



**RESERVOIR CHARACTERIZATION OF THE
JERIBE FORMATION (MIDDLE MIOCENE) FROM
SELECTED WELLS IN HAMRIN OIL FIELD,
NORTHERN IRAQ**

A Thesis
Submitted to the Council of
The College of Science at the University of Sulaimani
In partial fulfillment of the requirements for the degree of
Master of Science in Geology
(Petroleum Geology)

By
Muhamad Burhan M. Saeed
B.Sc. Geology (2009), Sulaimani of University

Supervised by
Dr. Dler Hussein Baban
Assistant Professor

January, 2017

Bafranbar, 2716

Supervisor Certification

I certify that the preparation of thesis titled "**Reservoir Characterization of the Jeribe Formation (Middle Miocene) from Selected Wells in Hamrin Oil Field, Northern Iraq**" accomplished by (Muhamad Burhan M. Saeed), was prepared under my supervision in the College of Science, University of Sulaimani, as partial fulfillment of the requirements for the degree of Master of Science in Geology (Petroleum Geology).

Signature:

Name: Dr. Dler Hussein Baban

Scientific Title: Assistant Professor

Date: 3 / 10 / 2016

In view of the available recommendation, I forward this thesis for debate by the examining committee.

Signature:

Name: Dr. Diary A. Amin

Scientific Title: Assistant Professor

Head of the department of Geology

Date: 3 / 10 / 2016

Linguistic Evaluation Certificate

This is to certify that I, Rebeen Abdullah Kareem have proofread this thesis entitled "**Reservoir Characterization of the Jeribe Formation (Middle Miocene) From Selected Wells in Hamrin Oil Field, Northern Iraq**" conducted by Muhamad Burhan M.Saeed. After marking and correcting the mistakes, the thesis was handed again to the researcher to make the corrections in this last copy.



Proofreader: Dr. Rebeen Abdullah Kareem


Date: 14/11 / 2016

Department of English, School of Languages, Faculty of Humanities,
University of Sulaimani.

Examining Committee Certification

We certify that we have read this thesis entitled "**Reservoir Characterization of the Jeribe Formation (Middle Miocene) from Selected Wells in Hamrin Oil Field, Northern Iraq**" prepared by (Muhamad Burhan M. Saeed), and as Examining Committee, examined the student in its content and in what is connected with it, and in our opinion it meets the basic requirements toward the degree of Master of Science in Geology "Petroleum Geology".

Signature: 
Name: **Dr. Fawzi M. Al-Beyati**
Title: **Assistant Professor**
Date: 15 / 1 / 2017
(Chairman)

Signature: 
Name: **Dr. Govand H. Sherwani**
Title: **Assistant Professor**
Date: 15 / 1 / 2017
(Member)

Signature:
Name: **Dr. Fouad M. Qader**
Title: **Lecturer**
Date: 15 / 1 / 2017
(Member)

Signature:
Name: **Dr. Dler H. Baban**
Title: **Assistant Professor**
Date: 15 / 1 / 2017
(Supervisor-Member)

Approved by the Dean of the College of Science.

Signature:
Name: **Dr. Bakhtiar Q. Aziz**
Title: **Professor**
Date: / / 2017

Dedication

**My father, my mother and my brothers;
My wife and my little son "Shko";** } (I hope this work makes them proud!)
**Our Heroes (Peshmarga), who gave their lives for Kurdistan Freedom; and
all people who love Science and love our country, Kurdistan.**

Acknowledgements

First of all, I praise Allah who gave me the health and power to finish this thesis. I would like to express my great thanks and appreciation for the crucial role to the thesis advisor, Dr. Dler Hussein Baban for proposing the idea of the project and his continuous advices during all steps of this work. I would like also to thank the chairman and staff of the Department of Geology at the College of Science at the University of Sulaimani for their support during different stages of this research.

I cannot express enough thanks to the North Oil Company in Kirkuk, for their cooperation and provision of the samples which were needed during this work. I am deeply grateful to the geologists Mr. Farhad Hamza, Mrs. Amal Nuradin and Mrs. Jiran Qadir for their kind help and assistance during sample collection stage.

I would like also to express my thanks to Dr. Fawzi Al-Beyati from Kirkuk Technical College for supporting me with very valuable references.

I appreciate the help of Dr. Ibrahim M.J. Mohialdeen for checking the Kurdish copy of the abstract.

Many thanks due to Mr. Sardar Saleem and Mr. Azad Sangawi for their support and help in the plotting issues.

I am very appreciative of the assistance and tolerance of my family, without which, I would not be able to finish this project. Last, but not least, my gratitude and thanks go to my wife for her patience and encouragement throughout this study.

Abstract

The Middle Miocene Jeribe Formation has been studied from reservoir potentiality point of view at three wells in Hamrin Oil Field, Northern Iraq. Thin sections of the cutting rock samples and different wireline logs of the wells Hr-49, Hr-50, and Hr-51 were the main data used for evaluating the formation which showed about 50m thickness and carbonate nature consisting of limestone, dolomitic limestone, and dolostones. Microfacies, pore types, and diagenesis features as appeared under microscope in the studied rock samples were all shown. The formation appeared to contain different ratios of shale with dispersed type of distribution. Highest ratio of shale concentrated in the middle part of the formation.

The calculated porosity from the Sonic, Density, and Neutron logs have been corrected from shale effect and showed variations from less than 5% in the rich shale zones to more than 20% in the upper and lower parts of the formation. The existence of the gas in the two wells of Hr-49 and Hr-51 detected from the relationship of the neutron and density logs. Secondary porosities contributed in the total porosity of the formation by different percentages reached in some intervals to about 7%. Permeability has been calculated for Jeribe Formation in this study depending on multilinear regression method using the available core analysis data (porosity and permeability) and log data from the well Hr-2. The equation best representing the relationship between the log data and the measured core permeability of the well Hr-2 has been applied on the log data of the mentioned three studied wells. The upper part of the formation showed permeabilities exceeded 30md (especially in the well Hr-49), whereas obvious fluctuations noticed in the permeability values of the middle and lower part of the formation in the two wells of Hr-50 and Hr-51 reflecting heterogeneity in the nature of the formation.

Four distinctive reservoir units have been identified in the studied Jeribe Formation depending on the variations in the shaleness, porosity, and permeability of the formation. The reservoir units named from the bottom to the top as RU-1, RU-2, RU-3 (subdivided to RU-3A and RU-3B subunits), and RU-4 (subdivided to RU-4A and RU-4B subunits).

Water saturations in Jeribe Formation are relatively higher in the well Hr-51 than the other two studied wells (especially the lower part of the formation). Most of the reservoir hydrocarbons in the well Hr-51 was movable and that in contrast to the hydrocarbons in the Jeribe Formation in the well Hr-50 which appeared containing the highest ratios of residual hydrocarbons.

Jeribe Formation in the studied wells can produce hydrocarbons associated with different volumes of water. The less produced water is in the reservoir unit RU-1 and the reservoir subunit RU-4B, and the highest water production is in the reservoir subunit RU-3A.

Grain packstone or dolopackstone are the dominant rock fabric of Jeribe Formation except the reservoir units RU-1 and RU-2 in the well Hr-50 which are mostly mud dominated packstone or wackstone. The pore throat sizes between the grains range mostly between 1.0 and 2.0 microns with being 2.0 micron much more dominated. Pore throat sizes of 0.5 micron exist rarely in some reservoir units of the formation like RU-2 in the well Hr-49. The flow in Jeribe Formation appeared to be from permeability provided by mainly connected matrix pores and by microfractures.

Four Flow Zone Indicators (FZI) representing four unique Hydraulic Flow Units (HFU) have been identified in the studied Jeribe Formation and that from the relationship between the calculated Reservoir Quality Index (RQI) and Normalized Porosity Index ($\emptyset z$).

Net to Gross ratios of reservoir, pay, and production have been calculated for Jeribe Formation using shaleness, porosity, permeability, and saturation cutoffs with taking values of Movable Hydrocarbon Index (MHI) in consideration.

The highest N/G ratios of reservoir, pay, and production for Jeribe Formation exist in the well Hr-51 (79.83%, 79.33%, and 78.68% respectively) and the lowest in the well Hr-50 (58.93%, 54.31%, and 25.98% respectively).

The well Hr-51 contains the highest production thickness of Jeribe Formation among the three studied wells which is totally equal to 37m, whereas the well Hr-50 contains the lowest which is totally equal to 13.25m.

CONTENTS

Abstract.....	I
Contents.....	IV
List of Figures.....	VII
List of Tables.....	XII

Chapter One: Introduction

1.1	Preface.....	1
1.2	Hamrin Oil Field.....	2
1.3	The Studied Wells.....	5
1.4	Geological setting.....	5
1.5	Jeribe Formation.....	8
1.5.1	Lithology and Thickness	9
1.5.2	Depositional environment.....	9
1.5.3	Boundaries and contacts.....	10
1.5.4	Age and Fossil.....	10
1.5.5	Equivalents.....	10
1.6	Methodology and Data Collection.....	11
1.6.1	Rock Samples.....	11
1.6.2	Well log data.....	11
1.7	Aims and Objectives.....	12
1.8	Previous studies.....	13

Chapter Two: Lithological and Shale Calculation

2.1	Preface.....	19
2.2	Identification of Microfacies.....	20
2.3	Lithology Determination from Porosity logs.....	28
2.3.1	Neutron – Density Crossplot.....	28
2.3.2	M-N Crossplot.....	31
2.4	Gamma Ray Log.....	34
2.5	Shale Volume Calculation.....	36

Chapter Three: Determination of Porosity, Permeability, and Reservoir Units

3.1	Preface.....	44
3.2	Determination of porosity.....	45
3.2.1	Sonic Log.....	46
3.2.2	Density Log.....	51
3.2.3	Neutron Log.....	56
3.3	Types of Shale Distribution in Reservoirs.....	59
3.4	Correction of Porosity From Shale Impact.....	64
3.5	Combination of Neutron-Density Porosity Logs.....	66
3.6	Detecting Existence of Gas Using Porosity Logs.....	72
3.7	Secondary Porosity Detection from Log Data.....	77
3.8	Permeability.....	82
3.9	Reservoir Units.....	87
3.9.1	Reservoir Unit 1 (RU-1).....	89
3.9.2	Reservoir Unit 2(RU-2).....	89
3.9.3	Reservoir Unit 3(RU-3).....	90
3.9.4	Reservoir Unit 4(RU-4).....	91

Chapter Four: Saturations and Reservoir Characterization

4.1	Preface.....	98
4.2	Resistivity Logs.....	99
4.3	Water Saturation	100
4.3.1	Calculation of Formation Water Resistivity (R_w).....	103
4.3.2	Determining the value of the Cementation Factor (m).....	104
4.4	Calculation of Water and Hydrocarbon Saturations in the studied wells.	108
4.5	Quick Look Methods.....	110
4.6	Bulk Volume Water (BVW) calculation.....	113
4.7	Moveability of Hydrocarbons.....	116
4.8	Rock Fabrics from Porosity - Permeability relationship.....	122
4.9	Flow Zone Indicators (FZI).....	130
4.10	Net to Gross Reservoir and Pay Ratios.....	136

Chapter Five: Conclusions and Recommendations

5.1	Conclusions.....	148
5.2	Recommendations.....	151
	References.....	153
	Appendix A.....	162
	Appendix B.....	165
	Appendix C.....	169

List of Figures

Figures No.	Figure Title	Page No.
1.1	A: Simplified tectonic map of Northern Iraq with indication for the studied Hamrin Oil Field (after Al-Ameri and Zumberg, 2012 with minor modifications), B: Location of the studied wells in Allas Dome (The satellite image is from Google Earth).....	3
1.2	(A) Structure cross-section across the Hamrin and Ajil fields showing the structure pattern and stratigraphic intervals; (B) Structure contour map on top of Jeribe Formation, Nukhaila and Allas domes, Hamrin Field, Northern Iraq (after NOC, 1992 in Mahdi, 2015).....	4
1.3	Structural elements of northern Iraq and location of Makhul-Hamrin lineament within Kirkuk-Hamrin Subzone (after Aqrawi et al., 2010).....	6
1.4	Schematic chronostratigraphic section for megasequence AP11 (34 Ma-present) and showing the position of Jeribe Formation within the MFS Ng20 (Sharland et al., 2001 with minor modifications).....	7
1.5	Paleogeographic setting of the Jeribe Formation (after Aqrawi et al., 2010).....	8
2.1	Classification of Dunhum (1962) with modifications by Embry and Klován (1972) for carbonate rocks.....	21
2.2	Classification of carbonate porosity, X indicates the most distinctive porosity types in carbonate reservoirs (after Choquette and Pray, 1970).....	21
2.3	Neutron-Density crossplot for lithology identification of the studied Jeribe Formation in the studied wells. The lithology of Dhiban and Lower Fars formations also identified (the crossplot is after Schlumberger, 1988).....	30
2.4	M-N crossplot for lithology identification of the studied Jeribe Formation in the studied wells. The lithology of Dhiban and Lower Fars formations also identified (the crossplot is after Schlumberger, 1989).....	33

2.5	Gamma ray log for Jeribe Formation including uppermost part of Dhiban and lowermost part of Lower Fars formations in the wells Hr-49, Hr-50 and Hr-51.....	35
2.6	Curve plots of the calculated volume of shale and shale content zonation along the studied sections of Hr-49, Hr-50 and Hr-51.....	38
2.7	Lithologic variations and gamma ray respond for the studied Jeribe Formation with the uppermost part of Dhiban and lowermost part of Lower Fars formations in the well Hr-49.....	41
2.8	Lithologic variations and gamma ray respond for the studied Jeribe Formation with the uppermost part of Dhiban and lowermost part of Lower Fars formations in the well Hr-50.....	42
2.9	Lithologic variations and gamma ray respond for the studied Jeribe Formation with the uppermost part of Dhiban and lowermost part of Lower Fars formations in the well Hr-51.....	43
3.1	Interval transit time (Δt) for the studied Jeribe Formation in the wells Hr-49, Hr-50 and Hr-51.....	49
3.2	Sonic porosity (\emptyset_s) for Jeribe Formation in the studied wells of Hr-49, Hr-50, and Hr-51.....	50
3.3	Bulk Density (ρ_b) for Jeribe Formation in the studied wells of Hr-49, Hr-50, and Hr-51.....	54
3.4	Density porosity (\emptyset_D) for Jeribe Formation in the studied wells of Hr-49, Hr-50, and Hr-51.....	55
3.5	Neutron porosity (\emptyset_N) for Jeribe Formation in the studied wells of Hr-49, Hr-50, and Hr-51.....	58
3.6	Clay distribution types in reservoirs (after Glover, 2008).....	60
3.7	Pore filling, pore lining, and pore bridging of Dispersed clay type in sandstone reservoir rocks (after Ellis and Singer, 2008).....	60
3.8	Thomas-Stieber plot for discriminating dispersed/laminated shale.....	62

3.9	Shale distribution type for the studied Jeribe Formation in the wells of Hr-49, Hr-50, and Hr-51 using Thomas-Stieber plot.....	63
3.10	Incorrected, corrected Sonic porosity from shale effect, and shale volume curves for the Jeribe Formation in the studied wells of Hr-49, Hr-50, and Hr-51.....	68
3.11	Incorrected and corrected Density porosity from shale effect and shale volume curves for Jeribe Formation in the studied wells of Hr-49, Hr-50, and Hr-51.....	69
3.12	Incorrected and corrected Neutron porosity from shale effect and shale volume curves for the studied Jeribe Formation in the wells of Hr-49, Hr-50, and Hr-51.....	70
3.13	Incorrected and corrected N-D porosity from shale effect and shale volume curves for the studied Jeribe Formation in the wells of Hr-49, Hr-50, and Hr-51.....	71
3.14	Neutron and Density porosity curve's crossovers as appeared in the studied Jeribe Formation for each of well Hr-49, Hr-50 and Hr-51.....	75
3.15	Gas effect as can be seen using MID crossplot for Jeribe Formation in the studied wells (the crossplot is after Schlumberger, 1972).....	76
3.16	Incorrected and Corrected Sonic porosity from gas effect for the studied Jeribe Formation in the wells Hr-49 and Hr-51.....	80
3.17	Secondary porosity plot for the studied Jeribe Formation in the studied wells of Hr-49, Hr-50 and Hr-51.....	81
3.18	Caliper log plot for the studied Jeribe Formation in the wells Hr-49, Hr-50 and Hr-51 with indication to the used bit size in each well.....	85
3.19	The measured permeability from core test analysis (red line) and the permeability values measured from log data (blue line) for the studied Jeribe Formation in the well Hr-2.....	87
3.20	Plots of the calculated permeability from the log data for the studied Jeribe	

Formation in the wells Hr-49, Hr-50, and Hr-51.....	88
3.21 Subdivision of the Jeribe Formation to reservoir units on the bases of the porosity, permeability, and shale volume for well Hr-49.....	92
3.22 Subdivision of the Jeribe Formation to reservoir units on the bases of the porosity, permeability, and shale volume for well Hr-50.....	93
3.23 Subdivision of the Jeribe Formation to reservoir units on the bases of the porosity, permeability, and shale volume for well Hr-51.....	94
3.24 Correlation between reservoir units of Jeribe Formation in the wells Hr-49, Hr-50, and Hr-51.....	97
4.1 The readings of the LLD, LLS, and MSFL logs for the studied Jeribe Formation in the wells Hr-49, Hr-50 and Hr-51.....	101
4.2 The Data Sp log for the Jeribe Formation in the well Hr-2.....	105
4.3 Cementation factor (m) from Pickett crossplot for Jeribe Formation, well Hr-49.....	106
4.4 Cementation factor (m) from Pickett crossplot for Jeribe Formation, well Hr-50.....	107
4.5 Cementation factor (m) from Pickett crossplot for Jeribe Formation, well Hr-51.....	107
4.6 Water saturation and Hydrocarbon saturation (Residual and Movable) with regard to porosity for the studied Jeribe Formation in the wells Hr-49, Hr-50 and Hr-51.....	109
4.7 Ro, Rxoo, and Rt curves as QLM (Movable Oil Plot) for Jeribe Formation in the three studied wells of Hr-49, Hr-50, and Hr-51.....	112
4.8 Buckles plot for the values of BVW for the reservoir units and subunits of Jeribe Formation in the well Hr-49.....	117
4.9 Buckles plot for the values of BVW for the reservoir units and subunits of Jeribe Formation in the well Hr-50.....	118
4.10 Buckles plot for the values of BVW for the reservoir units and subunits of	

	Jeribe Formation in the well Hr-51.....	119
4.11	The plot of Movable Hydrocarbon Index for the studied Jeribe Formation in the wells Hr-49, Hr-50 and Hr-51.....	121
4.12	Comparison of petrophysical-class fields and pore-throat sizes versus interparticle porosity and permeability (after Lucia, 1999).....	124
4.13	Porosity-permeability cross plot shows the pore throat size and petrophysical rock fabric classes of Jeribe Formation's reservoir units in Hr-49 well.....	125
4.14	Porosity-permeability cross plot shows the pore throat size and petrophysical rock fabric classes of Jeribe Formation's reservoir units in Hr-50 well.....	126
4.15	Porosity-permeability cross plot shows the pore throat size and petrophysical rock fabric classes of Jeribe Formation's reservoir units in Hr-51 well.....	127
4.16	Porosity-permeability cross plot showing the type of flow and pore throat sizes for Jeribe Formation in wells Hr-49, Hr-50 and Hr-51.....	129
4.17	Histogram of FZI values for the sample points of Jeribe Formation in the three studied wells of Hr-49, Hr-50, and Hr-51.....	133
4.18	Normal probability analysis for the calculated Flow Zone Indicator values for Jeribe Formation in each of the wells of Hr-49, Hr-50, and Hr-5.....	134
4.19	The three distinctive FZI values which identified from RQI- ϕ_z relationship for Jeribe Formation in the studied wells of Hr-49, Hr-50, and Hr-51.....	135
4.20	Comparison between the calculated MHI and FZI for the reservoir units of Jeribe Formation in the studied wells of Hr-49, Hr-50, and Hr-51.....	137
4.21	Porosity cutoff measurement for the case of oil bearing reservoir using porosity versus permeability crossplot for the core data from Hr-2 well.....	140
4.22	Porosity cutoff measurement for the case of gas bearing reservoir using porosity versus permeability crossplot for the core data from Hr-2 well.....	141
4.23	Water saturation cutoff determination using porosity versus water saturation crossplot for Hr-49.....	141
4.24	Water saturation cutoff determination using porosity versus water saturation	

	crossplot for Hr-50.....	142
4.25	Water saturation cutoff determination using porosity versus water saturation crossplot for Hr-51.....	142
4.26	Summary of all data that are used to finalize subdivision of reservoir units and reservoir potentiality by applying the cutoffs for Jeribe Formation in well Hr-49.....	145
4.27	Summary of all data that are used to finalize subdivision of reservoir units and reservoir potentiality by applying the cutoffs for Jeribe Formation in well Hr-50.....	146
4.28	Summary of all data that are used to finalize subdivision of reservoir units and reservoir potentiality by applying the cutoffs for Jeribe Formation in well Hr-51.....	147

List of Tables

Table No.	Tables Title	Page No.
1.1	The dimensions of the three domes of Allas, Nukhailah, and Albofodhool as appeared on top of Jeribe Formation and the API degrees of their reservoired oils (after NOC, 1994).....	5
1.2	The studied wells with their localities, elevations and coordinates.....	5
1.3	Thickness of the Jeribe Formation in the studied wells with the number of the selected rock samples in each well.....	11
1.4	The available and used wireline log data for the studied wells and the well Hr-2.....	12
2.1	Main lithology, microfacies, pore types, and diagenesis features identified in the studied Jeribe Formation in the well Hr-49.....	26
2.2	Main lithology, microfacies, pore types, and diagenesis features identified in	

the studied Jeribe Formation in the well Hr-50.....	26
2.3 Main lithology, microfacies, pore types, and diagenesis features identified in the studied Jeribe Formation in the well Hr-51.....	27
2.4 Minimum and maximum gamma ray readings used for calculating IGR for the three studied wells.....	36
2.5 Zonation on the bases of percentage of shale volume (after Ghorab, 2008).....	37
2.6 The depth intervals and thicknesses of Jeribe and the studied parts of Dhiban and Lower Fars formations in the Hr-49, Hr-50, and Hr-51 wells.....	39
2.7 Zonation of the Jeribe and the studied parts of Dhiban and Lower Fars formations studied formations depending on their average shale content and according to the standard proposed by Ghorab (2008).....	40
3.1 Matrix density values for common types of rocks (after Asquith and Krygowski, 2004).....	53
3.2 Description of porosity qualitatively as proposed by North (1985).....	72
3.3 Qualitative description of permeability as proposed by North (1985).....	86
3.4 Minimum, maximum, and average values of shale content, porosity, and permeability for the distinguished reservoir units of Jeribe Formation in the well Hr-49.....	95
3.5 Minimum, maximum, and average values of shale content, porosity, and permeability for the distinguished reservoir units of Jeribe Formation in the well Hr-50.....	95
3.6 Minimum, maximum, and average values of shale content, porosity, and permeability for the distinguished reservoir units of Jeribe Formation in the well Hr-51.....	96
4.1 Calculated R_w and other parameters for the studied Jeribe Formation in the Hr-2 well	104
4.2 BVW as a function of grain size and lithology (comparative table),(after Asquith and Krygowski, 2004).....	114

4.3	Calculated FZI and the hydraulic unit types for the studied wells.....	136
4.4	Calculated N/G reservoir and pay ratios for the studied Jeribe Formation in the well Hr-49.....	143
4.5	Calculated N/G reservoir and pay ratios for the studied Jeribe Formation in the well Hr-50.....	143
4.6	Calculated N/G reservoir and pay ratios for the studied Jeribe Formation in the well Hr-51.....	143

CHAPTER ONE

Introduction

1.1 Preface

The wealth of petroleum has made Iraq one of the most actively explored country of the world. Hamrin Oil Field is one of the Iraq's giant oil fields (Al-Mehadi, 2009) with several pay zones similar to the most of the other northern Iraqi oil fields.

Generally, reservoirs in the Hamrin Oil Field includes the Tertiary reservoirs (part of the Transition zone of L. Fars, Jeribe, Euphrates, and Kirkuk Group formations), and Cretaceous reservoirs (Shiranish, Kometan, Hartha, Sa'di, Khasib, Mishrif, Rumaila, Mauddud, Shu'aiba, and Yamama formations) (NOC, 1994).

The Middle Miocene Jeribe Formation considers as a significant carbonate reservoir within the Iraqi geological succession. The organic detrital limestone of Jeribe Formation in this field as observed from the drilled wells is overlain by the transition beds of the Middle Miocene Lower Fars (Fatha) Formation and underlain by the Lower Miocene Dhiban Formation.

Reservoir characterization which is to construction of realistic 3D image of petrophysical properties to be used predict reservoir performance (Lucia, 2007), is considered as an effective tool for evaluating any oil field economically.

In this study, different kinds of data have been collected about Jeribe Formation in Hamrin Oil Field for characterizing it as an important reservoir bed. As most of the reservoir characterizing procedures, log data represented the main source of information which had been used in evaluating the

formation.

As known, reservoir characterization to be best achieved for any reservoir, different kinds of data should be available with the best quality. In this study and due to the confidentiality and sensitivity of the required data not all the vital data been obtained from the official authorities. Accordingly, best attempt tried to be done with the available data to hit the targets of the study as good as possible.

1.2 Hamrin Oil Field

The studied Hamrin Oil Field is located within the Low Folded Zone, part of the Zagros Fold Belt of the Unstable Shelf ((Buday, 1980; Alsharhan and Nairn, 1997; Sharland et al. 2001; Aqrawi et al., 2010; Al-Ameri et al., 2011). It is nearly 10km from north of Salahaddin Governorate and about 80km southwest of Kirkuk City, north of Iraq (Fig. 1.1A).

Hamrin Oil Field structurally consists of an asymmetrical longitudinal anticline which has a reflection on the surface and extends to about 105km in length and about 4.5 km in width with a northwest-southeast axis trend (Fig 1.1A). Field mapping and seismic data indicated the presence of a large anticline which appeared to be composed of three domes namely (from northwest to southeast) Albofodhool, Nukhailah, and Allas (Fig. 1.1B). The domes separated by Darb Almilh Saddle (between Albofodhool and Nukhailah domes) and Ain Alnukhaila Saddle (between Nukhailah and Allas domes). The existence of a transverse fault is expected between those two mentioned saddles by which a displacement of about 450m occurred between the beds on both sides of the fault (NOC, 1994). Figure 1.2A shows the effect of the mentioned transverse fault as appears on the structural cross section along the domes of Allas and Nukhailah, whereas Figure 1.2B shows the trace of the fault on the structural map drawn for the top of Jeribe Formation.

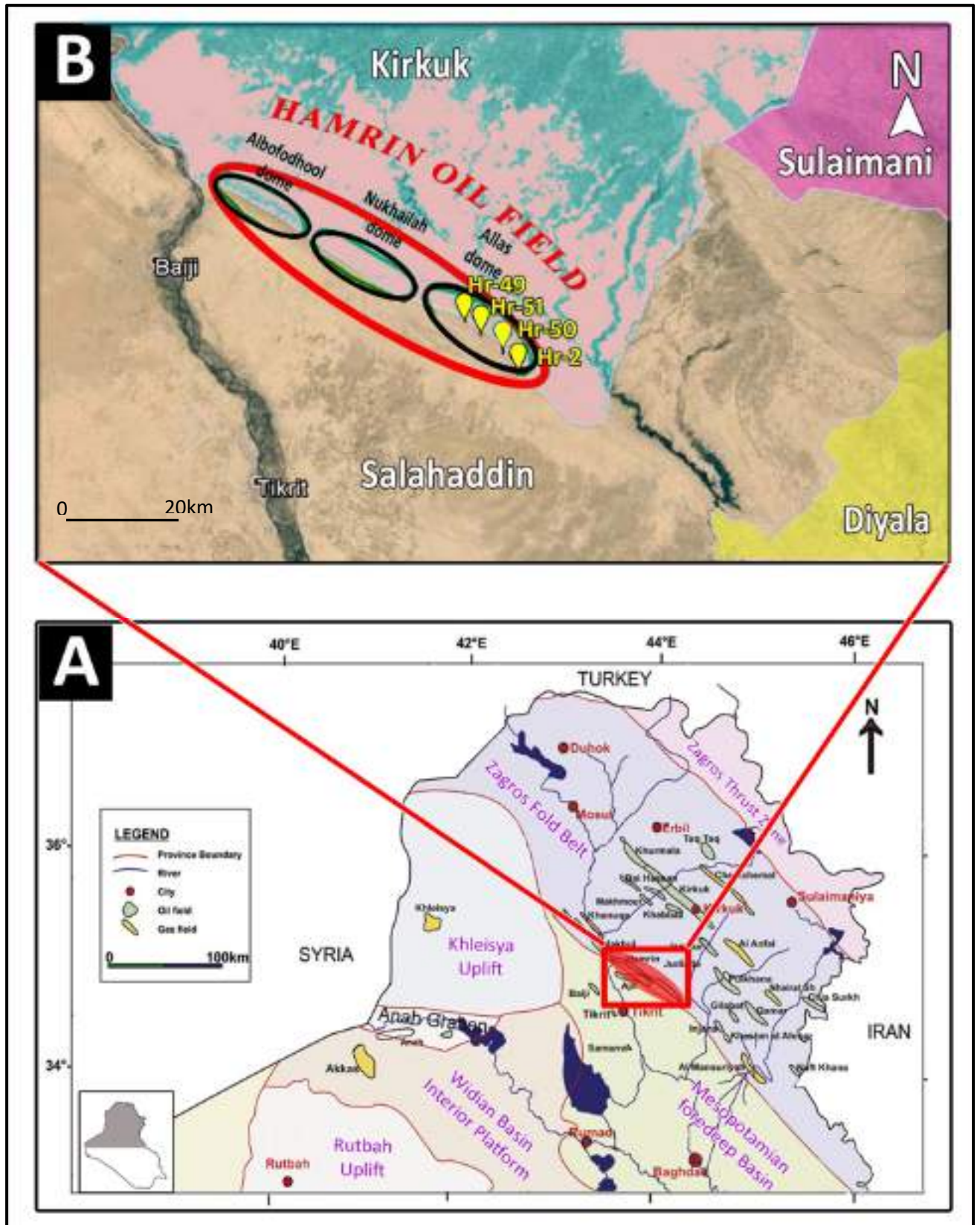


Figure 1.1: A: Simplified tectonic map of Northern Iraq with indication for the studied Hamrin Oil Field (after Al-Ameri and Zumberg, 2012 with minor modifications), B: Location of the studied wells in Allas Dome (The satellite image is from Google Earth).

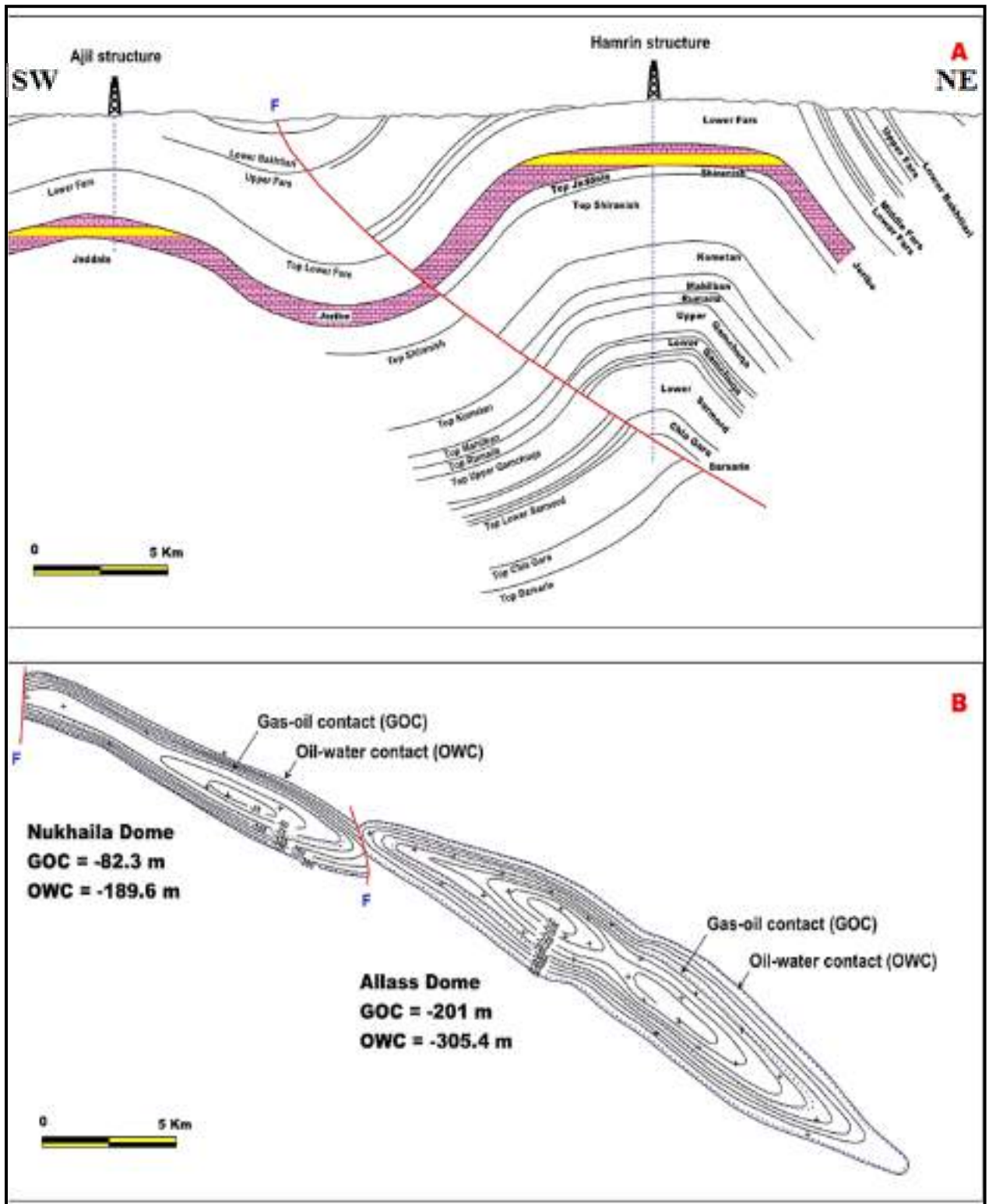


Figure 1.2: (A) Structure cross-section across the Hamrin and Ajil fields showing the structure pattern and stratigraphic intervals; (B) Structure contour map on top of Jeribe Formation, Nukhaila and Allas domes, Hamrin Field, Northern Iraq (after NOC, 1992 in Mahdi, 2015).

Table 1.1 summarizes the dimensions of the three domes with their closures on top of Jeribe Formation in addition to the API degrees of the reservoir oils in each dome.

Table 1.1: The dimensions of the three domes of Allas, Nukhailah, and Albofodhool as appeared on top of Jeribe Formation and the API degrees of their reservoir oils (after NOC, 1994).

Dome	Length(km)	Width (km)	Minimum Closure (m)	API° of the oil
Allas	28	3	130	32
Nukhailah	15	3	75	23
Albofodhool	26.5	4.5	325	16.5

1.3 The Studied Wells

In order to study Jeribe Formation in Hamrin Oil Field, three subsurface sections (wells) have been selected, namely Hr-49, Hr-50 and Hr-51 (Fig.1.1 B). Well locations, elevations, and coordinates are listed in table 1.2.

Table 1.2: The studied wells with their localities, elevations and coordinates.

Studied wells	Location	Elevation RTKB (m)	Coordinates
Hr-49	Allas Dome	313	Latitude: 34° 50' 22.20" Longitude: 44° 03' 32.60"
Hr-50		312	Latitude: 34° 47' 31.10" Longitude: 44° 07' 43.80"
Hr-51		326	Latitude: 34° 49' 06.00" Longitude: 44° 05' 15.10"

1.4 Geological setting

Hamrin Oil Field is located in the Iraqi Low Folded Zone which is characterized by outcropping Neogene sedimentary rocks; the cores of anticlines may expose Eocene limestone or Upper Cretaceous sedimentary rocks (Jassim and Buday, 2006).

Hamrin anticline represents the SW anticlinal line of the Kirkuk block (Embayment) portion of the Hamrin – Makhul Subzone (or Kirkuk-Hamrin as mentioned by Aqrawi et al., 2010) (Fig.1.3). The Hamrin- Makhul Subzone comprises long prominent NW-SE (or E-W) trending anticlines with decollement thrust faults originating at detachment surface at the base of the saliferous beds of the Fatha (Lower Fars) Formation (Jassim and Buday, 2006). The anticlines of the Hamrin-Makhul Subzone are over 100km long and are segmented into doubly plunging domes; the segmentation usually occurs at intersections with transversal faults where the axes of the anticlines are bent. The anticlines are often associated with longitudinal reverse faults on the S or SW flank, or occasionally on the N flank or on both flanks.

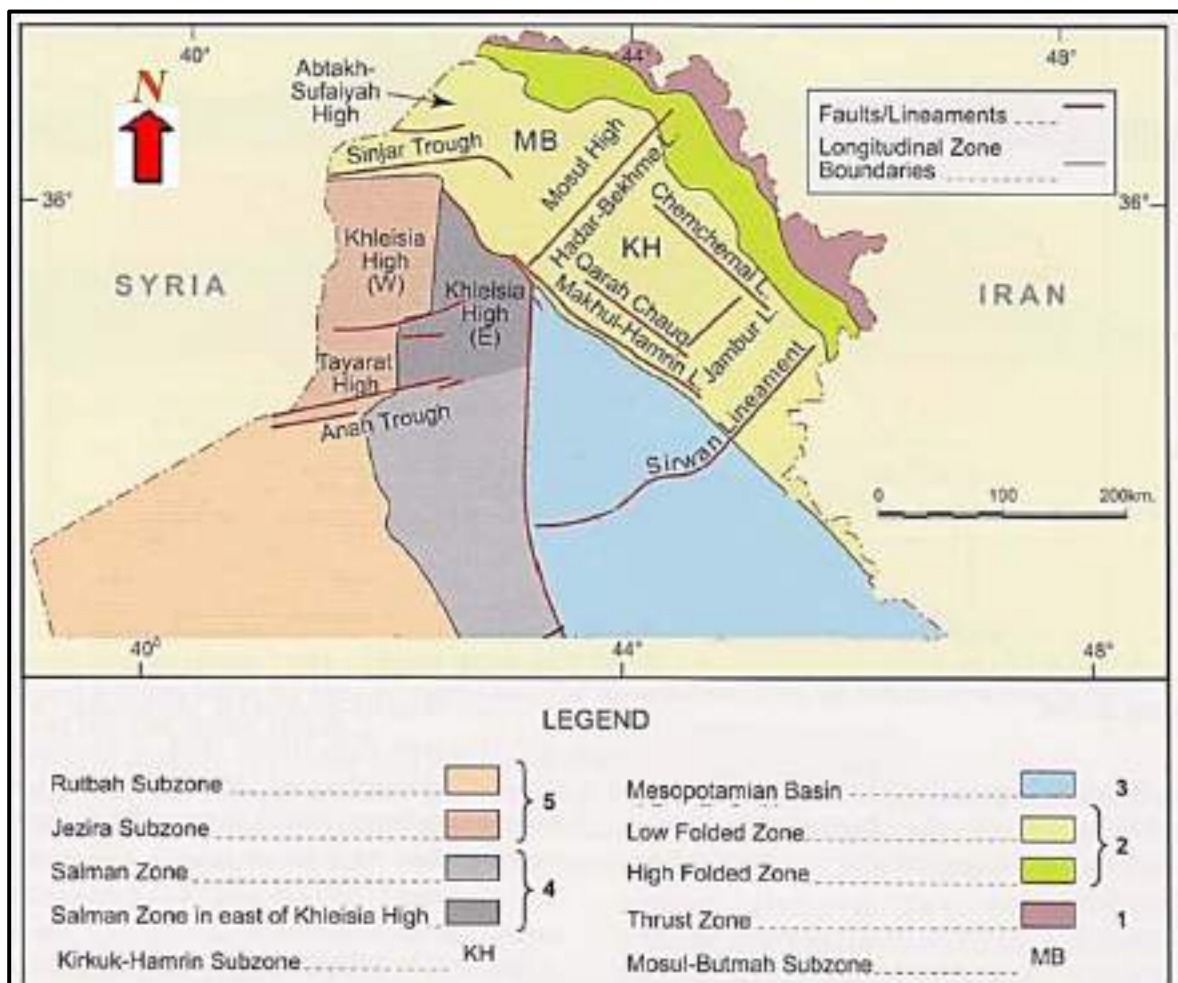


Figure 1.3: Structural elements of northern Iraq and location of Makhul-Hamrin lineament within Kirkuk-Hamrin Subzone (after Aqrawi et al., 2010).

The studied Jeribe Formation belongs to the Arabian Plate Megasequence 11 (AP11) of Sharland et al., (2001) within the Maximum Flooding Surface Ng 20 (MFS 20) (Fig. 1.4). According to Sharland et al., (2001) in Iraq and Syria, Jeribe Formation carbonate sedimentation was suppressed due to rapid deposition and plugging of accommodation space by sabkha cycles dominated by anhydrite, with halite deposited locally in the center of the shallow, saucer-like basin (Bellen et al., 1959; Aqrawi et al., 1989; Tucker, 1999). These events date the final closure of Neo-Tethys to the early Middle Miocene (Beydoun, 1993; Hooper et al., 1995).

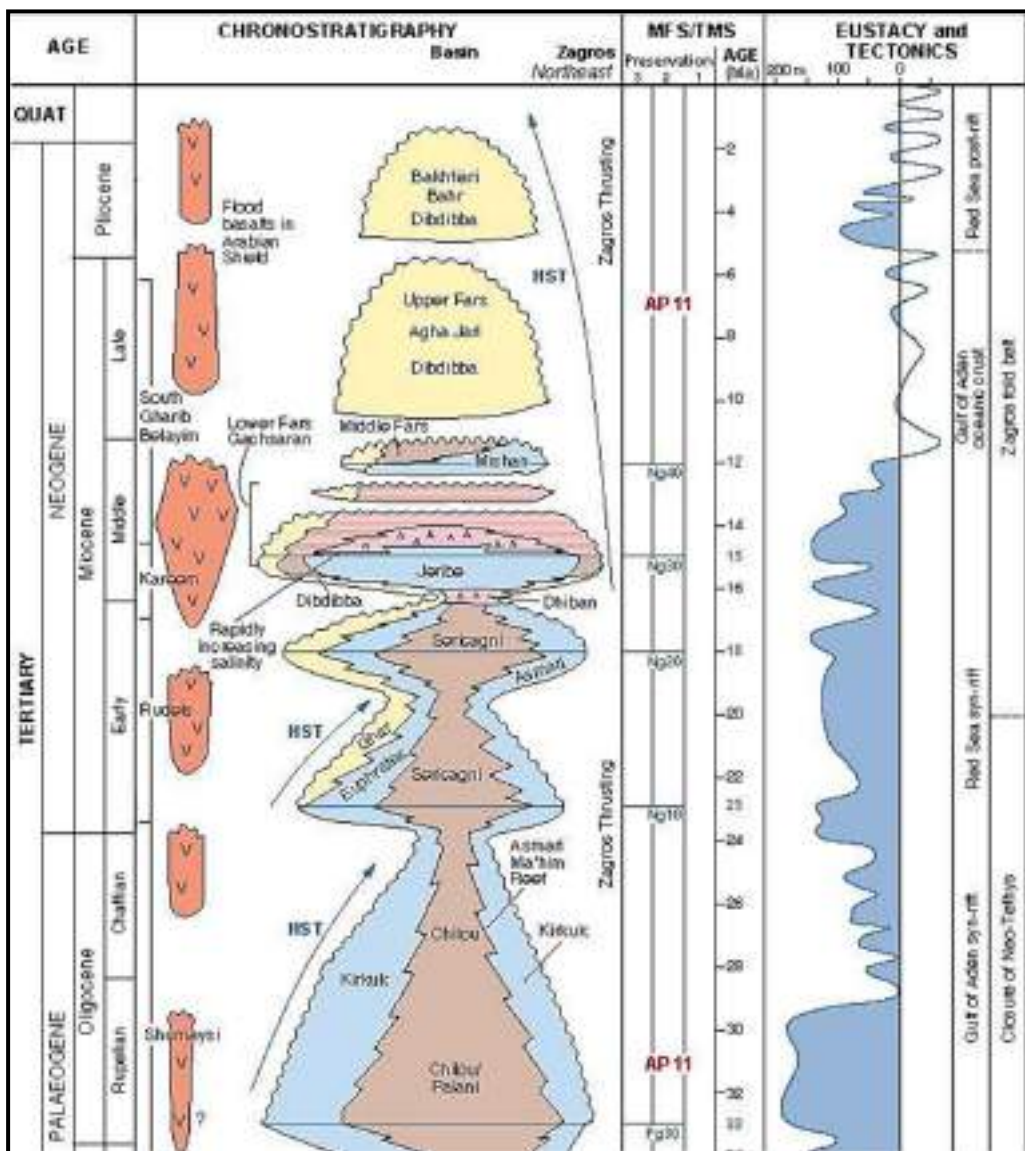


Figure1.4: Schematic chronostratigraphic section for megasequence AP11 (34 Ma-present) and showing the position of Jeribe Formation within the MFS Ng20 (after Sharland et al., 2001 with minor modifications).

The AP11 in Iraq can be divided into three supersequence based to the assumption of Aqrawi et al. (2010).

Jeribe Formation deposited relatively uniformly throughout the basin in which deposited (Fig.1.5). The maximum thickness is 70-75m in Makhul-Hamrin Subzone and Tigris Subzone (Jassim and Buday, 2006). In the basin center, cycles 1 to 10m thick occur in which porous open-marine carbonates are interbedded with relatively tight, restricted marine carbonates and evaporites (e.g. in the East Baghdad Field) (Aqrawi et al., 2010).

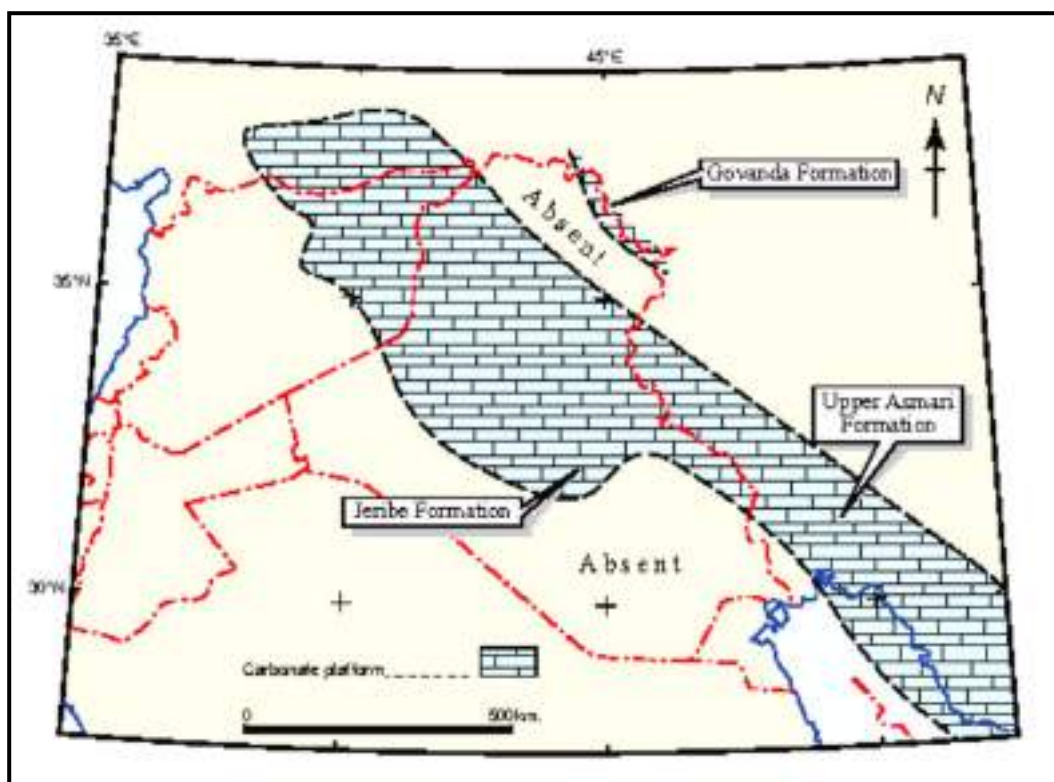


Figure 1.5: Paleogeographic setting of the Jeribe Formation (after Aqrawi et al., 2010).

1.5 Jeribe Formation

Damesin was the first who mentioned the Jeribe Formation in 1936 in unpublished report and then Bellen in 1957 defined and described it from the type locality near Jaddala Village, Jabal Sinjar, NW of Iraq at lat. 36°18'00" N, and long.41°41'00" E (Bellen et al., 1959).

1.5.1 Lithology and Thickness

The Jeribe Formation represents a heterogeneous formation originally described as organic detrital limestone. The Jeribe Formation comprises 70m of massive recrystallized and dolomitized limestones (Buday 1980; Jassim and Buday, 2006). However, Bellen et al. (1959) mentioned that the thickness of this formation ranges between 55 and 70m. Al-Juboury et al. (2007) recorded a thickness of 63m at well Injana-5.

As mentioned before, Jassim and Buday (2006) consider the maximum thickness of Jeribe Formation in Makhul - Hamrin Subzone and Tigris Subzone to be about 70-75m.

1.5.2 Depositional environment

According to Bellen et al. (1959); the type section gives most of the possible variations of the facies. They mentioned three main facies that interfinger extensively with each other. These are lagoonal facies, lithophyllid (reef) facies, and detrital facies that was probably deposited.

Al-Dayni (1979 in Ibrahim, 2008) determined the depositional environment of the Jeribe Formation as reefal (forereef - backreef) based on study of petrography, biostratigraphy and geochemistry of the formation in the northern part of Iraqi territory. According to Numan (1997); Jeribe Formation deposited in a marginal basin, whereas Al-Jouiny (2000) and Ibrahim (2008) stated that the formation deposited in an open platform and restricted platform generalized as shallow marine environment.

Aqrabi et al. (2010) consider Jeribe Formation as probably representing upward-shallowing carbonate ramp sequence. Al-Hietee (2012) determined the depositional environment of Jeribe as restricted, shallow open marine and shoal environments.

1.5.3 Boundaries and contacts

In the type area, the lower contact is unconformable with the Serikagni Formation where Dhiban Formation is absent and may be replaced by the Euphrates Formation (Bellen et al, 1959; Buday, 1980). In many areas conglomeratic beds occurs at the base of the Jeribe Formation. The formation passes gradationally into the overlying Lower Fars (Fatha) Formation. Jeribe Formation has a similar distribution to the underlying Euphrates Formation (Jassim and Buday, 2006).

In the studied wells Jeribe Formation appeared to be overlying by transition beds of Lower Fars (Fatha) Formation and underlying by the lagoonal evaporitic beds of Dhiban Formation.

1.5.4 Age and Fossil

The age of this formation is Middle Miocene (Karim, 1978) and also supposed to be early Miocene age (Bellen et al., 1959). However, the formation later assumed to be within the middle Miocene sequence (Jassim and Buday, 2006). Middle Miocene age is indicated by the presence of the *Orbulina* datum near the base of the formation (Prazak, 1974).

According to Buday (1980) fossils are sometimes abundant and the most conspicuous index fossil for the formation is *Borelis melo curdica*. He mentioned also that *Orbulina* occurs in the formation too. Besides, Bellen et al. (1959) mentioned the presence of *Amphistegina* sp., *Elphidium* sp., *Nonion* sp., *Rotalia beccarii*, *Dendritina cr. rangi*, *Peneroplis farsensis*, *Meandropsina anahensis*, fragments of gastropods, pelecypods, echinoids and lithophyllid algae in the formation also.

1.5.5 Equivalents

Govanda Limestone Formation is equivalent to Jeribe Formation in age and that in Northeast of Iraq (Jassim and Buday, 2006). In the southwestern Iran, the formation is equivalent to the Kalhur Limestone and part of Upper Asmari

Formation (Buday, 1980). Jeribe Formation is not recognized in southern Iraq (Bellen et al., 1959) (Fig.1.5), whereas it is also widespread at surface and in the northern oil fields of Iraq (Aqrawi et al., 2010).

1.6 Methodology and Data Collection

Rock samples (core and cutting) and logs are the main data that are used in characterizing Jeribe Formation in this study.

1.6.1 Rock Samples

Rock samples obtained from NOC for the studied formation from the wells Hr-49, Hr-50, and Hr-51 have been used to study microfacies, diagenesis, and determine visually the types of the porosity using optical transmitted light microscopy.

Table 1.3 shows the thickness of Jeribe Formation in the studied wells in addition to the depth intervals and number of the rock samples that used in this study.

Table 1.3: Thickness of the Jeribe Formation in the studied wells with the number of the selected rock samples in each well.

Wells	Total depth of the well (m)	Jeribe Formation			Number of the cutting samples
		Thickness (m)	Top (m)	Bottom (m)	
Hr-49	600	47	419.5	466.5	9
Hr-50	662	51	525	576	14
Hr-51	640	49	476.5	525.5	6

1.6.2 Well log data

Table 1.4 shows the available and used types of logs that were depended on in this study for characterizing Jeribe Formation in the studied wells. As seen in the table, log data from the well Hr-2 also used in this study for permeability calculation issues when combined with the available core

analysis data (porosity and permeability) for Jeribe Formation in the same well.

A number of softwares used in digitizing and plotting the log data including Getdata graph digitizer, Logplot-7, Adobe Photoshop, Adobe Illustrator, in addition to the conventional softwares of Excel and Grapher.

Table 1.4: The available and used wireline log data for the studied wells and the well Hr-2.

Wells	Gamma Ray Log	Caliper Log	Sonic Log	Density Log	Neutron Log	SP Log	Resistivity Logs		
							MSFL	LLS	LLD
Hr-2	X	X	X	X	X	X	-	-	-
Hr-49	X	X	X	X	X	-	X	X	X
Hr-50	X	X	X	X	X	-	X	X	X
Hr-51	X	X	X	X	X	-	X	X	X

1.7 Aims of the study

The main objective of this research is to evaluate Jeribe Formation from reservoir characteristics point of view from a selected wells in Hamrin Oil Field, Northern Iraq. Accordingly and in order to achieve that main target the following aims were taken in consideration:

1. Estimation of the petrophysical properties of Jeribe reservoir such as shale volume, porosity, and permeability.
2. Determination of the petrographic properties (microfacies and diagenesis) which affected the reservoir development.
3. Subdivision of the reservoir beds to units depending on the variations in reservoir properties.
4. Determination of the existed fluid types in the reservoir units and their saturations.
5. Identification of the potential flow zones within the studied formation.

6. Calculation of the net to gross reservoir and pay ratios for the studied reservoir units and collectively for Jeribe Formation in the Hamrin Oil Field.

1.8 Previous studies

Being Jeribe Formation an important reservoir in most of the Northern Iraqi oil fields, therefore a lot of studies and researches have been done to show the characteristics and properties of Jeribe Formation. The following is a summary of the most important studies in relation to the core title of this study.

Bellen et al. (1959) have described the type locality of Jeribe Formation and stated that Jeribe Formation is of low Miocene age; composed of recrystallized, detrital, and dolomitic limestone.

Lawa (1989) has studied the sedimentology and stratigraphy of the Oligocene-Miocene succession in Qayara area near Mosul City. He determined the paleodepositional environment of Jeribe Formation as semi-districted warm lagoon.

Ibrahim et al. (2002) studied the biostratigraphy of Euphrates and Jeribe formations in the Middle and Southern Iraq. They recorded the *Borelis milo curdica* Range zone as obvious character of Jeribe Formation. They also determined the age of the formation as Early Middle Miocene depending on the existence of the species *Borelis milo* (Fichtel&Moll) var *curdica Reichel*

Al-Ayobe (2004) has studied Jeribe Formation using more than 140 rock samples from three outcrop sections in Northwestern Iraq. Based on the field and petrographic features, the studied succession was divided stratigraphically into two informal rock units. The microfacies analysis showed that Jeribe Formation is composed of alternations of seven major facies; though, the algal bound stone facies is regarded as the most important facies. These facies are divided into (18) microfacies according to the types of grains and nature of

the matrix.

Markaryan (2005) has examined Jeribe Formation in a number of fields in Dyala Governorate. She claims that the porosities in the formation are of intraparticle, fracture, channels, vugs and moldic types. She also declared that Jeribe Formation has good reservoir properties with an average porosity about 20% and average permeability about 30md.

Al-Juboury et al. (2007) have studied the stratigraphic and depositional environment in the late-Early Middle Miocene. They mentioned two depositional basins, the first basin of Burdigalian age and the second of Langhian age including Jeribe and Fatha formations. They also mentioned that the Early Langhian age of the Kirkuk Basin characterized by a shallowing- upward sequence which begins by sediments rich in planktonic foraminifera for the lower part of the Jeribe Formation, and then shallow water and lagoonal carbonates for the upper part of the Jeribe Formation.

Abdulrahman (2007) studied the sedimentological and petrophysical properties of the Aquitanian-Lower Early Langhian succession in the well Kor Mor - 3. She concluded that Jeribe Formation represents a third order cycle with no hydrocarbon content. She mentioned that Jeribe in the studied well suffered from different kinds of cementation including Drusy, Fibrous, Granular, and Syntaxial.

Al-Ghri et al. (2007) Through their remarks on the age of the Miocene Euphrates Formation in Western Iraq, they thought that *Borelis melo curdica* does not need to be the official stamp of the Jeribe Formation.

Ibrahim (2008) studied the sedimentology and reservoir characteristics of Jeribe Formation from two wells of Tawke Oil Field, Kurdistan Region-Iraq. He mentioned that the formation which was of 63 and 87m thickness in the two wells is composed of limestone and dolomitic limestone including thin evaporite units. He distinguished four classes of porosity in the formation including fracture, intercrystalline, vuggy, and interparticle. The measured

porosity and permeability from 15 core samples revealed porosity up to 16.1% and permeability up to 36.8md.

Aqrawi et al. (2010) have stated that Jeribe Formation probably represents an upward- shallowing carbonate ramp sequence. Cycle stacking (ex. in East Baghdad Field) suggests that another sequence present locally at the formation's top.

Al-Ameri et al. (2011) have studied the hydrocarbon in the Middle Miocene Jeribe Formation in a number of oil fields in Dyala District. They found out that the oil accumulated in the Jeribe reservoir is originated from the Upper Jurassic-Lower Cretaceous Chia Gara Formation. They also explored that Jeribe Formation owns an average porosity about 12-27% in the studied oil fields.

Al-Dabbas et al. (2012) studied Jeribe Formation (Early Middle Miocene) in the central and southern Iraq and they concluded that four major depositional cycles are dominating in the formation. All the cycles exhibit shallowing, upwell regressive cycles. The upper part of the formation represents the fall of the sea level and marking the end of the regressive phase.

AL-Hietee (2012) studied the facies architecture and sequence stratigraphy of the Lower and Middle Miocene beds (including Jeribe Formation) in Kirkuk area. He noticed that Jeribe Formation consists mainly of mudstone, wackestone, and packstone with no recording of any grainstone facies.

Gharib (2012) has studied Jeribe and Euphrates formations from a number of wells in Ajeel Oil Field. He divided Jeribe Formation using log and microfacies data into two reservoir units separated in the middle part by a marl bed.

Fadhil (2013) has studied the sedimentological and reservoir characteristics of Jeribe Formation in five wells at Alass dome within Hamrin Oil Field/ NE Iraq. Four main microfacies were recognized within the formation

representing environments of deposition extending from semi closed platform to open platform and front slope. She divide Jeribe Formation depending mainly on log data into two reservoir units (A and B), separated by a layer of shale. She mentioned that Jeribe Formation has effective porosities ranging between 0 and 33%.

Kharajiany (2014) in his study about the stratigraphy of Ashdagh anticline near Darbandikhan Town, describes about 2m thick exposed Jeribe Formation overlying about 2m thick Dhiban Formation. He mentions that Jeribe in the studied sections consists of slightly marly gray limestone.

Kharajiany et al. (2014) have studied Oligocene and Miocene rock beds in Mamlaha anticline near Chamchamal Town. Through their study, they mention that Anah Formation is separated from Euphrates Formation as abrupt change in lithology, whereas Jeribe Formation lies beneath the claystone of Lower Fars Formation.

Hussein (2015) studied the Tertiary reservoir (including Jeribe Formation) from a number of wells in Khabbaz Oil Field. Poor permeability due to relatively high content of dispersed shale was the most noticeable conclusion of Hussein's study.

Mahdi (2015) during his study about source rock evaluation of some Upper Jurassic - Lower Cretaceous formations in northern Iraq, tried to correlate the generated oils with the reservoir oils within few selected oil fields. Among the selected oils was oil from Jeribe reservoir in Hamrin Oil Field that classified it as oil family no.4 and appeared to be generated from marine carbonate type IIS kerogen.

Sadeq et al., (2015) during their study about the permeability estimation of fractured and vuggy carbonate reservoir using permeability multiplier method in Bai Hassan Oil Field/Northern Iraq, exhibited in a comparison way (without details) porosity and permeability values for Jeribe Formation measured through cores and through using transformation equation. In this

study, Jeribe Formation mentioned mistakenly as of Oligocene age which is an older age for this formation that never been mentioned previously.

Al-Qayim et al. (2016) studied the Oligocene–Miocene carbonate sequence (including Jeribe Formation) at Golan Mountain, Kurdistan Region, and NE Iraq. In this study, Jeribe Formation was located at the upper most cycle (sequence-4) in their studied section with thickness about 3m. They mentioned that the lithologic character of Jeribe Formation was almost similar to the underlying Euphrates Formation. They subdivided Jeribe Formation to two members; the lower member (about 1.0 m thick), consists of thin-bedded, gray, hard, granular limestone of shoal environment, and the upper member (about 1.0 to 2.0 m-thick), which consists of gray, thin-bedded to laminated sandy dolomitic limestone or calcareous sandstone.

Sissakian et al. (2016) studied the Miocene sequence in Iraq emphasizing on the stratigraphy, paleogeography, and economic potential of the sequence. The authors attributed the wide subsurface extent of the Jeribe Formation to the basin configuration during Middle Miocene, as it was continued since the Early Miocene, as shallow marine, before starting the development of closed lagoons in which the Fatha Formation was deposited. According to Sissakian et al. (2016), the recognized cross bedding in the coquina bed within the Jeribe Formation is good indication for shallow marine near shore deposition.

Al-Jwaini and Gayara (2016a) studied the Upper Palaeogene -Lower Neogene succession in the fields of Kirkuk, Bai Hassan, and Khabbaz from reservoir characterization point of view. Among the studied formations in the succession was Jeribe Formation in the two fields of Bai Hassan and Khabbaz. They characterized Jeribe Formation as reservoir unit -1 and show the types of the microfacies in the formation and the types of the porosities with the diagenesis affected the properties of the formation. The formation also was evaluated depending on the log data from which, shale content, porosity values, and saturations in Jeribe Formation were determined in the

two mentioned fields.

Al-Jwaini and Gayara (2016b) as separate study analyzed the Palaeoenvironments and sequence development of the same mentioned succession above in the same mentioned fields also. Among the conclusions of this study was that a transgression during the Langhian Middle Miocene covered both Khabaz and Bai Hassan fields with shallow water but did not reach the Kirkuk Field, which led to the deposition of the Jeribe facies in a tidal flat environment in those two fields and absence of the formation in Kirkuk Field.

CHAPTER TWO

Lithological and Shale Calculation

2.1 Preface

Porosity and permeability as the most important properties characterizing reservoirs are mainly related to the lithology of the reservoir bed. Determining the lithology of the reservoirs can be done mostly either through studying the rock samples (core and cutting) or through analyzing the wireline log data.

Accurate porosity determination is necessary for effective log interpretation. When the lithology of a clean, liquid-filled formation is known or can be assumed with reasonable accuracy, representative porosity value can be derived from the reading of a porosity log. However, porosity determination becomes more involved when the lithology is not known or when it consists of two or more minerals of unknown proportions. Most reservoir rocks are composed of one of two main minerals and may contain various amounts of clay (Bassiouni, 1994).

Shale content as part of the lithology also has effective impact on potentiality of reservoirs. Calculating shale volume and determining the way by which it distributes is vital for characterizing any reservoir.

In this study, lithology and microfacies of the studied Jeribe Formation have been determined using both rock samples and logs as sources of data. More than one crossplot combining between different porosity logs used for determining the lithology as precisely as possible. On the other hand, shale content in the Jeribe reservoir has been measured through Gamma ray log for

the studied wells as a step to show the effect of shaleness on the reservoir properties and also its effect on the porosity logs.

2.2 Identification of Microfacies

According to Flugel (2010), microfacies is regarded as " the total of all sedimentological and paleontological data which can be described and classified from thin sections, peels, polished slabs or rock samples". Microscopic examination of thin sections considers as essential technique in studying carbonate rocks. Determining depositional environments, porosity types and value, and the effective porosity, in addition to destructive or constructive diagenesis processes all are important information that can be obtained from the microscopic study of carbonates which are of great assistance in best evaluating reservoir properties.

In this study, the prepared thin sections from the selected cutting rock samples of Jeribe Formation in the three studied wells have been studied using transmitted light microscopy. The classification proposed by Danhum (1962) for carbonate rocks was mainly depended on in describing and nominating the distinguished microfacies (Fig. 2.1). The types of porosity observed from the studied thin sections were described using the terms proposed by Choquette and Pray (1970) (Fig.2.2).

Plates 1-3 show selected photos for some of the identified microfacies in the studied Jeribe Formation with highlighting selective porosity or diagenesis types as observed during the microscopic study of the prepared thin sections.

Common lithology, microfacies type, porosity type, and distinguishable diagenesis for all the studied samples are listed in the tables 2.1-2.3 for Jeribe Formation in the three studied wells of Hr-49, Hr-50, and Hr-51.



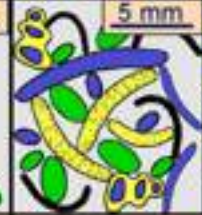
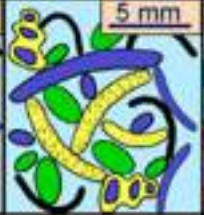




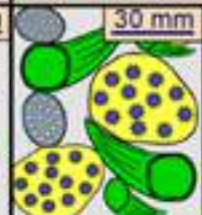
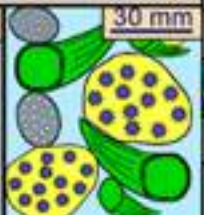


Depositional texture recognizable					Depositional texture not recognizable
Components not bound together during deposition			Components were bound together during deposition		
Contains carbonate mud (clay / fine silt)		Lacks mud and is grain supported			
Mud supported	Grain supported				
Less than 10% grains	More than 10% grains				
<i>Mudstone</i>	<i>Wackestone</i>	<i>Packstone</i>	<i>Grainstone</i>	<i>Boundstone</i>	<i>Crystalline</i>
					
	<i>Floatstone (large grains)</i>	<i>Rudstone (large grains)</i>		<i>Framestone</i>	
				<i>Bindstone</i>	
				<i>Bafflestone</i>	

Figure 2.1: Classification of Dunham (1962) with modifications by Embry and Klovan (1972) for carbonate rocks.

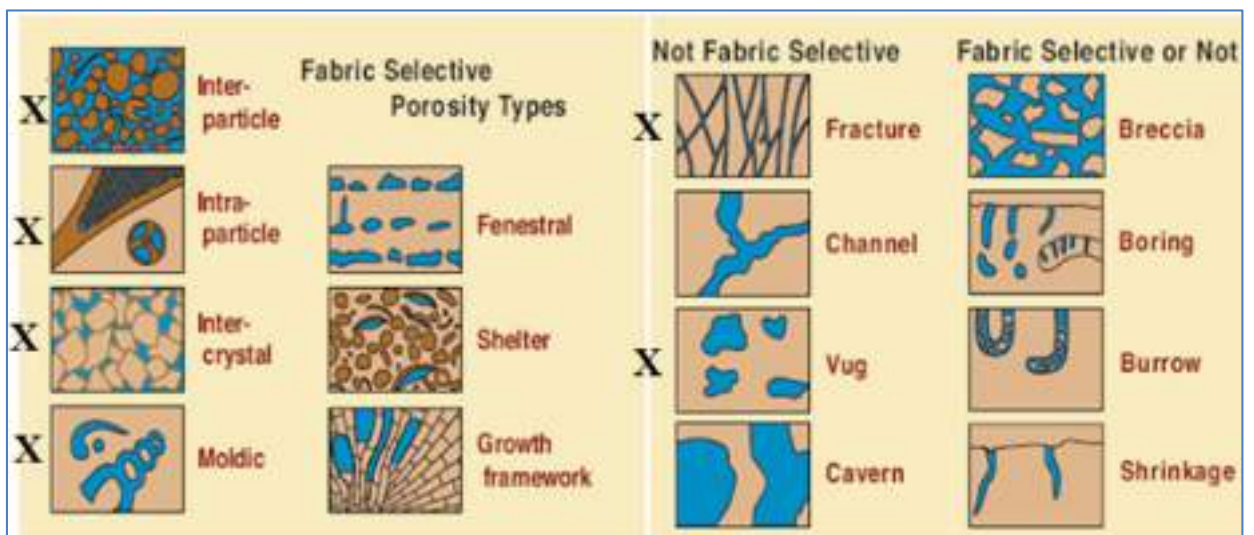


Figure 2.2: Classification of carbonate porosity, X indicates the most distinctive porosity types in carbonate reservoirs (after Choquette and Pray, 1970).

PLATE - 1

The bar = 100micron

- Fig. 1: Foraminifera bearing Grainstone Microfacies, Depth: 542m, well Hr- 50**
Fig. 2: Foraminifera bearing Grainstone/Packstone Microfacies, A: channel Porosity, B: intraparticle porosity, C: interparticle porosity, Depth: 548m, well Hr- 50 .
Fig. 3: Medium crystalline saccharosic dolostone, Dolowackestone Microfacies, A: bitumen filled fractures, Depth: 568m, well Hr- 50
Fig. 4: Quartz bearing Wackestone Microfacies, A: separated vugs, Depth: 568m, well Hr- 50
Fig. 5: Packstone/Grainstone Microfacies, Depth: 570m, well Hr- 50
Fig. 6: Foraminifera bearing Packstone Microfacies, A: intraparticle Porosity, Depth: 422m, well Hr- 49

PLATE - 2

The bar = 100micron

- Fig. 1: Foraminifera bearing Packstone Microfacies, A: shelter porosity, B: intraparticle porosity, Depth:426m, well Hr-49**
Fig. 2: Algal bearing Wackestone Microfacies, A: bitumen filled fractures, Depth: 436m, well Hr- 49
Fig. 3: Wackestone/Packstone Microfacies, A: moldic porosity, B: separated vugs, Depth: 464m, well Hr-49
Fig. 4: Packstone/Grainstone Microfacies, A: moldic porosity, B: shelter porosity, C: cement filled vug, Depth: 570m, well Hr-50
Fig. 5: Packstone/Wackestone Microfacies, Depth: 550m, well Hr-50
Fig. 6: Foraminifera bearing Grainstone/Packstone Microfacies, A: intraparticle porosity, B: interparticle porosity, Depth: 548m, well Hr- 50

PLATE - 3

The bar = 100micron

- Fig. 1: Wackestone/Packstone Microfacies, A: intraparticle porosity, B: interparticle porosity, Depth: 466m, well Hr-49**
Fig. 2: Packstone Microfacies, A: two sets of fractures, Depth: 452m, well Hr-49
Fig. 3: Foraminifera bearing Packstone Microfacies, A: intraparticle porosity, Depth: 422m, well Hr- 49
Fig. 4: Foraminifera bearing Grainstone/Packstone, A&B: interparticle porosity, Depth: 548 m, well Hr-50
Fig. 5: Wackestone/Packstone Microfacies, A: separated vugs, Depth: 520m, well Hr-51
Fig. 6: Algae bearing Packstone Microfacies, A: bitumen filled microfracture, Depth: 494m, well Hr- 51

PLATE - 1

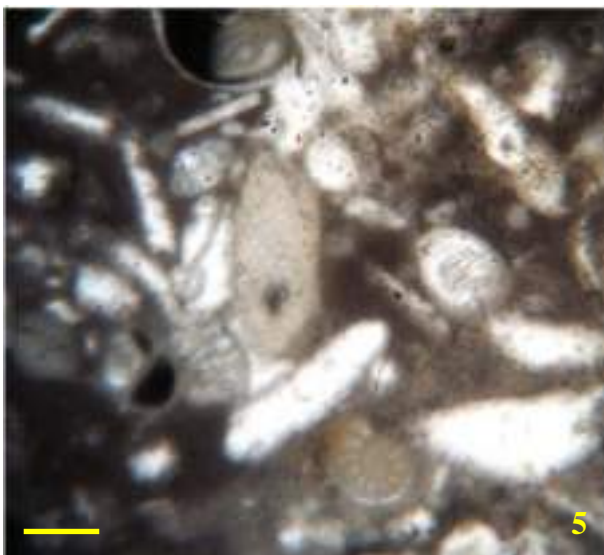
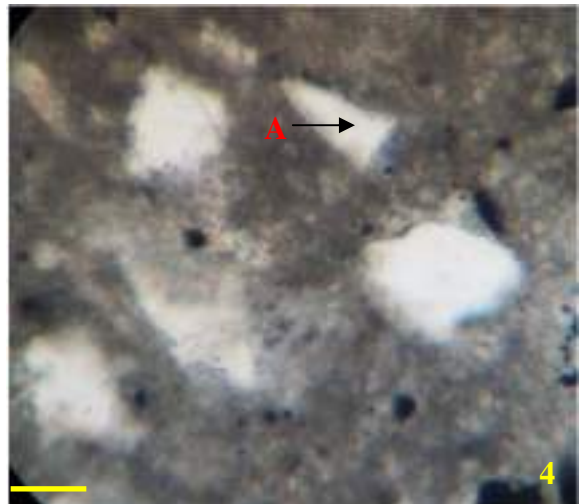
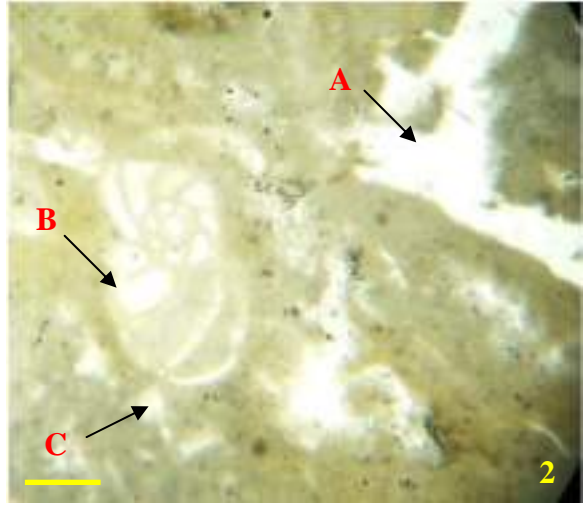
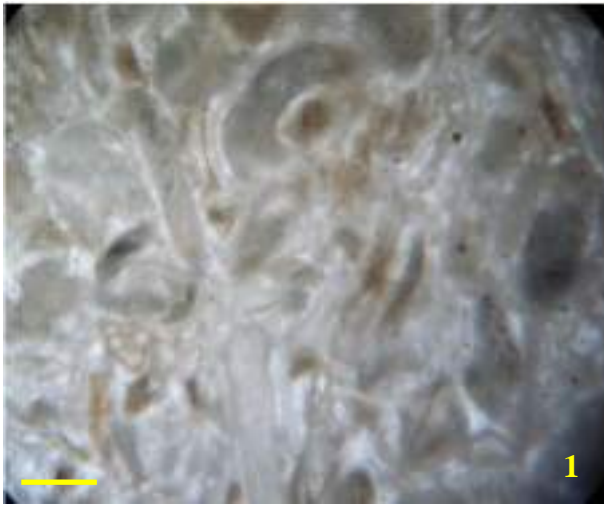


PLATE - 2

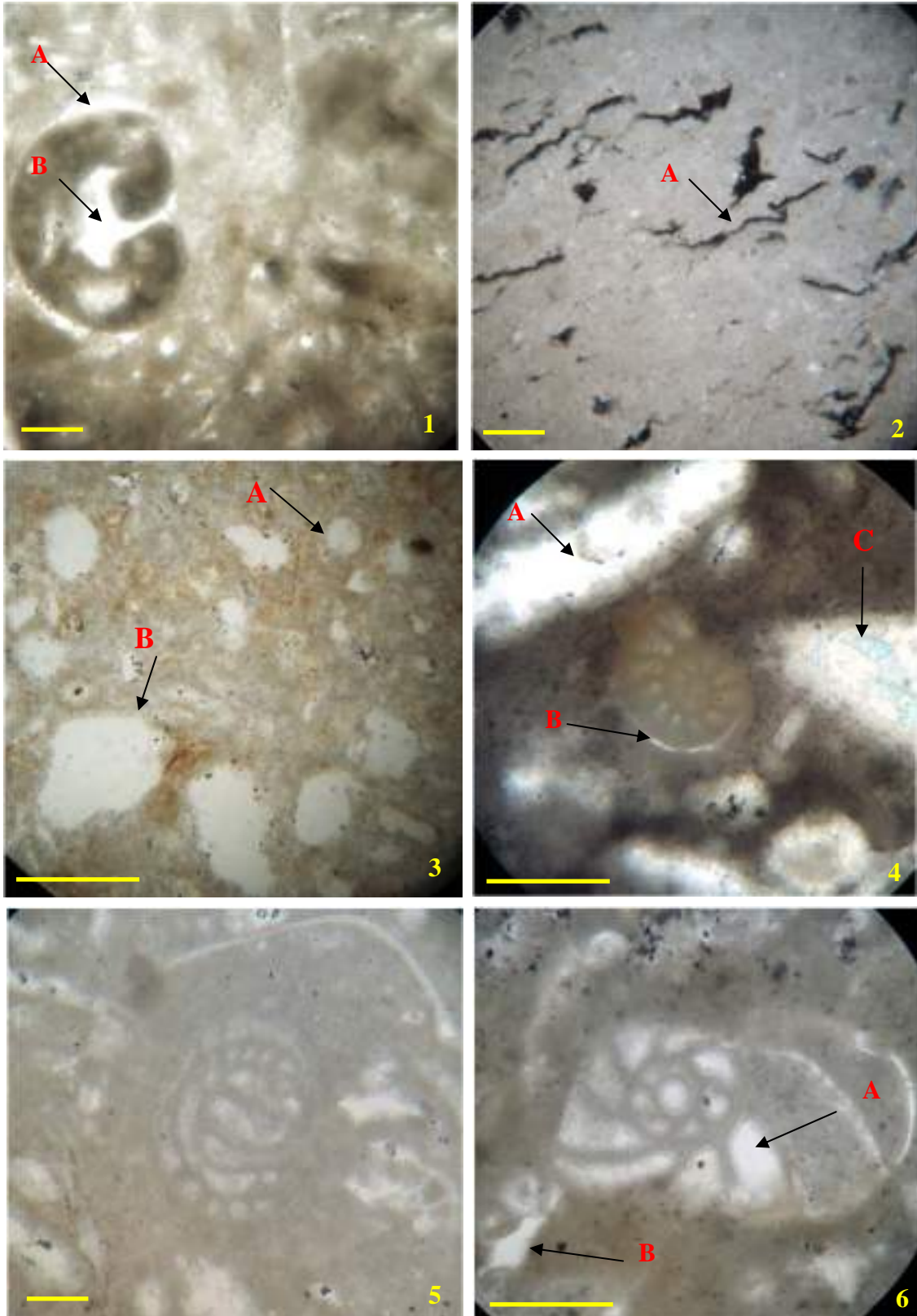


PLATE - 3

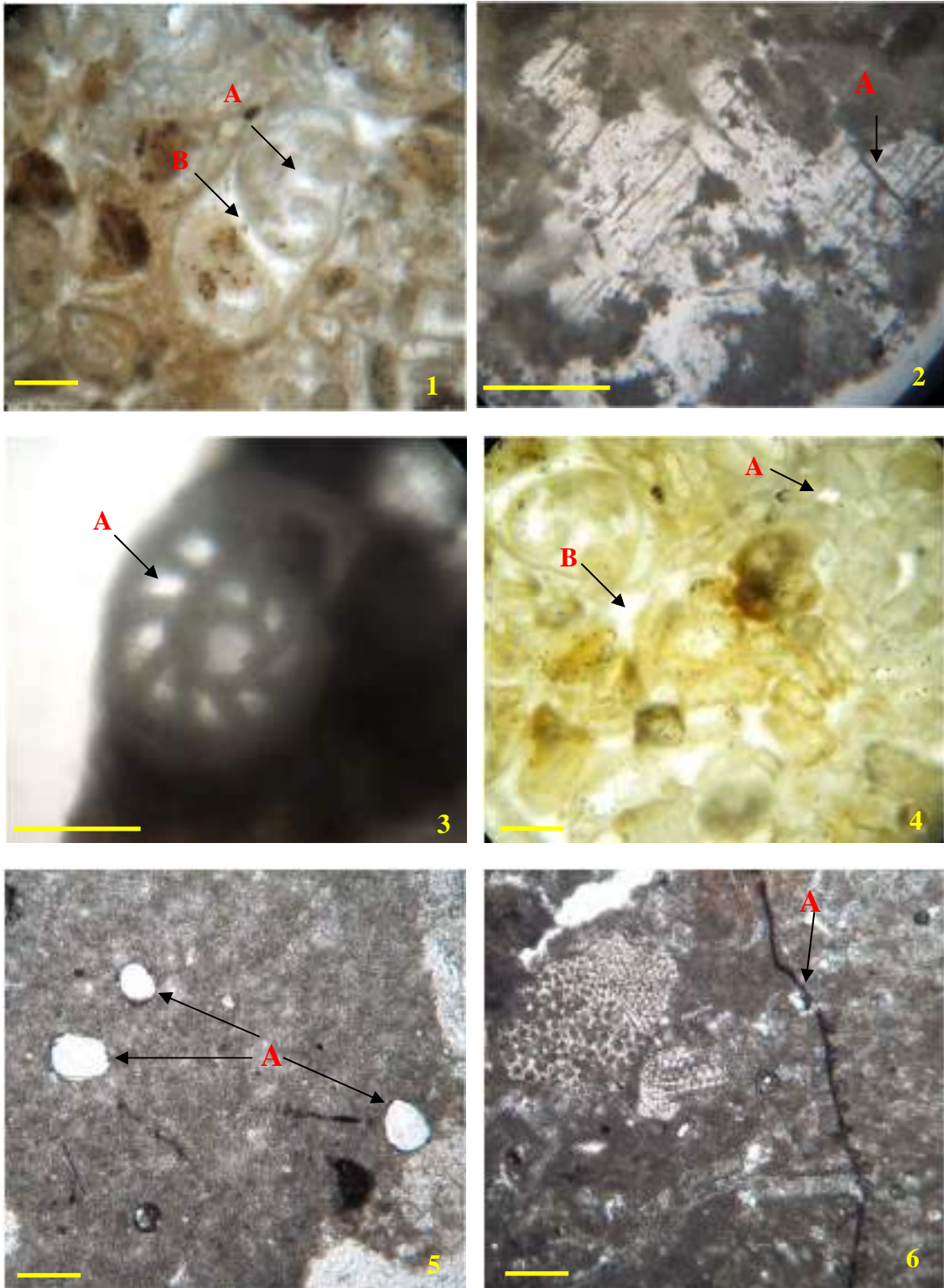


Table 2.1 Main lithology, microfacies, pore types, and diagenesis features identified in the studied Jeribe Formation in the well Hr-49.

Sample Depth (m)	Common lithology	Microfacies Type	Pore types	Diagenesis
420	Limestone	Wackestone	Intraparticle, moldic	Cementation, dissolution
422	Limestone	Foraminifera Bearing Packstone	Interparticle, intraparticle	Cementation
426	Limestone	Foraminifera Bearing Packstone	Intraparticle, shelter	Cementation
432	Argillaceous Limestone	Packstone / Grainstone	Interparticle, intraparticle, moldic	Cementation, dissolution
436	Argillaceous limestone	Algal Bearing Wackestone	Microfractures, vugs	Cementation, dissolution,
452	Limestone	Foraminifera Bearing Grainstone	Microfractures, vugs, interparticles, interparticles	Cementation, dissolution, dolomitization
456	Limestone	Wackestone / Packstone	Intraparticle, moldic, vugs	Dissolution
464	Dolomitic limestone	Wackestone / Packstone	Intraparticle, moldic, vugs	Cementation, dissolution, dolomitization
466	Limestone	Wackestone / Packstone	Intraparticle, interparticle, vugs	Cementation, dissolution

Table 2.2 Main lithology, microfacies, pore types, and diagenesis features identified in the studied Jeribe Formation in the well Hr-50.

Sample Depth (m)	Common lithology	Microfacies Type	Pore types	Diagenesis
527	Dolostone	Wackestone / Packstone	Interparticle, intraparticle	Cementation
528	Dolostone	Wackestone / Packstone	Intraparticle, moldic,	Cementation, dissolution, pyritization
530	Dolostone	Wackestone / Packstone	Intraparticle, interparticle, moldic,	Cementation, dissolution

533	Argillaceous dolostone	Packstone / Grainstone	Intraparticle, interparticle, moldic,	Cementation, dissolution
535	Argillaceous dolostone	Foraminifera Bearing Packstone	Microfractures, vugs, intercrystalline	Cementation, dissolution
537	Argillaceous dolostone	Grainstone / Packstone	Intraparticle, vugs, interparticle, moldic,	Cementation, dissolution, pyritization
539	Argillaceous dolostone	Grainstone / Packstone	Intraparticle, interparticle, moldic, vugs	Cementation, dissolution
542	Argillaceous dolostone	Foraminifera Bearing Grainstone	Intraparticle, interparticle, moldic, shelter, vugs	Cementation, dissolution
544	Dolostone with Anhydrite nodules	Packstone / Wackestone	Microfractures, vugs	Cementation, dissolution
548	Limestone	Foraminifera Bearing Grainstone/ Packstone	Interparticle, intraparticle, channel, shelter	Cementation
550	Dolostone	Packstone/ Wackestone	Interparticle, intraparticle	Cementation
564	Calcareous dolostone	Grainstone / Packstone	Intraparticle, interparticle, moldic	Dissolution, cementing
568	Dolostone	Quartz bearing Wackestone	Microfractures, vugs	Dissolution, cementing
570	Dolostone	Packstone / Grainstone	Shelter, moldic, vugs	Dissolution, cementing

Table 2.3 Main lithology, microfacies, pore types, and diagenesis features identified in the studied Jeribe Formation in the well Hr-51.

Sample Depth (m)	Common lithology	Microfacies Type	Pore types	Diagenesis
478	Limestone	Wackestone	vugs	Dissolution
486	Argillaceous limestone	Wackestone	vugs	Dissolution
494	Argillaceous limestone	Algae bearing Packstone	Microfractures, interparticle, intraparticle	Dissolution, cementation, pyritization

502	Limestone	Wackestone/ Packstone	Vugs, microfractures, interparticle, intraparticle	Dissolution, cementation
510	Limestone	Wackestone/ Packstone	Vugs, microfractures, interparticle, intraparticle	Dissolution, cementation
520	Limestone	Wackestone/ Packstone	Vugs, microfractures, interparticle, intraparticle	Dissolution, cementation

2.3 Lithology Determination from Porosity logs

The different log tools are responding to the lithology of the beds in different ways. Some are affected very effectively by certain types of lithology such as the effect of shale on Neutron log. Therefore, log data can aid in determining lithology especially if the data of different tools are combined through applicable equations and crossplots.

The most useful combinations used in this study for determining the lithology of the studied Jeribe Formation are Neutron-Density and M-N crossplots (additional MID crossplot also used to support the identified lithology in Chapter three of this study).

2.3.1 Neutron – Density Crossplot

The extensive use of the neutron-density combination may be due, in part, to the fact that they were among the first logging tools that could be physically combined and their data acquired in a single logging run. The response of the combination is such that for reconnaissance evaluation one can forego the crossplot and rely on recognition of the curve patterns (the position of the curves with respect to each other) to quickly determine the most likely predominant lithology and formation porosity (Asquith and Krygowski, 2004).

Both the neutron and the density logs are not easy to use for lithology

identification separately, but if they are combined, they become probably the best available indicator (Schlumberger, 1972; Rider, 2002).

The density-neutron crossplots were constructed for clean formation, liquid saturated formation and borehole filled water based mud or just water. The sufficient separation between quartz, limestone and dolomite lines in the chart indicate good identification for lithologies as well as the common evaporites such as anhydrite and rock salt can be easily indicated. The interpretation of the crossplot can be ambiguous when there is more than one mineralogy in the formation like dolomite-cemented sandstone (Halliburton, 2001).

The reading of both logs (Neutron porosity, $N\emptyset$ and Bulk density, ρ_b) for the studied formation in the three wells of Hr-49, Hr-50 and Hr-51 (appendix A) are used to identify the lithology using the Neutron-Density crossplot proposed by Schlumberger (1988) for the case of fresh mud drilling fluid (Fig. 2.3).

Through the distribution of the measured $N\emptyset$ and ρ_b on the N-D crossplot different pattern of distribution noticed for the three wells. In well Hr-50, the detected dolomite lithology is very noticeable, whereas in the other two wells a clear scattering of the points are seen with an obvious distortion toward gas effect field.

Accordingly, dolomite appears to be the dominant lithology of Jeribe Formation in the well Hr-50, whereas limestone and dolomitic limestone seem to be the lithology dominant of the formation in the other two wells of Hr-49 and Hr-51. On the other hand, the existence of gas in the wells Hr-49 and Hr-51 is highly expected.

Dhiban and Lower Fars formations represented by green and yellow color cycles respectively (Fig. 2.3) look as expected to be composed mainly of anhydrites (especially clear in the well Hr-50). The expected effects of gas are also noticeable on deflection of the points toward the gas field on the crossplot in the wells Hr-49 and Hr-51.

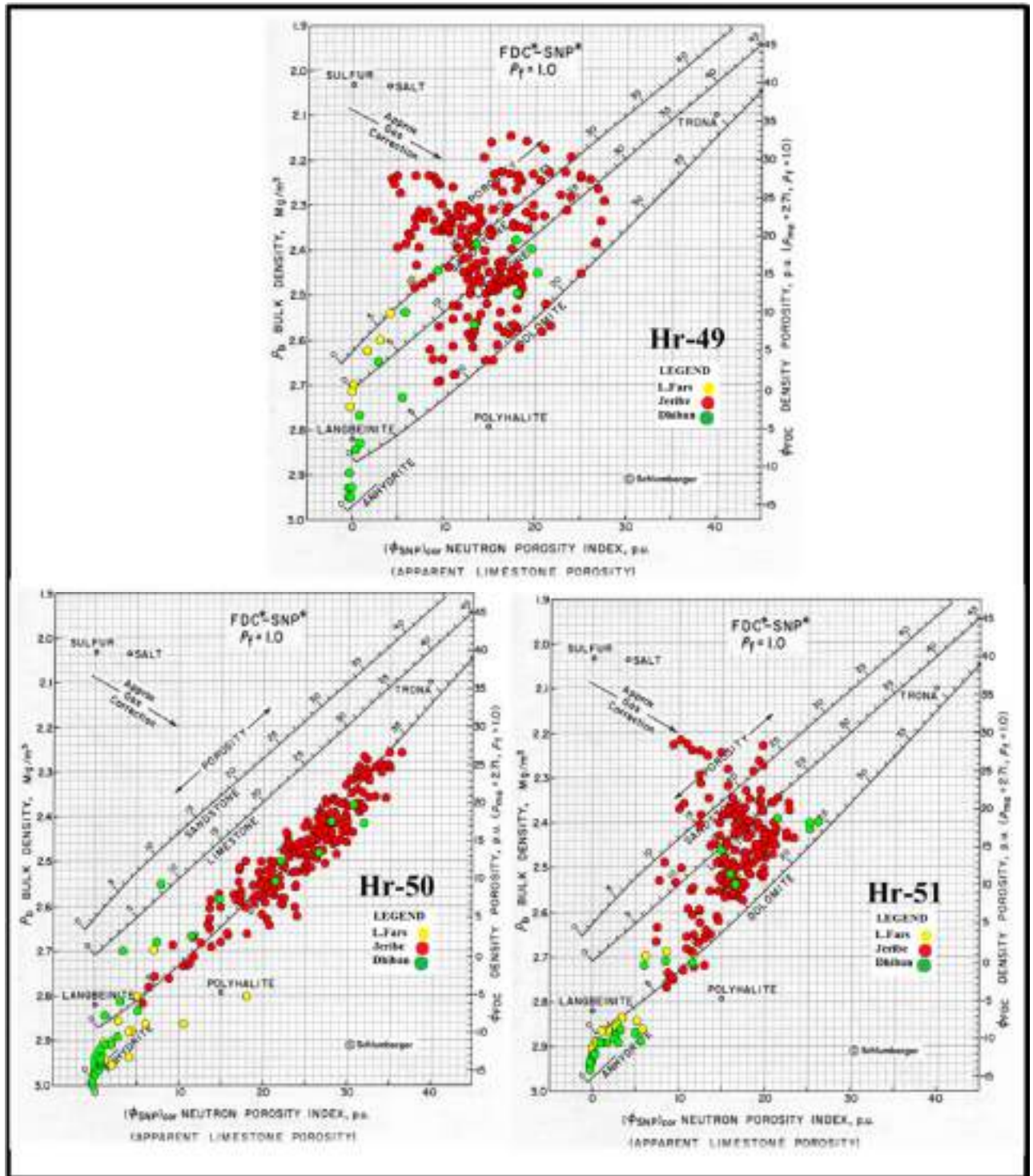


Figure 2.3: Neutron-Density crossplot for lithology identification of the studied Jeribe Formation in the studied wells. The lithology of Dhiban and Lower Fars formations also identified (the crossplot is after Schlumberger, 1988).

2.3.2 M-N Crossplot

The lithology interpretation in more complex mineral mixture is facilitated by use of the M-N plot. This plot combines the data of all three porosity logs to provide the lithology-dependent quantities M and N. M and N are simply the slopes of the individual lithology lines on the sonic-density and density-neutron crossplot chart respectively. Thus, M and N are essentially independent of porosity, and a crossplot provides lithology identification (Schlumberger, 1989).

M and N are mathematically defined as:

$$M = \frac{\Delta t_{fl} - \Delta t}{\rho_b - \rho_{fl}} * 0.01 \dots \dots \dots \text{E.q.2.1}$$

$$N = \frac{\emptyset_{Nfl} - \emptyset_N}{\rho_b - \rho_{fl}} \dots \dots \dots \text{E.q.2.2}$$

Where:

Δt_{fl} : interval transit time in the fluid in the formation

Δt : interval transit time in the formation (from log)

ρ_b : formation bulk density (from log)

ρ_{fl} : fluid density (generally, 1.0 for fresh mud and 1.1 for saline mud)

\emptyset_{Nfl} : neutron porosity of the fluid in the formation (usually 1.0)

\emptyset_N : neutron derived porosity (from log)

The multiplier 0.01 is used to make the M values compatible for easy scaling.

The M-N plot also displays arrows to indicate the direction along which points will move away from their true lithology locations owing to the effect of gas, secondary porosity, or shale. No unique shale point exists on the M-N plot because shales tend to vary in their characteristics. Most shales, however, will be situated below the line that joins the silica and anhydrite points (Bassiouni, 1994).

The calculate M and N values are listed in the appendix A.

As in the previous N-D crossplot, lithology easily identified for Jeribe Formation in the well Hr-50 using the M-N crossplot (Fig.2.4). The concentration of the M-N points in the dolomite field sings clearly to domination of this lithology in Jeribe Formation. Again, the effect of gas led to shift the points of M and N toward the gas zone in the wells Hr-49 & Hr-51 causing confusion in identifying the exact lithology of Jeribe in these two wells although limestone and dolomitic limestone look to be the correct lithology of the formation. Shale impact also can be observed in those two wells when observable points of M-N located at the lower right corner of the crossplot (shale region). On the other hand, the existence of secondary porosities (ex. fractures or vugs) is expected in the well Hr-49 as some points of the M-N distorted toward the upper part of the crossplot (due to high value of M factor). M factor commonly shows high values due to the low readings of density log (ρ_b) in fractured or vuggy zones; whereas sonic log will not respond to the effect of fractures or vugs and the measured Δt readings remain low representing the primary matrix porosities only. Such detection of secondary porosities using M-N plot gives advantage of this kind of crossplots on the previously used N-D crossplot.

The dominant anhydrite lithology of Dhiban and Lower Fars formations is very clear on the M-N crossplot with observing the following points:

1. Possible effect of gas on the lithology of Lower Fars Formation in the well Hr-49.
2. Possible effect of salt (rather than gas) on the lithology of Dhiban Formation in the studied three wells.
3. Higher shale content in the Lower Fars Formation (Transition Beds) in the well Hr-51 in comparison with the other two wells.

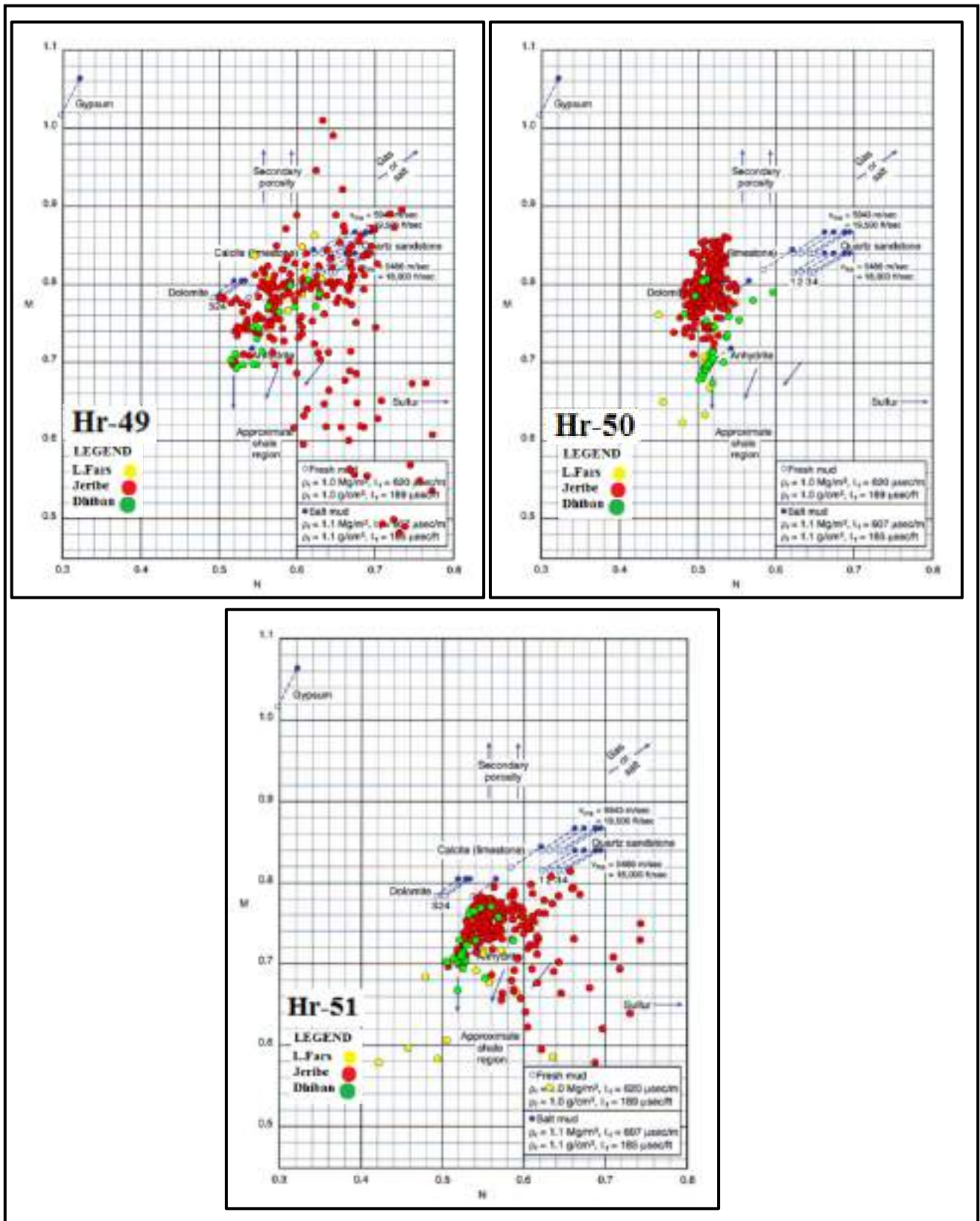


Figure 2.4: M-N crossplot for lithology identification of the studied Jeribe Formation in the studied wells. The lithology of Dhiban and Lower Fars formations also identified (the crossplot is after Schlumberger, 1989).

2.4 Gamma Ray Log

The gamma ray log is a record of formation radioactivity, the radiation emanates from naturally occurring uranium (U), thorium (Th) and potassium (K). In petroleum borehole logging the commonest natural radioactivity (by volume) is found in shale (clay), high gamma ray value frequently mean shale (Rider, 2002). The common uses of gamma ray log are for identifying lithologies and correlating zones in addition to its main application for calculating shale volumes in carbonate or sandstone (Asquith and Gibson 1982).

The Gamma ray measurements can be influenced by the logging speed. When logging speed is too high or slow it will mix the bed boundaries. The other main influence on gamma ray log is the increase of drilling mud between the measuring tool and the actual formation due to the caving. This effect will show lower gamma ray values. The gamma ray log also gives lower values in bad borehole conditions (Rider and Kennedy, 2011). All these factors should be considered while analyzing the gamma ray log.

Gamma ray log readings for Jeribe Formation in the three studied wells are listed in appendix A and plotted as curves in figure 2.5. The readings of the gamma ray from the bottom of the formation to above the middle show gradual increase reflecting may be a gradual increase in shale content. Near the top of the formation the deflection of the gamma ray curve starts reducing and that may be due to decrease in shale content.

The sudden decrease in the gamma ray deflection at the lower and upper contacts of Jeribe Formation with Dhiban and L. Fars formations respectively (Fig. 2.5) are mostly due to the anhydritic nature of those two formations.

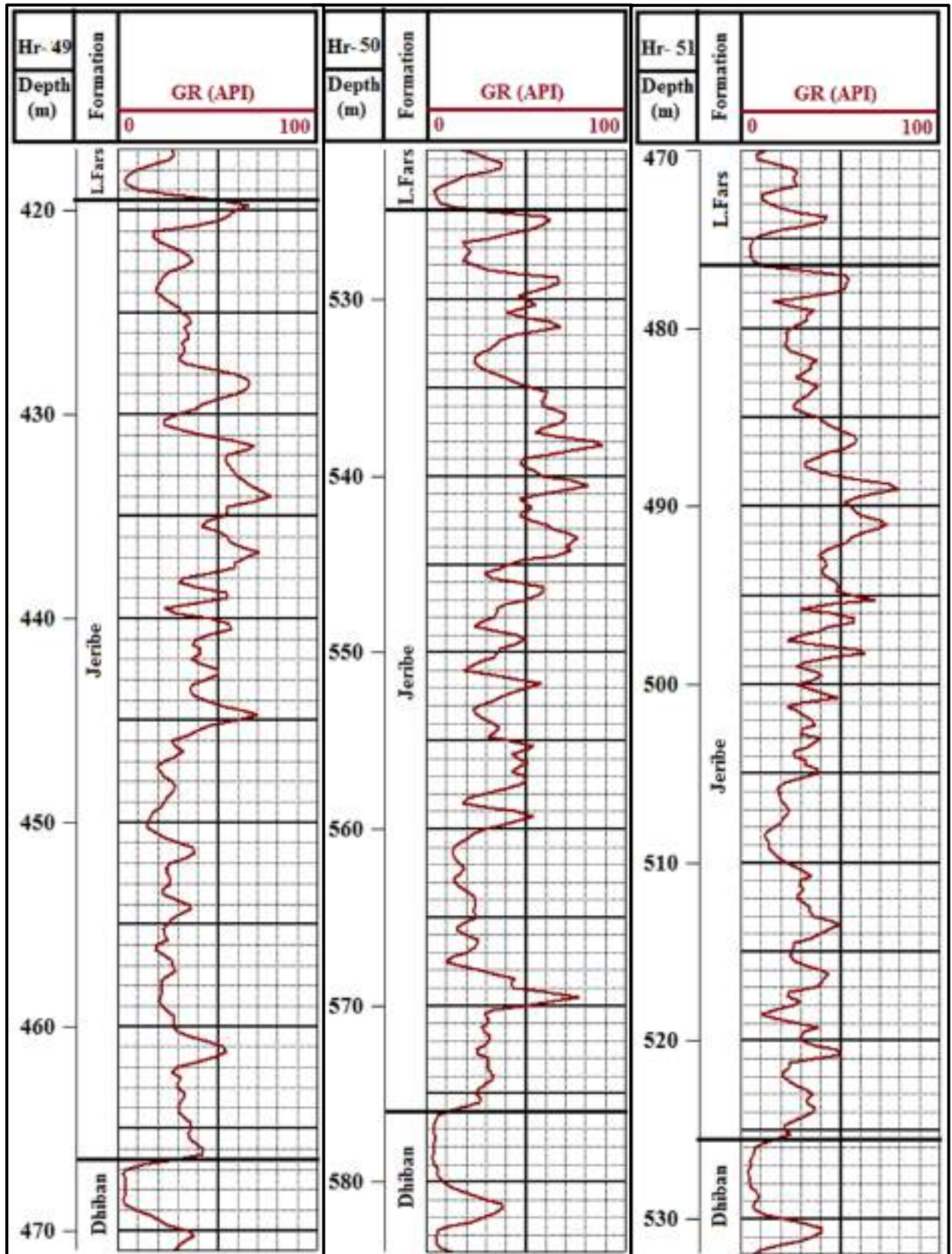


Figure 2.5: Gamma ray log for Jeribe Formation including uppermost part of Dhiban and lowermost part of Lower Fars formations in the wells Hr-49, Hr-50 and Hr-51.

2.5 Shale Volume Calculation

The simple gamma ray is sometimes called “shale log” because the radiation detected by gamma ray log is coming mainly from the radiation elements that exist in the shale. Therefore, gamma ray log can be used quantitatively to derive shale volume (Rider, 2002).

The volume of shale can be applied for analysis of shaly formations. The main step before calculating the shale volume is to calculate the gamma ray index (IGR), which can be calculated by using the equation Eq.2.3 as advised by Asquith and Gibson (1982):

$$\text{IGR} = \frac{\text{GR}_{\text{log}} - \text{GR}_{\text{min}}}{\text{GR}_{\text{max}} - \text{GR}_{\text{min}}} \dots \text{E.q.2.3}$$

Where:

GR_{log} = Gamma ray reading from log

GR_{min} = Minimum gamma ray reading from log (clean zone)

GR_{max} = Maximum gamma ray reading from log (shale zone)

Table 2.4 shows the selected minimum and maximum gamma ray readings with the depths at which the readings taken for calculating the IGR in the three studied wells.

Table 2.4: Minimum and maximum gamma ray readings used for calculating IGR for the three studied wells.

Wells	Depth (m)	GRmin (API)	Depth (m)	GRmax(API)
Hr-49	450.00	14.71	434.00	76.67
Hr-50	567.50	9.62	538.25	88.36
Hr-51	518.50	10.59	489.00	79.23

With existence of IGR values, volume of shale can be calculated. In this research, the equation proposed by Larionov (1969; in Asquith and Krygowski, 2004) for calculating shale volume in Tertiary rocks (Eq.2.4) has been used as the studied Jeribe Formation belongs to Tertiary period.

$$V_{sh} = 0.083 \{2^{(3.7 * IGR)} - 1.0\} \dots \dots \dots \text{E.q.2.4}$$

The calculated volumes of shale are listed in the appendix B and plotted as curves in the figure 2.6.

For distinguishing between zones of different shale contents within Jeribe Formation, the standard proposed by Ghorab (2008) has been used (Table 2.5) and shown also as zones in figure 2.6.

Table 2.5: Zonation on the bases of percentage of shale volume (after Ghorab, 2008).

Vsh (%)	Zone
<10	Clean Zone
10-35	Shaly Zone
>35	Shale Zone

The plotted shale content curves mostly reflect the shape of the gamma ray curves. Accordingly, the interval above the middle part of Jeribe Formation in the three studied wells showed the highest shale content as noticed previously in the gamma ray curves.

The depth intervals and thicknesses of Jeribe and the studied parts of Dhiban and Lower Fars formations are listed in table 2.6, whereas the details of the shaleness according to the mentioned standard of Ghorab (2008) for the whole studied sections arranged in the table 2.7.

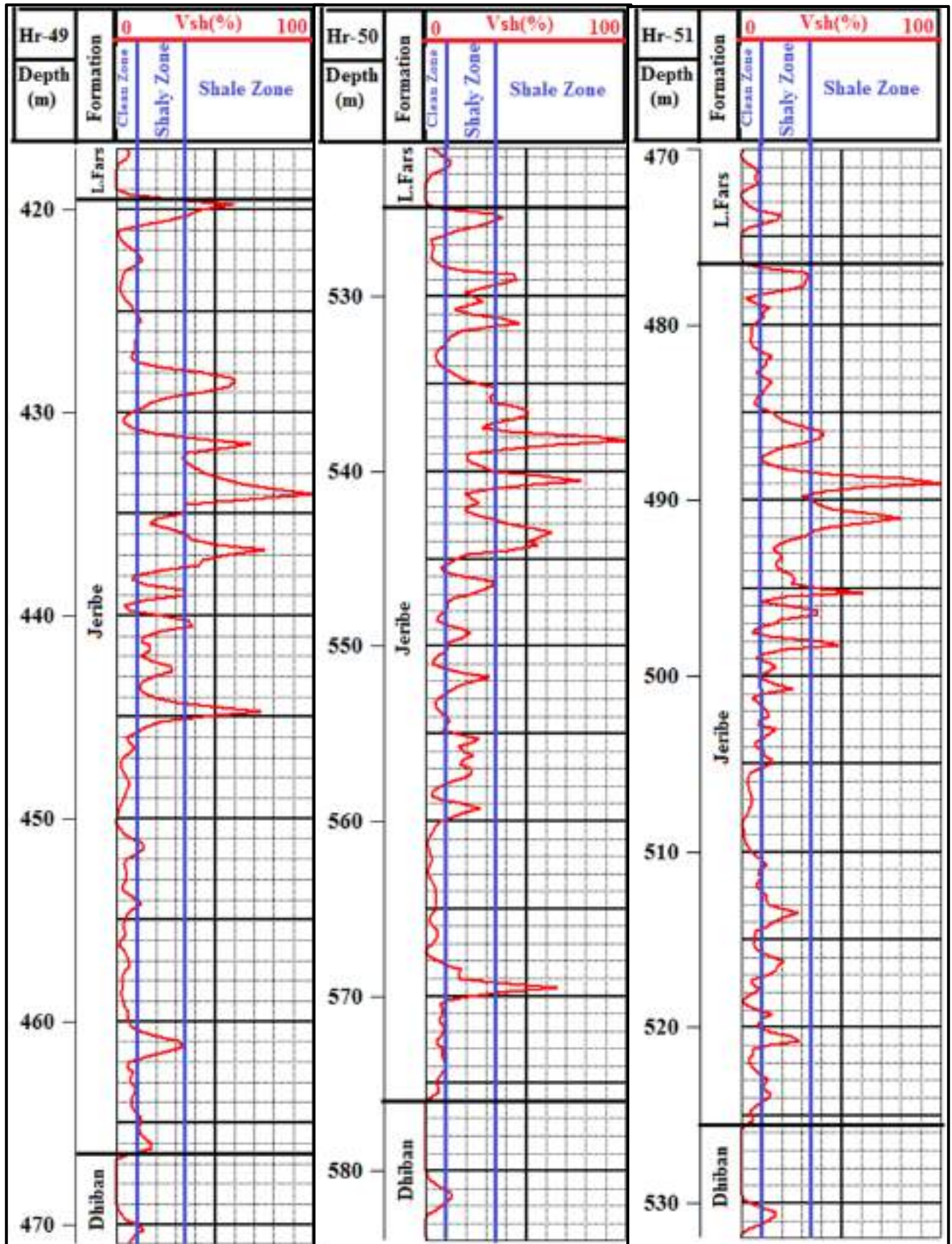


Figure 2.6: Curve plots of the calculated volume of shale and shale content zonation along the studied sections of Hr-49, Hr-50 and Hr-51.

Table 2.6: The depth intervals and thicknesses of Jeribe and the studied parts of Dhiban and Lower Fars formations in the Hr-49, Hr-50, and Hr-51 wells.

Wells	Formations	Depth interval (m)	Thickness (m)
Hr-49	L.Fars	417.00-419.50	02.50
	Jeribe	419.50-466.50	47.00
	Dhiban	466.50-471.00	04.50
Hr-50	L.Fars	521.50-525.00	03.50
	Jeribe	525.00-576.00	51.00
	Dhiban	576.00-584.00	08.00
Hr-51	L.Fars	470.00-476.50	06.50
	Jeribe	476.50-525.50	49.00
	Dhiban	525.50-532.00	06.50

The results of the average shale content zonation showed that Lower Fars and Dhiban formations in all of the studied sections contain less than 10% of shale for which they classified as clean zones. The same is true also with the lower part of Jeribe Formation and partly with its upper part. It is worth mentioning that even in the middle part of Jeribe Formation where shale zones identified (maximum gamma ray readings), kind of exaggeration in the shale content expected. Any maximum recording of gamma ray will show 100% shale when IGR calculated and shale volume measured although the zone may be only shaly and not shale.

Figures 2.7-2.9 are drawn to show more clearly the lithology of the studied sections with the gamma ray responds against each of the specific type of lithology.

Table 2.7: Zonation of the Jeribe and the studied parts of Dhiban and Lower Fars formations studied formations depending on their average shale content and according to the standard proposed by Ghorab (2008).

Wells	Formations	Zone	Depth interval (m)
Hr-49	L.Fars	Clean zone	417.00-419.50
	Jeribe	Clean zone	419.50-428.00
		Shale zone	428.00-438.00
		Shaly zone	438.00-445.00
		Clean zone	445.00-466.50
	Dhiban	Clean zone	466.50-471.00
Hr-50	L.Fars	Clean zone	521.50-525.00
	Jeribe	Shaly zone	525.00-535.00
		Shale zone	535.00-545.00
		Shaly zone	545.00-560.00
		Clean zone	560.00-576.00
	Dhiban	Clean zone	576.00-584.00
Hr-51	L.Fars	Clean zone	470.00-476.50
	Jeribe	Clean zone	476.50-488.00
		Shale zone	488.00-493.00
		Shaly zone	493.00-501.00
		Clean zone	501.00-525.50
	Dhiban	Clean zone	525.50-532.00

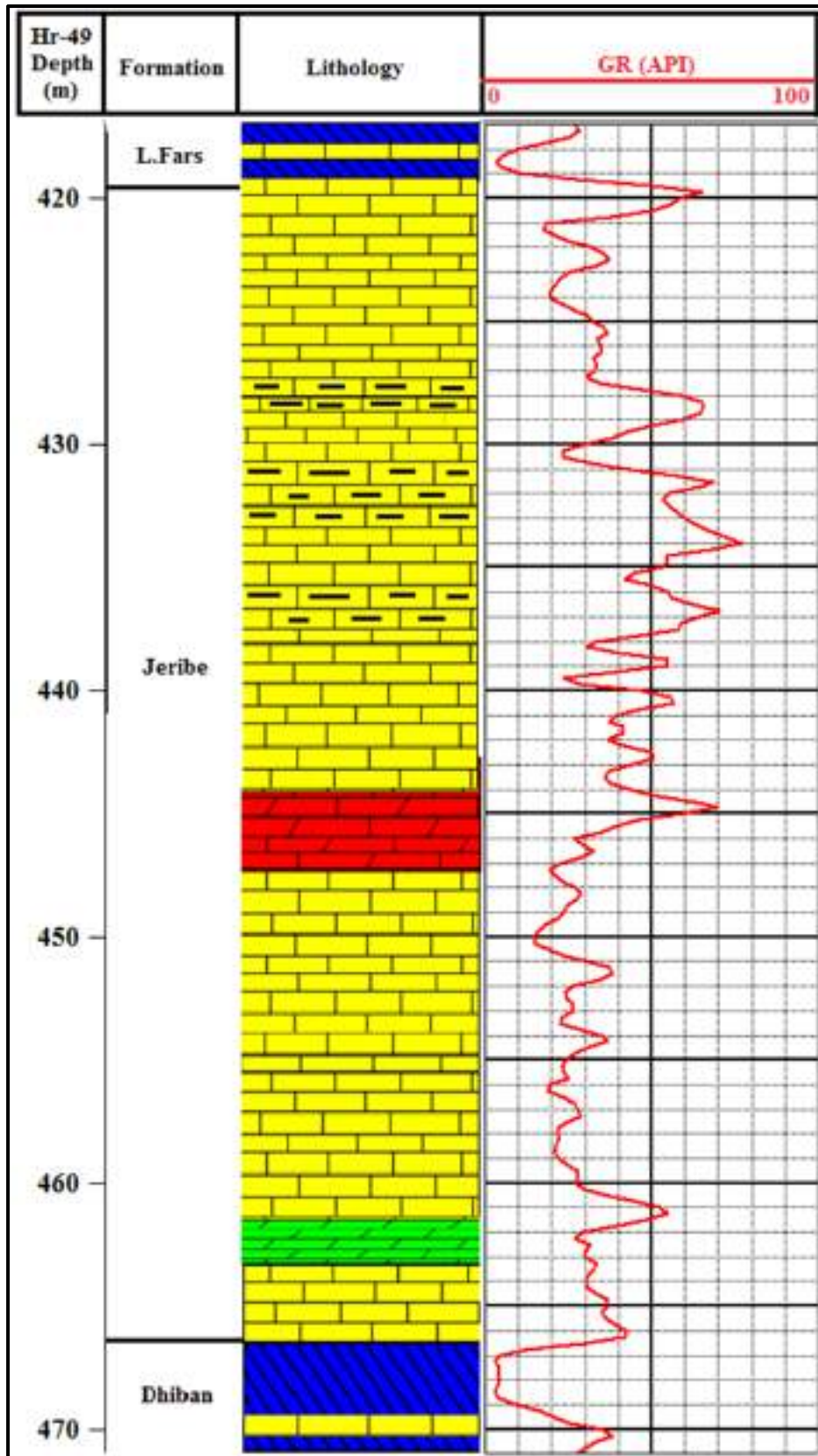


Figure 2.7: Lithologic variations and gamma ray response for the studied Jeribe Formation with the uppermost part of Dhiban and lowermost part of Lower Fars formations in the well Hr-49.



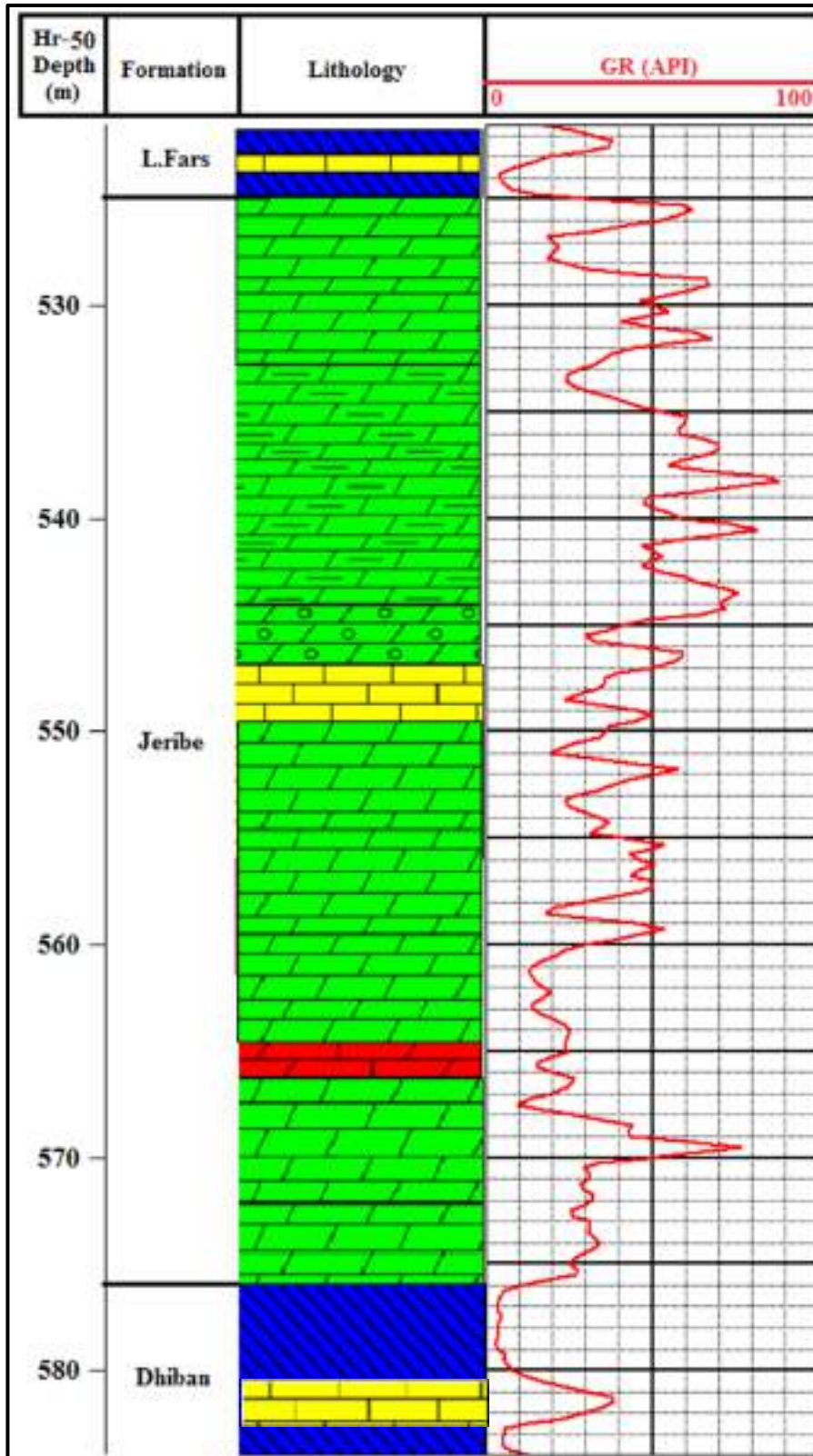


Figure 2.8: Lithologic variations and gamma ray response for the studied Jeribe Formation with the uppermost part of Dhiban and lowermost part of Lower Fars formations in the well Hr-50.



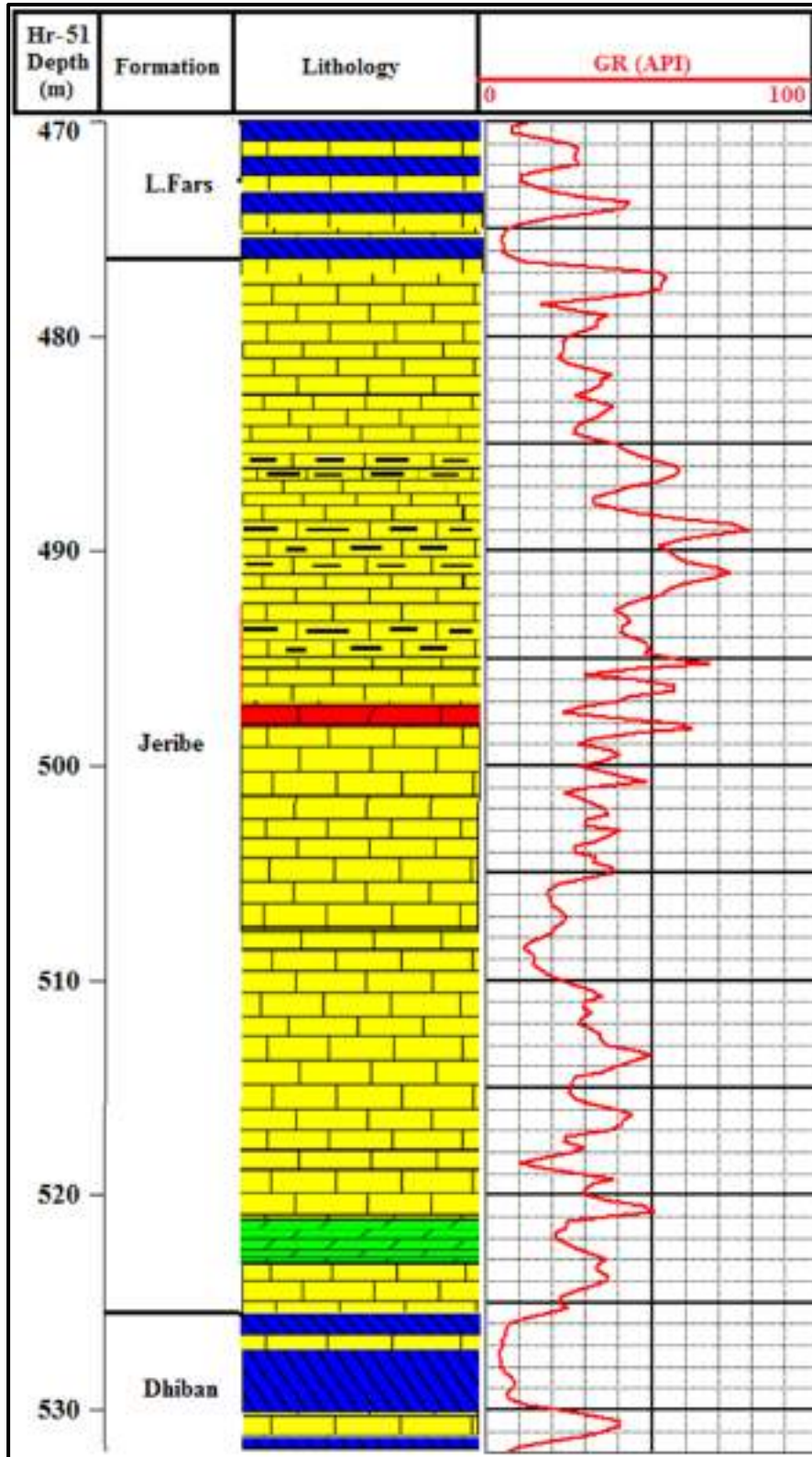


Figure 2.9: Lithologic variations and gamma ray response for the studied Jeribe Formation with the uppermost part of Dhiban and lowermost part of Lower Fars formations in the well Hr-51.



CHAPTER THREE

Determination of Porosity, Permeability, and Reservoir Units

3.1 Preface

The main goal of this study in part is to determine porosity, permeability, and reservoir units from the available logs and core test data. Reservoir characterization entails the application of petrophysical parameters to evaluate reservoirs. Among the important petrophysical parameters needed to evaluate a reservoir are porosity and permeability (with estimating the effect of shaleness on both parameters).

A reservoir is a subsurface rock that has effective porosity and permeability that usually contains commercially exploitable quantity of hydrocarbon. Reservoir characterization is undertaken to determine its capability to both store and transmit fluid (Ulasi et al., 2012).

Porosity can be defined as the ratio of voids to the total volume of rock. It is represented as a decimal fraction or as a percentage and is usually represented by the Greek letter phi (ϕ). The amount of internal space or voids in a given volume of rock is a measure of the amount of fluid a rock may hold. The amount of void space that is interconnected, and thus able to transmit fluids is called effective porosity (ϕ_e). Isolated pores and pore volume occupied by adsorbed water are excluded from a definition of effective porosity but are included in the definition of total porosity (Asquith and Krygowski, 2004). With the existence of shale, the

filled pore spaces by water in the shale are added to the total porosity (ϕ_t) (Bassiouni, 1994). The storage capacity of a reservoir rock always depends on the effective porosity, since it contains the reservoir fluids (Heinemann, 2005).

Permeability is the capacity of a reservoir rock to permit fluid flow. It is a function of interconnectivity of the pore volume; therefore, a rock is permeable if it has an effective porosity (Ulasi et al., 2012).

Porosity of subsurface formations can vary widely. Dense carbonates (limestones and dolomites) and evaporites (salt, anhydrite, gypsum, sylvite, etc.) may show practically zero porosity; well-consolidated sandstones may have 10 to 15% porosity; unconsolidated sands may have 30%, or more, porosity. Shales or clays may contain over 40% water-filled porosity, but the individual pores are usually so small, the rock is impervious to the flow of fluids (Schlumberger, 1989).

3.2 Determination of porosity

Devices that measure porosity are sensitive to both rock matrix and the fluid filling the pore space. Thus, the measurement of porosity reflects not only porosity, but also the type of rock, the clay content, and the fluid type (Bateman, 1985).

Rock porosity is generally determined from the measurements from one, or a combination of, the following logs:

Acoustic log,

Density log,

Neutron log, and

Nuclear Magnetic Resonance (NMR) log

Data from the mentioned first three types of porosity logs were available for this study whereas no NMR logging is done for the studied wells.

The measurements of the sonic, density, and neutron logs depend not only on porosity (\emptyset) but also on the formation lithology, on the fluid in the pores, and in some instances, on the geometry of the pore structure.

3.2.1 Sonic Log

The sonic log is a porosity log that measures interval transit time (Δt , delta t, or DT) of a compressional sound wave traveling through the formation along the axis of the borehole. The sonic log device consists of one or more ultrasonic transmitters and two or more receivers. Modern sonic logs are borehole-compensated (BHC) devices (Asquith and Krygowski, 2004).

The speed of sound in sedimentary formations depends on many parameters. Principally, it depends on the rock matrix material (sandstone, limestone, dolomite etc.) and on the distributed porosity (Rider, 2002).

The sonic log seems to be affected also by the fluid contents of the pores: water, oil, gas, or even disseminated shale.

The sonic velocity varies inversely with the recorded time interval (Δt). Thus, a hard formation has a high sonic velocity and transmits sound faster than a soft formation, which has a low sonic velocity. The dominant influence on sonic velocity variations is porosity. The higher the proportion of open space in a rock, the less the speed of sound and the greater the recorded time interval (Miller, 1970).

The recorded interval transit time (Δt) for Jeribe Formation in the studied wells are listed in the appendix A and shown as curve in the figure 3.1.

The recorded Δt values for the lower and middle part of the formation in the three studied wells are generally less than 90 μ sec/ft with more or less similar deflections. The upper part of the formation in the well Hr-50 continued with

relatively same Δt values, whereas high Δt records noticed in the upper part of the formation in the both wells of Hr-49 and Hr-51. Such variations in the Δt are mainly due to either increasing of porosity or changing in fluid properties especially their densities.

Because Δt is dependent upon both lithology and porosity; therefore, the formation matrix interval transit time (Δt_{ma}) must be known to derive sonic porosity by Wyllie time-average equation (Eq.3.1) (Wyllie et al, 1958: in Asquith and Gibson, 1982).

$$\phi_s = \frac{\Delta t_{log} - \Delta t_{ma}}{\Delta t_{fl} - \Delta t_{ma}} \dots\dots\dots \text{Eq.3.1}$$

Where:

ϕ_s : Sonic porosity (fraction).

Δt_{log} : Interval transit time in the formation ($\mu\text{sec}/\text{ft}$).

Δt_{fl} : Fluid travel time (freshwater mud = 189 $\mu\text{sec}/\text{ft}$, and saline water mud = 185 $\mu\text{sec}/\text{ft}$).

Δt_{ma} : interval transit time of formation's matrix ($\mu\text{sec}/\text{ft}$).

As the lithology of Jeribe Formation in the studied three wells has been determined through the N-D and M-N point techniques (Chapter two), accordingly the Δt_{ma} of limestone (47.6 $\mu\text{sec}/\text{ft}$) used for calculating sonic porosities in wells Hr-49 and Hr-51, whereas Δt_{ma} of dolomite (43.5 $\mu\text{sec}/\text{ft}$) used for the sonic porosity calculation in the well Hr-50. Both used values of limestone and dolomite Δt_{ma} are after Schlumberger (1972). Regarding the Δt_{fl} , the value of 189 $\mu\text{sec}/\text{ft}$ used for the three studied wells as the used drilling fluid in the three cases was fresh mud.

The calculated sonic porosity values for Jeribe Formation in the three studied wells are listed in the appendix B and shown in the figure 3.2 as curves.

It is clear from the plotted ϕ s that the upper part of the Jeribe Formation is of higher porosity than the lower part. Porosity values more than 50% were calculated in the interval depths between 421 and 427m in the well Hr-49, whereas porosities of more than 40% observed in the depth interval 433 - 439m of the same well, and also in two depth intervals of Hr-51 well (between depths 478 and 482m and between depths 492 and 495m). The upper part of the formation in the well Hr-50 showed relatively lower porosity values (around 30%) in comparison with the same part of the formation in the other two wells.

The lower part of the formation in the three studied wells show no obvious differences and all are generally showing porosity values between 15 and 25%. High porosities (>22%) also observed in the lowermost part of the formation near the contact with Dhiban Formation. These abnormal high porosities in such a carbonate reservoir like Jeribe Formation can preliminarily be interpreted as due to either existence of high shale content (shale effect), or may be due to existence of low density hydrocarbons such as gas.

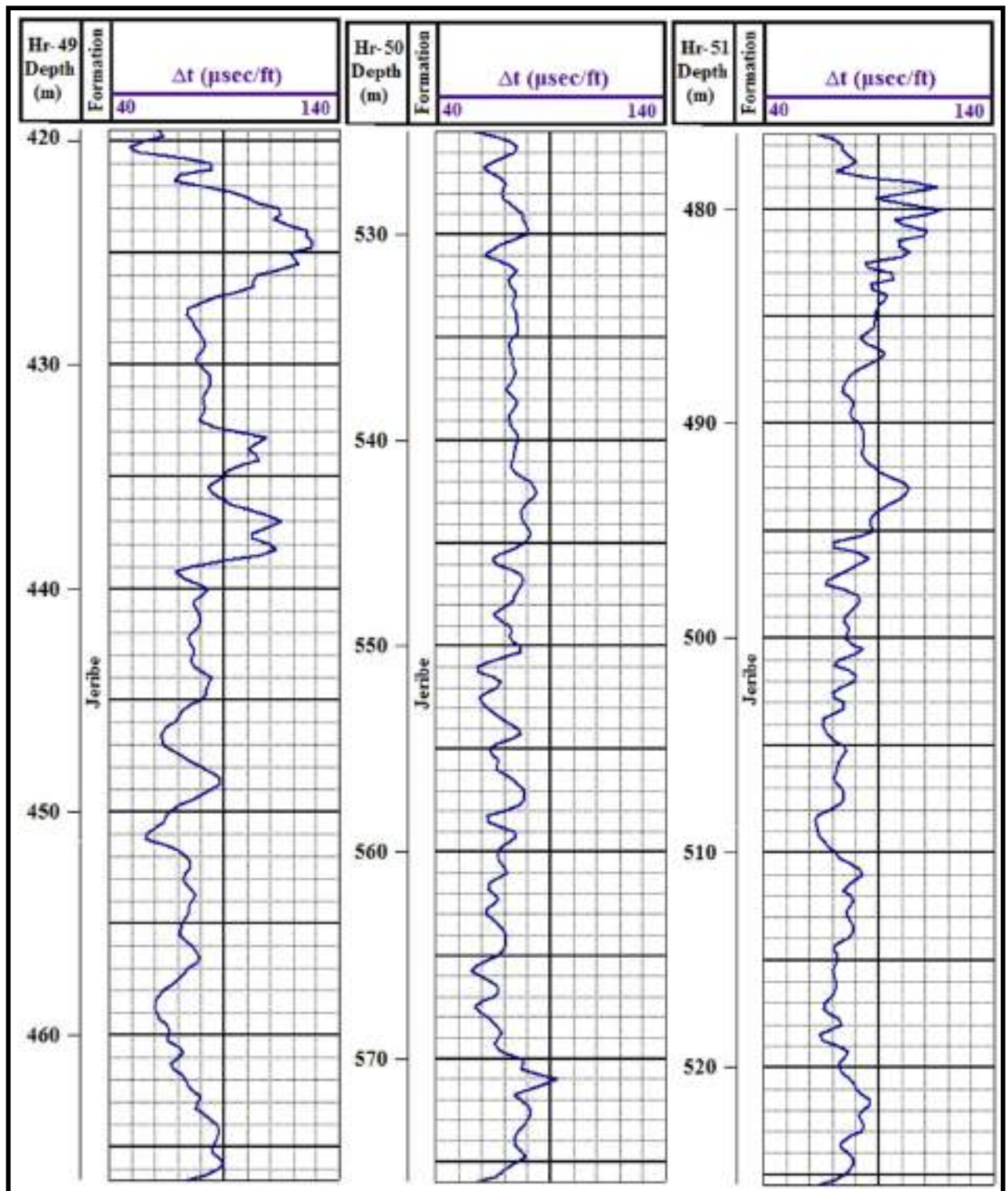


Figure 3.1: Interval transit time (Δt) for the studied Jeribe Formation in the wells Hr-49, Hr-50 and Hr-51.

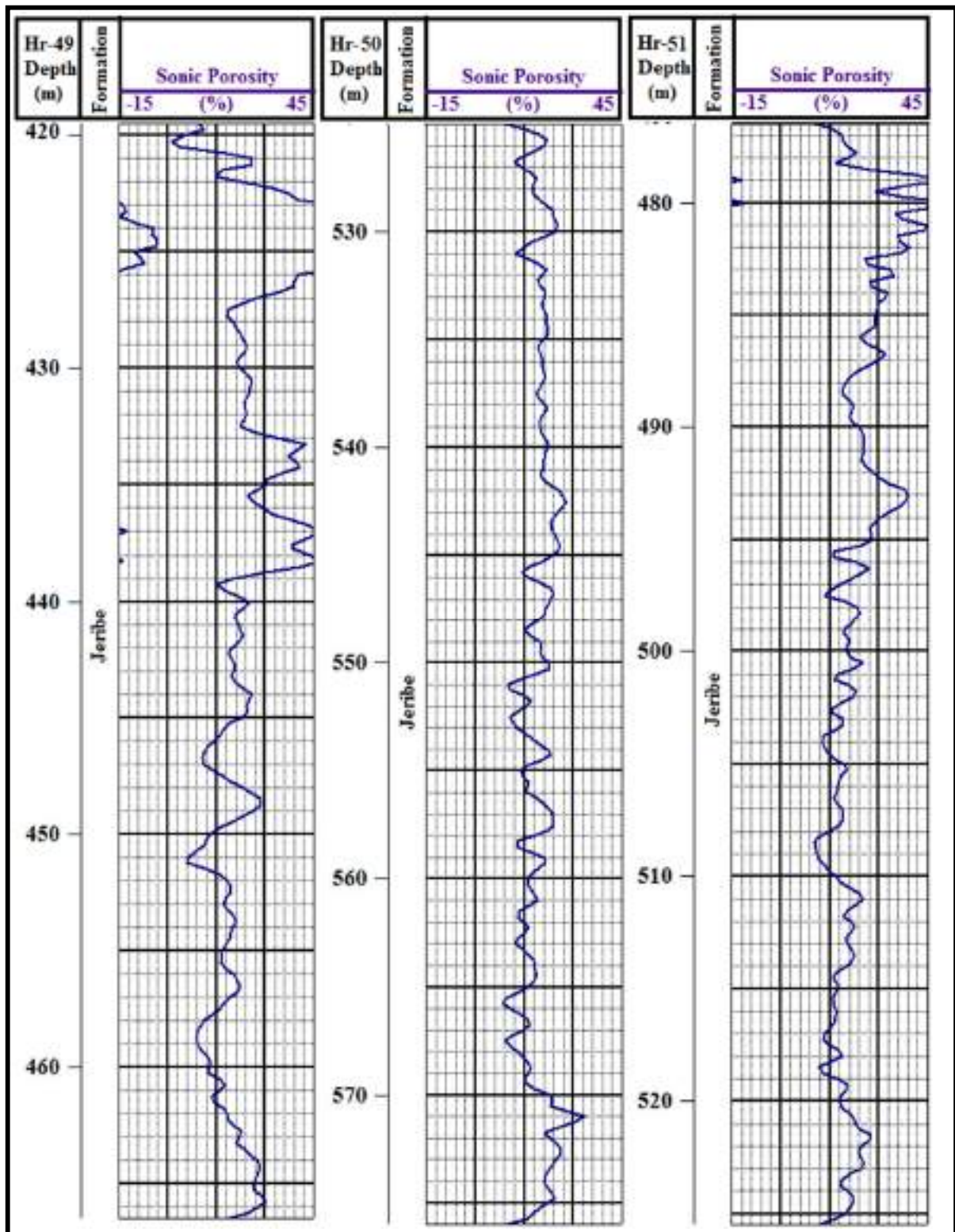


Figure 3.2: Sonic porosity (ϕ_s) for Jeribe Formation in the studied wells of Hr-49, Hr-50, and Hr-51.

3.2.2 Density Log

The Density log is a radioactivity tool, which is based on the response of the rock to induced, medium-energy gamma rays. The result is an approximate measurement of the bulk density of the rock. The bulk density, as used in well logging, is the number of grams or mass weight of a substance divided by its volume (Miller, 1970). The technique of density logging includes injecting gamma rays into the logged beds around the borehole and then scattering the gamma rays by electrons in the beds through a process known as Compton Scattering. The scattered gamma rays are finally detected by the detectors (Darling, 2005).

The two identical density values used by the density log are: the bulk density (ρ_b or RHOB) and the matrix density (ρ_{ma}). The first is the density of the whole formation (solid and fluid parts) as measured by the density logging tool, whereas the matrix density is the density of the solid framework of the rock (Asquith and Krygowski, 2004).

The density tool investigates the fluid in the pores of the permeable formations within relatively shallow zones (about 6in.) which is mostly mud filtrate. This mud filtrate may have a density ranging from about 1gm/cc (fresh water) to more than 1.1gm/cc depending upon its salinity, temperature, and pressure (Schlumberger, 1989).

The recorded ρ_b by the density tool for Jeribe Formation in the three studied wells are listed in the appendix A and plotted as curves in the figure 3.3. As a general note: the upper part of the formation is of lower density than the lower part. This feature can more easily be observed in the well Hr-49. The last five meters of the formation at its bottom shows decreasing in density again. As ρ_b represents the bulk density of the formation (matrix type, porosity, fluid type and content), therefore decreasing in the recorded ρ_b values may be due to change in

the properties of the formation including increasing the porosity or decreasing the density of the reservoir fluid.

The mentioned Eq.3.2 below is the common equation used for calculating porosity from the recorded ρ_b by the density logging tool:

$$\phi_D = \frac{\rho_{ma} - \rho_b}{\rho_{ma} - \rho_{fl}} \dots \dots \dots \text{Eq.3.2}$$

Where:

ϕ_D : density porosity (fraction).

ρ_{ma} : density of the matrix (gm/cc)

ρ_{fl} : fluid density (1.0gm/cc for fresh water mud and 1.1gm/cc for saline water mud)

ρ_b : bulk density (log reading, gm/cc)

The selected value for matrix density in the Eq.3.2 varies with lithology and affects greatly the calculated porosity. In dense formations like anhydrite, negative values of the calculated density porosity are not uncommon as the assumed matrix density is less than the actual formation density (Krygowski, 2003).

As the case with the sonic log, limestone matrix (2.71gm/cc) suggested for the wells Hr-49 and Hr-51, whereas dolomite matrix (2.87gm/cc) suggested for the well Hr-50 during ϕ_D calculation. Table 3.1 shows values of matrix density for different types of lithologies as mentioned by Asquith and Krygowski (2004).

The porosity calculated from bulk density will also be affected by the choice of fluid density (ρ_{fl}), which varies with fluid type and salinity. As mentioned before, the used drilling fluid was a fresh water base mud for the three studied wells, therefore, 1.0g/cc used as value for the ρ_{fl} during calculation process of the ϕ_D .

Generally, the zone investigated by the density tool is assumed to be completely saturated with mud filtrate (Krygowski, 2003).

The porosity values derived from the bulk density readings of the density logging tool are listed in the appendix B and drawn as curves in the figure 3.4. Except the lower most 5.0 to 6.0m of Jeribe Formation in the three studied wells, the porosity is gradually increasing upward till more than 27% at the upper part of the formation before starting decreasing at the upper most 2.0 to 3.0m near the contact with the above Lower Fars Formation. It is important to mention that no high porosities as that recorded by the sonic log at the upper part of the formation observed in the calculated density porosity and that should be due to the different responses of the two porosity logs to the reservoired fluids.

Table 3.1: Matrix density values for common types of rocks (after Asquith and Krygowski, 2004).

Lithology	Density(g/cm³)
Sandstone	2.65
Limestone	2.71
Dolomite	2.87
Anhydrite	2.98

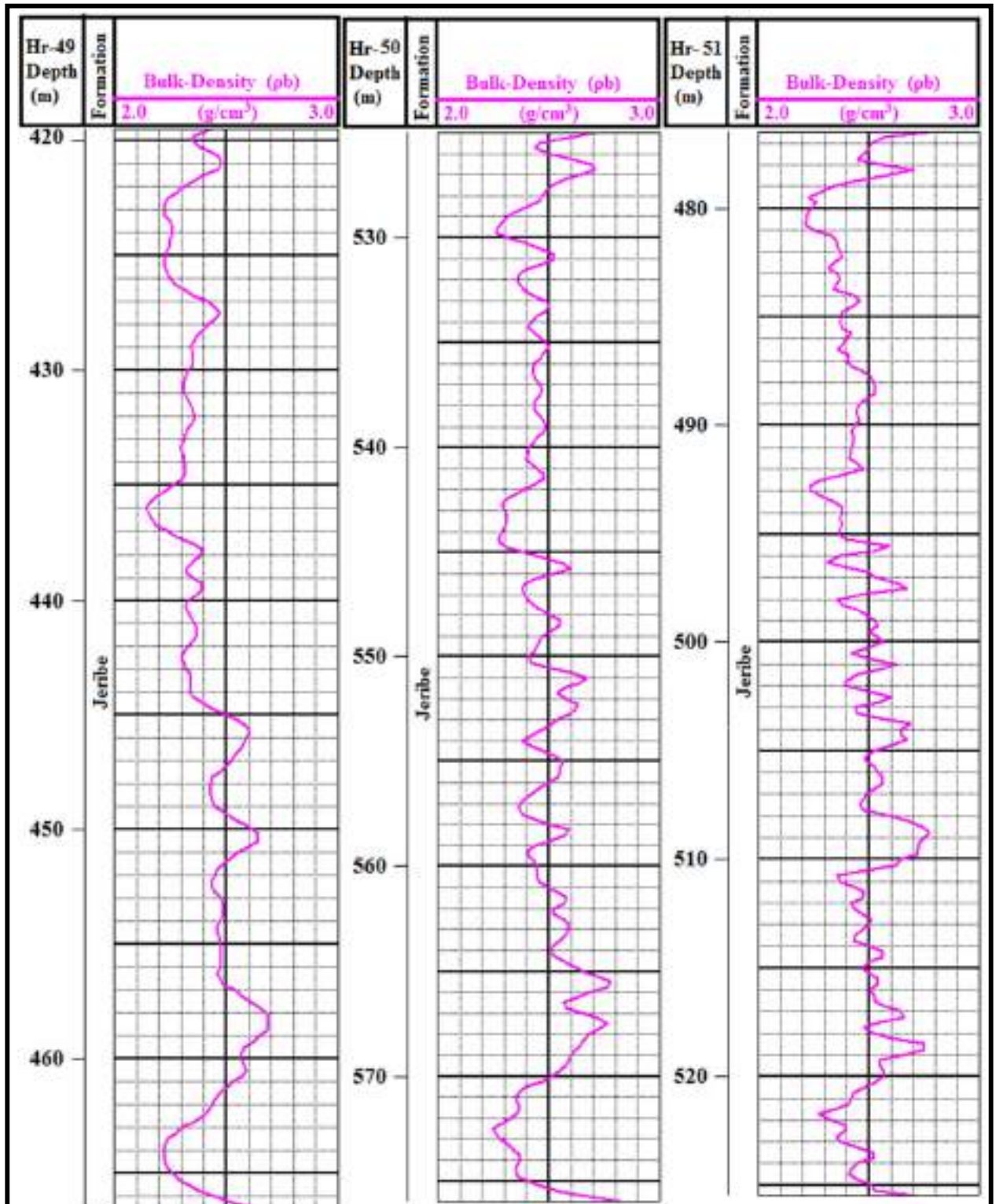


Figure 3.3: Bulk Density (ρ_b) for Jeribe Formation in the studied wells of Hr-49, Hr-50, and Hr-51.

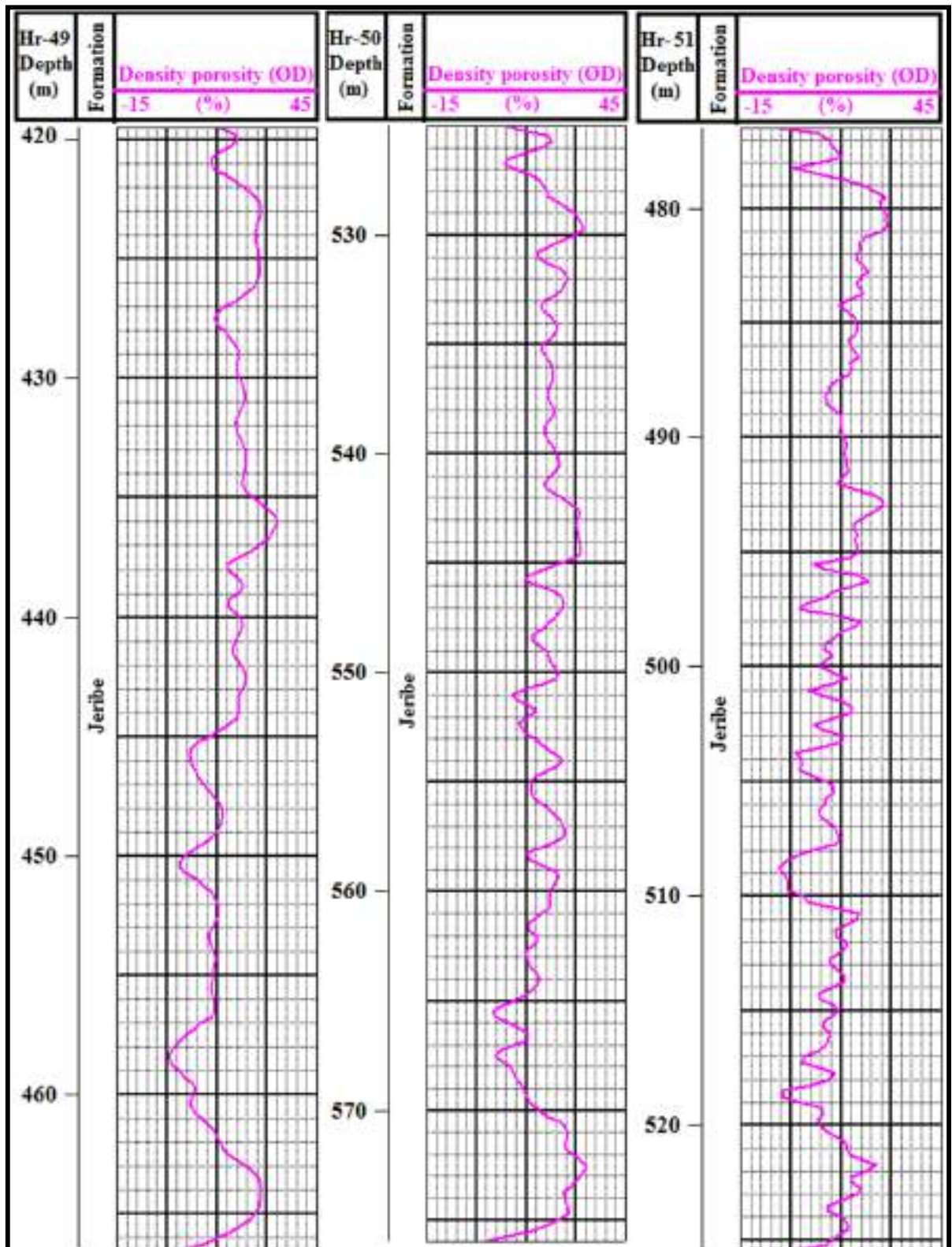


Figure 3.4: Density porosity (ØD) for Jeribe Formation in the studied wells of Hr-49, Hr-50, and Hr-51.

3.2.3 Neutron Log

Neutron logs measure porosity of the beds through measuring the hydrogen concentration in the formation. In shale free formations where porosity filled with oil or water, the tool measures the liquid filled porosity (Asquith and Krygowski, 2004).

High neutron count rate indicates low porosity, while low neutron count rate indicates high porosity (Baker Hughes, 1992).

The derived porosity from the Neutron log is affected by the existing quantity of hydrogen in the fluid content in the pore spaces and the hydrogen within the formation matrix itself (Bassiouni, 1994).

Accordingly and as mentioned by Schon (2015), for any porous rock composed of different mineral components, shale, and fluids, the porosity derived from the neutron log can be represented as:

$$\varnothing_N = \varnothing \cdot \varnothing_{N,fl} + \{(1 - V_{shale}) \cdot \varnothing_{N,ma} + V_{shale} \cdot \varnothing_{N,shale}\} \dots\dots\dots \text{Eq. 3.3}$$

Where:

\varnothing : rock porosity

\varnothing_N : measured neutron porosity

$\varnothing_{N,fl}$: neutron response of the fluid

$\varnothing_{N,ma}$: neutron response of the matrix

$\varnothing_{N,shale}$: neutron response of the shale

V_{shale} : the shale content

The recorded neutron porosity for Jeribe Formation in the studied wells are listed in the appendix B and shown in the figure 3.5.

The neutron porosity showed its highest values at the upper part of the formation (between depths about 529 to 545m) in the well Hr-50. Porosities more than 25% are common in the mentioned interval. The recorded neutron porosity appeared to be generally higher in the well Hr-50 than the other two

studied wells of Hr-49 and Hr-51. Jeribe Formation in the latest two wells showed very similar neutron porosity values especially in the lower part of the formation which was around 15%. Noticeable increase in the neutron porosity exists in the lower most part of the formation near its contact with Dhiban Formation. Porosities of more than 30% recorded in this part of the formation in the well Hr-50.

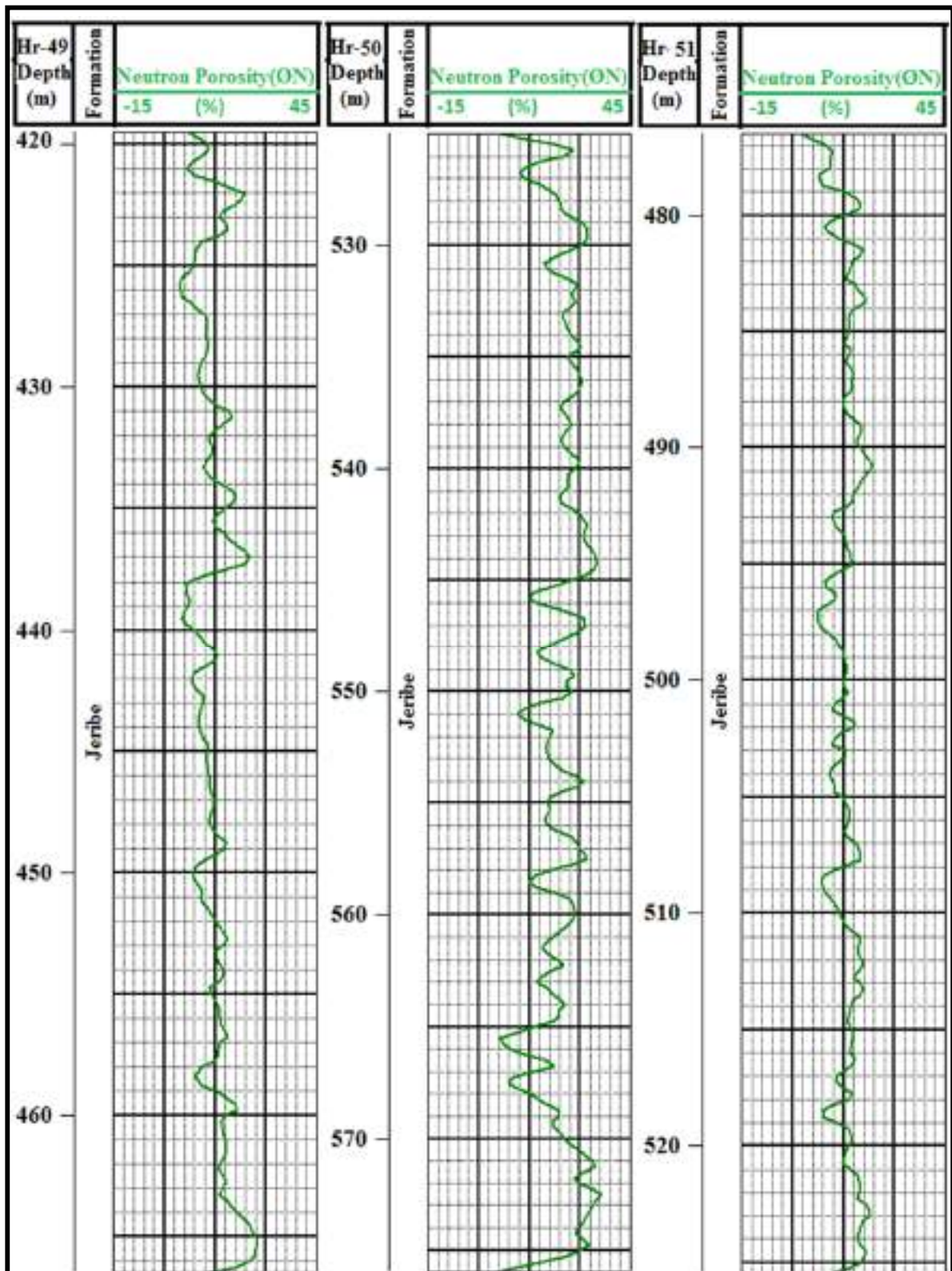


Figure 3.5: Neutron porosity (\emptyset_N) for Jeribe Formation in the studied wells of Hr-49, Hr-50, and Hr-51.

3.3 Types of Shale Distribution in Reservoirs

Evaluation of the formations containing clay minerals (shaly formations) is not an easy task because clay minerals have an impact on all well logging measurements. Therefore, reservoir properties such as porosity and water saturation have to be corrected from the effect of shale (Bassiouni, 1994).

The amount of the shale and its physical properties are both affecting the log readings along with the way by which the shale is distributing in the formation (Schlumberger, 1989).

There are three common types of clay distribution in the formations as identified by log analysts, namely; dispersed, structural, and laminated (Glover, 2008) (Fig. 3.6).

"Dispersed shale is present throughout the pore space, and reduces the original porosity without affecting the grain space. Structural shale is part of the framework structure, so that the original porosity is not altered. Laminated shale appears as discrete interspersed layers of shale in otherwise clean formation, with the shale reducing the volume of both matrix and porosity" (Ellis and Singer, 2008).

The three mentioned types of shale distribution can occur at the same time in the same formation (Schlumberger, 1989) with being the dispersed type of greatest interest (even if it occurs at small volume concentrations) for hydrocarbon reservoir evaluation (Ellis and Singer, 2008).

Through the technique of Scanning Electron Microscope, several types of dispersed shale have been identified; pore filling, pore lining, and pore bridging. The photomicrographs of the mentioned three types are shown in figure 3.7 (Ellis and Singer, 2008).

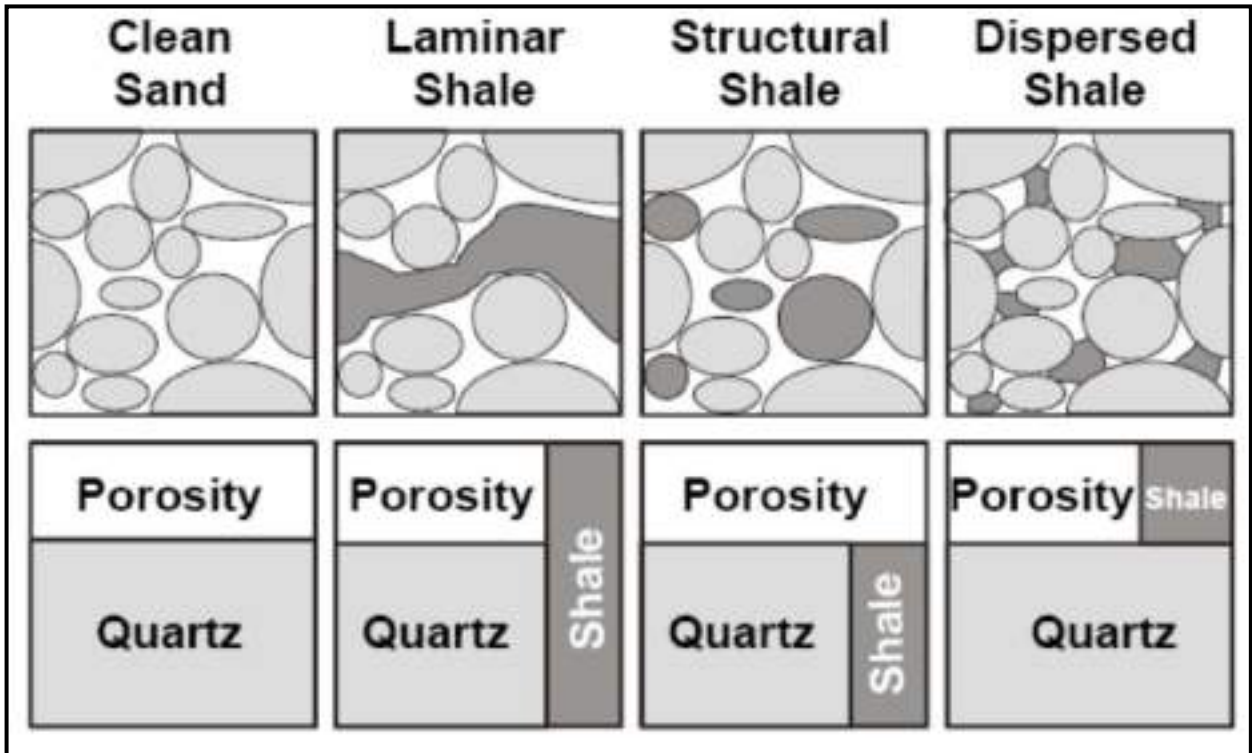


Figure 3.6: Clay distribution types in reservoirs (after Glover, 2008).

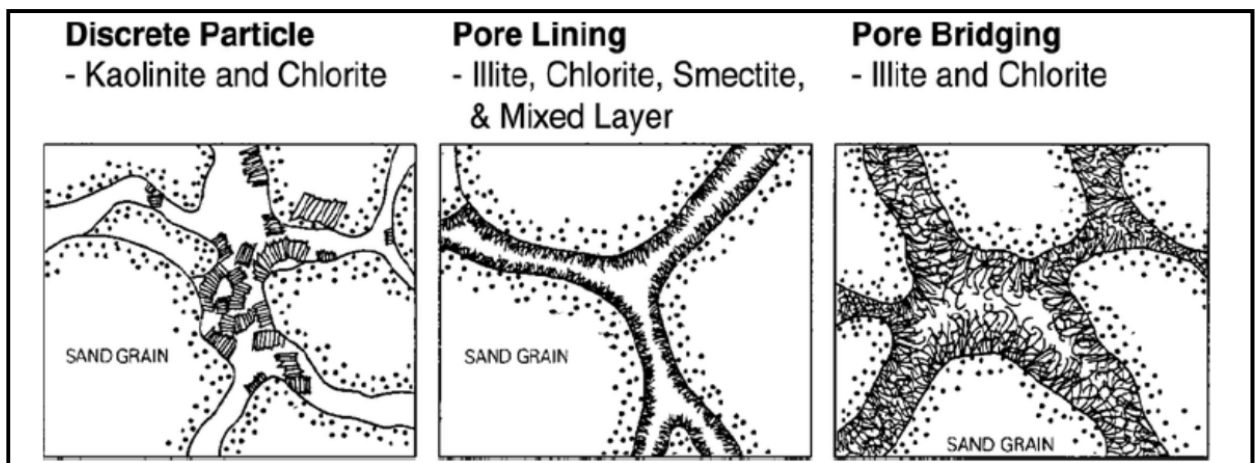


Figure 3.7: Pore filling, pore lining, and pore bridging of Dispersed clay type in sandstone reservoir rocks (after Ellis and Singer, 2008).

Darling (2005) clarifies the way by which $\emptyset D$ and $\emptyset N$ may be predicted in a shaly formation in the three shale distribution types as follows:

Let the shale porosity be denoted by \emptyset_{sh} , and the clean sand porosity be denoted by \emptyset_{csa} . The hydrogen index (HI) of the shale is denoted by HI_{sh} and of water as HI_w , assuming that the shale and quartz have a similar matrix density and that the formation is water bearing;

Laminae:

$$\emptyset_n = V_{lam} * (HI_{sh} + \emptyset_{sh} * HI_w) + (1 - V_{lam}) * \emptyset_{csa} * HI_w \dots\dots\dots Eq.3.4$$

$$\emptyset_d = V_{lam} * \emptyset_{sh} + (1 - V_{lam}) * \emptyset_{csa} \dots\dots\dots Eq.3.5$$

Where V_{lam} is the volume fraction of laminated shale.

Dispersed:

$$\emptyset_n = HI_{sh} * V_{sh} + HI_w * \emptyset_d \dots\dots\dots Eq.3.6$$

$$\emptyset_d = \emptyset_{csa} - V_{sh} * (1 - \emptyset_{sh}) \dots\dots\dots Eq.3.7$$

Where V_{sh} is the volume fraction of shale.

Structural:

$$\emptyset_n = \emptyset_{csa} * HI_w + V_{sh} * \emptyset_{sh} * HI_w + V_{sh} * HI_{sh} \dots\dots\dots Eq.3.8$$

$$\emptyset_d = \emptyset_{csa} + V_{sh} * \emptyset_{sh} \dots\dots\dots Eq.3.9$$

The three mentioned types of shale distribution are graphically presented through the relationship between $\emptyset D$ and $\emptyset N$ which is known as Thomas and Stieber’s method for determining shale distribution types (Fig. 3.8).

Through application of the Thomas and Stieber’s method on the calculated $\emptyset D$ and $\emptyset N$ for Jeribe Formation in the studied wells (Fig. 3.9), dispersed shale appeared to be the main type by which the existed shale in the formation has distributed.

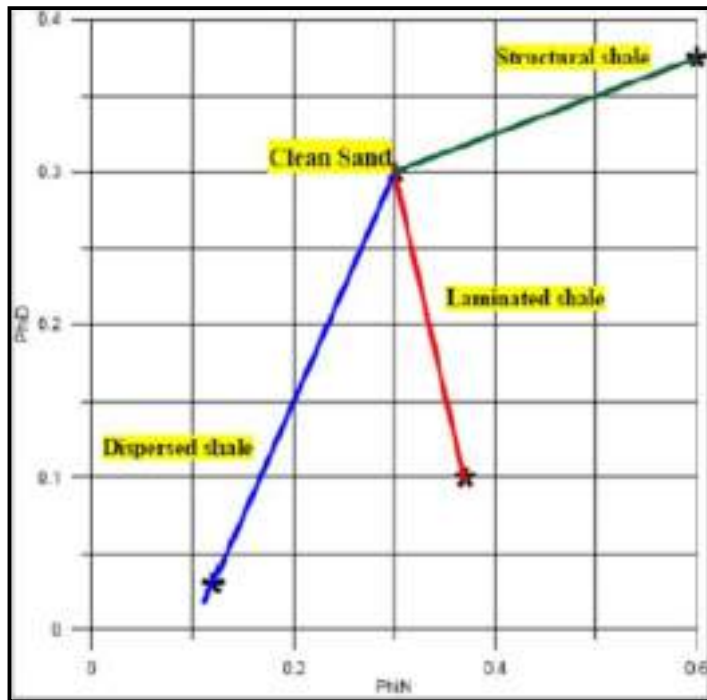


Figure 3.8: Thomas-Stieber plot for discriminating dispersed/laminated shale.

It's important to mention that if the studied Jeribe reservoir in Hamrin Field was containing gas (as it expected especially in the wells Hr-49 and Hr-51), this will not affect the readings of the Density and Neutron log tools in a manner that will change the result of the application of the ØD and ØN on Thomas-Stieber plot. This is true because the existence of the gas in the reservoir will result in overestimation of the calculated ØD and underestimation of the ØN . Accordingly, any correction for removing the effect of the gas on the ØD and ØN will lead to decrease the values of the first one and increase the values of the second one but they will remain within the field of dispersed shale distribution types on the Thomas-Stieber plot.

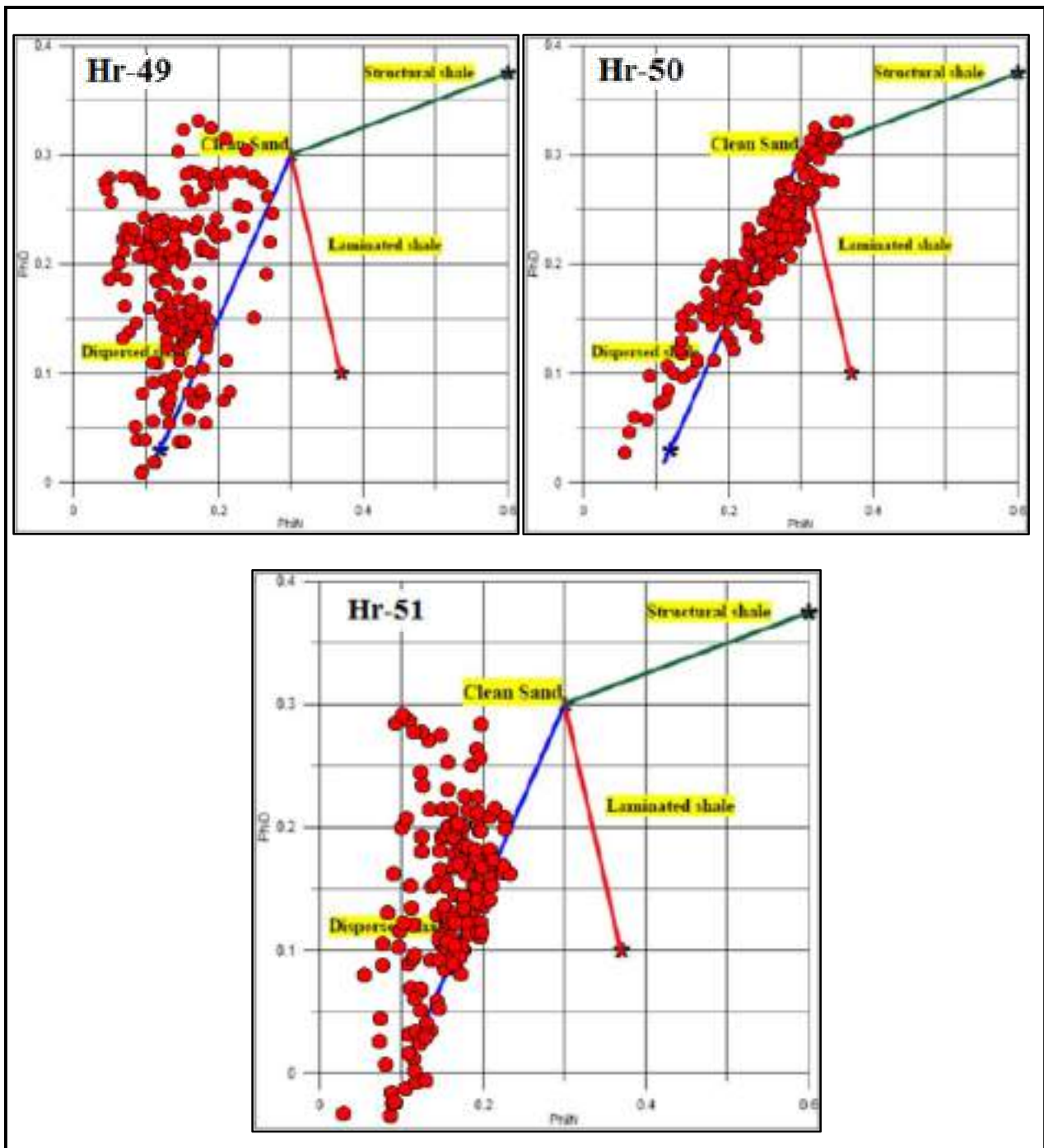


Figure 3.9: Shale distribution type for the studied Jeribe Formation in the wells of Hr-49, Hr-50, and Hr-51 using Thomas-Stieber plot.

3.4 Correction of Porosity from Shale Impact

The porosity log tools have different responses to shale content due to the different characteristics of shales, therefore the presence of shale in any reservoir will complicate the interpretation of the calculated porosities (Bassiouni, 1994).

Whenever shale is present in a formation, all the porosity tools (Sonic, Density, and Neutron) will record too high porosity values and this is true for all common types of reservoirs (sandstone, limestone, and dolomite reservoirs) (Asquith and Gibson, 1982).

For example, clays and shales present a problem for all Neutron porosity interpretations because of the hydroxyls associated with the clay mineral structure. The large apparent porosity values are due primarily to the hydrogen concentration associated with the shale matrix (Ellis and Singer, 2008).

The presence of shale or clay in the reservoir will distort the measurement of true effective porosity. To correct for shaliness, it is necessary to estimate the fractional shale volume from other logs (Khan, 1989).

In chapter two of this study, the shale volume in Jeribe Formation has been determined through gamma ray log, whereas type of the distribution for the existed shales determined through the calculated ϕ_D and The readings of ϕ_N using Thomas-Stieber plot and appeared to be of dispersed shale distribution type.

Accordingly, all the calculated porosity values using Sonic, Density and Neutron logs in this study were corrected from the effect of shale using appropriate equation for each type of porosity and as shown below:

a. For correcting Sonic porosity

$$\phi_{\text{Sonic}} = \frac{\Delta t_{\text{log}} - \Delta t_{\text{ma}}}{\Delta t_{\text{fl}} - \Delta t_{\text{ma}}} - V_{\text{sh}} \times \frac{\Delta t_{\text{sh}} - \Delta t_{\text{ma}}}{\Delta t_{\text{fl}} - \Delta t_{\text{ma}}} \quad \dots \text{Eq.3.10, from Dresser Atlas (1979)}$$

Where:

$\emptyset S_{\text{corr}}$: sonic porosity corrected for shale

Δt_{log} : interval transit time of formation

Δt_{ma} : interval transit time of formation's matrix

Δt_{fl} : interval transit time of fluid (189 $\mu\text{sec}/\text{ft}$ for fresh mud and 185 $\mu\text{sec}/\text{ft}$ for salt mud)

Δt_{sh} : interval transit time of adjacent shale

b. For correcting Density porosity

$$\emptyset_{\text{Dcorr}} = \frac{\rho_{\text{ma}} - \rho_{\text{b}}}{\rho_{\text{ma}} - \rho_{\text{fl}}} - V_{\text{sh}} \times \frac{\rho_{\text{ma}} - \rho_{\text{sh}}}{\rho_{\text{ma}} - \rho_{\text{fl}}} \dots \dots \text{Eq.3.11, from Dresser Atlas (1979)}$$

Where:

\emptyset_{Dcorr} : density log derived porosity corrected for shale

ρ_{ma} : matrix density of formation

ρ_{b} : bulk density of formation

ρ_{sh} : bulk density of adjacent shale

ρ_{fl} : fluid density (1.0 gm/cm³ for fresh mud and 1.1 gm/cm³ for salt mud)

V_{sh} : volume of shale

c. For correcting Neutron porosity

$$\emptyset_{\text{Ncorr}} = \emptyset_{\text{N}} - V_{\text{sh}} \times \emptyset_{\text{Nsh}} \dots \dots \text{Eq.3.12, from Dewan (1983)}$$

Where:

\emptyset_{Ncorr} : neutron log derived porosity corrected for shale

\emptyset_{N} : neutron log derived porosity uncorrected for shale

\emptyset_{Nsh} : neutron porosity for adjacent shale

V_{sh} : volume of shale

The corrected porosity values using the mentioned equations above are listed in the appendix B and shown along with calculated volume of shale and the uncorrected porosity values (for comparison purposes) in the figures 3.10-3.12 .

As mentioned by Asquith and Gibson (1982), the existence of the shale in any reservoir causes overestimating for the calculated porosities using common porosity tools of Sonic, Density, and Neutron. So, it's expected that the corrected porosities from the effect of shale will show a decrease in the porosity values proportionally to the calculated shale volume in each depth. Accordingly, the corrected porosity values of \emptyset_S , \emptyset_D , and \emptyset_N showed the highest decrease in the middle part of Jeribe Formation where the highest values of shale content were measured in the three studied wells (Figs. 3.10-3.12). The reduction in the porosity values in this part of the formation exceeds 25% in some depth intervals.

No effective changes in the porosity values (after correction) can be observed in the upper and lower parts of the formation which is mainly due to no existence of appreciable shale content in those parts.

It is worth to mentioning that in some intervals the \emptyset_{scorr} shows unusual high porosities (>45%) especially in the upper part of the formation in the wells Hr-49 and Hr-51. Such a case may be a good sign to the probability of the existence of low density hydrocarbons (gas) in those intervals.

3.5 Combination of Neutron-Density Porosity Logs

To avoid errors in the measured porosity values from porosity logs (even after correction from shale effect), combination of at least two porosity logs is done. The common combination is between Density and Neutron porosity logs by which the different responses of these two porosity tools for the different reservoir properties such as lithology and gas effect can be solved.

In most cases like in limestone lithology, porosity can be read directly from the neutron log. For other lithologies, it should be used by taking the average of porosity calculates from density and neutron logs to avoid the lithologic effects (Rider and Kennedy, 2011).

The used equation for calculating the Neutron-Density porosity combination for Jeribe Formation in this study is as follows:

$$\varnothing_{N-D} = \frac{N_{corr} + \varnothing D_{corr}}{2} \dots\dots\dots \text{Eq.3.13}$$

Where:

\varnothing_{N-D} : neutron-density porosity corrected for shale

$\varnothing_{N_{corr}}$: neutron porosity corrected for shale

$\varnothing_{D_{corr}}$ density porosity corrected for shale

The calculated corrected \varnothing_{N-D} values for Jeribe Formation in the studied wells are listed in appendix B and plotted as curved line in the figure 3.13 along with the shale volume and uncorrected \varnothing_{N-D} curves.

This calculated corrected \varnothing_{N-D} values will be used mainly for the purpose of evaluating and characterizing Jeribe Formation in this study. On the other hand, the standard proposed by North (1985) for evaluating porosities (Table 3.2) will depend on for describing the porosities of Jeribe Formation qualitatively.

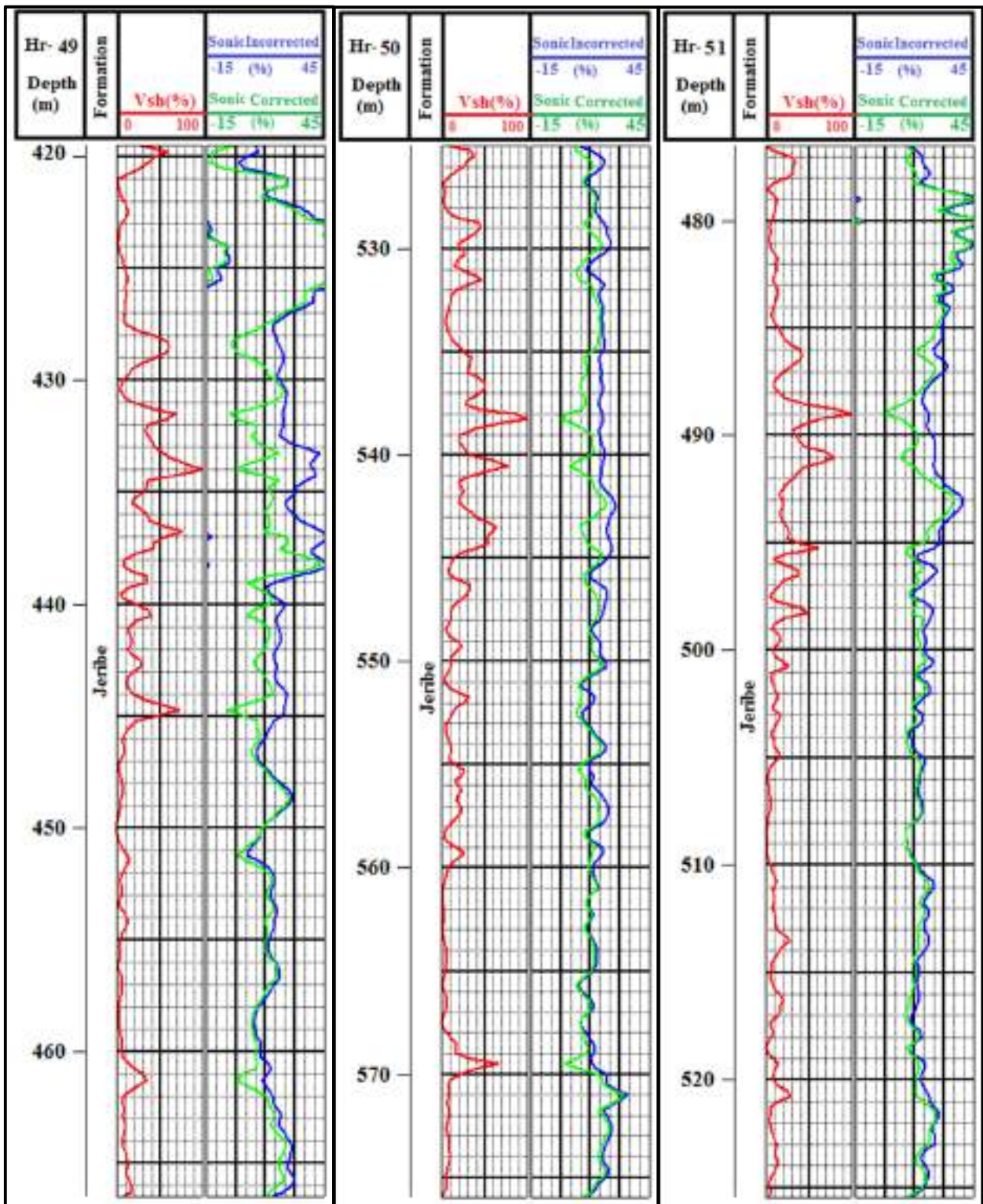


Figure 3.10: Incorrected, corrected Sonic porosity from shale effect, and shale volume curves for the Jeribe Formation in the studied wells of Hr-49, Hr-50, and Hr-51.

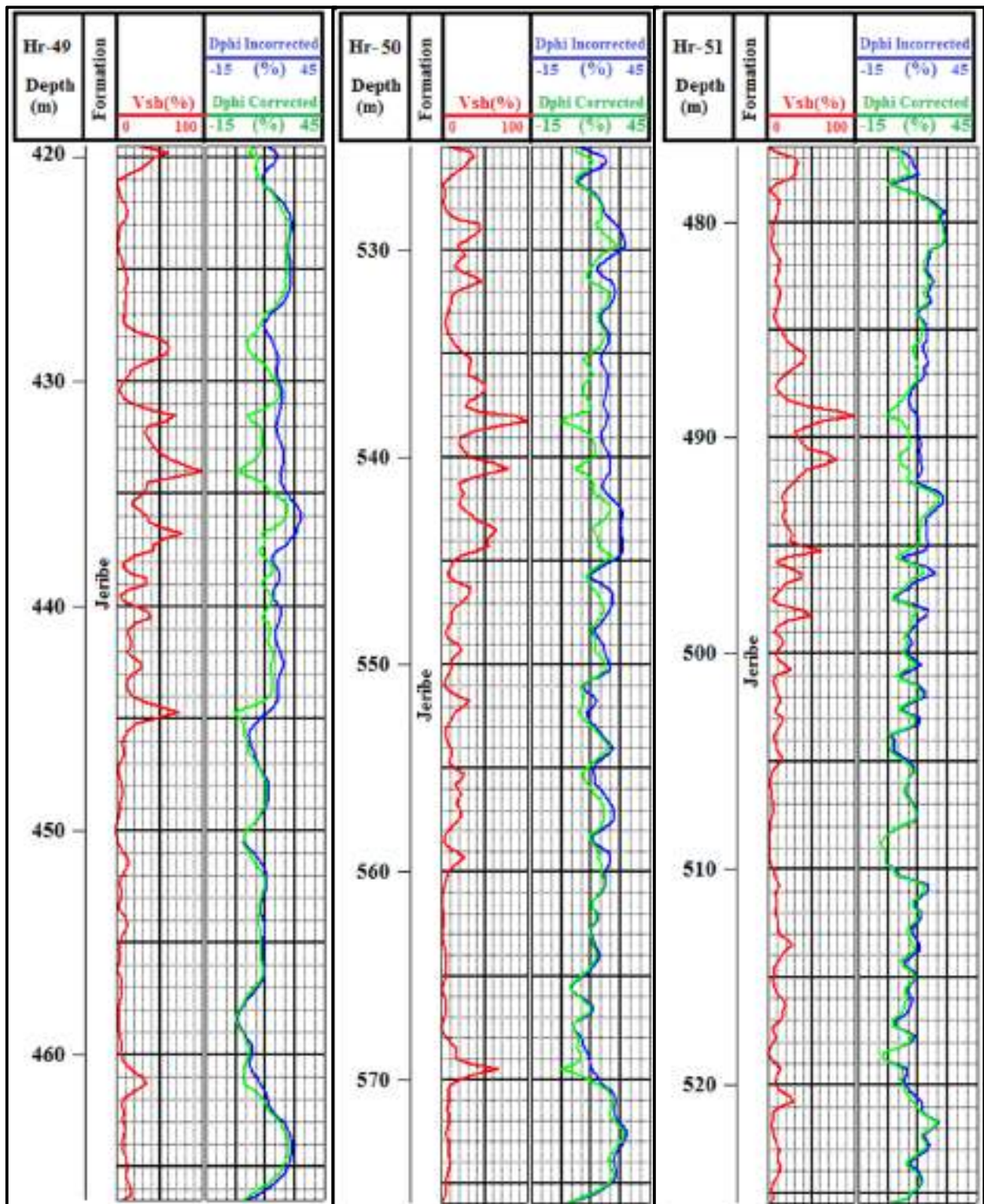


Figure 3.11: Incorrected and corrected Density porosity from shale effect and shale volume curves for Jeribe Formation in the studied wells of Hr-49, Hr-50, and Hr-51.

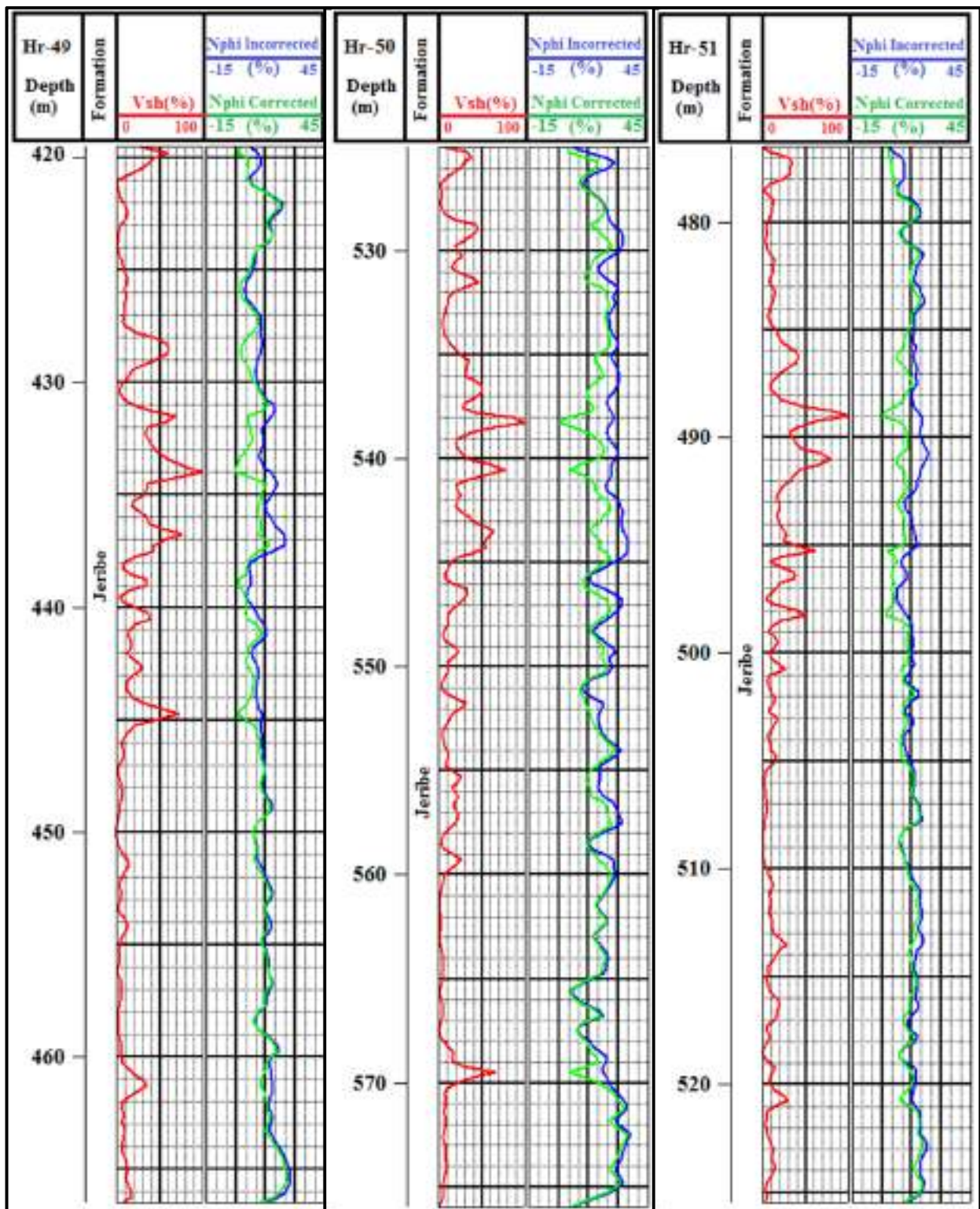


Figure 3.12: Incorrected and corrected Neutron porosity from shale effect and shale volume curves for the studied Jeribe Formation in the wells of Hr-49, Hr-50, and Hr-51.

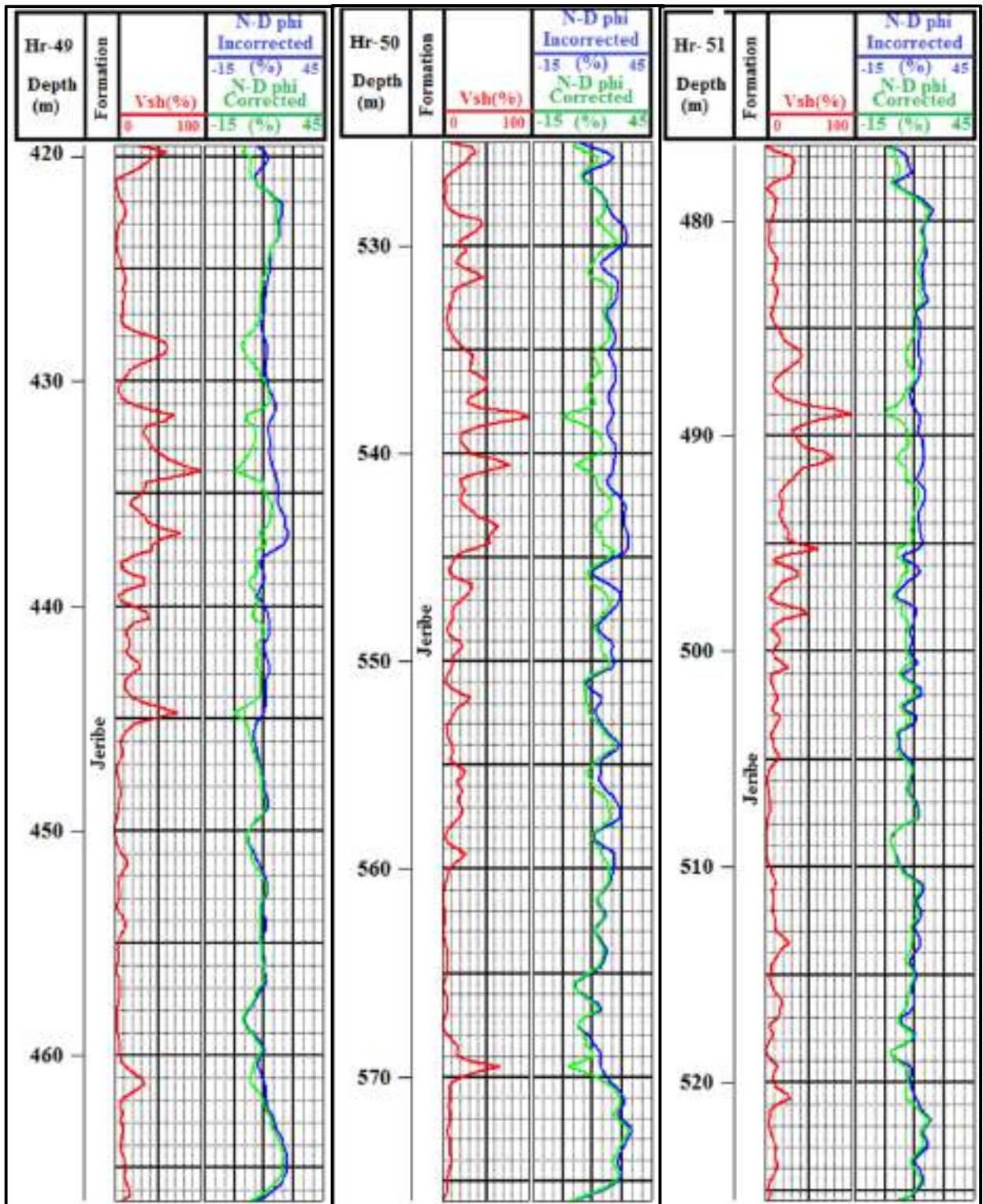


Figure 3.13: Incorrected and corrected N-D porosity from shale effect and shale volume curves for the studied Jeribe Formation in the wells of Hr-49, Hr-50, and Hr-51.

Table 3.2: Description of porosity qualitatively as proposed by North (1985).

Porosity (%)	Qualitative Description
0-5	Negligible
5-15	Poor
15-20	Good
20-30	Very Good
>30	Excellent

3.6 Detecting Existence of Gas Using Porosity Logs

"Whenever pores are filled with gas rather than oil or water, the reported neutron porosity is less than the actual formation porosity. This occurs because there is a lower concentration of hydrogen in gas than in oil or water. This lower concentration is not accounted for by the processing software of the logging tool, and thus is interpreted as low porosity. A decrease in neutron porosity by the presence of gas is called gas effect" (Asquith and Krygowski, 2004).

Liquid hydrocarbons have hydrogen indexes close to that of water. Gas, however, usually has a considerably lower hydrogen concentration that varies with temperature and pressure. Therefore, when gas is present near enough to the borehole to be within the tool's zone of investigation, a neutron log reads too low porosity. This characteristic allows the neutron log to be used with other porosity logs to detect gas zones and identify gas/liquid contacts (Rider, 2002).

On the other hand, porosity values derived from density logging tool in zones containing gas are mostly overestimated and that due to the low concentration of electrons in gas if compared to liquid oil or water. Therefore, a neutron and density log combination provides a more accurate porosity and a value of minimum gas saturation (Rider, 2002). Hilchie (1978; in Asquith and Gibson,

1982) suggests using gas density of 0.7g/cm^3 for fluid density in the density porosity formula if gas density is unknown. As gas in the pores causes the density porosity to be too high (gas has a lower density than oil or water) and causes the neutron porosity to be too low (there is a lower concentration of hydrogen atoms in gas than in oil or water) (Asquith and Krygowski, 2004), therefore using the technique of plotting the two curves of ØD and ØN on the same track will show separation between the two curves in gas bearing zones and become closer to each other in oil bearing zones, whereas the two curves show nearly no separation in water bearing zones. Figure 3.14 is the plot of ØD and ØN (after correction from shale effect) for Jeribe Formation in the studied wells.

According to Kulyk and Bondarenko (2016) the reliable identification of the gas reservoirs needs to be the difference between the ØD and ØN ($\Delta\text{Ø}$) greater than the total error of porosity determination with the neutron and density logging tool. They estimated the absolute total error of difference $\Delta\text{Ø}$ in practice to be less than about $\pm 3\%$.

Depending on above, Jeribe reservoir looks to be containing mainly gas rather than oil or water in the two wells of Hr-49 and Hr-51 of Hamrin Oil Field and that in contrast to the well Hr-50 in which Jeribe Formation seems to be containing oil as appears from the nature of the overlay between the two curves of ØD and ØN .

As mentioned in chapter two, the matrix identification (MID) plot can be relied on for detecting gas in pores in addition to the main use of this plot for lithology determination.

As with the M-N plot, the matrix-identification plot requires data from neutron, density, and sonic logs (Asquith and Krygowski, 2004).

The first step in constructing a matrix identification plot is to determine values

for the apparent matrix parameters, apparent matrix density $(\rho_{ma})_a$ and apparent matrix travel time $(\Delta t_{ma})_a$. These values are calculated from neutron ($\emptyset N$), density (ρ_b) and sonic (Δt) data using the following equations (Western Atlas, 1995).

$$(\rho_{ma})_a = \frac{\rho_b - \emptyset ND * \rho_{fl}}{1 - \emptyset ND} \dots\dots\dots E.q.3.14$$

$$(\Delta t_{ma})_a = \frac{\Delta t - \emptyset SN * \Delta t_{fl}}{1 - \emptyset SN} \dots\dots\dots E.q.3.15$$

Where:

$(\rho_{ma})_a$ = apparent grain density in g/cm^3 or Kg/m^3 .

$(\Delta t_{ma})_a$ = apparent matrix interval transit time in $\mu sec/ft$ or $\mu sec/m$.

ρ_b = bulk density from the log

ρ_{fl} = density of fluid

Δt = interval transit time from the log

Δt_{fl} = interval transit time of fluid

$\emptyset ND$ = neutron-density porosity (uncorrected $\emptyset N$ and $\emptyset D$ used)

$\emptyset SN$ = sonic-neutron porosity (uncorrected $\emptyset S$ and $\emptyset N$ used)

The calculate $(\rho_{ma})_a$ and $(\Delta t_{ma})_a$ values are listed in the appendix A.

In this technique as shown in figure 3.15, the observed lithology has no great difference with the previously identified lithology for Jeribe Formation in the three studied wells using the two techniques of N-D and M-N (chapter two). The same dolomite lithology domination was confirmed for Jeribe Formation in Hr-50 well with limestone and dolomitic limestone for the other two studied wells.

Characteristic gas effect also can be seen in the wells of Hr-49 and Hr-51 were the sample points show great distortion toward the gas effect field of the crossplot (even out of the common used values of the crossplot's axis). As seen in the overlay curves of neutron and density (Fig.3.14) the well Hr-50 showed no

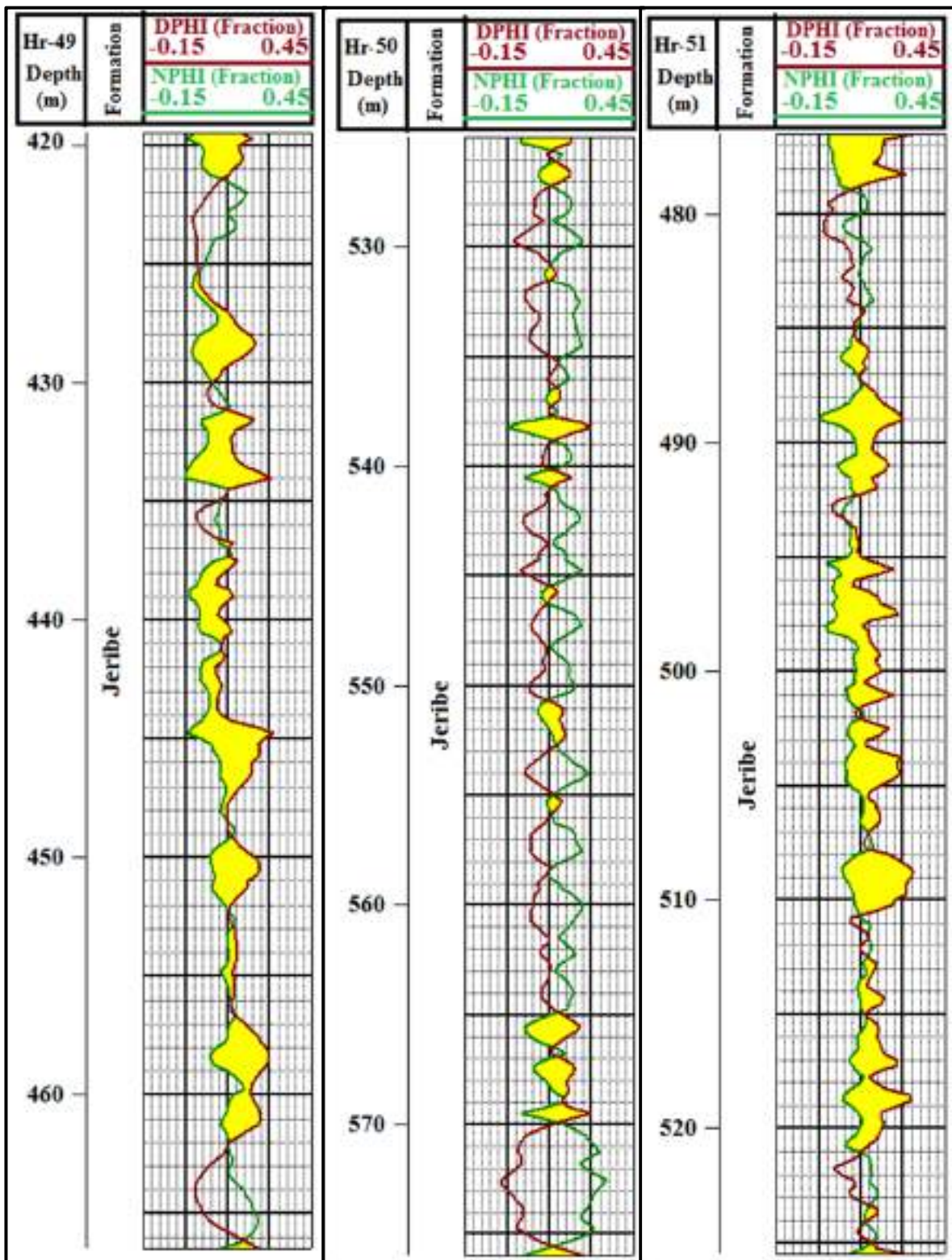


Figure 3.14: Neutron and Density porosity curve's crossovers as appeared in the studied Jeribe Formation for each of well Hr-49, Hr-50 and Hr-51.

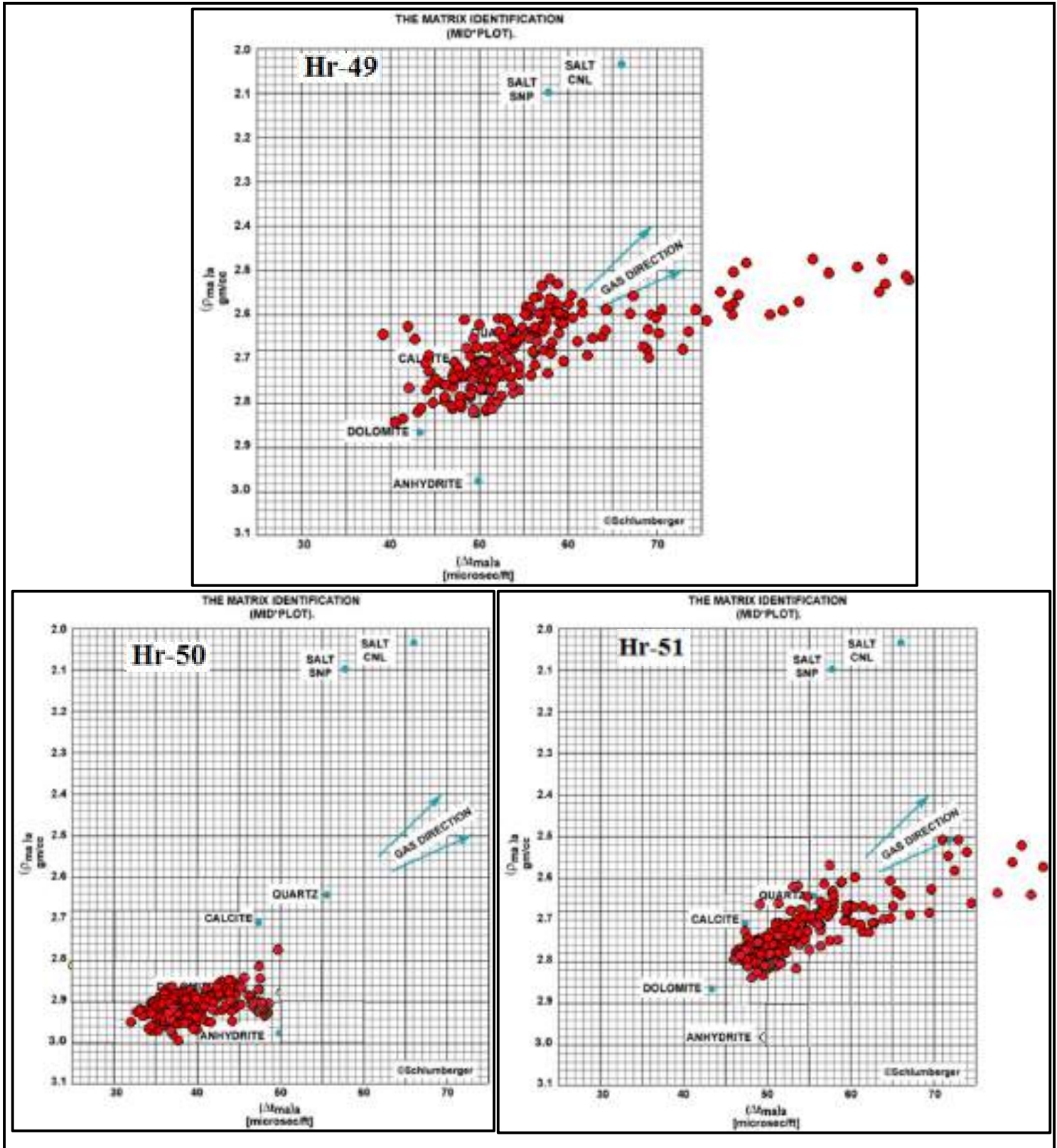


Figure 3.15: Gas effect as can be seen using MID crossplot for Jeribe Formation in the studied wells (the crossplot is after Schlumberger, 1972).

indications of gas accumulation in Jeribe Formation, this fact can be noticed also in the MID crossplot of this well when no significant distortion of the sample points toward the gas effect field occurred.

3.7 Secondary Porosity Detection from Log Data

Generally, intergranular pore spaces in any rock are known as primary porosity, whereas porosities created after deposition or after burial, e.g. vugs or fractures in carbonates are known as secondary porosity (Schlumberger, 1989).

The formula for calculating sonic porosity can be used to determine porosity in consolidated sandstone and carbonates with intergranular porosity or intercrystalline porosity (sucrosic dolomites). However, when sonic porosities of carbonates with vuggy or fracture porosity are calculated by Whille formula, porosity values are too low. This happens because of the sonic log only record matrix porosity rather than secondary porosity (Asquith and Gibson, 1982), therefore the porosity derived from the sonic log will tend to be too low by an amount approaching the secondary porosity.

Thus, if the total porosity (\emptyset_t) of a formation exhibiting primary and secondary porosity is available (from a neutron and/or density log, for example) the amount of secondary porosity (\emptyset_2) representing fractures or vugs can be estimated through the following formula:

$$\emptyset_2 = \emptyset_t - \emptyset_s \dots\dots\dots \text{Eq.3.16}$$

Where:

\emptyset_2 : secondary porosity

\emptyset_t : total porosity (from neutron and density logs)

\emptyset_s : primary porosity (from sonic log)

On the other hand, the interval transit time (Δt) of a formation is increased due to the presence of hydrocarbons (i.e., hydrocarbon effect). If the effect of

hydrocarbons is not corrected, the sonic-derived porosity is too high (Asquith and Krygowski, 2004). Hilchie (1978, in Asquith and Gibson, 1982) suggests the following empirical corrections for gas effect:

$$\emptyset = \emptyset_s * 0.7 \text{ (Gas)Eq.3.17}$$

Where:

\emptyset : Corrected porosity

\emptyset_s : Sonic porosity

To get best results about the percentage of the existing secondary porosities in Jeribe Formation in Hamrin Oil Field, firstly equation 3.17 applied for correcting the sonic porosity from the impact of gas (only for the wells Hr-49 and Hr-51 in which existence of gas was previously been proved) then the equation 3.16 has been applied for the three studied wells to show how far secondary porosity contributed in the total porosity of Jeribe reservoir. Figure 3.16 shows the reduction in the calculated sonic porosity after removing the effect of gas for the mentioned two wells of Hr-49 and Hr-51, whereas figure 3.17 shows the calculated secondary porosity as curves for the three studied wells. Appendix B contains the values of the calculated secondary porosity.

By looking at the figure 3.17 it is clear that secondary porosity contributed in enhancing the porosity of Jeribe Formation in different rates either vertically in the same well or laterally in the different wells. Jeribe in the well Hr-50 seems to be affected by secondary porosity more than the other two wells. The entire of the formation in this well showed secondary porosity rate which sometimes exceeded 7%. The least affecting by secondary porosity was Jeribe Formation in the well Hr-51 in which less than 4% contribution in the total porosity and that mostly in the lower part of the formation. The middle and upper part of Jeribe in this well showed nearly no affecting by or any other secondary porosity type.

The contribution of secondary porosity in the total porosity of Jeribe

Formation in the well Hr-49 looked different from the other two wells. Variations in the secondary porosity values was obvious within the different depth intervals with being the few meters at the top of the formation of the highest calculated secondary porosity (more than 10% as average). Less than 6% secondary porosity was the common feature of Jeribe Formation in this well with being some intervals of no secondary porosity at all as appears in the figure 3.17.

The cases of vugs or fractures are of substantially different responses regarding their display values as secondary porosity.

Different types of fractures also show different results in their contributing to the total porosity. The most important classification of fractures in reservoirs which related to fracture porosity is what known as macrofractures and microfractures (Van Golf-Racht, 1982).

“Macrofractures are extended fractures with wide openings which develop through varies layers; while microfractures (or fissures) are fractures with narrow openings and limited extent, often limited to a single layer” (Van Golf-Racht, 1982).

The maximum fracture porosity (ϕ_f) with relation to the total porosity(ϕ_t) can be expected to be less than 0.1 of the ϕ_t when ϕ_t is less than 10%, and ϕ_f expected to be less than 0.4 of the ϕ_t when ϕ_t is greater than 10%(Van Golf-Racht, 1982). Depending on such assumption the detected secondary porosity in the Jeribe Formation should be not only from fractures but most likely from vugs and fractures.

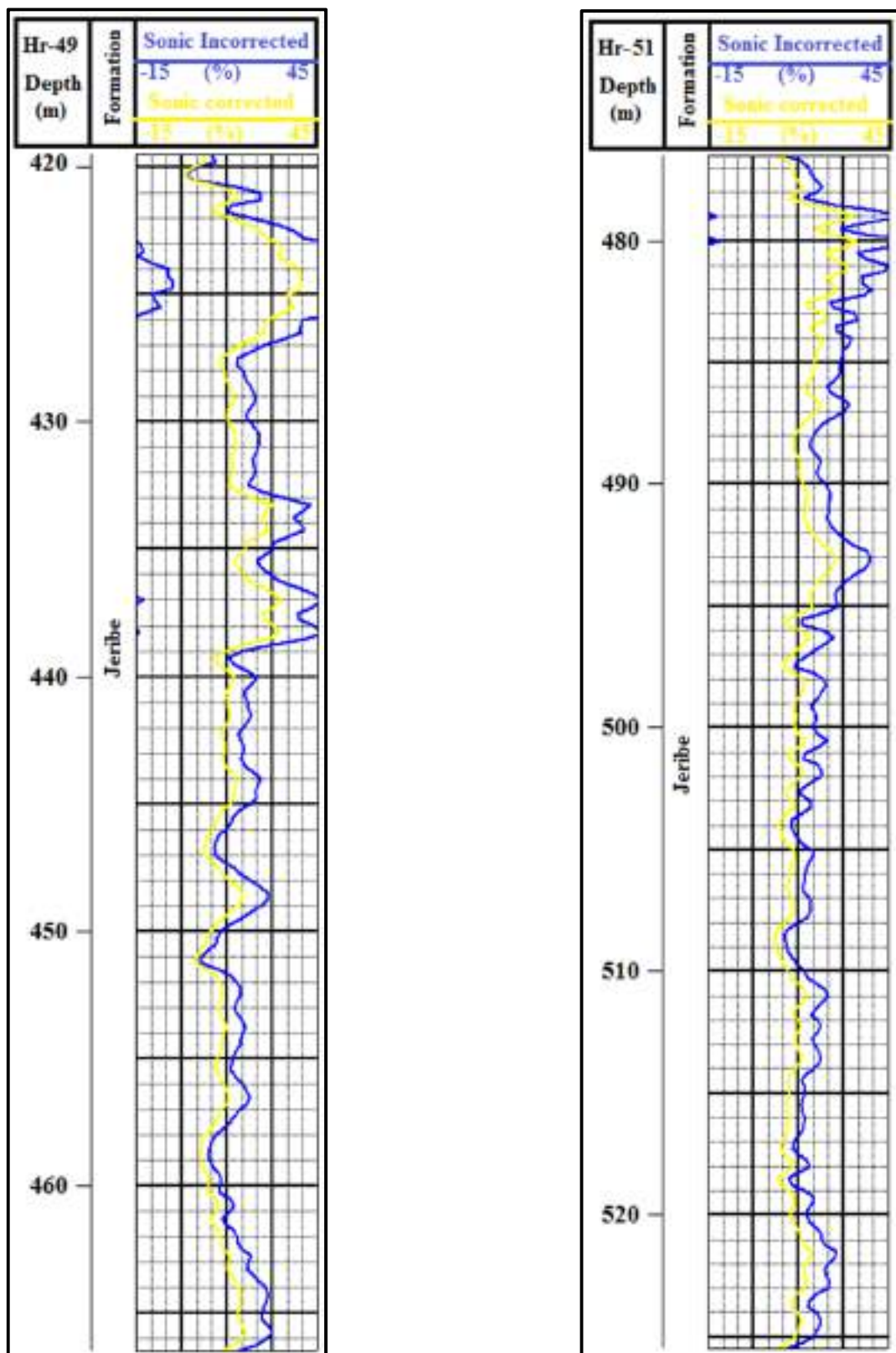


Figure 3.16: Incorrected and Corrected Sonic porosity from gas effect for the studied Jeribe Formation in the wells Hr-49 and Hr-51.

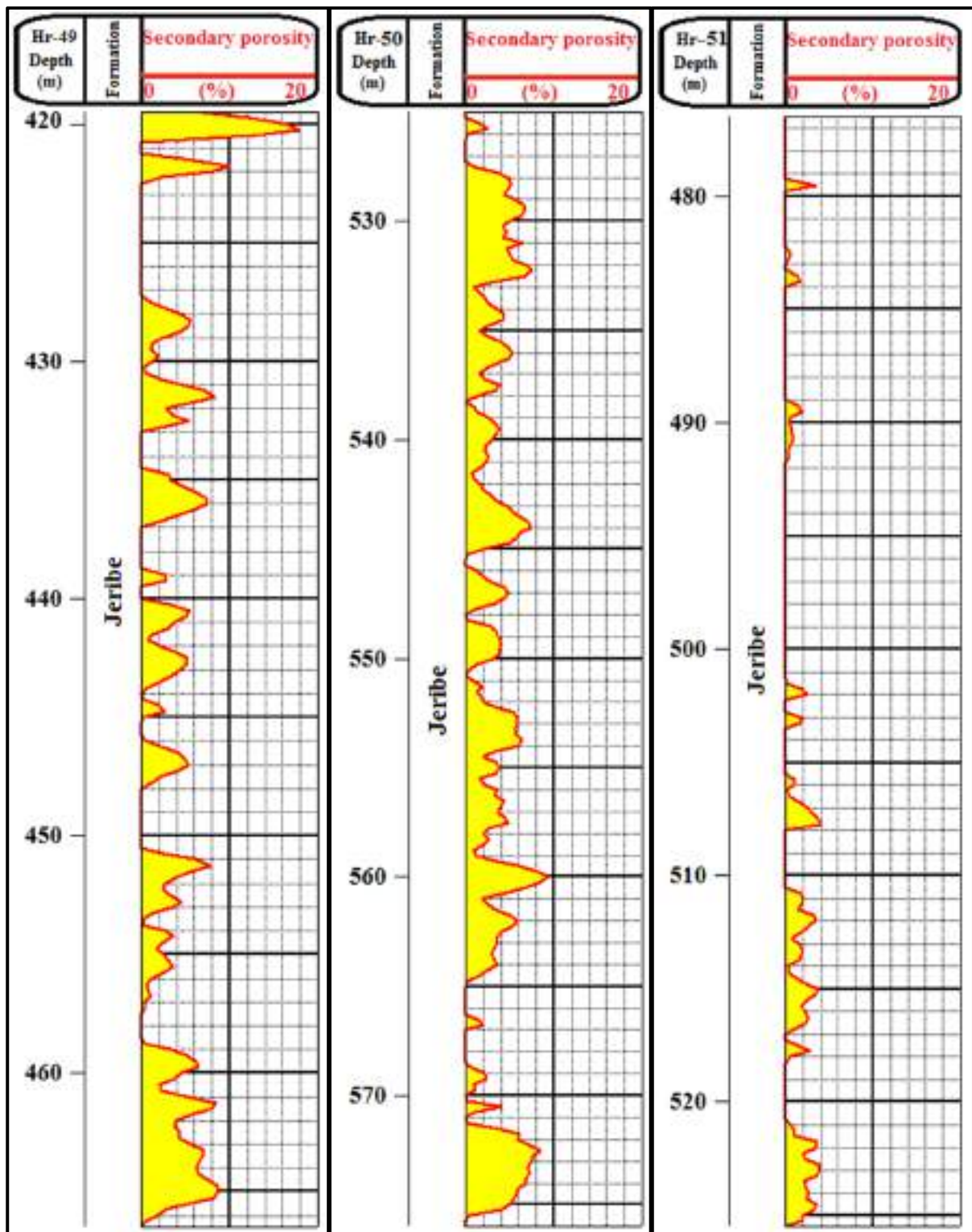


Figure 3.17: Secondary porosity plot for the studied Jeribe Formation in the studied wells of Hr-49, Hr-50 and Hr-51.

3.8 Permeability

"Permeability is a measure of the ease with which a formation permits a fluid to flow through it. To be permeable, a rock must have interconnected porosity (pores, vugs, capillaries, fissures, or fractures). Greater porosity usually corresponds to greater permeability, but this is not always the case. Pore size, shape, and continuity, as well as the amount of porosity, influence formation permeability "(Schlumberger, 1989).

Permeability can be estimated indirectly using wireline logging and pressure transient methods, or directly with core analysis techniques. Indirect methods often prove to be unreliable; however, integration of methods at all scales yields the best estimate of reservoir permeability. Formation testers, Sonic (Stoneley-wave velocity), and nuclear (geochemical) logging tools are commonly used to estimate permeability of reservoirs (Al-Saddique et al, 2000).

Deriving permeability in carbonates and correlating it with porosity mostly result in problems and that due to the complex pore structure and diversity of carbonates (Schon, 2015). According to Lucia (2007), reservoir properties are controlled by two basic pore networks:

1. Interparticle pore network (intergranular and intercrystalline porosity).
2. Vuggy pore network (leached particles, fractures, and irregular cavities). The effect of vugs on reservoir properties is strongly controlled by the type of interconnection as if they are separate vugs or touching vugs.

Usually permeability is estimated based either on simple logarithmic regressions evaluating permeability from log derived porosity or on empirical correlations which relate permeability to various log responses (Chandra, 2008).

Most reliable permeability estimation can be obtained from core samples tested under reservoir condition in the laboratories (although such kind of testing

is not fully out of limitations and problems). As not all parts of a reservoir may contain cores for permeability testing, therefore, other types of data will depend on for the permeability estimation.

Several authors have attempted to detect permeability values from log data as it is of low cost and sufficient accuracy (Abed, 2014). Conventional logs which usually depend on in detecting permeable zones (qualitatively) include SP log and Caliper log. As no SP is logging done for the studied three wells, Caliper log data recorded for Jeribe Formation was followed to detect under-gauge zones resulted from creation of mudcake opposite the permeable intervals. Figure 3.18 shows the caliper log curve compared to the 8.5inch bit size used in drilling the logged interval. Jeribe Formation in the wells Hr-49 and Hr-51 shows nearly a continuous creation of mud cake along the formation reflecting permeable nature of the zone. The same formation in the well Hr-50 did not show same condition of mudcake creation but mostly on-gauge or over-gauge zones were recorded by the caliper log.

Being the studied Jeribe Formation in the wells Hr-49, Hr-50, and Hr-51, of no available core test data (porosity and permeability), therefore permeability values from core testing for Jeribe Formation in the well Hr-2 has been depended on in formulating the relationship between the permeability values and the log responses in Hr-2 firstly and the other studied three wells secondly.

Multiple Linear Regressions as the more accurate procedure used for predicting permeability values from the available log data. The multilinear regression method is an extension from the regression analysis which incorporates independent values, to predict a dependent value (Mohaghehet et al, 1997). In such a case, predicted permeability values from the log data consider as dependent values, whereas the well log data themselves are the independent values.

In this study, the gamma ray, sonic, neutron, and density log data are utilized as independent values to predict the dependent permeability values. By applying this regression method, expectation is that the dependent permeability will negatively relate to independent gamma ray and density log values and positively with sonic and neutron porosity values (Tagavi, 2005).

Equation 3.18 is the best representative for the relationship between the permeability measured from the core test and the permeability predicted from the log data for Jeribe Formation in the well Hr-2.

$$\text{Log K} = 211.0461 + (-0.016569 * \text{GR}) + (0.59611 * \Delta t) + (0.097265 * \text{ØN}) + (-97.5214 * \rho_b) \dots \dots \dots \text{E.q.3.18}$$

Where:

K: permeability.

GR: gamma Ray.

Δt : interval Transit Time.

ØN: neutron Porosity.

ρ_b : bulk Density.

Figure 3.19 shows graphically the rate of matching between the permeability values measured from core testing for Jeribe Formation in the well Hr-2 (depth interval between 491 and 540m) and the calculated permeability values using the equation 3.18 depending on the available log data for the same depth interval.

Being confident with the results obtained for permeability from the log data in the well Hr-2, the same equation of 3.18 has been applied on the log data of Jeribe Formation in the studied wells of Hr-49, Hr-50, and Hr-51 (the calculated permeability values are listed in the appendix B, and shown as plot in the figure 3.20). The qualification description of permeability proposed by North (1985) (Table 3.3) is used for describing and evaluating the calculated permeability for the studied formation.

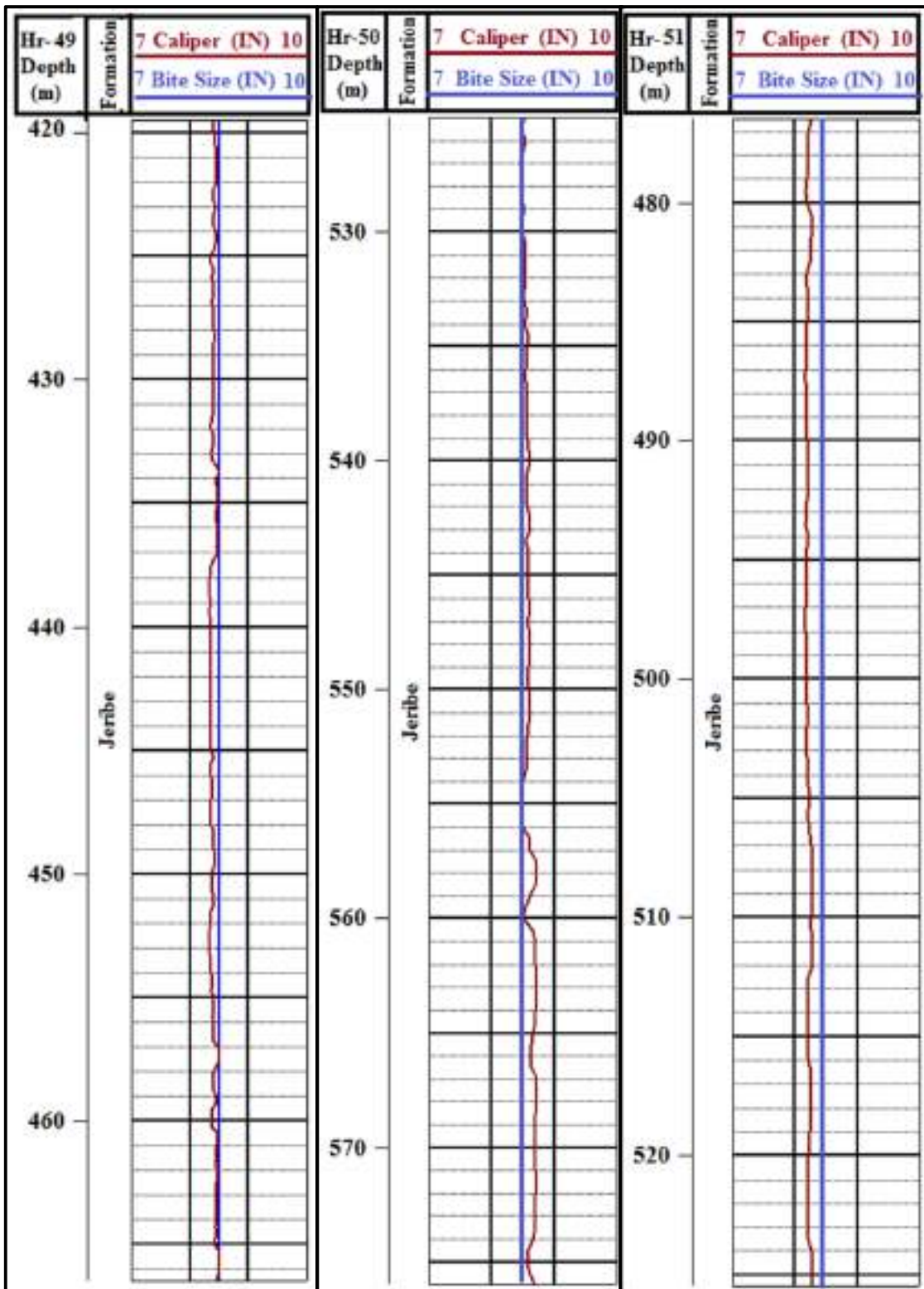


Figure 3.18: Caliper log plot for the studied Jeribe Formation in the wells Hr-49, Hr-50 and Hr-51 with indication to the used bit size in each well.

Table 3.3: Qualitative description of permeability as proposed by North (1985).

Qualitative description	K- value (md)
Poor to Fair	1.0-15
Moderate	15-50
Good	50-250
Very Good	250-1000
Excellent	>1000

As appears in the figure 3.20, the upper 25m of Jeribe Formation in the well Hr-49 owns as average more than 30md permeability, whereas the remaining lower part showed relatively lower permeability (less than 20md as average) including intervals of impermeable or poor zones.

The other two wells of Hr-50 and Hr-51 showed large similarity in the permeability for Jeribe Formation. The upper part of the formation (about 20m thickness) in those two wells showed continuous moderate permeability ranged between 15 and 30md (being relatively higher in the well Hr-51).

The middle part of the formation till the last 5meters showed an obvious fluctuation in the permeability values reflecting noticeable heterogeneity in the reservoir properties of Jeribe Formation. Impermeable, poor, and moderate permeability zones with variable thicknesses can be observed in this part of the formation in the mentioned two wells.

The few meters at the lower most part of the Jeribe Formation showed moderate permeability in the studied three wells.

As a general note, no zones of higher than moderate permeability recorded for Jeribe Formation in this study.

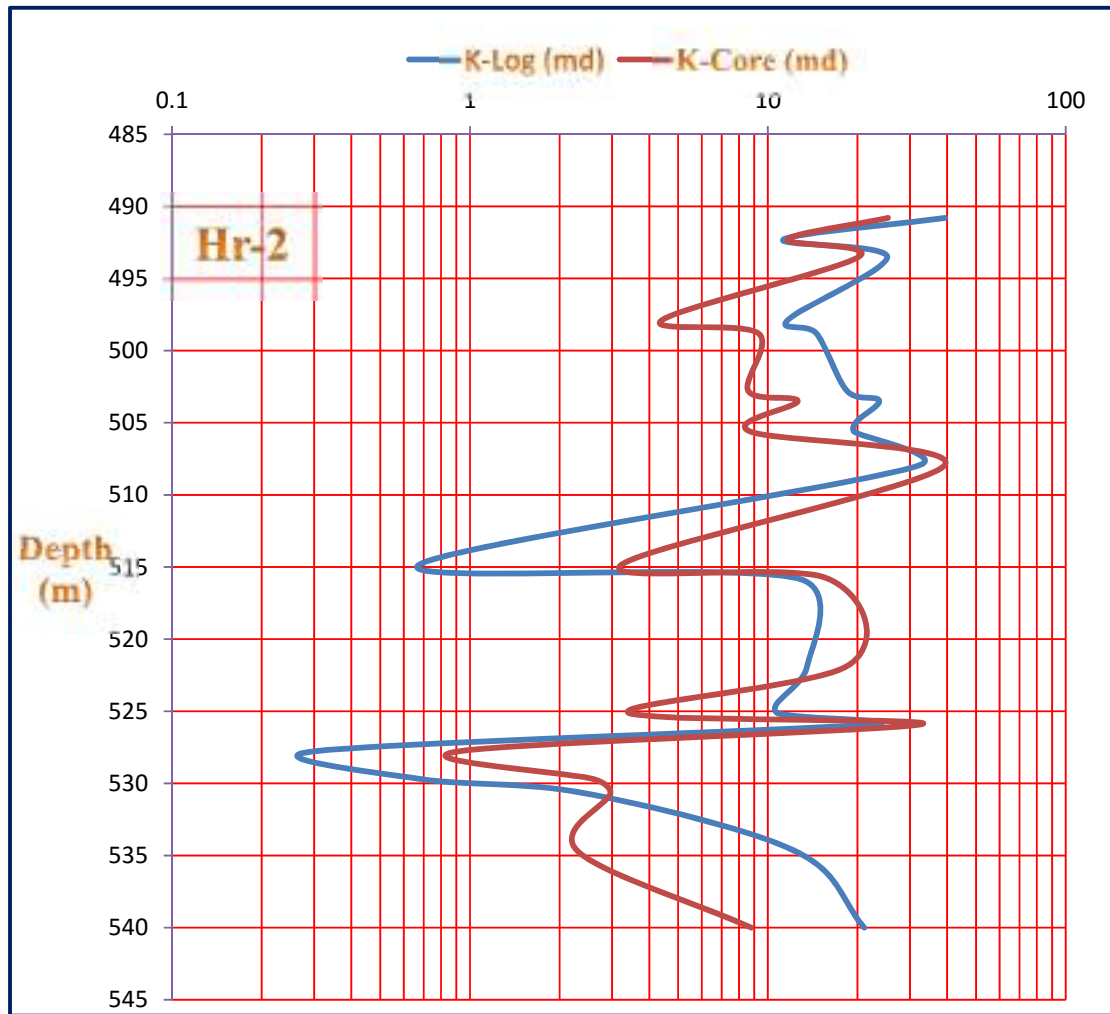


Figure 3.19: The measured permeability from core test analysis (red line) and the permeability values measured from log data (blue line) for the studied Jeribe Formation in the well Hr-2.

3.9 Reservoir Units

In order to distinguish between the horizons of different reservoir capacity and hence subdividing Jeribe Formation in the studied wells to different reservoir units, three main rock properties depended on which are shaleness, porosity, and permeability. Such a subdivision shows only variation in the storage capacity of the units (depending on the shaleness and porosity) and preliminarily their production capacity (depending on the shaleness and permeability) regardless the type of the fluid content.

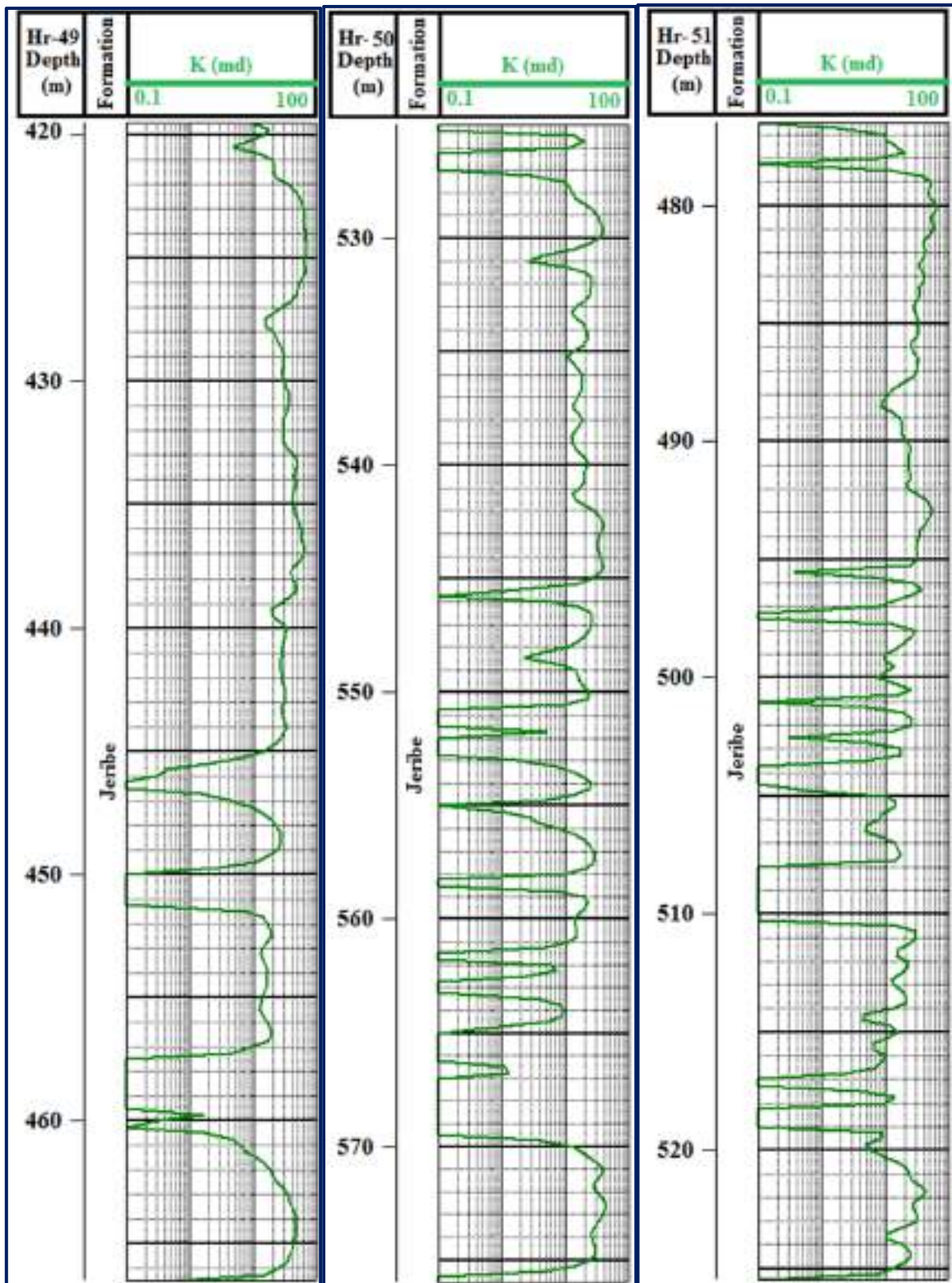


Figure 3.20: Plots of the calculated permeability from the log data for the studied Jeribe Formation in the wells Hr-49, Hr-50, and Hr-51.

The figures 3.21, 3.22, and 3.23 show the division of the Jeribe Formation to reservoir units on the bases of the mentioned parameters in the studied three wells. Tables 3.4, 3.5, and 3.6 summarize the minimum, maximum, and average values of the mentioned three parameters for the distinguished reservoir units of the studied Jeribe Formation in the studied wells Hr-49, Hr-50, and Hr-51 respectively. The tables also show the depth interval of each unit within the studied wells.

It's important to mention that Jeribe Formation in the studied wells did not show distinguishable lateral variations in its lithological properties, so the same reservoir units observed in the three studied wells. This also means that even no diagenetic processes affected the formation laterally in such a different way leading to changing the reservoir properties of the formation in each well from the other. Below is description and evaluation of each reservoir unit.

3.9.1 Reservoir Unit 1 (RU-1)

This unit represents the lower most part of Jeribe Formation (about 5m thickness) with about 11% average shaleness and good porosity. Moderate permeability is obvious feature of this reservoir unit which looks to be partly resulting from vugging or fracturing (especially in the well Hr-49). This unit is composes mainly of limestone and dolomitic limestone in the two wells of Hr-49 and Hr-51 whereas composes of dolostone in the well Hr-50.

3.9.2 Reservoir Unit 2 (RU-2)

This unit is about 16 m thick in the wells Hr-49 and Hr-51 and about 10m thick in the well Hr-50. This unit is characterized by the lowest average shale content among all the distinguished reservoir unit of Jeribe Formation in this study.

Average porosity of this unit in the wells Hr-49 and Hr-51 is about 11%

(moderate porosity) with fair permeability (about average 9.0md) whereas, this unit owns about 16% average porosity (good porosity) with about 5.0md average permeability (poor permeability) in the well Hr-50. Lithologically, this unit composes mainly of limestone and dolomitic limestone.

3.9.3 Reservoir Unit 3 (RU-3)

This unit has about 18m thickness in the wells Hr-49 and Hr-51 with a relatively higher thickness (about 24m) in the well Hr-50. Depending mainly on the variation in the shale content, this unit has been subdivided to two subunits (RU-3A and RU-3B). The lower RU-3A subunit is of the lower average shale content (between 14 and 23%) with porosities ranging in average between 10% and 18% (being highest in the well Hr-50) and fair permeability in the wells Hr-50 and Hr-51 and moderate average permeability in the well Hr-49 (about 29 md). The lithology of this subunit is mainly limestone and dolomitic limestone in the two wells of Hr-49 and Hr-51 whereas composes of dolostone with anhydrite nodules in the well Hr-50.

The reservoir subunit RU-3B is characterized by the highest shale content among the distinguished reservoir units with an average shaleness exceeded 40% in the wells Hr-49 and Hr-50. The average porosity in this subunit ranged between about 11 and 16% with an average moderate permeability ranged between 22 and 27md in the wells Hr-50 and Hr-51, whereas higher average permeability recorded for this subunit in the well Hr-49 reached to about 40md. Vugging and fracturing expected to be the main reason in enhancing the permeability in this shaly reservoir subunit which is mainly composed of argillaceous limestone in Hr-49 and Hr-51 wells whereas argillaceous dolostone is the main lithology composing this subunit in the well Hr-50.

3.9.2 Reservoir Unit 4 (RU-4)

This unit represents the uppermost 10m of Jeribe Formation in the studied wells which is composed mainly of slightly argillaceous limestone and limestone in the wells Hr-49 and Hr-51. The same unit showed slightly argillaceous dolostone and dolostone lithology in the well Hr-50.

Two subunits are distinguished from this reservoir unit namely RU-4A and RU-4B. The subunit RU-4A is characterized by relatively low shale content (average shaleness ranging between about 7% and 18%) and good average porosity (between about 16% and 20%) coupled with moderate average permeability (between about 18 and 47md).

The uppermost 2m of Jeribe Formation is represented by the subunit RU-4B and is characterized by relatively high average shale content (between about 20% and 34%) and poor to moderate average porosity (between about 4% and 11%). Poor to fair permeability is the obvious feature of this subunit with an average permeability of less than 12md.

As a general note and regardless of hydrocarbon saturations, RU-1 and RU-4A are of the best reservoir properties within Jeribe Formation in the studied wells, whereas the subunit RU-3B is of the least reservoir property.

Figure 3.24 shows a lateral correlation between the identified reservoir units in Jeribe Formation as appears in each wells. The most obvious different in the greater thickness of RU-3A in the well Hr-50 in comparison with the other two wells, and in the lower thickness of the RU-2 in the same well in comparison with the other two wells of Hr-49 and Hr-51.

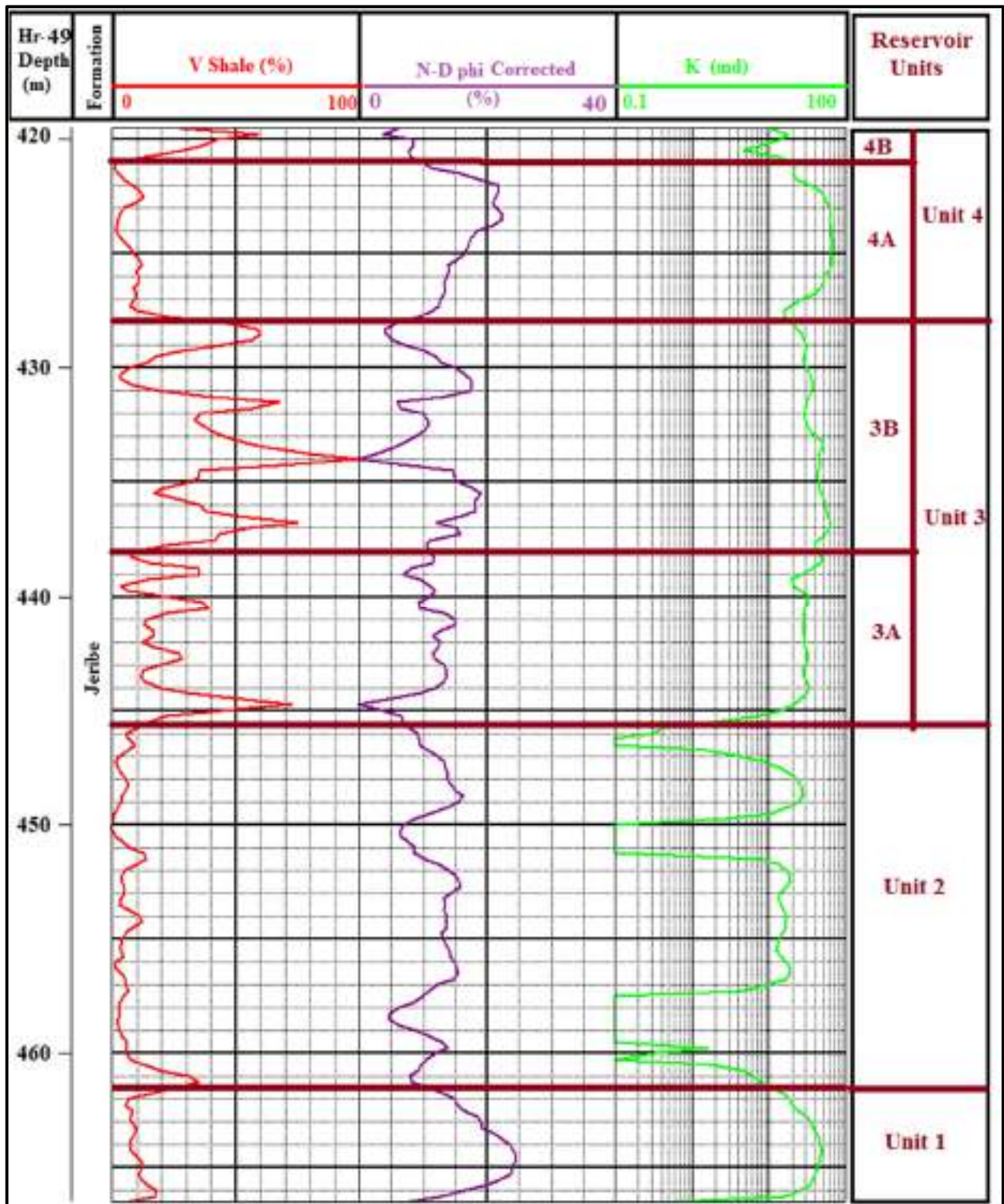


Figure 3.21: Subdivision of the Jeribe Formation to reservoir units on the bases of the porosity, permeability, and shale volume for well Hr-49.

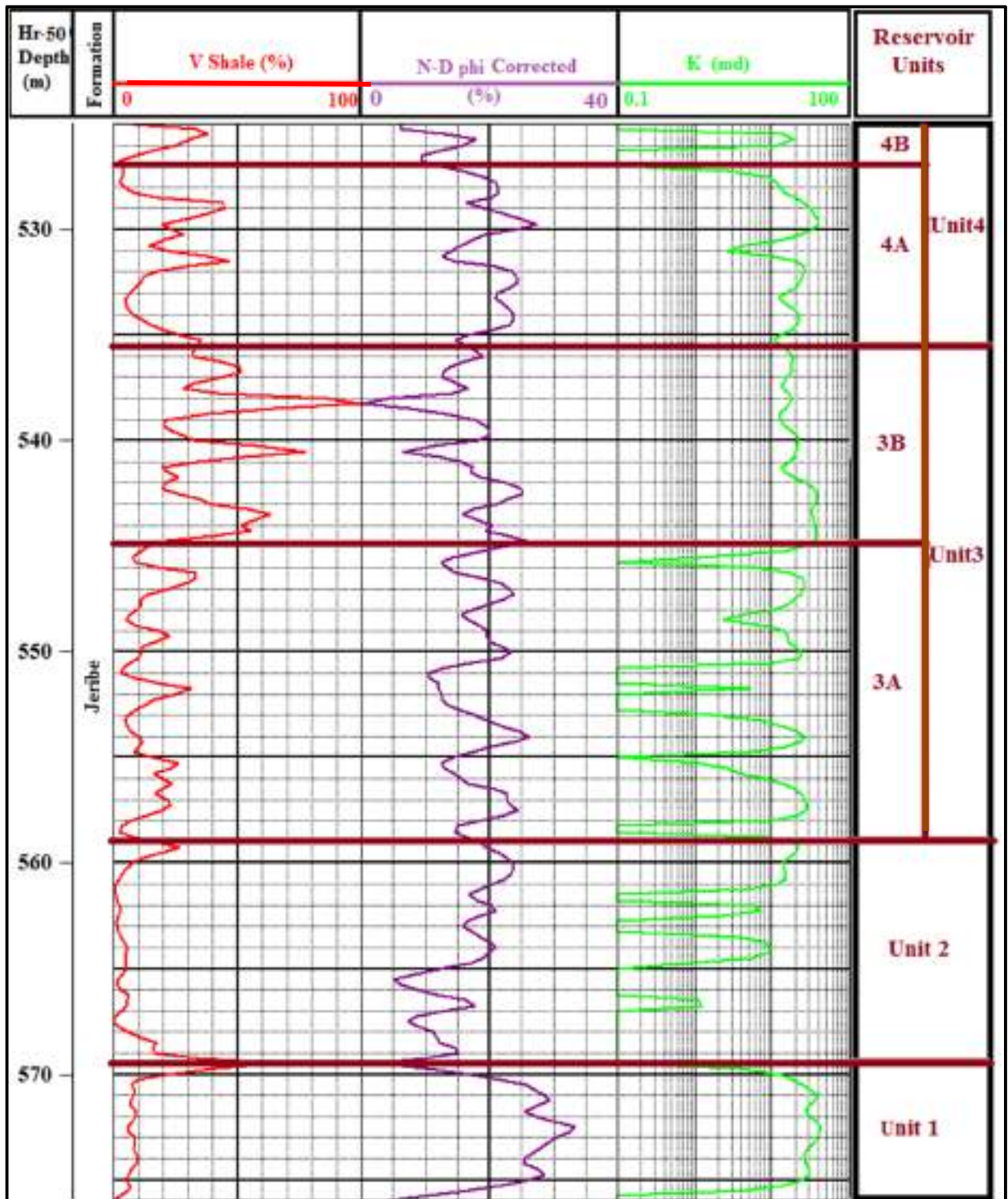


Figure 3.22: Subdivision of the Jeribe Formation to reservoir units on the bases of the shale volume, porosity, and permeability for well Hr-50.

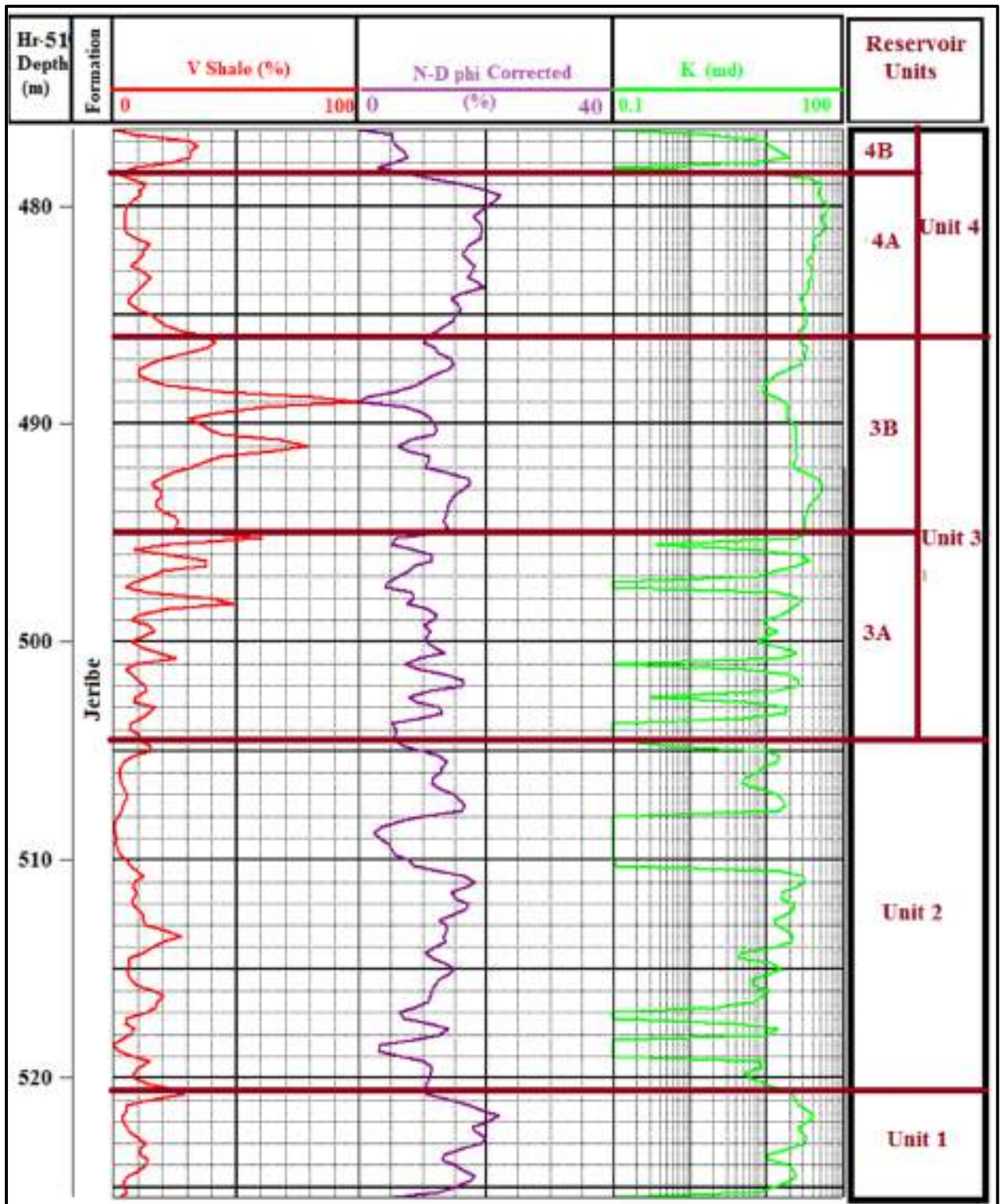


Figure 3.23: Subdivision of the Jeribe Formation to reservoir units on the bases of the shale volume, porosity, and permeability for well Hr-51.

Table 3.4: Minimum, maximum, and average values of shale content, porosity, and permeability for the distinguished reservoir units of Jeribe Formation in the well Hr-49.

Reservoir Units	Depth Interval (m)	Statistics	Vsh (%)	Porosity (%)	Permeability (md)	Main Lithology
RU-4B	421-419	Min	13.15	3.71	4.71	Limestone
		Max	59.06	8.51	17.75	
		Average	34.42	7.11	11.21	
RU-4A	428-421	Min	1.00	9.23	15.39	Slightly Argillaceous limestone
		Max	22.60	22.45	69.30	
		Average	7.68	16.36	47.09	
RU-3B	438-428	Min	3.75	0.00	20.11	Argillaceous Limestone
		Max	99.55	18.95	62.60	
		Average	40.40	11.54	39.82	
RU-3A	445.5-438	Min	3.66	0.00	7.18	Limestone, Calcareous dolostone
		Max	72.88	15.08	47.74	
		Average	23.10	10.59	29.21	
RU-2	461.5-445.5	Min	0.00	4.67	0.00	Limestone, Dolomitic limestone
		Max	34.81	16.25	27.95	
		Average	6.41	11.46	9.09	
RU-1	466.5-461.5	Min	5.43	7.94	0.60	Limestone, Dolomitic limestone
		Max	25.77	24.59	47.89	
		Average	11.07	18.78	31.49	

Table 3.5: Minimum, maximum, and average values of shale content, porosity, and permeability for the distinguished reservoir units of Jeribe Formation in the well Hr-50.

Reservoir Units	Depth Interval (m)	Statistics	Vsh (%)	Porosity (%)	Permeability (md)	Main Lithology
RU-4B	527-525	Min	2.81	6.08	0.00	Dolostone
		Max	37.88	17.75	18.97	
		Average	20.33	11.28	5.54	
RU-4A	535.5-527	Min	2.81	11.87	0.00	Slightly Argillaceous dolostone
		Max	46.51	27.42	39.84	
		Average	18.60	20.14	18.85	
RU-3B	545-535.5	Min	19.60	0.15	12.30	Argillaceous dolostone
		Max	99.57	25.77	38.62	
		Average	41.55	16.58	22.55	

RU-3A	559-545	Min	2.63	10.47	0.00	Dolostone, Limestone with Anhydrite nodules
		Max	33.36	26.16	28.44	
		Average	14.24	18.03	11.87	
RU-2	569.5-559	Min	0.00	5.13	0.00	Limestone, Dolomitic limestone
		Max	33.74	23.70	22.10	
		Average	6.69	16.03	4.93	
RU-1	576-569.5	Min	0.17	2.74	0.00	Dolostone
		Max	65.65	33.28	42.77	
		Average	11.17	23.68	24.74	

Table 3.6: Minimum, maximum, and average values of shale content, porosity, and permeability for the distinguished reservoir units of Jeribe Formation in the well Hr-51.

Reservoir Units	Depth Interval (m)	Statistics	Vsh (%)	Porosity (%)	Permeability (md)	Main Lithology
RU-4B	478.5-476.5	Min	0.43	0.00	0.00	Limestone
		Max	34.24	7.79	19.47	
		Average	21.47	4.98	7.96	
RU-4A	486-478.5	Min	2.07	7.79	12.66	Slightly Argillaceous limestone
		Max	28.46	22.15	62.90	
		Average	10.62	16.98	40.67	
RU-3B	495-486	Min	10.66	0.08	8.78	Argillaceous Limestone
		Max	99.55	17.40	54.38	
		Average	35.41	11.35	27.20	
RU-3A	504.5-495	Min	5.02	4.17	0.00	Limestone, Calcareous dolostone.
		Max	60.52	16.46	36.31	
		Average	17.68	9.65	13.70	
RU-2	520.5-504.5	Min	0.00	2.47	0.00	Limestone, Dolomitic limestone
		Max	27.78	18.24	30.40	
		Average	8.59	11.14	9.10	
RU-1	525.5-520.5	Min	3.17	5.47	0.00	Limestone, Dolomitic limestone
		Max	28.61	22.02	42.38	
		Average	9.86	15.86	22.11	

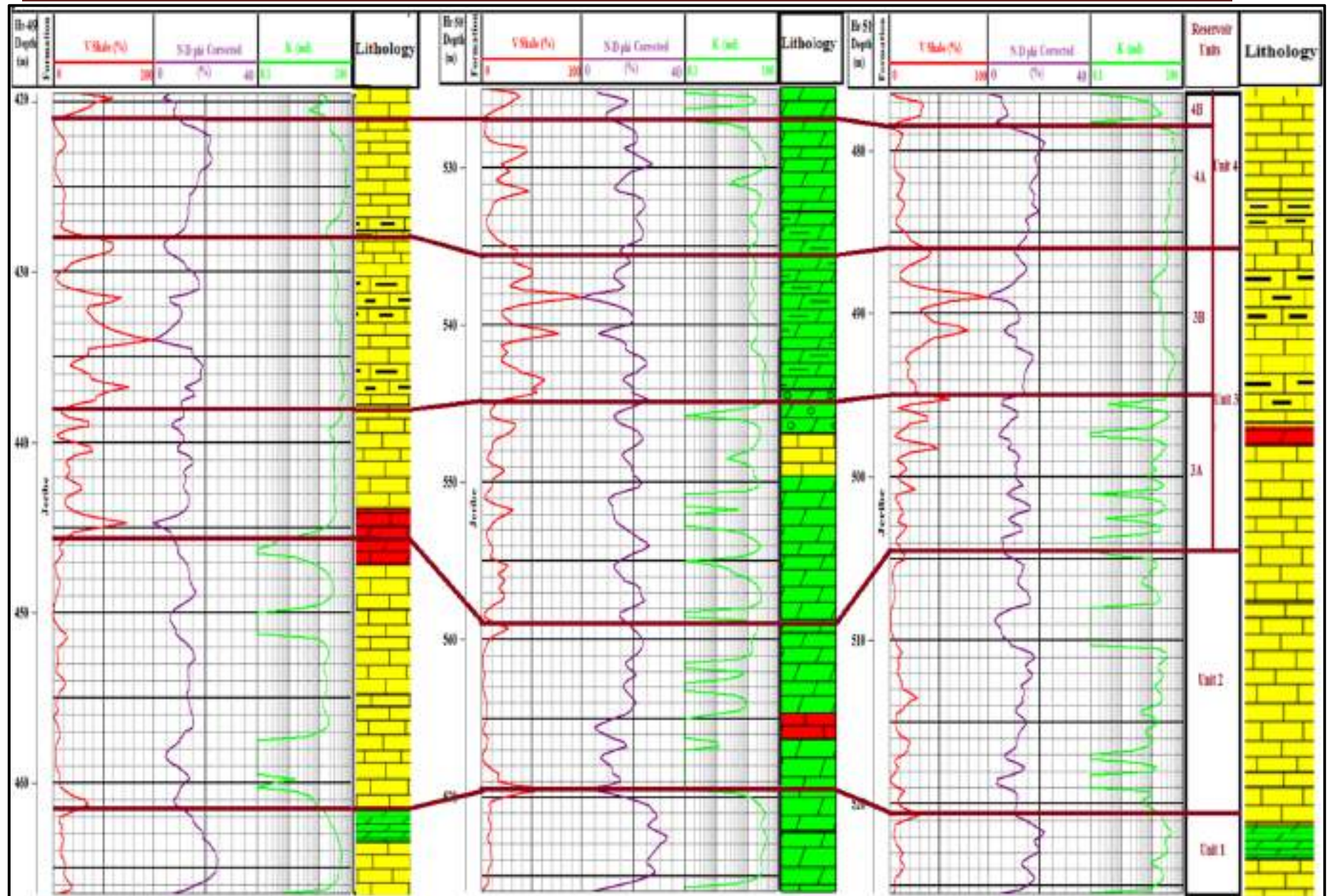


Figure 3.24: Correlation between reservoir units of Jeribe Formation in the wells Hr-49, Hr-50, and Hr-51.



CHAPTER FOUR

Saturations and Reservoir Characterization

4.1 Preface

One of the main goals of reservoir characterization is determining the initial water saturation within the studied formation as it has an enormous impact on the calculation and production of original hydrocarbon in place. Electrical logs are considered as essential tools for determining water saturation because they can provide economically and continuously information about resistivity (reciprocal of conductivity) of the penetrated formation.

The conductivity of any reservoir rock is the result of the presence of water or a combination of water and hydrocarbons in the pore space as a continuous phase. The actual conductivity will depend on the conductivity of the water in the pores and the quantity of water present. Lithology of the rock matrix, its clay content, and its texture (grain size and the distribution of pores, clay, and conductive minerals) also affects conductivity, but to a lesser extent. It's important to mention that conductivity of a reservoir bed will depend strongly on temperature (Ellis and Singer, 2008).

Accordingly, and in order to best evaluate a reservoir, attention should be paid to all of the petrophysical properties of the reservoir which affect calculation of water or hydrocarbon saturation. Non-pay zones within any reservoir bed should be identified to avoid mistakes in calculating reserves or production capacity of the reservoir.

4.2 Resistivity Logs

Resistivity measurement is generally used to estimate the amount of hydrocarbon present in the well depending on resistivity of the formation water (R_w), the amount of water and pore structure geometry. The electric currents are forced to flow in the formation either by direct contact from electrodes, or by induction. The formation resistivity is measured by measuring the currents and voltages produced.

Through resistivity logging we need to know resistivity rather than resistance because resistance is a function not only of the resistivity measured, but also of the geometry of the body of material on which the measurement is being made. The geometry of the body is not of prime interest to the well logger. The measurement that characterizes the rock, as far as fluid content is concerned, is the resistivity and not the resistance (Bateman, 1985).

In this study, the available resistivity log data were resistivity values derived from Microspherically Focused Log (MSFL), Shallow Laterolog (LLS), and Deep Laterolog (LLD) which their values represented resistivity of flushed zone (R_{xo}), resistivity of transition zone (R_i), and resistivity of uninvaded zone (R_t , true resistivity) respectively.

Appendix A contains the recorded values of resistivity for Jeribe Formation in the studied wells, whereas figure 4.1 shows the plots of the mentioned resistivity values.

The feature of the separation between the three resistivity curves most of the time gives an idea about the expected fluid type within the reservoir pore spaces (with giving attention to the type of the drilling mud).

As the used drilling mud for the three studied wells was of fresh water base, a relatively high resistivity values were expected to be seen along the studied section of Jeribe Formation. Accordingly, non-separated curve intervals were considered to be of most interest and most likely to be intervals

containing hydrocarbons. Among the non-separated curve intervals, the zones of low resistivity values are the most interest because those zones are most the time porous intervals (low matrix content and hens low resistivity).

The deflection of the three resistivity curves in the three studied wells are quite correlatable especially deflection of the two curves of R_i and R_t . Separation of the R_{xo} curve from the other two curves in some intervals (especially in the wells Hr-49 and Hr-50) in a different way in each well is mainly due to the effect of borehole wall condition and the nature of the mudcake (R_{xo} resistivity value represents a very shallow investigation depth of the reservoir from the borehole wall). Variations in water saturations or high ratio of residual hydrocarbons should also be expected to be a reason causing such separation of the R_{xo} curve.

Non-separation or low separation is the common feature of the three resistivity curves especially in the well Hr-51 as seen in figure 4.1. Accordingly, hydrocarbons with different saturations are expected to be existing in Jeribe Formation in the studied wells.

4.3 Water Saturation (S_w)

Water saturation as defined by Asquith and Gibson (1982) "is the percentage of pore volume in a rock which is occupied by formation water". S_w is the symbol used for expressing water saturation which is measured in percent or fraction.

Calculating water saturation is very important as it helps in determining hydrocarbon saturation of a reservoir and that by subtracting water saturation from the value 1.0 which is equal to 100% water saturation.

Resistivity logging tools with different radial depth of investigation capacity are used to evaluate water saturation in the uninvaded zone (virgin zone with no effect of mud filtrate) and water saturation in the invaded zone (flushed zone where mud filtrate replaces the reservoir movable fluids).

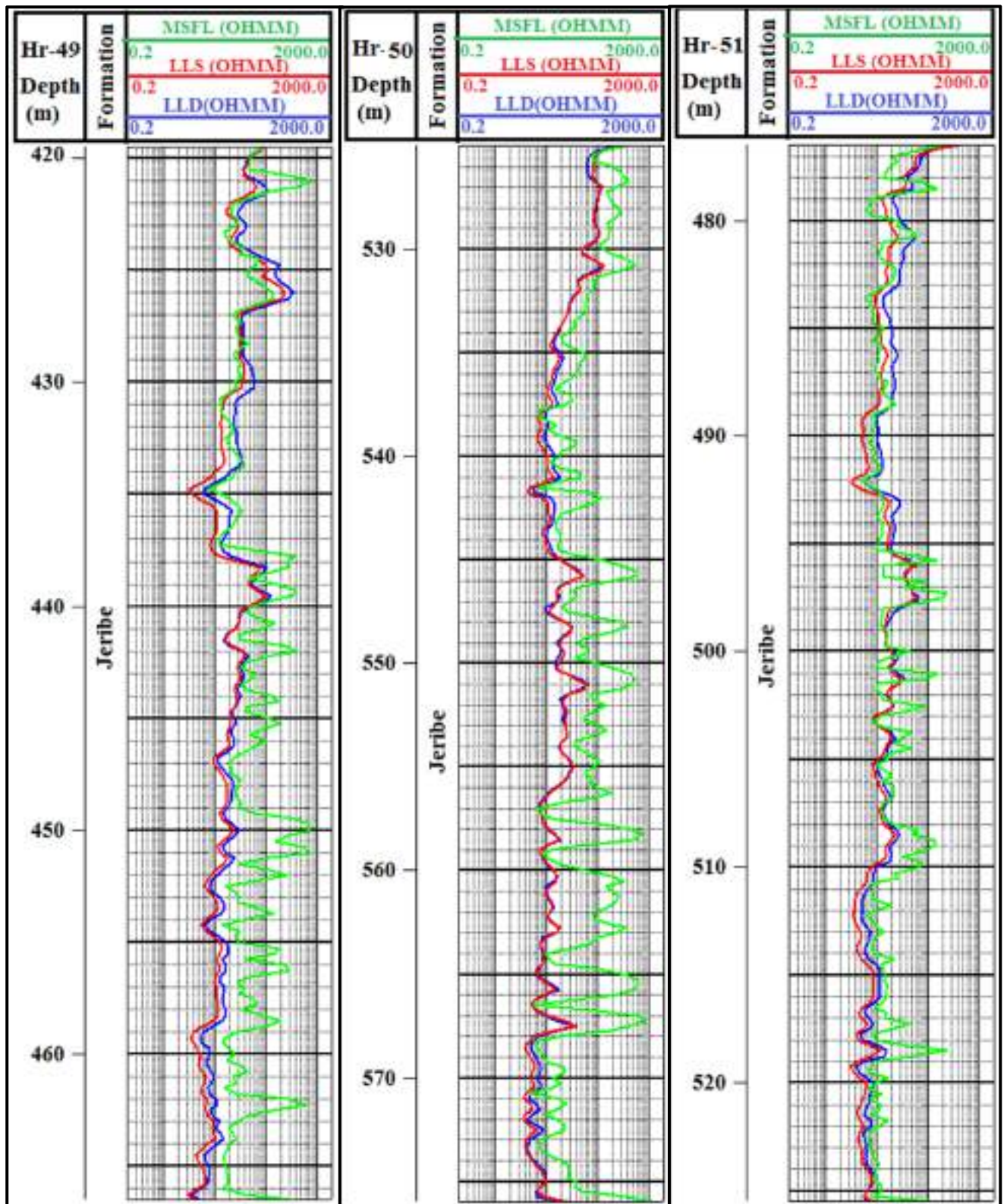


Figure 4.1: The readings of the LLD, LLS, and MSFL logs for the studied Jeribe Formation in the wells Hr-49, Hr-50 and Hr-51.

Archie equation (Eq.4.1) is the most popular equation used for calculating water saturation from log data.

$$S_w = \sqrt[n]{\frac{F \cdot R_w}{R_t}} \dots\dots\dots \text{E.q.4.1}$$

Where:

S_w : Water saturation in the uninvaded zone (in fraction)

F : Formation resistivity factor

R_w : Formation water resistivity (in $\Omega.m$)

R_t : True resistivity (in $\Omega.m$)

n : Saturation exponent (its value ranges from 1.8 to 2.5 but mostly equal to the value 2.0 which is also the value used in this study)

Formation resistivity factor (F) as suggested by Archie (1942 in Asquith and Gibson, 1982) can be related to porosity by the following equation:

$$F = \frac{a}{\phi^m} \dots\dots\dots \text{Eq. 4.2}$$

Where:

F : Formation resistivity factor

a : Tortuosity factor (complexity of the paths and is equal to the value 1.0 for carbonates, the case of this study)

ϕ : Porosity

m : Cementation factor

On the other hand, water saturation in the flushed zone (S_{xo}) also similarly can be calculated using Eq.4.3 in which formation water resistivity (R_w) replaced by mud filtrate resistivity (R_{mf}) and true resistivity (R_t) replaced by resistivity of the flushed zone (R_{xo}).

$$S_{xo} = \sqrt[n]{\frac{F \cdot R_{mf}}{R_{xo}}} \dots\dots\dots \text{Eq.4.3}$$

Where:

S_{xo}: Water saturation in the flushed zone (in fraction)

F: Formation resistivity factor.

R_{mf}: Resistivity of mud filtrate (in $\Omega.m$)

R_{xo} : Resistivity of the flushed zone (in $\Omega.m$)

As appears from the equations of water saturation calculation (Eq.4.1& Eq.4.3), more than one factor should be determined for water saturation to be precisely calculated. Formation water saturation (R_w) and Cementation factor (m) are the two critical factors that should be determined following certain procedures as will described in the following sections.

4.3.1 Calculation of Formation Water Resistivity (R_w)

Formation water or so called "connate water" is the water held by capillary pressure in the pores of the reservoir rock which serves to inhibit the transmission of hydrocarbons. This water takes up space both in the pores and in the throats between pores. As a consequence, it may block or reduce the ability of hydrocarbons to move through the rock (Asquith and Gibson, 1982).

Formation water resistivity (R_w) can be found from the readings of the SP log, water catalogs, produced water sample, or water saturation equation in a 100% water bearing reservoir (Schlumberger, 1989).

One of the methods for determining the value of R_w (which is also used in this study) is through the readings of Spontaneous Potential log (SP) by following a known procedure explained by Asquith and Gibson (1982), Bateman (1985), Asquith and Krygowski (2004), Schon (2015), and others.

As no runs of SP log done in the studied wells of Hr-49, Hr-50, and Hr-51, therefore data of SP log for Jeribe Formation in the well Hr-2 (Fig. 4.2) has been used for determining the value of the R_w. Although fresh mud is used in drilling this well no intense deflection can be seen in the curve of the SP log.

Such a case may be due to low permeability of the zone or existence of hydrocarbons.

Table 4.1 shows the values of the factors and parameters used for calculating the value of the R_w in the Hr-2 well which appeared to be 0.05 $\Omega.m$.

Table 4.1: Calculated R_w and other parameters for the studied Jeribe Formation in the well Hr-2.

Parameter	Value
SP reading	-12millivolt
Depth of SP reading	513m
Rmf@ Ts (83°F)	0.547 $\Omega.m$
Rmf@ Tf (103°F)	0.42 $\Omega.m$
BHT	108°F
R_w	0.05 $\Omega.m$

4.3.2 Determining the value of the Cementation Factor (m)

Cementation factor (m) reflects the nature of grain size, grain size distribution, and the complexity of the paths between pores known generally as tortuosity which in turn depends mainly on type of lithology and the diagenesis activity. The higher the value for tortuosity, the higher the m value.

The values of cementation factor range from about 1.3 to as high as 3.0. The values of m most commonly applied to log interpretation problems range from 1.8 to 2.2 (Asquith, and Krygowski, 2004).

The common known methods for determining the value of cementation factor for any reservoir are either through special core analysis or through using Pickett crossplot.

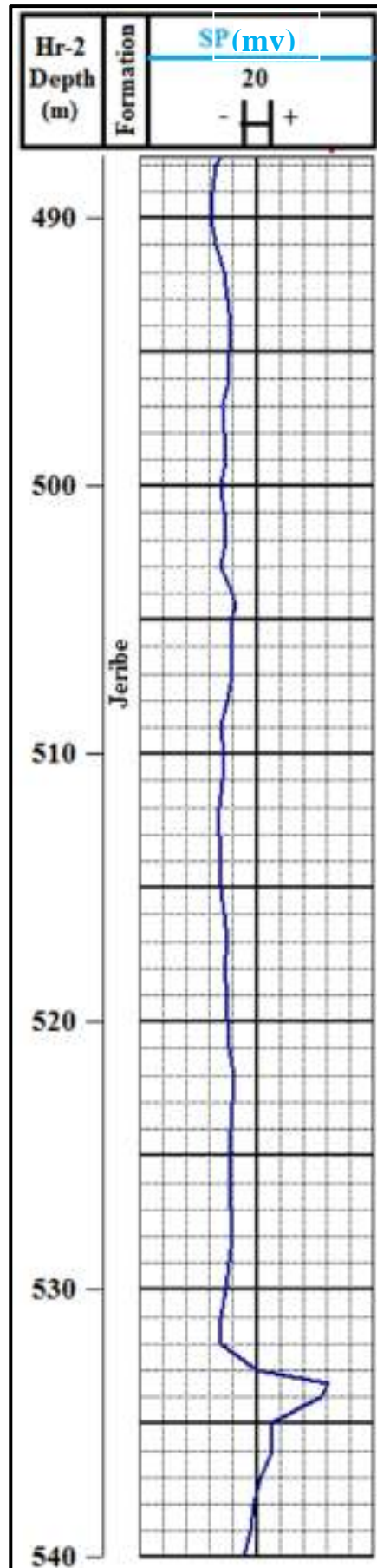


Figure 4.2: The Data SP log for the Jeribe Formation in the well Hr-2.

In this study the second method was used in which the calculated values of porosity (ϕ) plotted against their readings of true resistivity (Rt) on a log-log paper with paying attention to the value of R_w which represents the value of resistivity in no matrix case (100% porosity). According to this method the line connecting between the points of lowest resistivity in each porosity case starting from the R_w value is plotted in which the slope of this line will represent the value of the cementation factor (Figs. 4.3-4.5).

The calculated values of cementation factor for Jeribe Formation in the three studied wells Hr-49, Hr-50, and Hr-51 are 1.81, 1.78, and 1.80 respectively as appears from the figures 4.3 to 4.5.

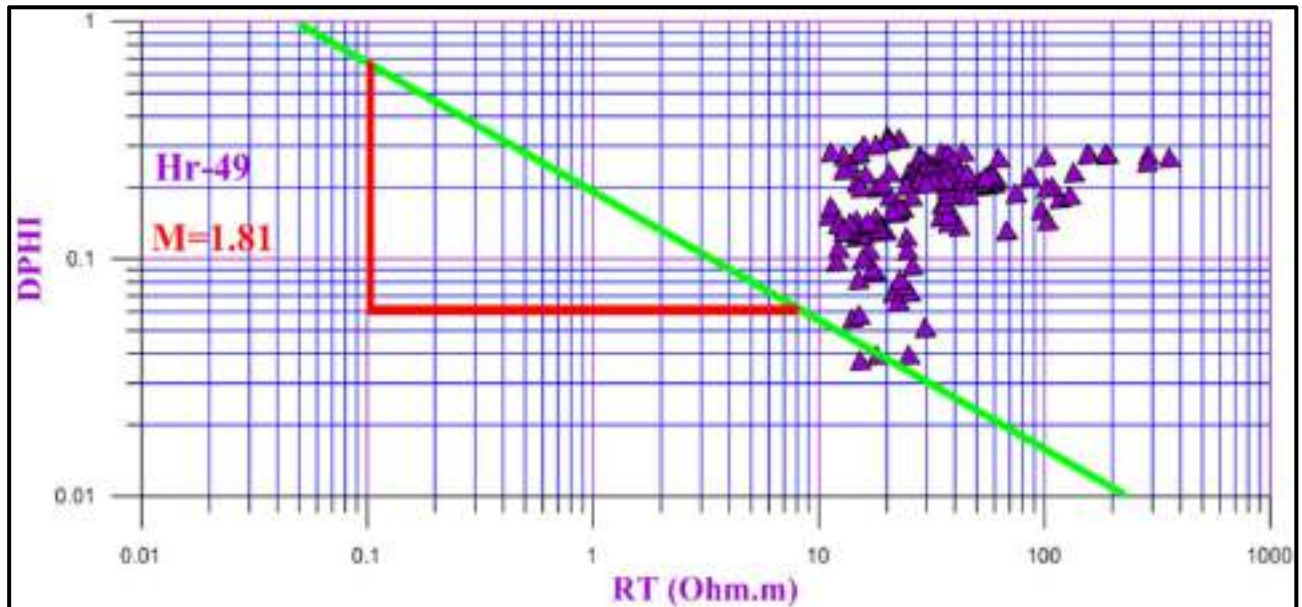


Figure 4.3: Cementation factor (m) from Pickett crossplot for Jeribe Formation, well Hr-49.

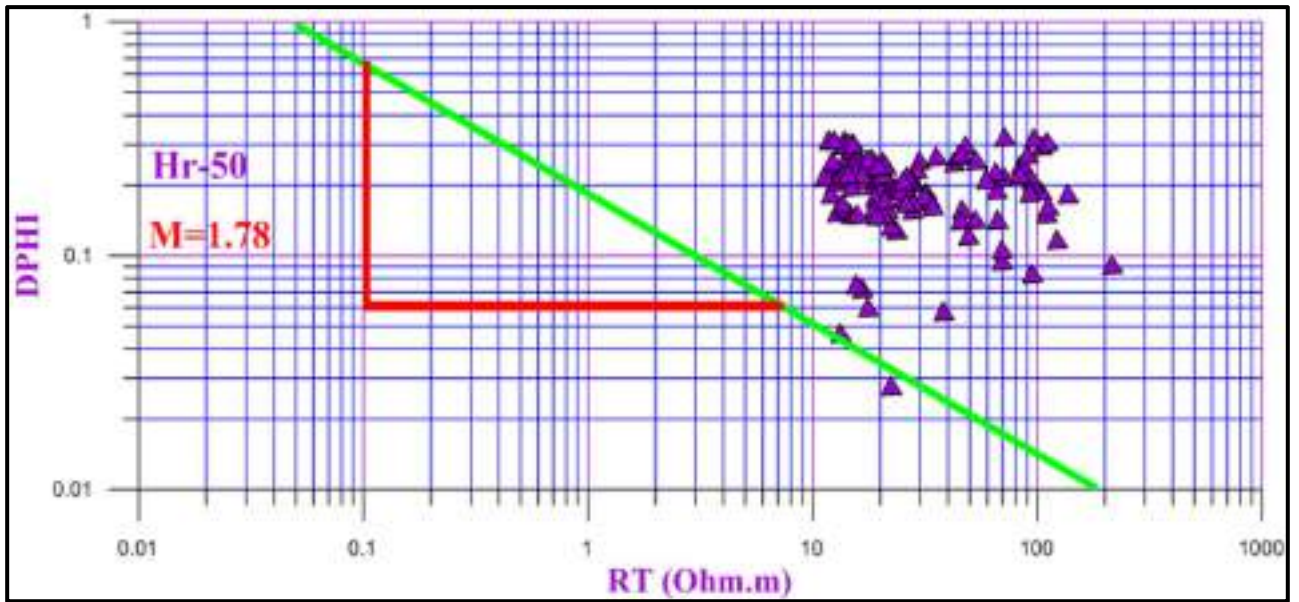


Figure 4.4: Cementation factor (m) from Pickett crossplot for Jeribe Formation, well Hr-50.

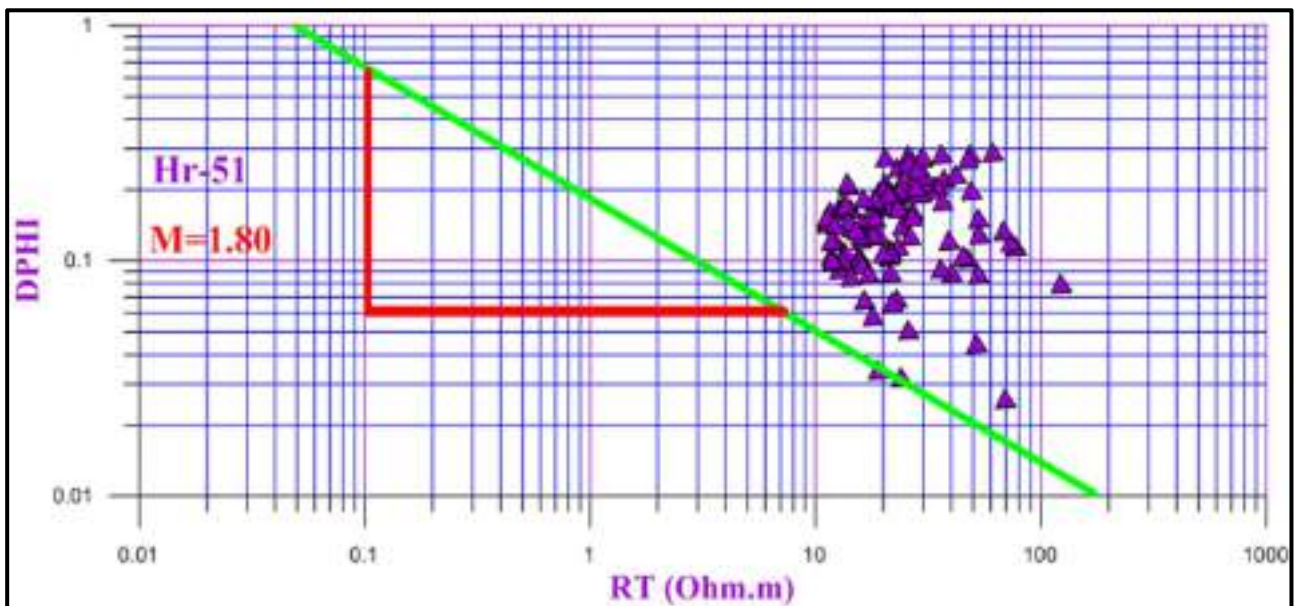


Figure 4.5: Cementation factor (m) from Pickett crossplot for Jeribe Formation, well Hr-51.

4.4 Calculation of Water and Hydrocarbon Saturations in the studied wells

As values for all the requested factors become available for applying Archie's equation, water saturations for Jeribe Formation in the studied wells have been calculated and listed in the appendix C and plotted as curve line with regard to the porosity value in the figure 4.6(the blue field). As appears from the values and from the figure, the upper part of the Jeribe Formation contains lower percent of water saturation than the lower part (as was expected). It's also noticed that water saturation in the well Hr-51 is relatively higher than the other two studied wells especially in the lower part of Jeribe Formation. It has been noticed also that narrow zones (less than one meter) of full water saturation exist in more than one depth interval in the studied wells (depth 443m in Hr-49, depth 537m in Hr-50, and depths 488, 508, and 518m in the well Hr-51).

Hydrocarbon saturations for Jeribe Formation also have been simply calculated by subtracting the value of water saturation in each depth from the value 1.0. Residual hydrocarbon saturations also calculated through the following equation:

$$\mathbf{Rhs = 1.0 - Sxo} \dots \dots \dots \text{Eq.4.4}$$

Where:

Rhs: Residual hydrocarbon saturation

Sxo: Water saturation in the flushed zone

The values of hydrocarbon saturations and residual hydrocarbon saturations are listed in the appendix C and shown in the figure 4.6 as red + green field and red field respectively.

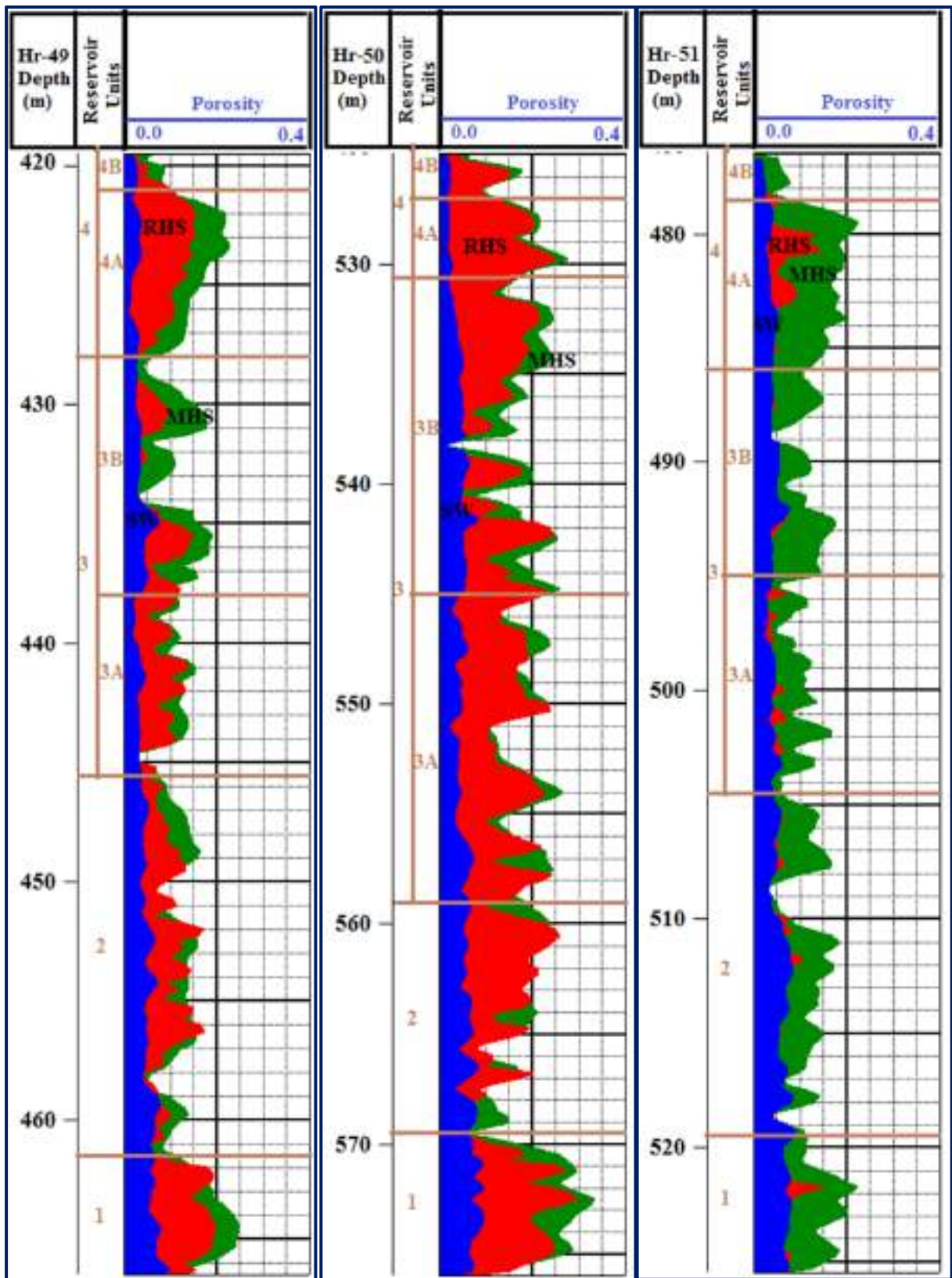


Figure 4.6: Water saturation and Hydrocarbon saturation (Residual and Movable) with regard to porosity for the studied Jeribe Formation in the wells Hr-49, Hr-50 and Hr-51.



The most noticeable feature of the hydrocarbon saturations in the figure 4.6 is that Jeribe Formation in the well Hr-51 contains the least residual hydrocarbon saturations, whereas most of the existed hydrocarbons within the formation in the well Hr-50 are residual hydrocarbons. Such a condition may be related mainly to the nature of the reservoired hydrocarbons in the well Hr-50 which is expected to be mostly oil, whereas the hydrocarbon type in the other two wells is expected to be mostly gas especially in the well Hr-51 (Chapter Three).

4.5 Quick Look Methods

Quick Look Methods (QLM) "are helpful to the geologist because they provide flags, or indicators, that point to possible hydrocarbon zones requiring investigation" (Asquith and Krygowski, 2004).

Most quick look methods are widely used by log analysts for wellsite evaluations and they can be applied without any special equipment and produce quite acceptable results. Their great appeal lies in their simplicity and subtlety and their analysis refers to a number of techniques for plotting log data in a reasonably effortless and simple way that reveals either the formation content or the formation lithology (Bateman, 1985).

The main three branches of quick look analysis include compatible overlays of curves, crossplots of selected curve readings, and simple algorithms for calculators.

In this study, and depending on the available log data, a logarithmic Movable Oil Plot (MOP) is used as a quick look method to detect existence of movable oil and to trace the ratio of residual to movable hydrocarbons. This technique need that two overlays be made, one to indicate S_w and a second to indicate S_{xo} .

The production of a MOP proceeds in two stages. First, the formation factor (F) curve is normalized to true resistivity of the uninvaded zone (R_t) in

a wet zone and the resulting wet resistivity (R_o) curve traced onto the resistivity log. Second, the F curve is normalized to the resistivity of the flushed zone (R_{xo}) trace in a wet zone, and the resulting R_{xoo} curve ($R_{xoo} = R_{xo}$ in a rock 100% saturated with a fluid of resistivity R_{mf}) is traced onto the resistivity log.

Figure 4.7 shows the way that the three curves of R_o , R_{xoo} , and R_t are overlay. As a quick look analysis, water bearing zones should show non-separation of the three mentioned curves, whereas hydrocarbon bearing zones should show separation between the curves with being R_t curve of the highest value.

As seen in figure 4.7, there is a clear separation between the R_o and the R_t curves in all of the reservoir units of Jeribe Formation in the three studied wells indicating to being Jeribe a hydrocarbon bearing formation (except the previously mentioned water bearing narrow horizons). High residual hydrocarbon saturation intervals can be detected when a clear separation between the three curves can be observed (as the case of RU-4 in the three studied wells, and RU-1 with RU-3A in the wells Hr-49 and Hr-50). Zones of high movable hydrocarbon saturation shows clear separation between R_o and R_t curves with no separation between R_{xoo} and R_t curves or even being R_{xoo} of higher resistivity value than R_t (as the case of RU-1, RU-2, and RU-3A in the well Hr-51).

According to this technique, the space between the R_o and R_t curves is representative of the hydrocarbon filled pore spaces (moveable plus residual hydrocarbons). The detail about the ratio between residual and movable hydrocarbons can be detected from the wideness of the spaces between the three curves (residual between R_o and R_{xoo} curves, movable between R_{xoo} and R_t curves). So, such a presentation helps in identifying the most productive intervals within the studied reservoirs.

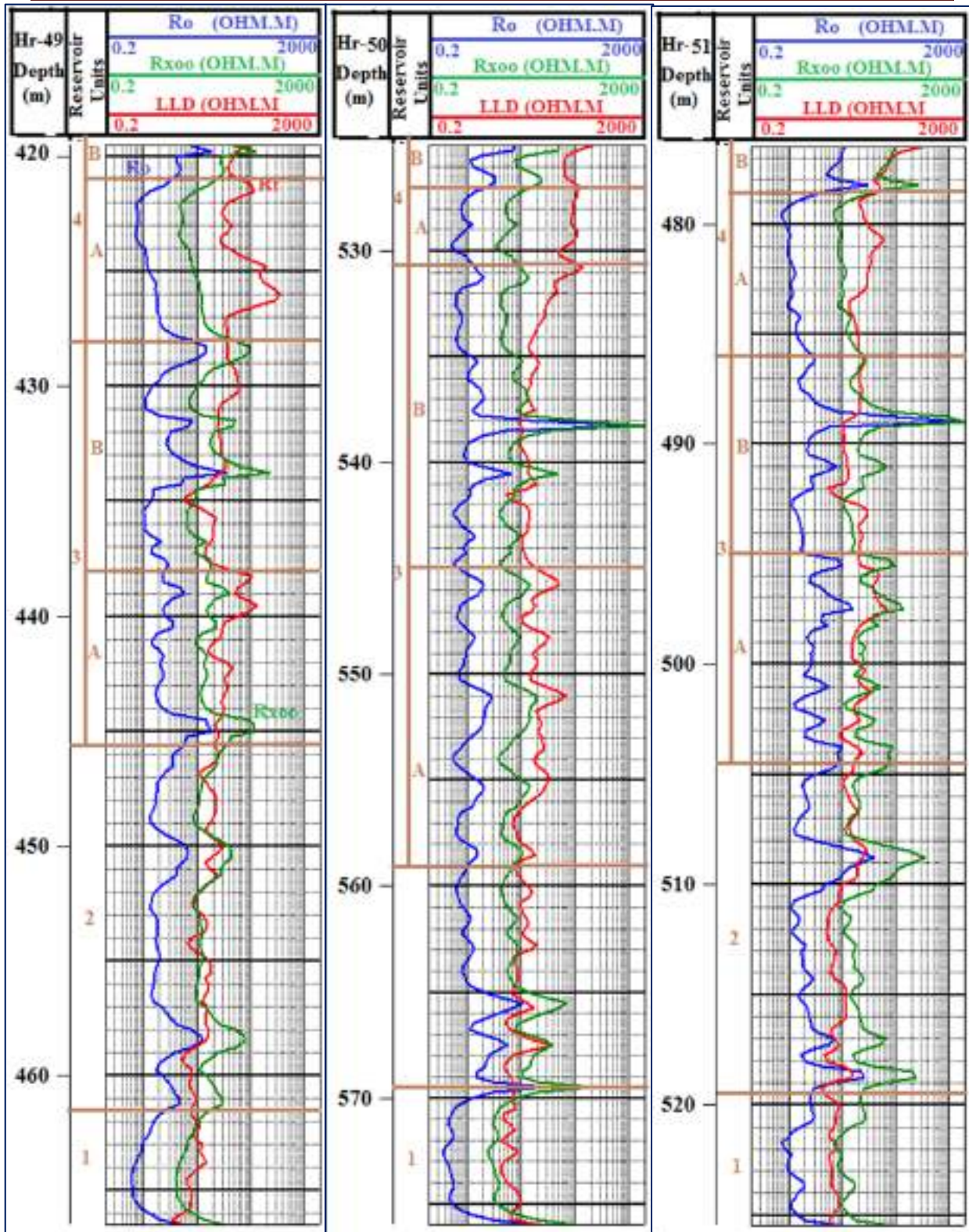


Figure 4.7: R_o , R_{xoo} , and R_t curves as QLM (Movable Oil Plot) for Jeribe Formation in the three studied wells of Hr-49, Hr-50, and Hr-51.

4.6 Bulk Volume Water (BVW) calculation

Bulk Volume Water is the product of the reservoirs water saturation and its porosity as shown in equation 4.5.

$$\mathbf{BVW = S_w * \emptyset} \dots\dots\dots \text{E.q. 4.5}$$

Where:

BVW: Bulk Volume Water

S_w: Water Saturation of uninvasion zone

∅: Porosity

When values of BVW at different depths of a reservoir appear to be constant or very close to constant that means the reservoir is homogeneous and it's at irreducible water saturation (S_{wirr}) condition (Asquith and Gibson, 1982). Any reservoir at irreducible water saturation produces water free hydrocarbons, whereas reservoirs not at irreducible water saturation commonly show wide variations in the values of BVW.

As the amount of water hold by capillary pressure in a reservoir will increase with decreasing grain size, therefore the BVW values also increase with decreasing grain size (Asquith and Krygowski, 2004). The relationship of BVW values to decreasing grain size and lithology is shown in the table 4.2.

In this study, Buckles plot is used to find out which of the identified reservoir units of Jeribe Formation are in irreducible water saturation condition and which are not. Buckles plot according to Asquith and Krygowski (2004) is a graph of porosity versus water saturation suggested by Buckles in 1965. Points of equal BVW form hyperbolic curves across this plot. If BVW is plotted using data from a formation at irreducible water saturation, the points fall along a single hyperbolic curve. If the data come from reservoirs with higher percentages of produced water, the points are more scattered.

Table 4.2: BVW as a function of grain size and lithology (comparative table),(after Asquith and Krygowski, 2004).

Lithology	Grain Size in Millimeters	BVW
<i>Clastic</i>		
Coarse	1.0 to 0.5	0.02 to 0.025
Medium	0.5 to 0.25	0.025 to 0.035
Fine	0.25 to 0.125	0.035 to 0.05
Very Fine	0.125 to 0.062	0.05 to 0.07
Silt	< 0.0625	0.07 to 0.09
<i>Carbonate</i>		
Vuggy		0.005 to 0.015
Vuggy and Intercrystalline (intergranular)		0.015 to 0.025
Intercrystalline		0.025 to 0.04
Chalky		0.05

The calculated BVW for the identified reservoir units of Jeribe Formation in the studied wells are listed in appendix C and their Buckles plot are shown in the figures 4.8 - 4.10.

As a rule of thumb, reservoirs in irreducible water saturation condition show decreasing in water saturation as porosity increases, otherwise production of water in different rates become expectable.

By observing figures 4.8 to 4.10, different cases of relationship between porosity and water saturation values can be seen reflecting variable values of BVW.

RU-1 showed nearly constant distribution of BVW values mostly around 0.06 hyperbolic line in the three studied wells, whereas RU-2 showed much scattered points around 0.04 and 0.06 BVW hyperbolic lines in the wells Hr-49 and Hr-50 with much more scattering points reaching till the hyperbolic line of 0.08 value in the well Hr-51.

Most of the BVW points related to the reservoir subunit RU-3A concentrated around the hyperbolic line value 0.04 especially in the well Hr-51, whereas the points additionally scattered toward the line 0.02 in the well Hr-49 and toward the line value 0.06 in the well Hr-50. The reservoir subunit RU-3B showed a little bit different condition than RU-3A by concentrating of the BVW points mostly around the hyperbolic line of 0.04 especially in the well Hr-49 with scattering points toward the hyperbolic line of 0.06 also in the wells Hr-50 and Hr-51.

Finally, the points of BVW related to the reservoir unit RU-4 generally showed concentrating around the hyperbolic line value 0.02 especially the subunit RU-4B with scattering towards the 0.04 value BVW hyperbolic line in the subunit RU-4A particularly in the wells Hr-50 and Hr-51.

As a general conclusion, the reservoir units of Jeribe Formation in the studied wells can produce hydrocarbons with different rates of water. The less expected produced water is in the reservoir unit RU-1 and the reservoir subunit RU-4B, and the highest expected water production is in the reservoir subunit RU-3A, the remained reservoir units and subunits are expected to produce hydrocarbons with different rates in between depending on the porosity and saturation of each interval.

On the other hand, and according to the relationship between BVW values and the expected types of porosity as a function of grain size and lithology (table 4.2), the existence of vuggy porosities are much more expected to be seen in the reservoir unit RU-4 (upper part of Jeribe Formation) and much more chalky porosities in the lower part of the formation (RU-1) with being the middle part of mostly intercrystalline.

4.7 Moveability of Hydrocarbons

According to Asquith and Krygowski (2004); "Water saturation of the flushed zone (S_{xo}) can be used as an indicator of hydrocarbon moveability. For example, if the value of S_{xo} is much larger than S_w , then hydrocarbons in the flushed zone have probably been moved or flushed out of the zone nearest the borehole by the invading drilling fluids (R_{mf})".

What is known as the *ratio method* is an identification of the hydrocarbons from the difference between water saturations in the flushed zone (S_{xo}) and the uninvaded zone (S_w). When the equation of S_w calculation (Eq. 4.1) is divided by the equation of S_{xo} calculation (Eq. 4.3), the following equation is results:

$$\frac{S_w}{S_{xo}} = \sqrt{\frac{\frac{R_{xo}}{R_t}}{\frac{R_{mf}}{R_w}}} \dots\dots\dots \text{Eq. 4.6}$$

If the ratio S_w/S_{xo} (known as Moveable Hydrocarbon Index, MHI) is equal to or greater than 1.0, then hydrocarbons were not moved during invasion (regardless of whether or not a formation contains hydrocarbons). Whenever the ratio S_w/S_{xo} is less than 0.7 for sandstones or less than 0.6 for carbonates, moveable hydrocarbons are indicated (Schlumberger, 1972).

MHI values have been calculated for the identified reservoir units of Jeribe Formation in the studied wells and listed in the appendix C Plotting the MHI values as curve lines is shown in the figure 4.11.

As the studied Jeribe Formation is composed of carbonate lithology, the 0.6 value is used as cutoff value to separate the zones containing moveable hydrocarbons from non-moveable hydrocarbon zones (or zones with no hydrocarbon content).

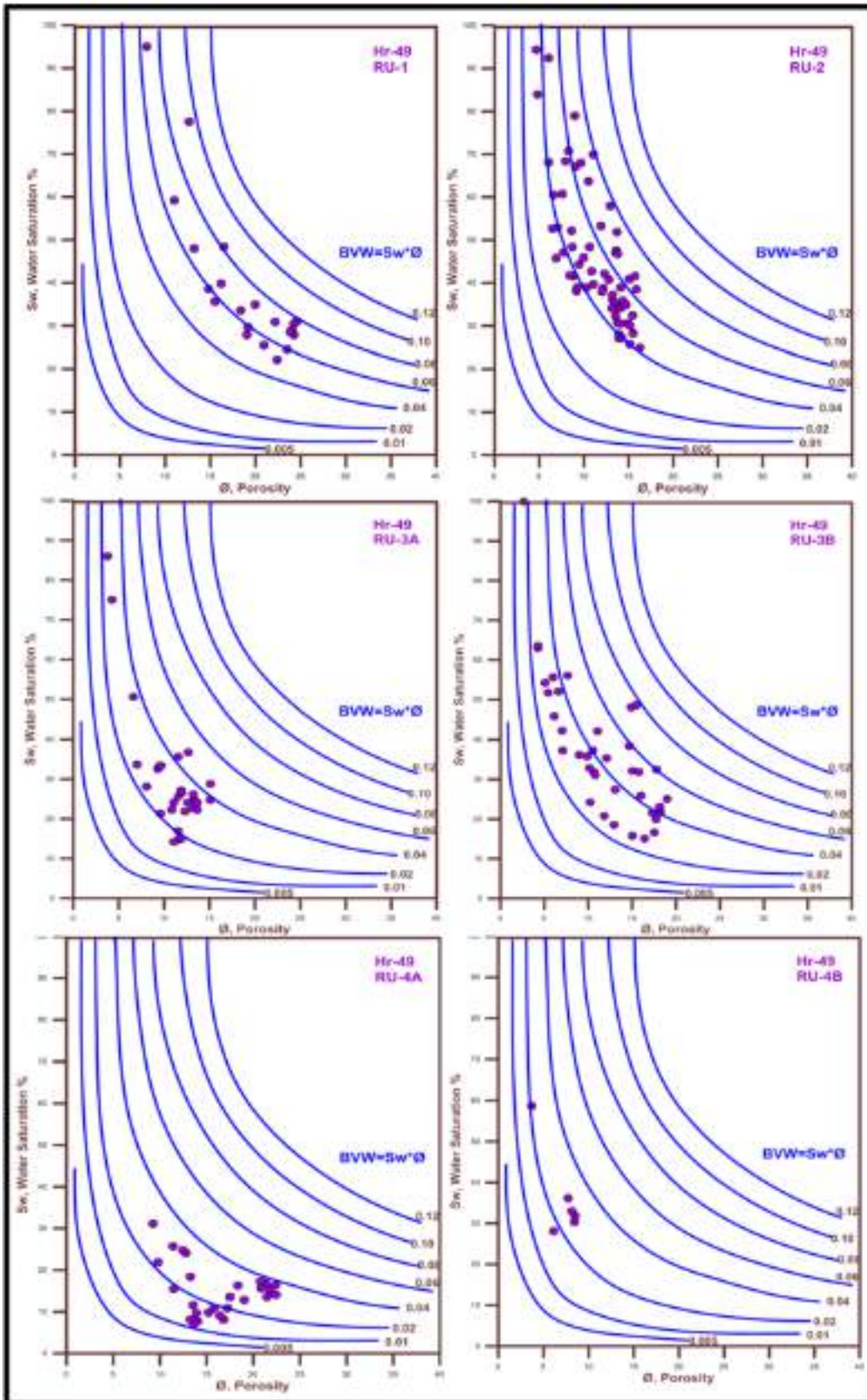


Figure 4.8: Buckles plot for the values of BVW for the reservoir units and subunits of Jeribe Formation in the well Hr-49.

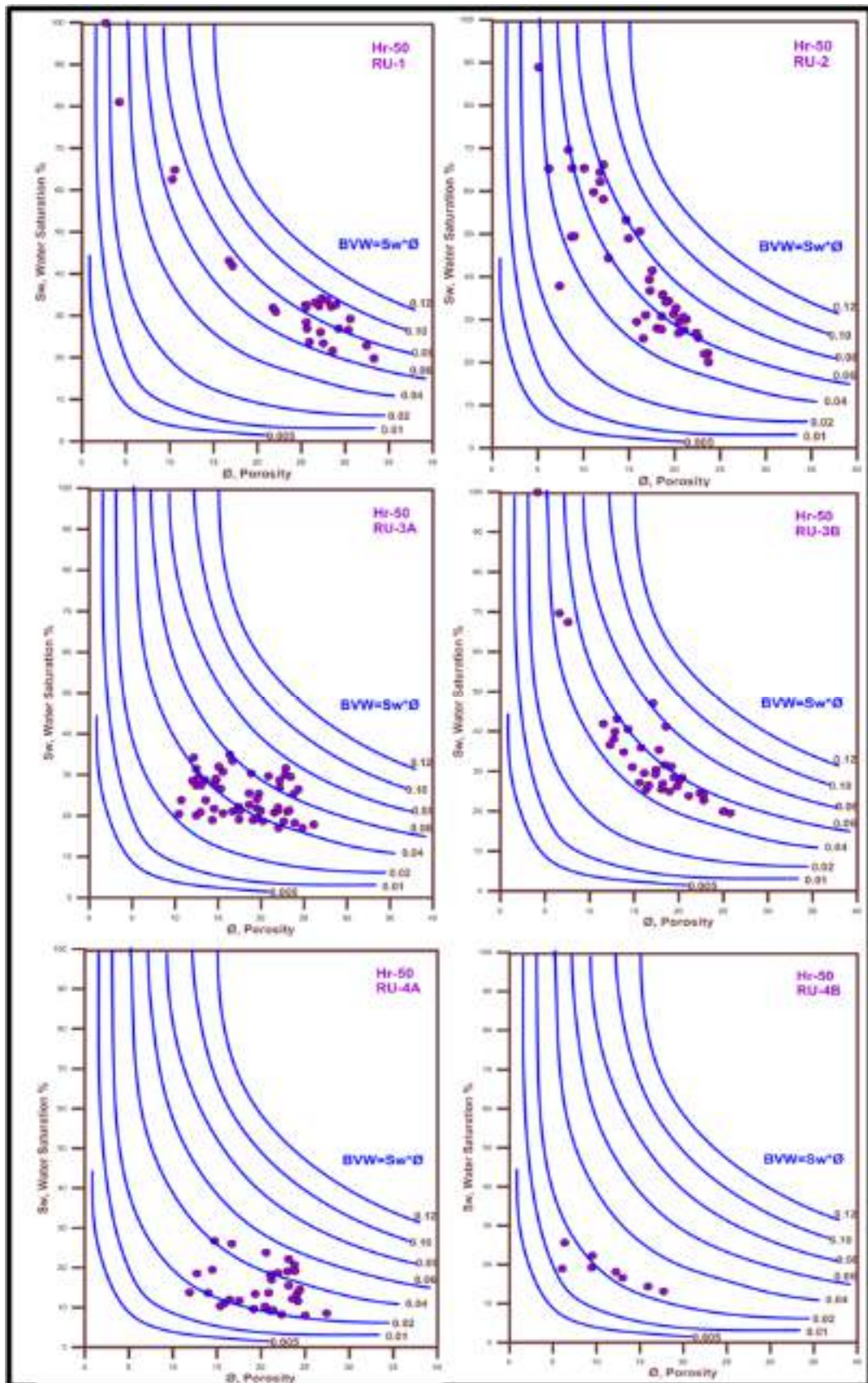


Figure 4.9: Buckles plot for the values of BVW for the reservoir units and subunits of Jeribe Formation in the well Hr-50.

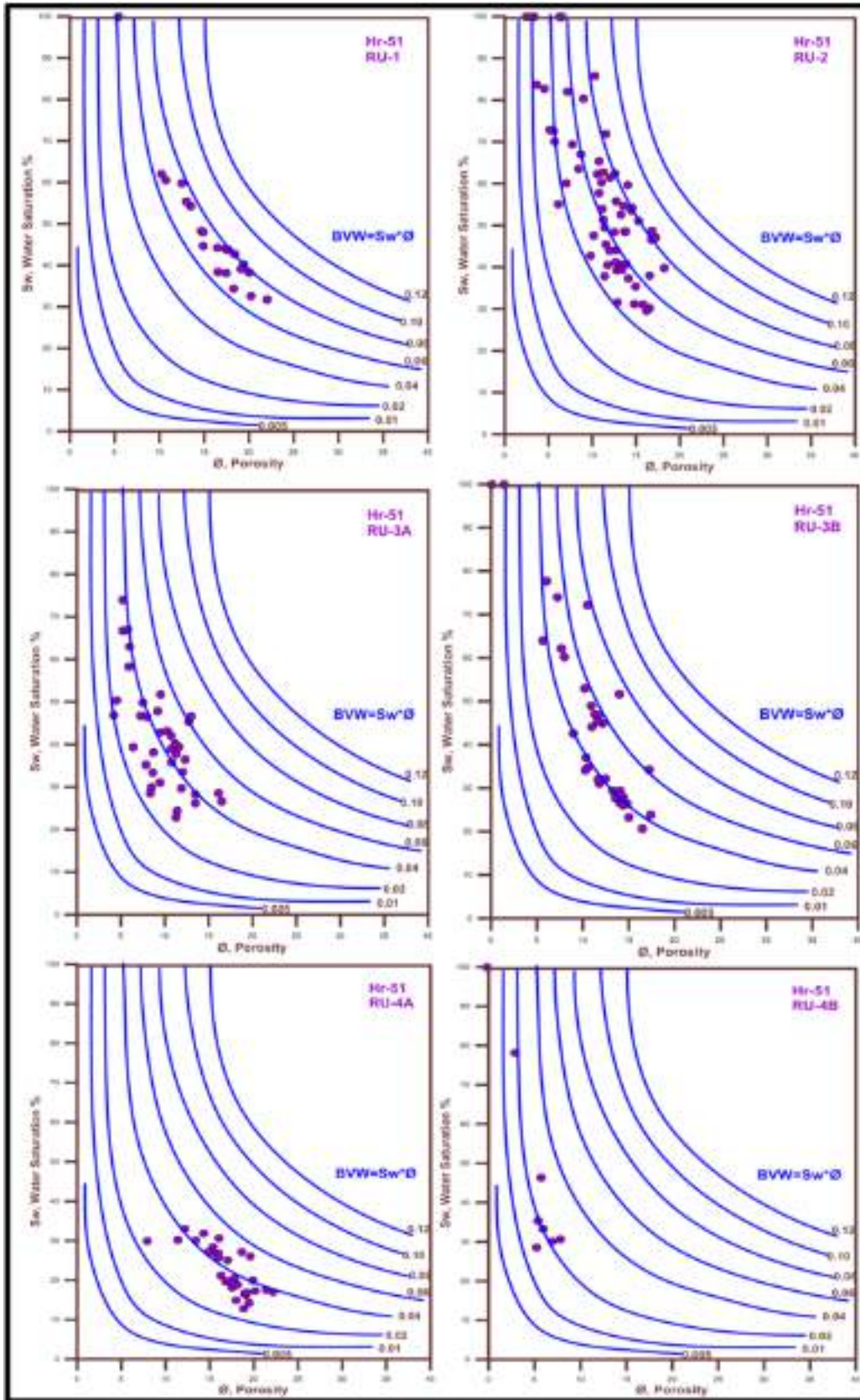


Figure 4.10: Buckles plot for the values of BVW for the reservoir units and subunits of Jeribe Formation in the well Hr-51.

The following points can be observed from the plot of MHI in the figure 4.11:

1. Almost the whole parts of Jeribe Formation in the well Hr-51 contain moveable hydrocarbons.
2. The interval of Jeribe Formation representing the reservoir unit RU-4 and the reservoir subunit RU-3B in the three studied wells are composed of zones containing moveable hydrocarbons.
3. Most parts of the reservoir subunit RU-3A in the two wells of Hr-49 and Hr-51 contains moveable hydrocarbons, whereas the same subunit in the well Hr-50 mostly represents an interval of non-moveable hydrocarbon content.
4. The reservoir unit RU-2 contains a lot of zones with non-moveable hydrocarbons in the two wells of Hr-49 and Hr-50.
5. Most parts of the reservoir unit RU-1 contain moveable hydrocarbons in the two wells of Hr-49 and Hr-50 except the lower most part of unit near the contact of the Jeribe Formation with Dhiban Formation which contains no moveable hydrocarbons even in the well Hr-51.

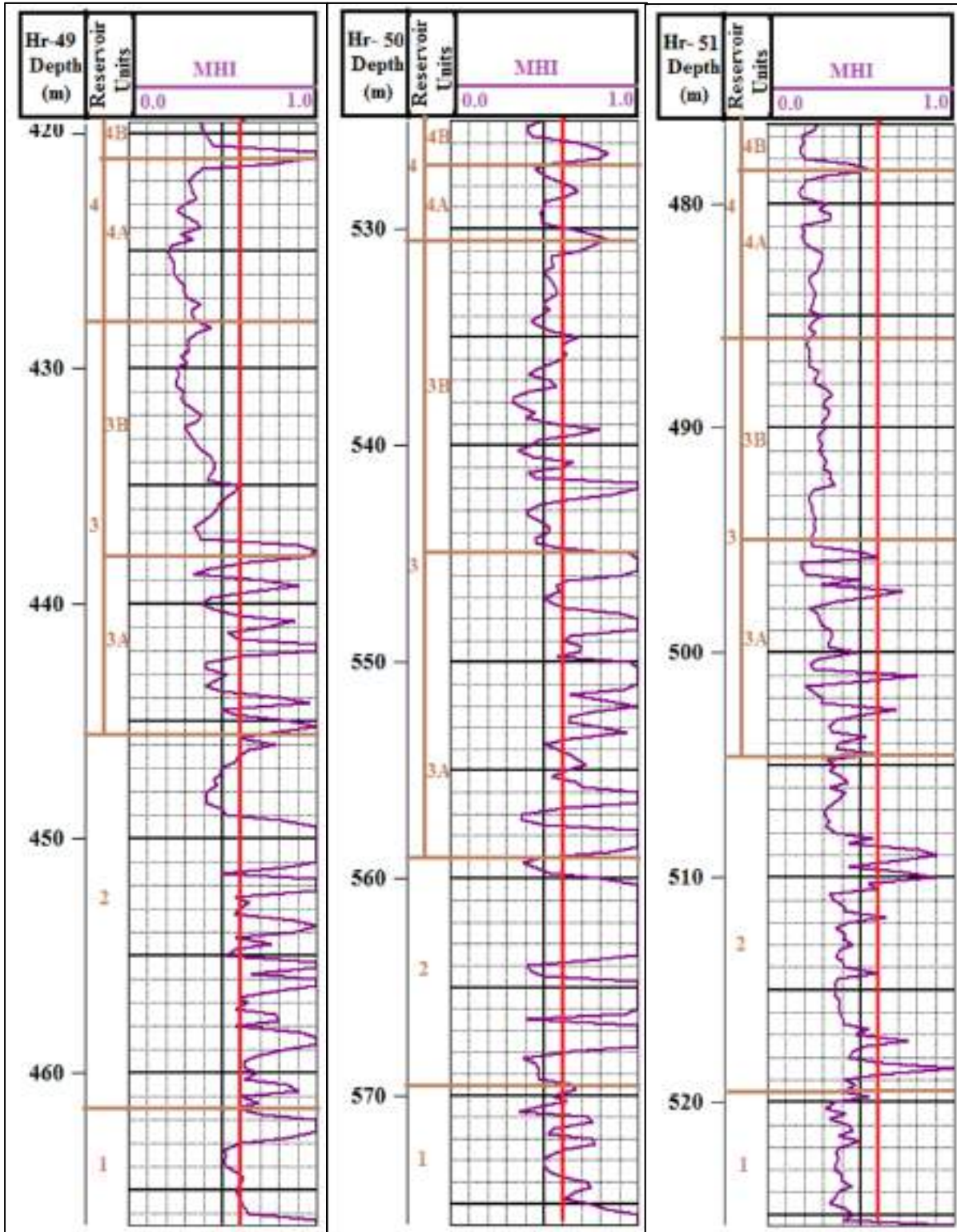


Figure 4.11: The plot of Movable Hydrocarbon Index for the studied Jeribe Formation in the wells Hr-49, Hr-50 and Hr-51.

4.8 Rock Fabrics from Porosity - Permeability relationship

Lucia (1999) distinguished three classes of carbonate rock fabrics on the basis of the relationship between porosity and permeability (on a log-log paper) and as a function of the pore throat size (Fig. 4.12).

Class 1 on Lucia's graph represents three rock fabrics which are: (1) grainstones, (2) dolomitized grainstones, and (3) large crystalline dolostones, which may be dolograins, grain-dominated dolopackstones or mud-dominated dolostones.

Class 2 represents three rock fabrics which are: (1) grain-dominated packstones, (2) fine to medium crystalline grain-dominated dolopackstones, and (3) medium crystalline mud dominated dolostones.

Finally, the field of class 3 represents two types of rock fabrics which are: (1) mud-dominated fabrics (mud-dominated packstone, wackestone, and mudstone) and (2) fine crystalline mud-dominated dolostones.

Lucia (1999) mentioned that although the eight rock fabrics are divided into three clear petrophysical classes but actually in nature there is no sharp boundary between the rock fabrics.

As a general note on Lucia's graph, grain dominated fabrics (Class 1) are those which own higher permeability for a certain value of porosity if compared to the more mud dominated fabrics (class 3) with the same porosity value.

The application of the porosity - permeability relationship mentioned above using the data of this study is shown in the figures 4.13 - 4.15.

The following are the main notes about the above porosity - permeability crossplots regarding the rock fabric type of each reservoir unit of Jeribe Formation in the studied wells:

1. The rock fabric types and pore throat sizes of the reservoir units of Jeribe Formation in the two wells of Hr-49 and Hr-51 are almost

similar to each other and that in contrast to the well Hr-50 which the reservoir units showed kind of variations in comparison with the other two wells.

2. Some reservoir units show homogeneity in the class type and throat size (ex. RU-1 in the wells Hr-49 and Hr-50, RU-4B in the well Hr-50), whereas other reservoir units show more heterogeneity in rock fabrics and pore throat sizes (ex. RU-2 in the wells Hr-49 and Hr-51, RU4A in the well Hr-50).
3. Rock fabric class 3 which is expected to be more mud dominated has been seen only in the reservoir units of Jeribe Formation in the well Hr-50.
4. The pore throat sizes of the Jeribe Formation in the studied wells ranged mostly between 1.0 and 2.0 microns with being 2.0 micron much more dominated. Pore throat sizes of 0.5 micron recorded rarely in some reservoir units like RU-2 in the well Hr-49.
5. The reservoir unit RU-3B showed points locating out of the three classified rock fabric types (before class 1). Such a condition is mostly due to the effect of fracturing or existence of vugs which causes high permeability in a low porosity zone.
6. Except the reservoir units RU-1 and RU-2 in the well Hr-50, the dominated rock fabric of Jeribe Formation is expected to be mostly grain dominated packstone or dolopackstone. Mud dominated packstone or wackstone are mostly expected to be seen in the RU-1 and RU-2 in the well Hr-50.

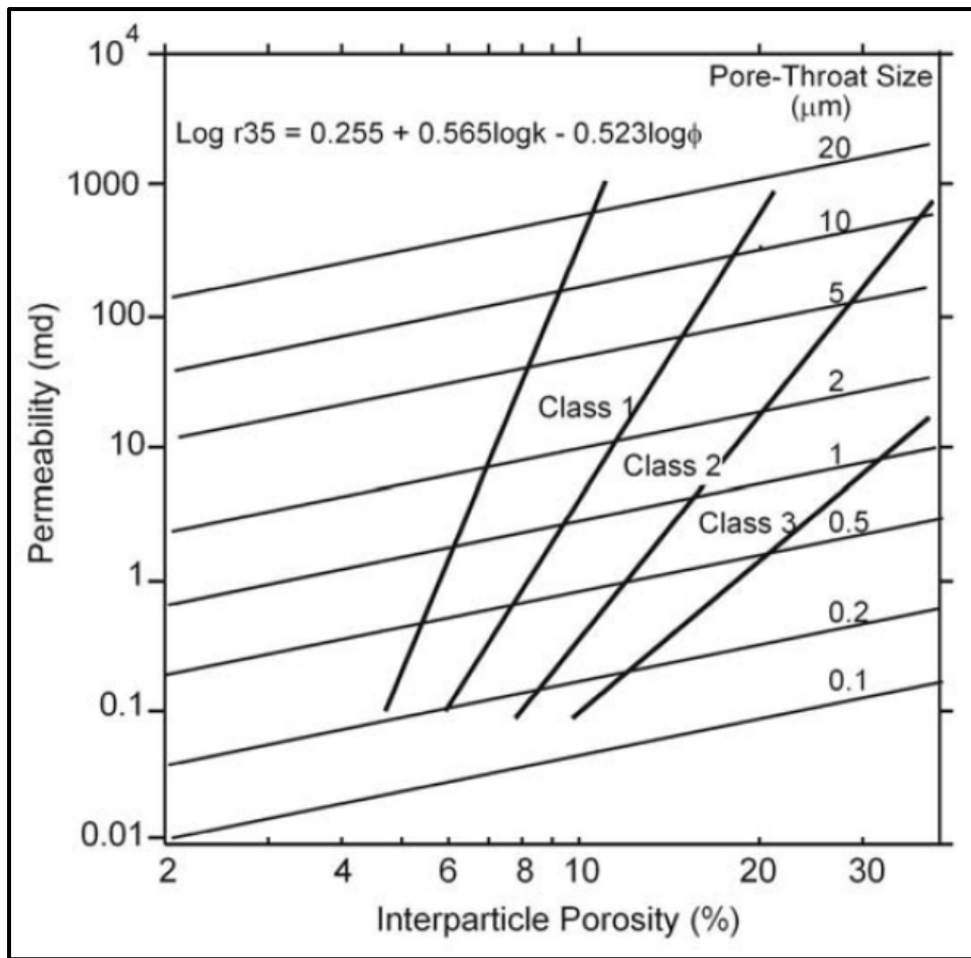


Figure 4.12: Comparison of petrophysical-class fields and pore-throat sizes versus interparticle porosity and permeability (after Lucia, 1999).

Similarly, and from the relationship between porosity and permeability, an attempt done for detecting the type of the flow in Jeribe Formation as either flow occurs due to permeability from fractures, fractures and matrix, or mainly matrix (with taking porosity and storage capacity in consideration).

The idea of such crossplot is mainly based on the technique of R35 proposed by Winland in the year 1972 who combined data from routine core analysis with capillary pressure data and developed an empirical relationship between porosity, air permeability, and the pore throat size equivalent to a mercury non-wetting phase of 35% (R35) (Rivas et al., 2014).

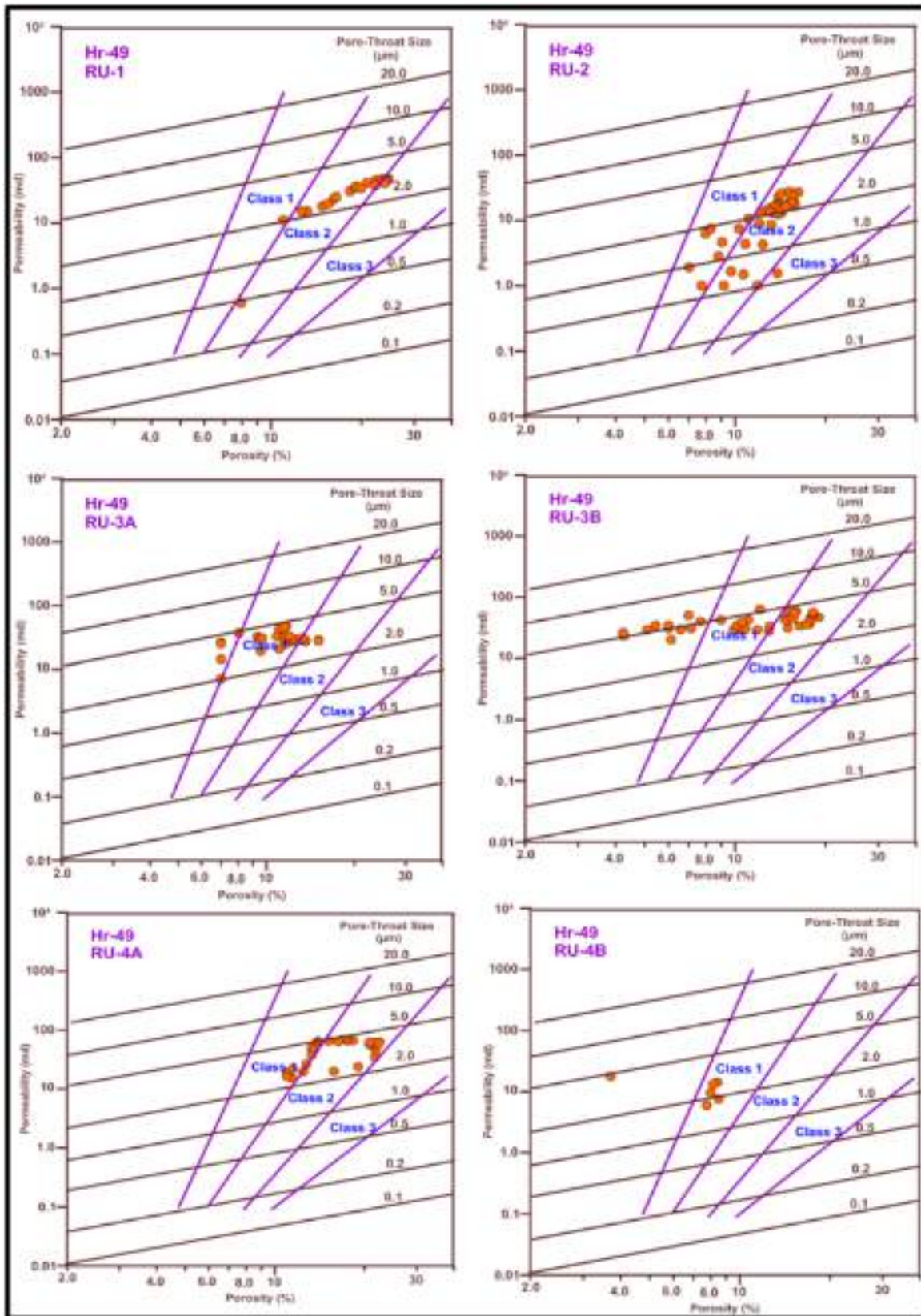


Figure 4.13: Porosity-permeability cross plot shows the pore throat size and petrophysical rock fabric classes of Jeribe Formation’s reservoir units in Hr-49 well.

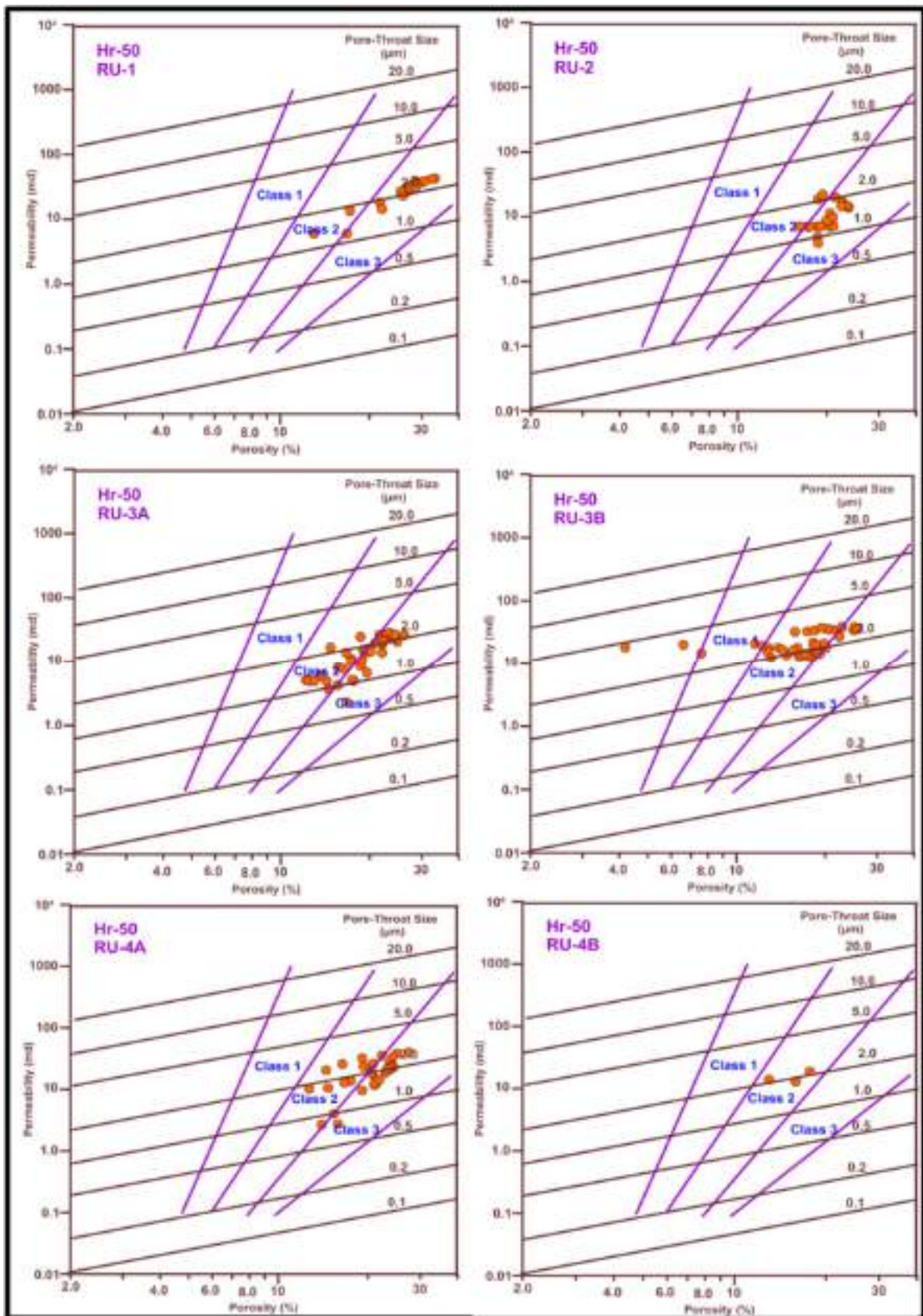


Figure 4.14: Porosity-permeability cross plot shows the pore throat size and petrophysical rock fabric classes of Jeribe Formation’s reservoir units in Hr-50 well.

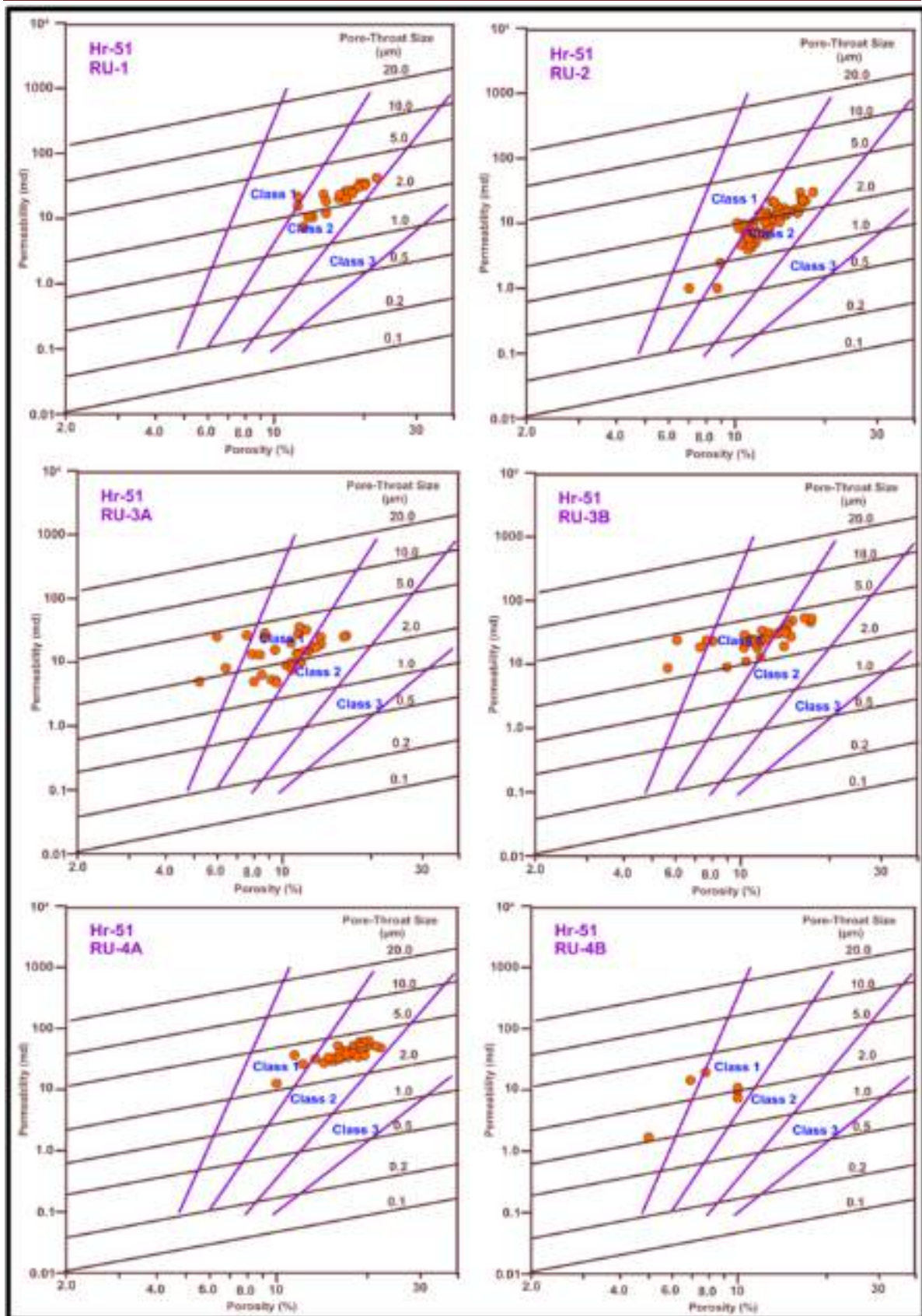


Figure 4.15: Porosity-permeability cross plot shows the pore throat size and petrophysical rock fabric classes of Jeribe Formation’s reservoir units in Hr-51 well.

As no measured porosity and permeability from core samples are available for Jeribe Formation in this study, so the calculated porosity and permeability from the log data used to apply this technique.

The crossplot as shown in the figure 4.16 combines between the values of porosity and permeability with existence of contour lines representing iso K/ϕ ratios (Humbolt, 2006) in addition to exhibiting the expected pore throat sizes in microns.

Regarding storage capacity of rocks, the accuracy of the evaluation of fracture porosity (ϕ_f) is of very limited importance, since it is generally negligible when compared with the matrix porosity. But from the point of view of storage capacity, especially in relation to the transient flow problem, the accuracy of ϕ_f may play an important role. It is important to evaluate the ϕ_f value only when ϕ_t is very small ($\phi_t < 5\%$) (Van Golf-Racht, 1982).

From figure 4.16, it is clear that the fluid flow from Jeribe Formation in the studied wells are mainly due to permeability provided by pores within the matrix with contribution from the existed fractures. The figure also shows that the least contribution of fractures in providing the permeability is in the well Hr-50.

It is important to mention that as not all the sample points are clustering around one single K/ϕ contour line, that means the system is not completely homogeneous but definitely heterogeneity as a result of either depositional environment or due to the later processes of diagenesis have affected the reservoir property of the formation. However, Jeribe Formation in the well Hr-51 shows the least heterogeneity in comparison with the other two studied wells.

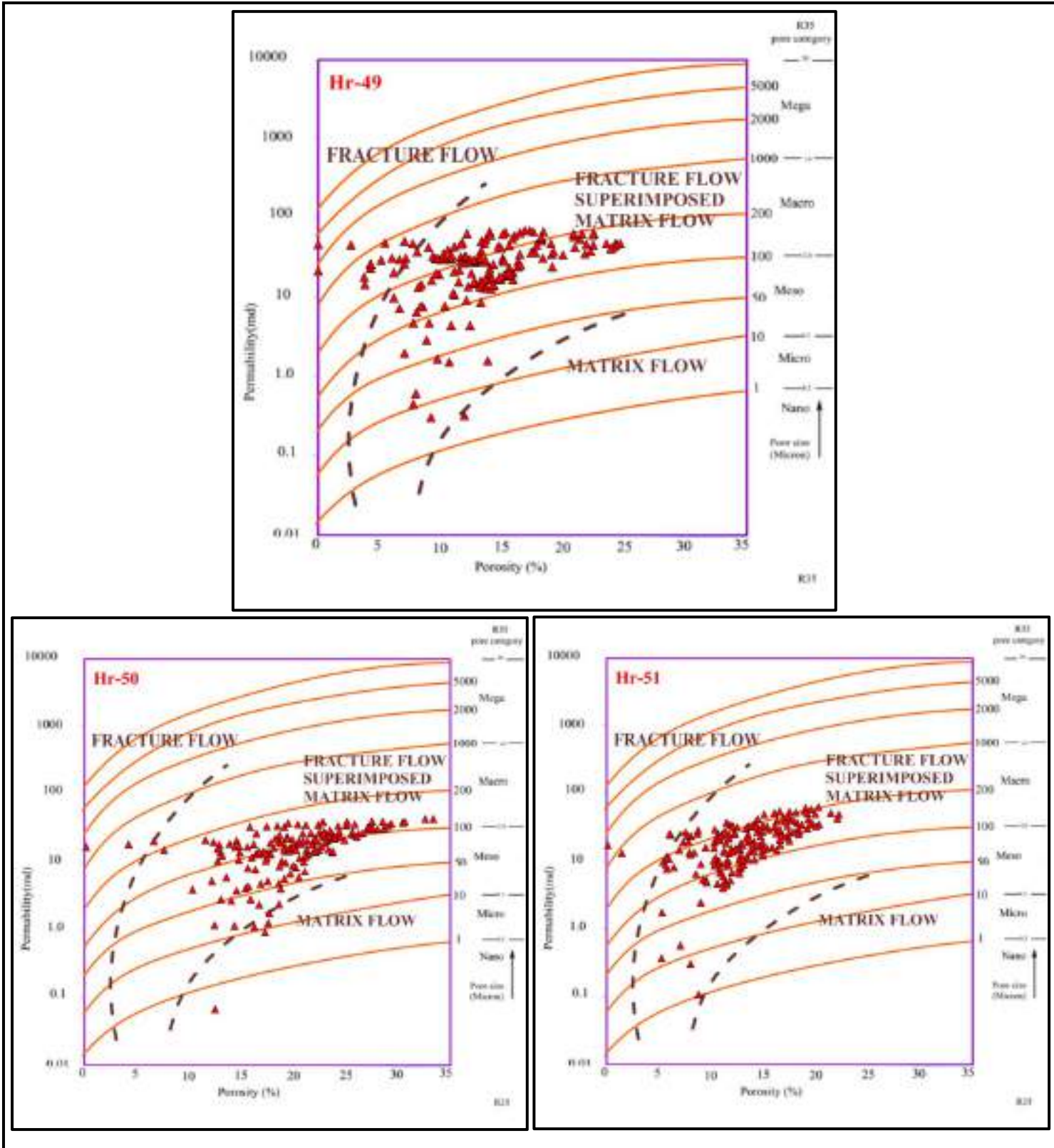


Figure 4.16: Porosity-permeability cross plot showing the type of flow and pore throat sizes for Jeribe Formation in wells Hr-49, Hr-50 and Hr-51.

4.9 Flow Zone Indicators (FZI)

Flow Zone Indicator (FZI) as defined by Amaefule et al. (1993) "is a unique parameter that incorporates the geological attributes of texture and mineralogy in the discrimination of distinct pore geometrical facies (hydraulic units)". This means that FZI is an indicator to the grain shape and size with the sorting of the grains and tortuosity of the paths between them.

The technique of FZI was initially proposed by Amaefule et al. (1993) to better identify the porosity and permeability correlation for a given rock type. They designed the approach as a unique parameter that varies inversely with tortuosity, shape factor and grain surface area, which are the critical factors determining the flow in the rock (Teh and Willhite, 2011). Accordingly, the FZI value discriminates the pore geometry of facies into flow zones, in which a high FZI value indicates that the rock exhibits coarse, well-sorted grains and lower shape factor. In the same manner, a low FZI value represents a rock constituent of fine and poorly sorted grained.

The value of FZI for any interval depends mainly on the measured Reservoir Quality Index (RQI) and the Normalized Porosity Index (\emptyset_z) which both can be obtained from the effective porosity and permeability of the interval as shown in the equations Eq.4.7 - Eq.4.9.

$$RQI = 0.0314\sqrt{k/\emptyset_e} \dots\dots\dots E.q.4.7$$

$$\emptyset_z = \frac{\emptyset}{1-\emptyset_e} \dots\dots\dots E.q.4.8$$

$$FZI = RQI / \emptyset_z \dots\dots\dots E.q.4.9$$

Where:

RQI: Reservoir Quality Index

K: Permeability in md

\emptyset_z : Normalized Porosity Index

\emptyset_e : Effective porosity in fraction

\emptyset : Porosity in fraction

FZI: Flow Zone Indicator in μm

The calculated values of RQI, \emptyset_z , and FZI for the Jeribe Formation in the studied wells are listed in the appendix C.

Figure 4.17 is a histogram showing the values of FZI for the sample points of Jeribe Formation in the three studied wells. By such a presentation it is easier to preliminarily separate the FZI values as groups. Four groups of FZI are considered of values <0.15 , $0.15-0.25$, $0.25-0.50$, and >0.50 for Jeribe Formation in the well Hr-49, and <0.06 , $0.06-0.10$, $0.10-0.2$, and >0.2 in the well Hr-50, whereas values of <0.15 , $0.15-0.20$, $0.20-0.40$, and >0.40 are considered for Jeribe Formation in the well Hr-51.

Normal probability analysis (S shape curve) is another helpful technique for recognizing the different groups of FZI values which in turn are representing different HFUs. Figure 4.18 shows the distribution and arrangement of the calculated FZI values for Jeribe Formation in the three studied wells. The slope by which a group of FZI values are arranging is distinguishing it from the neighboring groups. As can be seen in the figure 4.18 four groups of FZI with distinguished ranges can be identified in each of the studied wells which are of the same range values as mentioned above.

On the other hand through plotting the values of RQI against \emptyset_z on a log - log paper (Fig.4.19) the points which are representing FZI values are distributed as groups with different unit slope. Each group of points with distinctive unit slope represents a unique Hydraulic Flow Unit (HFU).

A hydraulic flow unit represents a volume of the total reservoir rock within which the fluid flow is affected by specific geological and petrophysical properties, and each HFU is internally consistent and predictably different from properties of other rock volumes (Thomas, 2002).

Table 4.3 summarizes the range values of the distinguished FZI groups for Jeribe Formation in the studied wells and the average value of each FZI group with the name of the HFU representing the FZI groups.

A comparison between the calculated MHI and FZI values for Jeribe Formation is drawn as curves in the figure 4.20. Being the two values representatives for moveability of the fluids, therefore zones with high FZI values are expected to have low MHI values (lower than 0.6) and vice versa. Such a relationship is clearly observed in the studied wells especially for the reservoir unit RU-2 which contains a lot of horizons with non-moveable hydrocarbons especially in the two wells of Hr-49 and Hr-50.

By a simple comparison between the average values of the identified HFU units one can conclude that the HU-4 in the well Hr-50 (RU-3B) has the highest potentiality of fluid production than the other identified hydraulic units.

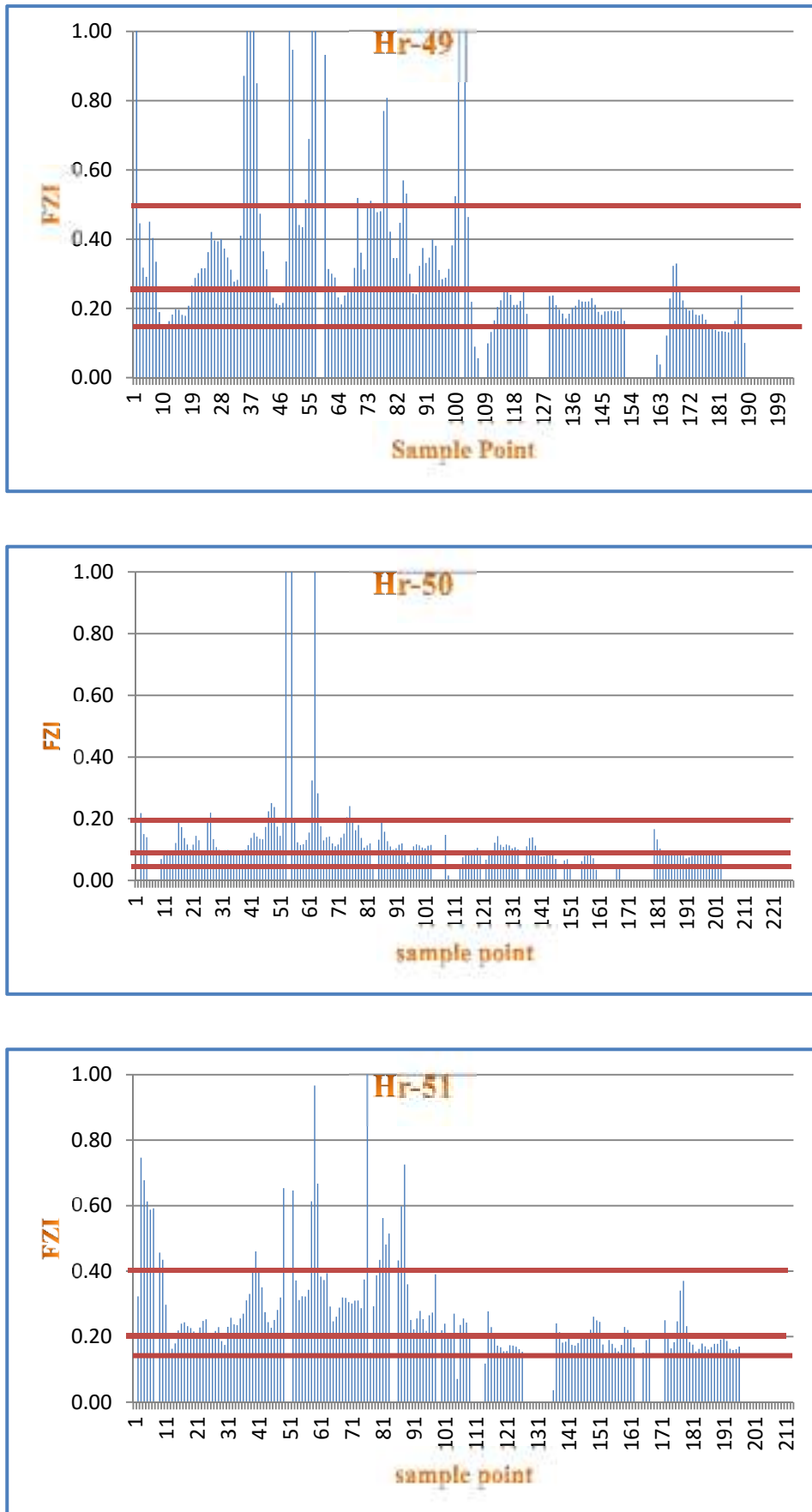


Figure 4.17: Histogram of FZI values for the sample points of Jeribe Formation in the three studied wells of Hr-49, Hr-50, and Hr-51.

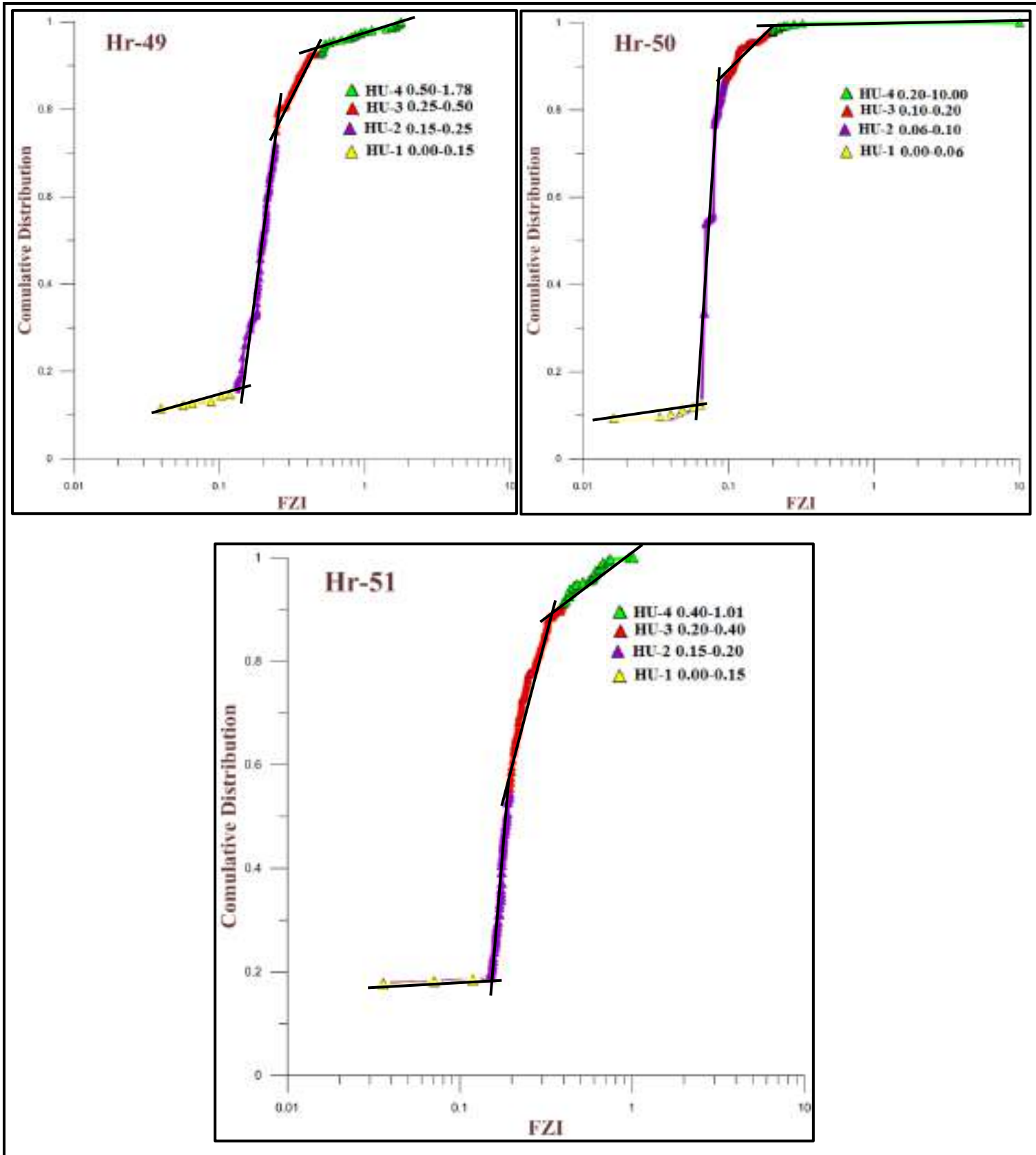


Figure 4.18: Normal probability analysis for the calculated Flow Zone Indicator values for Jeribe Formation in each of the wells of Hr-49, Hr-50, and Hr-51.

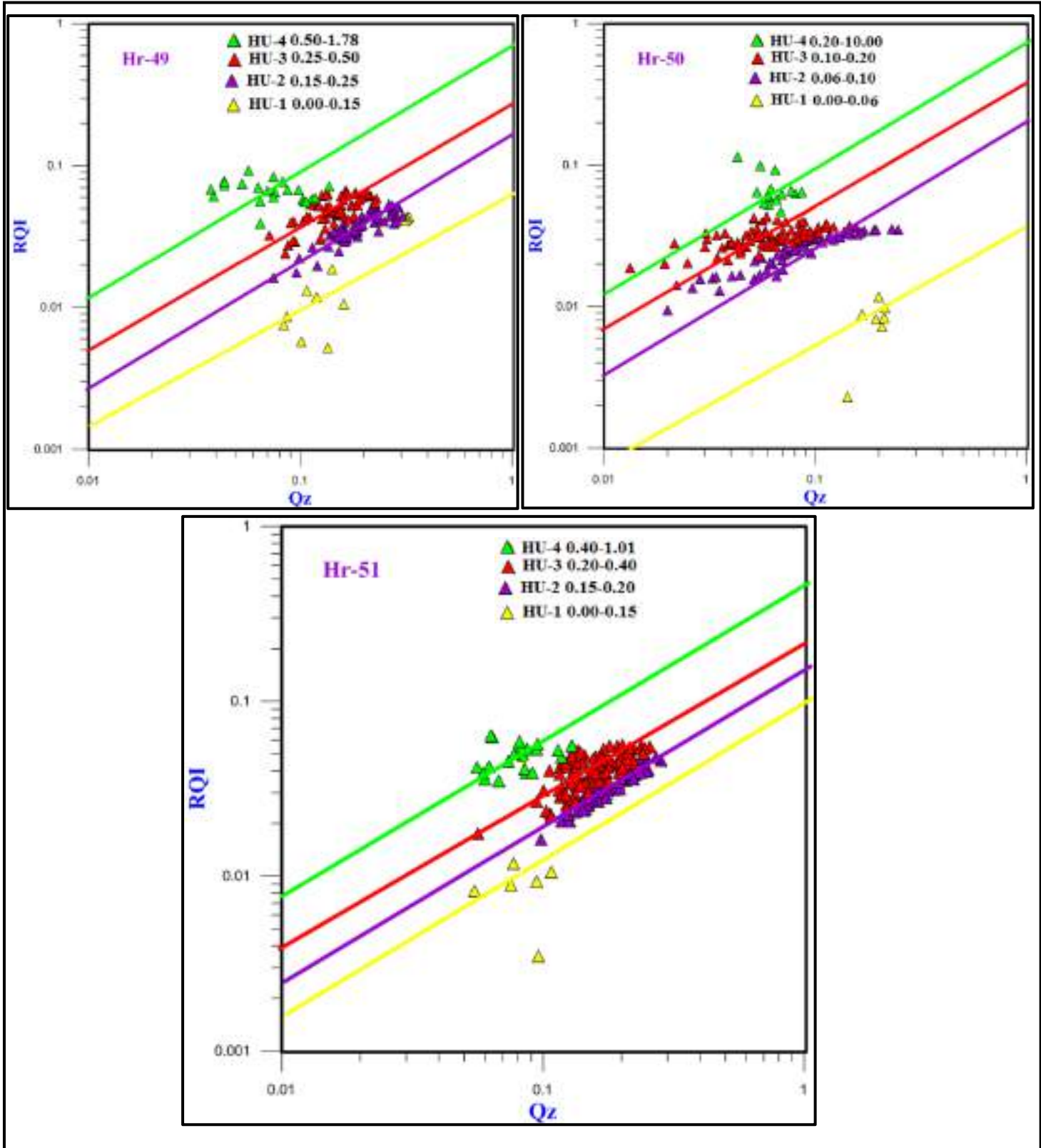


Figure 4.19: The three distinctive FZI values which identified from RQI- \emptyset_z relationship for Jeribe Formation in the studied wells of Hr-49, Hr-50, and Hr-51.

Table 4.3: Calculated FZI and the hydraulic unit types for the studied wells.

wells	FZI Range	Average FZI	Hydraulic Units
Hr-49	0.00-0.15	0.042	HU-1
	0.15-0.25	0.201	HU-2
	0.25-0.50	0.380	HU-3
	0.50-1.78	1.190	HU-4
Hr-50	0.00-0.06	0.0079	HU-1
	0.06-0.10	0.0885	HU-2
	0.10-0.20	0.14	HU-3
	0.20-10.00	5.00	HU-4
Hr-51	0.00-0.15	0.06	HU-1
	0.15-0.20	0.18	HU-2
	0.20-0.40	0.28	HU-3
	0.40-1.01	0.60	HU-4

4.10 Net to Gross Reservoir and Pay Ratios

As most of the reservoirs (especially the carbonate reservoirs) are not homogeneous either vertically or laterally, therefore not all the intervals within the reservoir are expected to have the required properties of potential reservoir. The layers which have no porosity or limited permeability are generally defined as 'non-reservoir' intervals. The thickness of productive (net) reservoir rock within the total (gross) reservoir thickness is termed the net-to-gross or N/G ratio (Jahn et al., 2003). The calculated N/G ratio for any formation may range between 1.0 (100% reservoir) and 0.0 (non-reservoir).

According to Dikkers (1985); net productive thickness is the thickness of those intervals in which porosity and permeability are known (or supposed) to be high enough for the interval in order to produce oil or gas, whereas net oil-bearing thickness includes those intervals in which oil is present in such saturation, the interval may be expected to produce oil, if penetrated by a properly completed well.

To discriminate between reservoir and non-reservoir rock each sample point had to meet a shale, porosity, and permeability cutoffs.

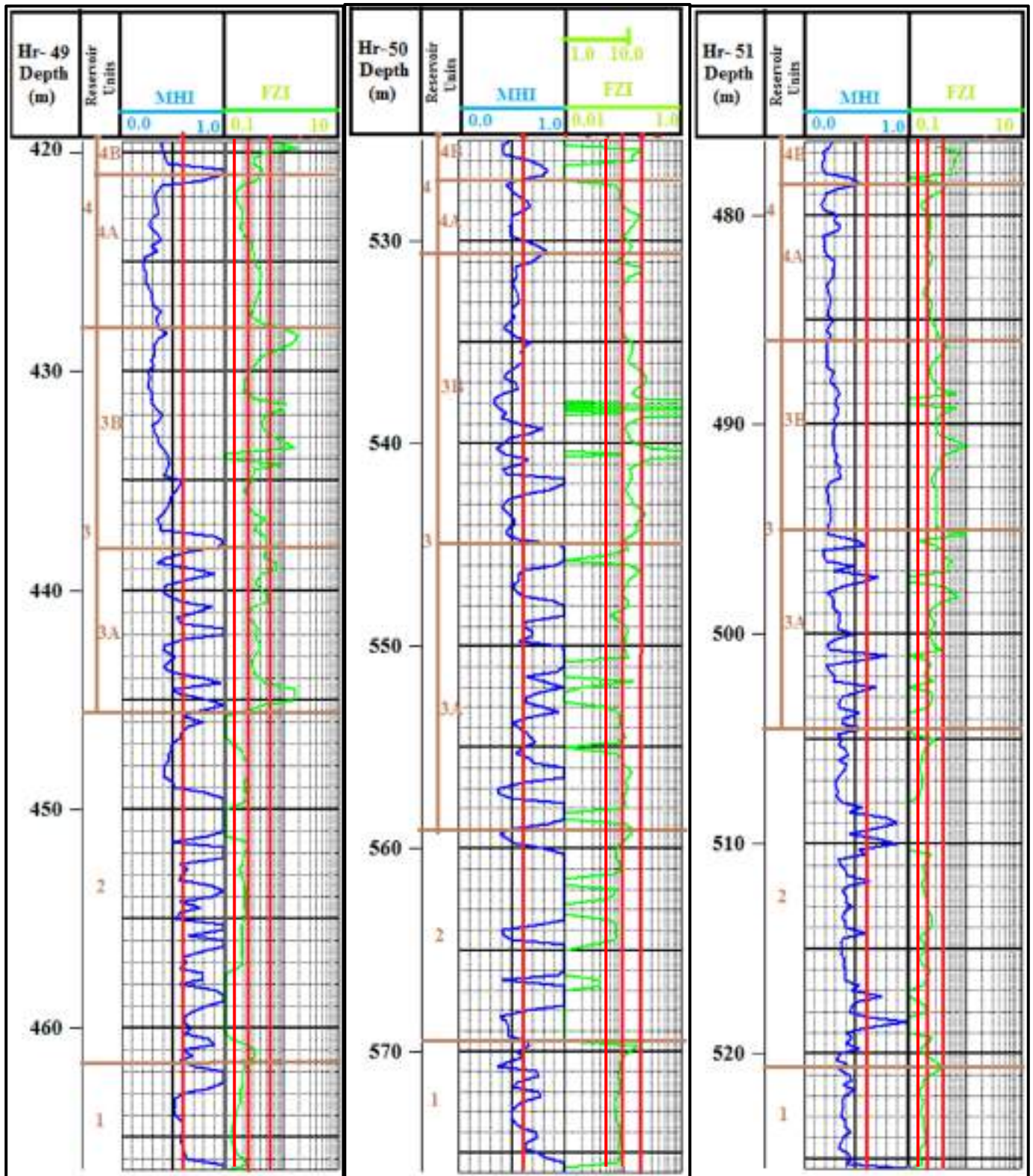


Figure 4.20: Comparison between the calculated MHI and FZI for the reservoir units of Jeribe Formation in the studied wells of Hr-49, Hr-50, and Hr-51.

What is meant by cutoff is a value of a certain reservoir property which represents a limit for distinguishing between reservoir and non-reservoir horizons. Cutoff value may represents a maximum requested value for a certain reservoir property (such as shale content and water saturation) in which higher values of any sample point will lead to consider it as non-reservoir sample point. On the other hand, some cutoff values of other reservoir properties (such as porosity and permeability) represent a minimum requested value to consider any sample point as a reservoir, and points of less than that cutoff will be considered as non-reservoir points.

In this study, and in order to distinguish between reservoir and non-reservoir intervals of Jeribe Formation in the studied wells, three cutoffs have been selected representing shale content, permeability, and porosity.

The value of 35% has been selected as the shale content (V_{sh}) cutoff value in this study and that due to considering this value as a limit for distinguishing between shaly and shale intervals (chapter two).

According to Schlumberger (1989); the range of permeabilities of producing formations is extremely wide-from less than 0.1md to over 10,000md. The lower limit of permeability for a commercial well depends on several factors: thickness of pay, whether production is oil or gas, hydrocarbon viscosity, formation pressure, water saturation, value (price) of the oil or gas, well depth, etc. In this study, permeability cutoff of 1.0md selected to be the minimum requested value of permeability for Jeribe Formation in the well Hr-50 which believed to be containing oil, whereas 0.1md used as permeability cutoff value for Jeribe Formation in the other two wells of Hr-49 and Hr-51 which believed to be containing gas rather than oil. Selecting those two values is on the base of literature reviews (Peters, 2001; Law et al., 2001; Tiab and Donaldson, 2004; Darling, 2005; and Parnell et al., 2010)

Using porosity versus permeability crossplot for the data obtained from the core analysis in the well Hr-2 (Figs. 4.21 & 4.22), two porosity cutoff values have been determined for the two cases of oil bearing reservoir (using 1.0md permeability cutoff, Fig.4.21) and gas bearing reservoir (using 0.1md permeability cutoff, Fig. 4.22).

Accordingly, 14.8% and 2.95% values were the two porosity cutoff values which are determined to be used for calculating N/G reservoir ratio in the oil bearing (Hr-50 well) and gas bearing reservoirs (Hr-49 & Hr-51 wells) respectively.

The above used three cutoffs of shale content, porosity, and permeability can only be used for distinguishing reservoir from non-reservoir intervals without determining the payable zones (zones containing acceptable hydrocarbon saturations). To determine payable zones, additional cutoff of water saturation has been used whose values have been determined from the relationship between porosity and water saturations (Figs. 4.23 - 4.25) with paying attention to the both cases of oil and gas bearing reservoirs as mentioned above. The values of 58.50%, 35%, and 73% decided to be used as water saturation cutoffs for the wells Hr-49, Hr-50, and Hr-51 respectively.

For determining actual producible horizons within the previously determined payable zones (using water saturation cutoffs), an attempt was done to take benefit from the measured MHI using 0.6 value as a cutoff to distinguish horizons of movable hydrocarbons from horizons which maybe of high hydrocarbon saturation but without movement ability (horizons of high residual hydrocarbon saturation).

The measured gross, net reservoir, net pay, and net production thicknesses with the calculated N/G reservoir, N/G pay, and N/G production ratios for the identified reservoir units of Jeribe Formation in the studied wells are listed in the tables 4.4 - 4.6.

The following are a few notes about the values and statistics within the mentioned three tables:

1. Jeribe in the well Hr-51 has the highest N/G ratio of reservoir, pay, and production (79.83%, 79.33%, and 78.68% respectively) and the lowest in the well Hr-50 (58.93%, 54.31%, and 25.98% respectively).
2. RU-4A is the best production reservoir unit in Jeribe Formation with N/G production ratios of 85.71%, 52.94%, and 100% in the wells Hr-49, Hr-50, and Hr-51 respectively.
3. The highest production thickness among the reservoir units of Jeribe Formation observed in the RU-2 of the well Hr-51 (11.25m).
4. The highest production thickness of Jeribe Formation among the three studied wells exists in the well Hr-51 (37.00m) and the lowest in the well Hr-50 (13.25m).

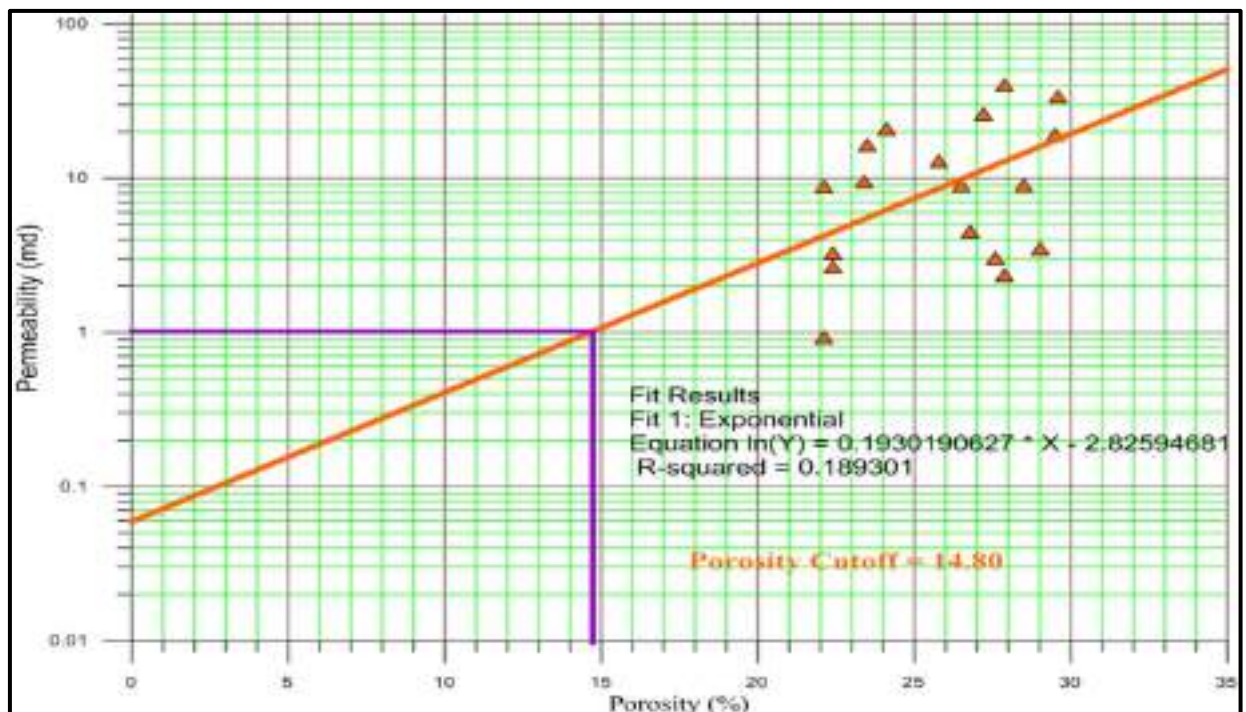


Figure 4.21: Porosity cutoff measurement for the case of oil bearing reservoir using porosity versus permeability crossplot for the core data from Hr-2 well.

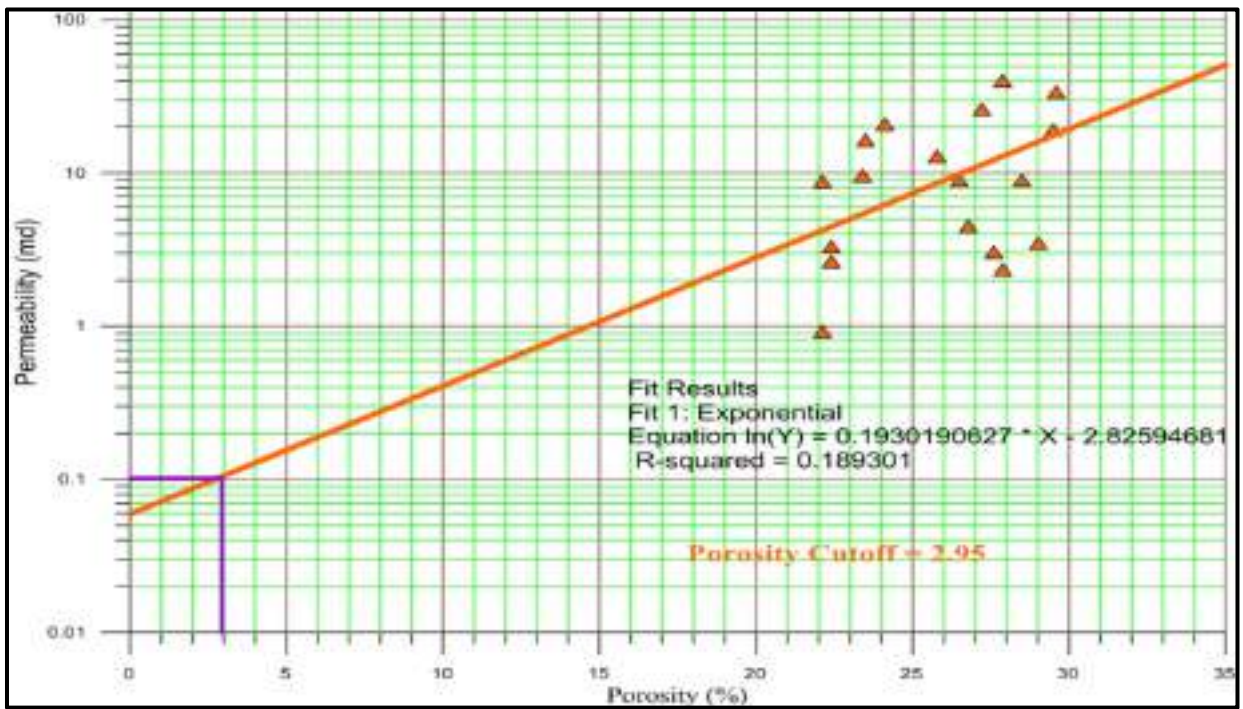


Figure 4.22: Porosity cutoff measurement for the case of gas bearing reservoir using porosity versus permeability crossplot for the core data from Hr-2 well.

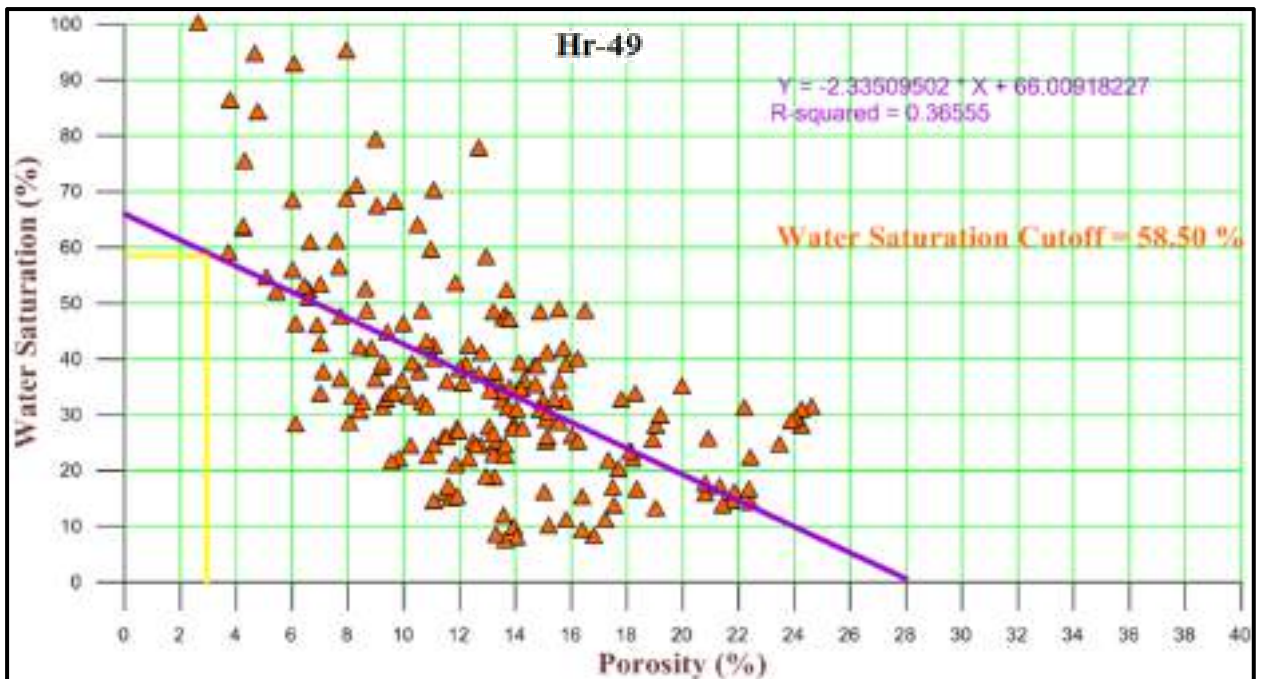


Figure 4.23: Water saturation cutoff determination using porosity versus water saturation crossplot for Hr-49.

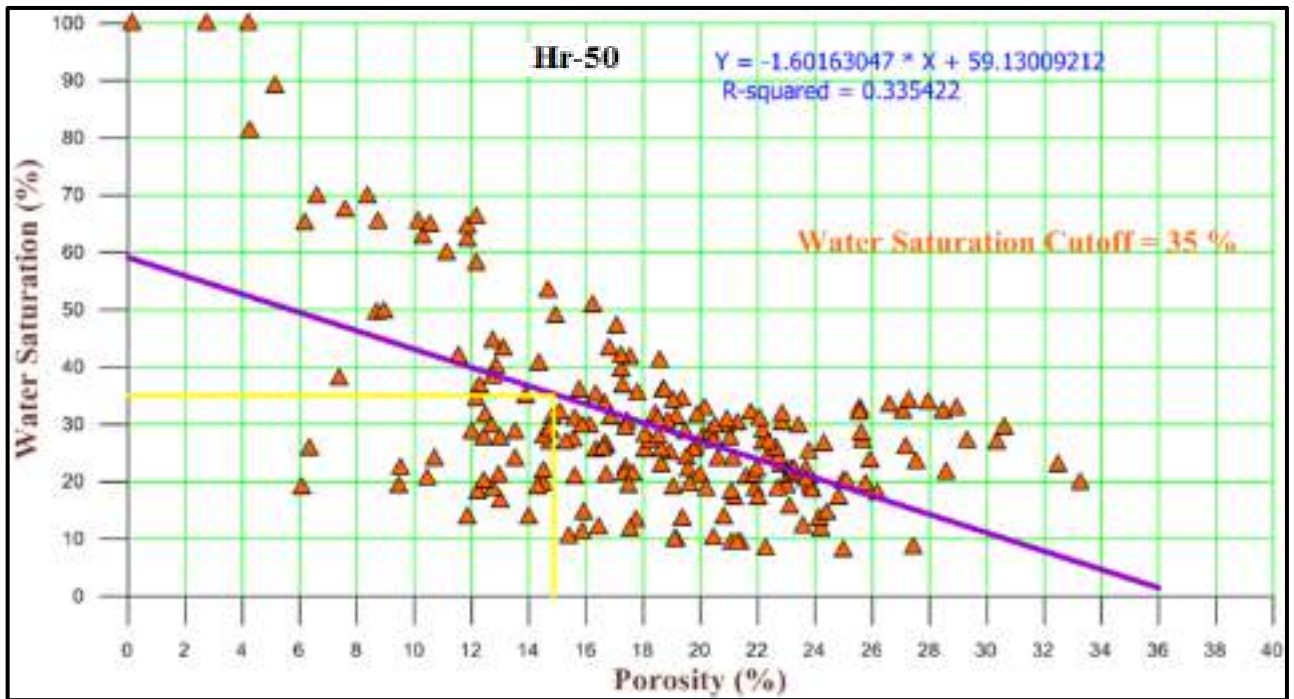


Figure 4.24: Water saturation cutoff determination using porosity versus water saturation crossplot for Hr-50.

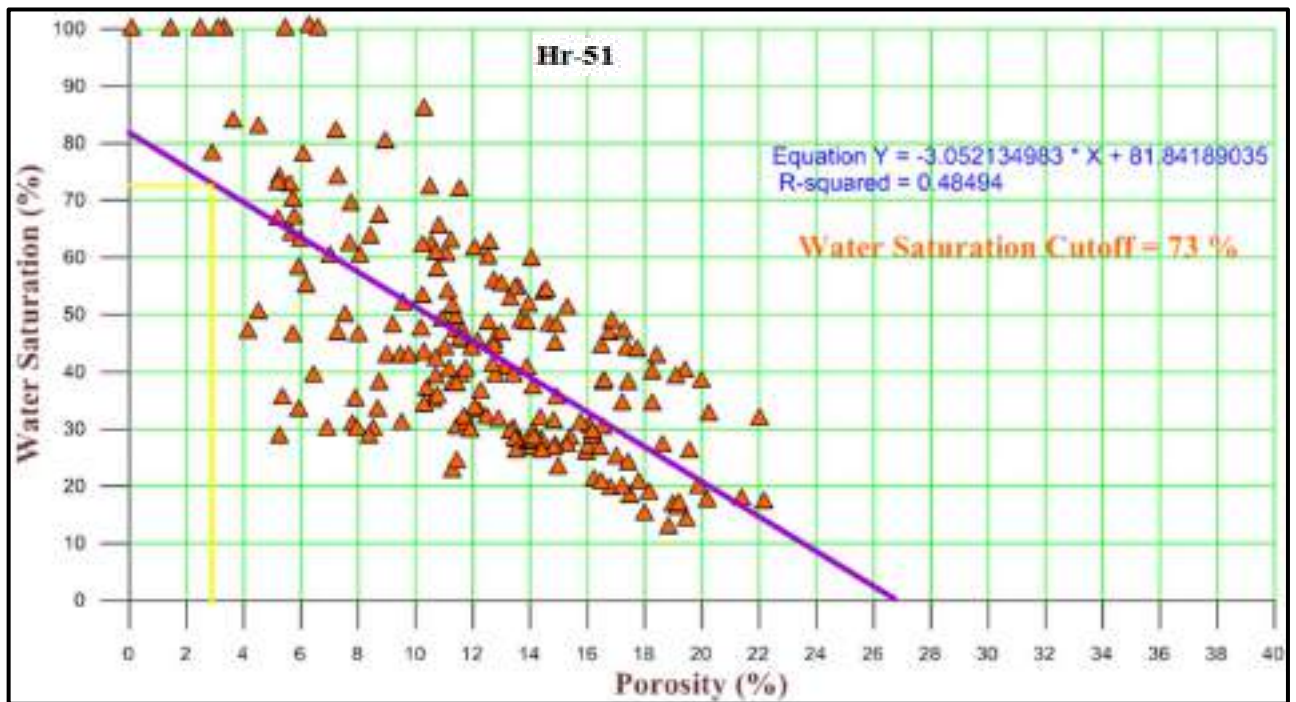


Figure 4.25: Water saturation cutoff determination using porosity versus water saturation crossplot for Hr-51.

Table 4.4: Calculated N/G reservoir and pay ratios for the studied Jeribe Formation in the well Hr-49.

Formation	Reservoir Units	Gross thickness (m)	Net reservoir thickness (m)	Net pay thickness (m)	Net production thickness (m)	N/G Reservoir (%)	N/G Pay (%)	N/G Production (%)
Jeribe	4B	1.50	0.75	0.75	0.50	50.00	50.00	33.33
	4A	7.00	7.00	7.00	6.00	100.00	100.00	85.71
	3B	10.00	3.50	3.50	3.25	35.00	35.00	32.50
	3A	7.50	6.00	6.00	3.25	80.00	80.00	43.33
	2	16.00	11.50	10.50	5.00	71.88	65.63	31.25
	1	5.00	5.00	4.50	2.25	100.00	90.00	45.00
Total		47.00	33.75	32.25	20.25	72.81	70.10	45.18

Table 4.5: Calculated N/G reservoir and pay ratios for the studied Jeribe Formation in the well Hr-50.

Formation	Reservoir Units	Gross thickness (m)	Net reservoir thickness (m)	Net pay thickness (m)	Net production thickness (m)	N/G Reservoir (%)	N/G Pay (%)	N/G Production (%)
Jeribe	4B	2.00	0.50	0.50	0.25	25.00	25.00	12.50
	4A	8.50	6.50	6.50	4.50	76.47	76.47	52.94
	3B	9.50	4.75	3.75	2.25	50.00	39.47	23.68
	3A	14.00	9.25	9.25	2.50	66.07	66.07	17.85
	2	10.50	5.00	4.00	1.50	47.62	38.10	14.28
	1	6.50	5.75	5.25	2.25	88.46	80.77	34.61
Total		51.00	31.75	29.25	13.25	58.93	54.31	25.98

Table 4.6: Calculated N/G reservoir and pay ratios for the studied Jeribe Formation in the well Hr-51.

Formation	Reservoir Units	Gross thickness (m)	Net reservoir thickness (m)	Net pay thickness (m)	Net production thickness (m)	N/G Reservoir (%)	N/G Pay (%)	N/G Production (%)
Jeribe	4B	2.00	1.50	1.50	1.50	75.00	75.00	75.00
	4A	7.50	7.50	7.50	7.50	100.00	100.00	100.00
	3B	9.00	5.50	5.50	5.50	61.00	61.00	61.00
	3A	9.50	6.50	6.50	6.25	68.00	68.00	65.78
	2	16.00	12.00	11.50	11.25	75.00	72.00	70.31
	1	5.00	5.00	5.00	5.00	100.00	100.00	100.00
Total		49.00	38.00	37.50	37.00	79.83	79.33	78.68

As Jeribe Formation in the studied three wells includes non-reservoir intervals and hence non-pay or non production intervals, therefore figures 4.26- 4.28 have been drawn to show the depth intervals of the mentioned non-productible zones of Jeribe reservoir in each well. Such information is vital for perforation processes and production assessments.

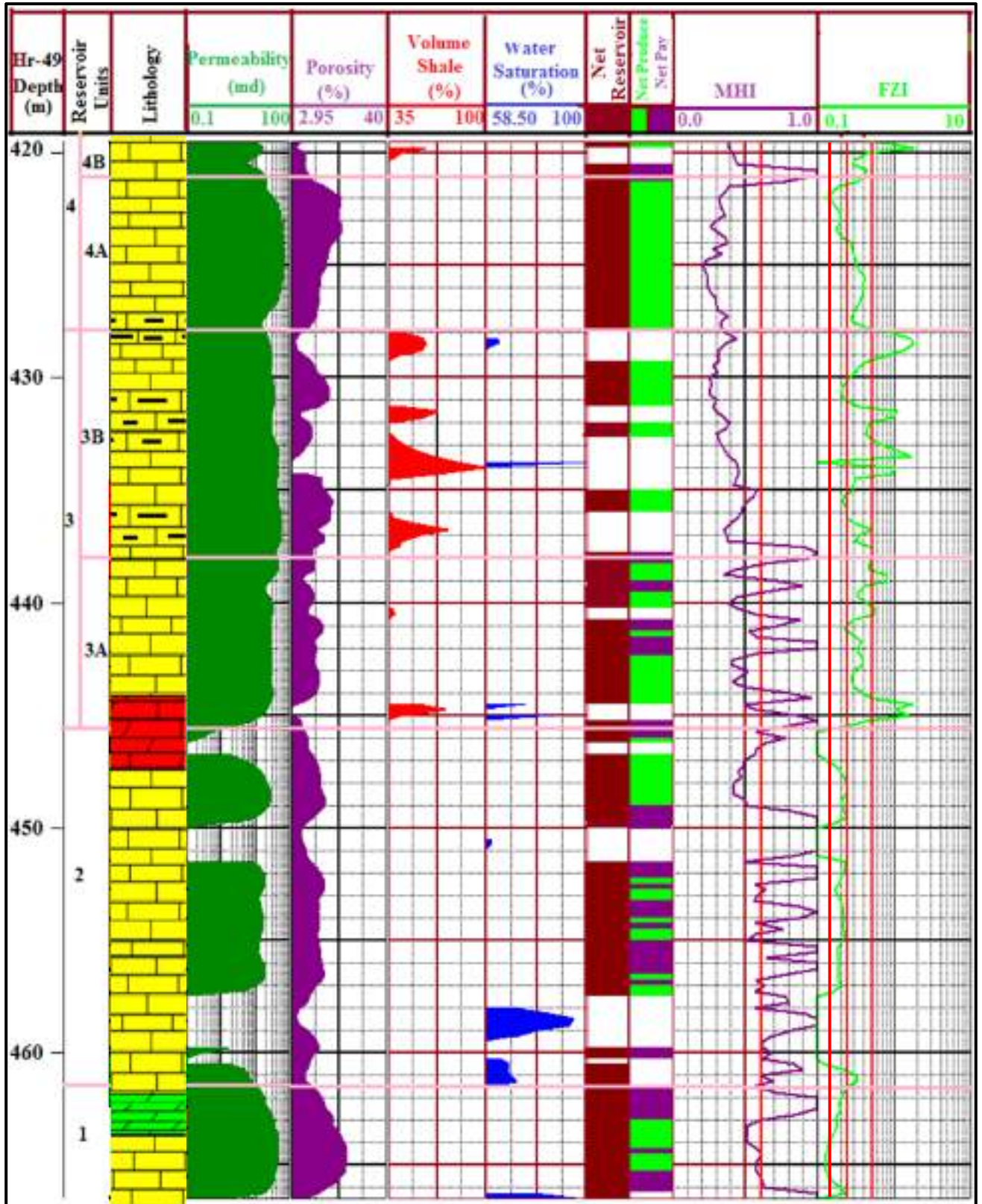


Figure 4.26: Summary of all data that are used to finalize subdivision of reservoir units and reservoir potentiality by applying the cutoffs for Jeribe Formation in well Hr-49.

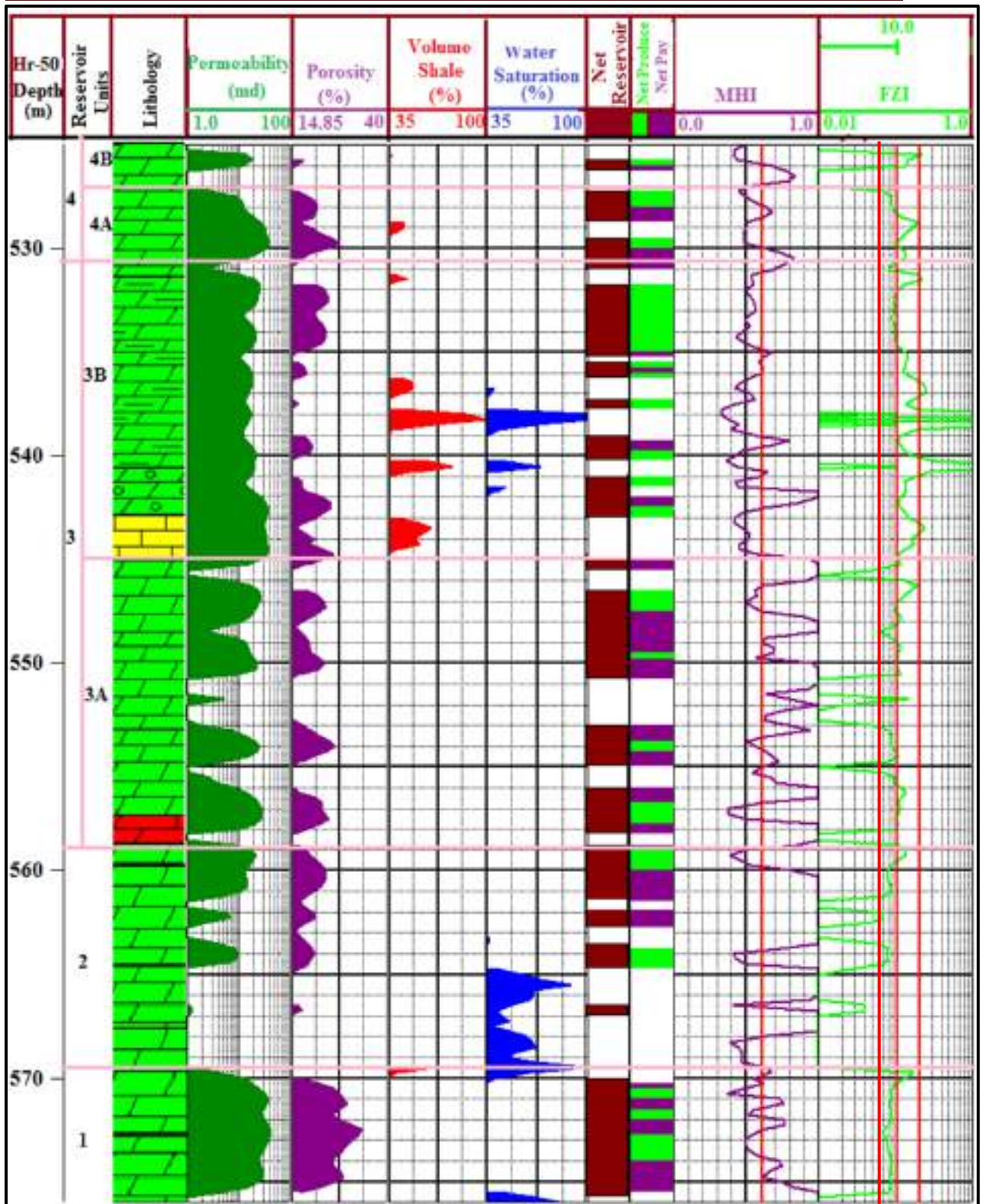


Figure 4.27: Summary of all data that are used to finalize subdivision of reservoir units and reservoir potentiality by applying the cutoffs for the Jeribe Formation in well Hr-50.

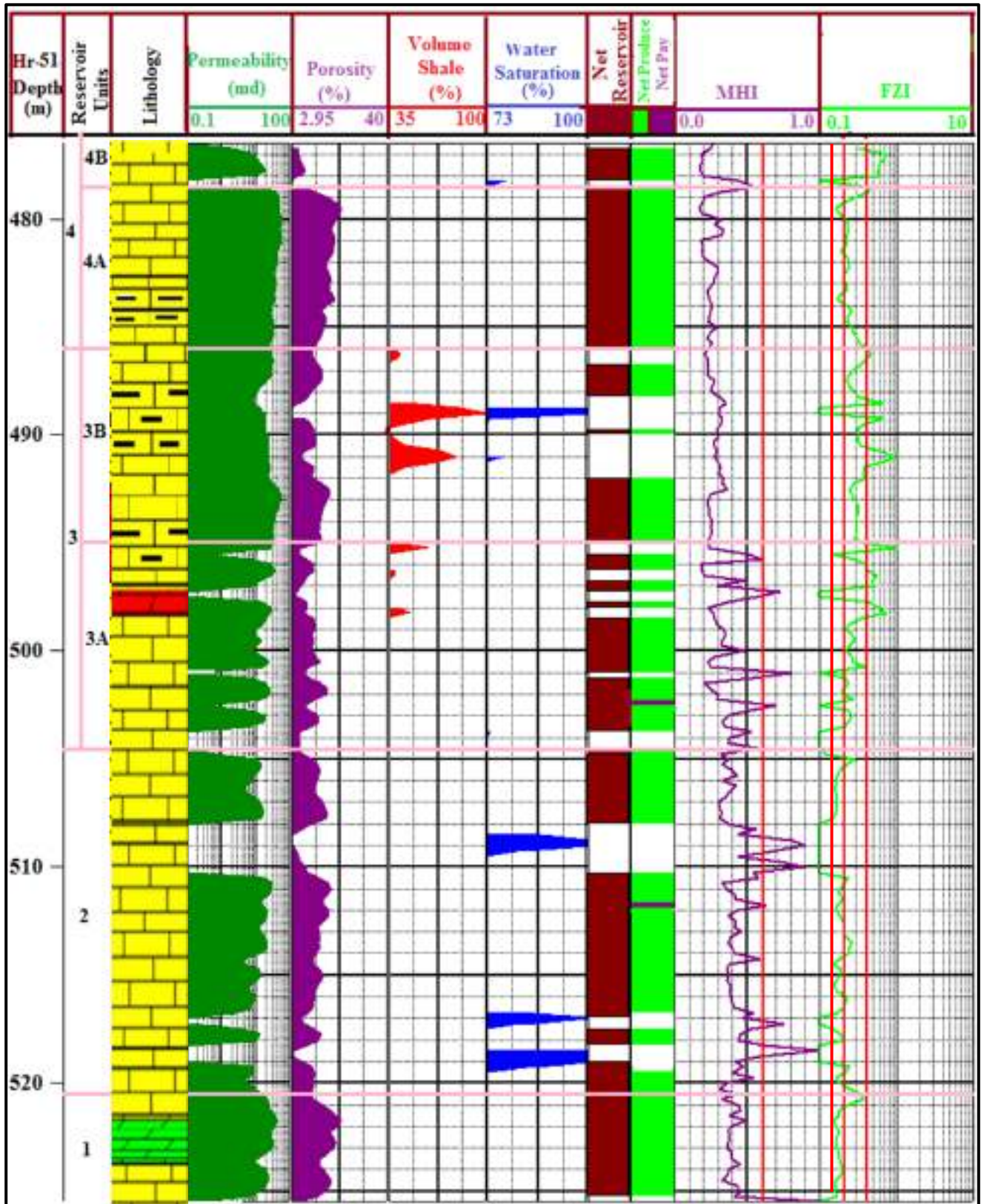


Figure 4.28: Summary of all data that are used to finalize subdivision of reservoir units and reservoir potentiality by applying the cutoffs for the Jeribe Formation in well Hr-51.

CHAPTER FIVE

Conclusions and Recommendations

5.1 Conclusions

From the results the present study the following conclusions can be made:

1. Jeribe Formation in the studied wells of Hamrin Oil Field has a thickness around 50m with a lithology which varies from limestone, dolomitic limestone dominant as in the wells Hr-49 and Hr-51 to dolostone dominant as in the well Hr-50.
2. The lithology of Jeribe Formation contains variable ratios of shale which exceeds 35% in some intervals especially in the middle part of the formation. The existed shale is of dispersed distribution type which generally has a negative effect on the porosity and permeability of the reservoirs.
3. The porosity of Jeribe Formation in the well Hr-50 is relatively higher than the other two studied wells (more than 15% porosity as an average in the well Hr-50). The upper part and the lowermost part of the formation are of higher porosity than the middle and the lower part. The lowest porosity values (less than 5%) exist within the middle part where the highest shale content exists.
4. Jeribe Formation in the two wells of Hr-49 and Hr-51 is mainly contains gas, whereas oil is the reservoired hydrocarbon within the formation in the well Hr-50.
5. Jeribe Formation in the well Hr-50 owns secondary porosity (mostly

vugs) more than the other two wells in which exceed 7% in some intervals. The least affecting by secondary porosity is in the well Hr-51 in which generally less than 4% contribution to the total porosity is recorded in the lower part of the formation with being most of the middle and upper part of the formation in this well of no secondary porosity.

6. Jeribe Formation in the studied wells contains no intervals of higher than moderate permeability (15-50md). The upper part of the formation in the well Hr-49 (the upper 25m) owns as average more than 30md permeability, whereas the lower part is relatively of lower permeability (less than 20md as average) including intervals of impermeable or poor zones. Jeribe Formation in the other two wells of Hr-50 and Hr-51 is generally of large similarity in the permeability with being the upper part of the formation (about 20m thickness) of continuous moderate permeability ranging between 15 and 30md (being relatively higher in the well Hr-51). The middle part of the formation till the last lower 5meters in the two wells of Hr-50 and Hr-51 is of an obvious fluctuate permeability values reflecting noticeable heterogeneity in the reservoir properties of Jeribe Formation. Impermeable, poor, and moderate permeability zones with variable thicknesses also exist in this part of the formation in the mentioned later two wells.
7. Depending on the variability in shaleness, porosity, and permeability values, Jeribe Formation in the studied wells can be divided into four reservoir units (with different reservoir potentialities). The reservoir subunit RU-4A at the upper part of the formation is of highest reservoir potentiality among the identified reservoir units, whereas RU-4B is of the least reservoir potentiality.

8. Water saturation in Jeribe Formation in the well Hr-51 is relatively higher than the other two studied wells (especially the lower part of the formation). The formation also contains narrow zones of full water saturation.
9. Jeribe Formation in the well Hr-51 contains the least residual hydrocarbon saturations, whereas most of the existing hydrocarbons within the formation in the well Hr-50 are residual hydrocarbons. Such a condition is interpreted as a consequence of the nature of the reservoir hydrocarbons (gas in the wells Hr-49 and Hr-51, oil in the well Hr-50).
10. Jeribe Formation in the studied wells can produce hydrocarbons associated with different volumes of water. The less produced water is in the reservoir unit RU-1 and the reservoir subunit RU-4B, and the highest water production is in the reservoir subunit RU-3A. The produced hydrocarbons from the remained reservoir units and subunits will accompanied by in between volumes of water depending on the porosity and saturation of each interval.
11. Almost the whole parts of Jeribe Formation in the well Hr-51 contain moveable hydrocarbons, whereas the formation in the other two studied wells contains a lot of horizons with non-moveable hydrocarbons especially in the middle and lower part of the formation.
12. Jeribe Formation in the studied wells composes mainly of grain dominated packstone or dolopackstone except the reservoir units RU-1 and RU-2 in the well Hr-50 which are mostly mud dominated packstone or wackstone.
13. The pore throat sizes between the grains of the Jeribe Formation in the studied wells ranges mostly between 1.0 and 2.0 microns with

being 2.0 micron much more dominated. Pore throat sizes of 0.5 micron exist rarely in some reservoir units of the formation like RU-2 in the well Hr-49.

14. The fluid flow from Jeribe Formation is mainly due to permeability capacity created from connected pores within the matrix and from microfractures.
15. Jeribe Formation characterizes by four Flow Zone Indicators representing four unique hydraulic flow units.
16. The highest N/G ratio of reservoir, pay, and production for Jeribe Formation exist in the well Hr-51 (79.83%, 79.33%, and 78.68% respectively) and the lowest in the well Hr-50 (58.93%, 54.31%, and 25.98% respectively).
17. The well Hr-51 contains the highest production thickness of Jeribe Formation among the three studied wells which is equal to 37m, whereas the well Hr-50 contains the lowest which is equal to 13.25m.

5.2 Recommendations

For better evaluating Jeribe Formation in the studied Hamrin Oil Field, the following suggestions are highly recommended:

1. Full package data always results in better evaluating reservoirs, therefore much more rock samples (core and cuttings with condensed depth intervals) associated with data of core analysis and well tests for Jeribe will definitely improve the evaluation process of the formation.
2. Applying techniques of reservoir evaluation on Jeribe Formation in those wells which penetrated the true thickness of the formation and best covering the whole structure of the field.

3. Comparing the results of the log analysis between the log data from the old wells with the log data from the newly drilled wells and that for following the changes in the reservoir dynamic properties which occurred to Jeribe Formation due to periods of production.

REFERENCES

Abdulrahman, N. A. (2007) "Sedimentological and Petrophysical Properties study of Stratigraphic Succession for (Aquitanian-Lower Early Langhian) Stage in Well KorMor/3 at Kirkuk Area", *M.Sc .thesis*, University of Mosul, Mosul, Iraq.

Abed, A. A. (2014) "Hydraulic flow units and permeability prediction in a carbonate reservoir, Southern Iraq from well log data using non-parametric correlation", *International Journal of Enhanced Research in Science Technology & Engineering*, 3(1): 480-486.

Al-Ameri, T. K. and Zumberge, J. (2012) "Middle and Upper Jurassic hydrocarbon potential of the Zagross Fold Belt, North Iraq", *Marine and Petroleum Geology*, 36: 13-34.

Al-Ameri, T. K., Zumberg, J. and Markarian, Z. M. (2011) "Hydrocarbons In the Middle Miocene Jeribe Formation Dyala Region, NE Iraq", *Journal of Petroleum Geology* 34(2): 199-216.

Al-Ayobe, N. S. (2004) "Microfacies and Modeling of Jeribe Formation (Early Middle Miocene) Northwest of Iraq", *M.Sc .thesis*, Basra University, Basra, Iraq.

Al-Dabbas, M. A., Al-Sagri, K. E. A., Al-Jassim, J. A., and Al-Jwaini, Y. S. (2012) "Sedimentological and diagenetic study of the Early Middle Miocene Jeribe Limestone Formation in selected wells from Iraq northern oilfields (Ajil; Hamrin; Jadid; Khashab)" *Journal of Baghdad for Science* 10(1): 207-216.

AL-Ghreri, M. F. (2007) "Biostratigraphic Succession of the Formations of Euphrates Valley between Hit and AL-Qaim in Iraq", *Ph.D.dissertation*, Baghdad University, Baghdad, Iraq.

AL-Hietee, S. A. A. (2012) "Facies architecture and Sequence Stratigraphy of the Lower and Middle Miocene, Kirkuk area, North Iraq", *M.Sc.thesis*, Baghdad University, Baghdad, Iraq.

Al-Jouiny, Y. S. K. (2000) "Sedimentological Study of Jeribe Limestone in selected wells from Northern Hamrin, Saddam, Khashab, and Judiada Fields", *MSc thesis* (unpublished), Baghdad University, Baghdad, Iraq.

Al-Juboury A. L., Al-Tarif, A. M. and Al-Eisa, M. (2007)"Basin analysis

of the Burdigalian and Early Langhian successions, Kirkuk Basin, Iraq", *Geological Society*, London, Special Publications, 285(1): 53-68.

Al-Jwaini, Y. S. and Gayara, A. D. (2016a) "Upper Palaeogene-Lower Neogene Reservoir Characterization in Kirkuk, Bai Hassan and Khabaz Oil Fields, Northern Iraq" *Tikrit Journal of Pure Science*, 21(3): 82-101.

Al-Jwaini, Y. S. and Gayara, A. D. (2016b) "Palaeoenvironments and sequence development of the Upper Palaeogene-Lower Neogene Succession in Kirkuk, Bai Hassan and Khabaz oil Fields, Northern Iraq" *Tikrit Journal of Pure Science*, 21(3): 102-113.

Al-Mehaidi, K. (2009) "Prudent Oil Field Development, Iraq".

Al-Qayim, B., Ibrahim, A. and Kharajiany, S. (2016) "Microfacis and Sequence stratigraphy of the Oligocene–Miocene sequence at Golan Mountain, Kurdistan, Iraq" *Carbonates and Evaporites*, Springer-Verlag, Berlin Heidelberg, 31(3): 259-276.

Al-Saddique, M. A., Hamada, G. M. and Al-Awad, M. N. (2000) "Recent Advances in Coring and Core Analysis Technology" *New Technique to Improve Reservoir Evaluation, Engineering Journal of the University of Qatar*, 13:29-52.

Alsharhan, A. S. and Nairn, A. E. M. (1997) "Sedimentary Basins and Petroleum Geology of the Middle East", Elsevier, Amsterdam, 942 p.

Amaefule, J. O., Altunbay, M., Tiab, D., Kersey, D. G. and Keelan, D. K. (1993) "Enhanced Reservoir Description: Using core and log data to identify hydraulic (flow) units and predict permeability in Uncored Intervals/Wells", 68th Annual Tech. Conf. And Exhibit. Houston, TX Paper SPE26435.

Aqrawi, A. A. M., Goff, J. C., Horbury, A. D., and Sadooni, F. N. (2010) *Petroleum Geology of Iraq*, Scientific press Lt Po box 21, Beaconsfield, Bucks HP9 1NS, UK.

Aqrawi, A. A. M., Al-Hakim, M. K. and Ashoor, A. M. A. (1989) "The stratigraphic subdivision of the Lower Fars Formation (Miocene) in southern Mesopotamian Basin, Iraq." *Journal of Geological Society of Iraq*, 22(2):25-34.

Asquith, G. B. and Gibson, C. R. (1982) *Basic Well Analysis for*

Geologist, The American Association of Petroleum Geologists, Tulsa, Oklahoma .USA.

Asquith, G. and Krygowski, D. (2004) "Chapter 1: Basic Relationships of Well Log Interpretation", in *Basic Well Log Analysis*, (Second edition) edited by Asquith, G., and Krygowski, D., pp. 1-20. AAPG Methods in exploration 16, Tulsa, Oklahoma.

Asquith, G. and Krygowski, D. (2004) "Chapter 4: Porosity Logs", in *Basic Well Log Analysis*, (Second edition) edited by Asquith, G., and Krygowski, D., pp. 37-76. AAPG Methods in exploration 16, Tulsa, Oklahoma.

Asquith, G. and Krygowski, D. (2004) "chapter 7: Log Interpretation", in *Basic Well Log Analysis*, (Second edition) edited by Asquith, G., and Krygowski, D., pp. 115-135. AAPG Methods in exploration 16, Tulsa, Oklahoma.

Asquith, G. and Krygowski, D. (2004) "Chapter 8: Petrophysical Techniques", in *Basic Well Log Analysis*, (Second edition) edited by Asquith, G., and Krygowski, D., pp. 137-149. AAPG Methods in exploration 16, Tulsa, Oklahoma.

Baker Hughes (1992) *Advanced Wire line and MWD Procedure Manual*, Houston.

Bassioui Z. (1994) *Theory, Measurement, and Interpretation of Well Logs*, Society of Petroleum Engineers, Richardson, Texas.

Bateman, R. M. (1985) *Open-Hole Log Analysis and Formation Evaluation*, 137 Newbury Street, Boston.

Bellen, R. C. Van. M., Dunnington, H. V. and Wetyzel, R. and Morton, D. (1959) *Lexique stratigraphique International*. Asie, Fscicule 10a, Iraq, Paris.

Buday, T. (1980) "Volume I: Stratigraphy and Paleontology" in *The Regional Geology of Iraq*, Dar Al-Kutub publishing house, University of Mosul. Iraq.

Chandra T. (2008) "Permeability estimation using flow zone indicator from well log data", *7th International Conference and Exposition on Petroleum Geophysics (P140)*, Hyderabad, Pakistan.

- Choquette, P. W., and Pray, L. C. (1970) "Geological Nomenclature and Classification of Porosity in Sedimentary Carbonates" *AAPG Bulletin*, 54(2): 207-250.
- Darling, T. (2005) *Well Logging and Formation Evaluation*, Elsevier, Amsterdam.
- Dewan, J. (1983) *Essentials of Modern Open-Hole Log Interpretation*: PennWell Publishing Company, Tulsa, Oklahoma, 361 p.
- Dijkers, A.J. (1985) *Geology in Petroleum Production* (Developments in Petroleum Science, 20), Elsevier, Amsterdam.
- Dresser Atlas (1979) *Log interpretation charts*: Dresser Industries, Inc., Houston, Texas, 107p.
- Dunham, R.J. (1962) "Classification of carbonate rocks according to depositional texture". In Ham, W.E., ed., *Classification of Carbonate rocks*, AAPG-Publ-Memoris 1, Tulsa, Oklahoma.
- Ellis, d. V., and Singer, J. M. (2008) *Well Logging for Earth Scientists*, Second Edition, Springer.
- Embry, A. F. and Klovan, J. E. (1972) "Absolute water depth limits of Late Devonian paleoecological zones" *Geologische Rundschau*, 61(2): 672-686.
- Fadhil, T. D. (2013) "Sedimentological and Reservoir Characterization for Jeribe Formation at Alass Dome/North Hamrin Oil Field", *M.Sc. thesis*, (unpublished) University of Tikrit, Tikrit, Iraq.
- Flügel, E. (2010) *Microfacies of Carbonate Rocks* (Analysis, Interpretation and Application, 2nd Edition), Springer, Heidelberg.
- Gharib, A. F. (2012) "Sedimentological and Reservoir Characterization of Euphrates and Jeribe Formations in Selected Wells in Ajeel Oil Field/Northern Iraq", *M.Sc.thesis (unpublished)*, University of Tikrit, Tikrit, Iraq.
- Ghorab, M., Ramadan, A. M., and Nouh, A. Z. (2008) "The relation between shale origin (source or nonsource) and its type for Abu Roash Formation at Wadi-El Naturn area, south of Western Desert, Egypt," *Australian Journal of Basic Applied Sciences*, 2(3): 360-371.

Glover, P. (2008) *Petrophysics MSc course notes*, University of Aberdeen, UK.

Halliburton, (2001) *Basic Petroleum Geology and Log Analysis*.

Hambolt, A. (2006) "Genetic pore typing as a means of characterizing reservoir flow units: San andres, Sunflower field, Terry County, Texas", *MSc thesis (unpublished)*, Texas A&M University.

Hooper, R. J., Baron, I. R., Agah, S. and Hatcher, R.D. (1995) "The Cenomanian to Recent development of the southern Tethyan margin in Iran", In M.I. Al-Husseini (Ed.), *Middle East Petroleum Geosciences, Geo'94*. Gulf PetroLink, Bahrain, 2: 505-516.

Hussein, H. S. (2015) "Characterization of the Tertiary Reservoirs in Khabbaz Oil Field, Kirkuk Area, Northern Iraq" *MSc. thesis (unpublished)*, Sulaimani University, Sulaimani, Iraq.

Ibrahim, D. M. (2008), "Sedimentology and reservoir characteristics of Jeribe Formation (Middle Miocene) in Tawke Oil Field, Zakho, Kurdistan Region - Iraq", *MSc thesis (unpublished)*, Salahaddin University, Erbil, Iraq .

Ibrahim, Y. k., AL-Sheikhily, S. S. and AL-Jassim, J. A. (2002) "The biostratigraphy of Euphrates and Jeribe formations in the Middle and Southern Iraq" *Journal Iraqi Science* 43(2): 32-49.

Jahn, F., Cook, M. and Graham, M. (2003) *Hydrocarbon Exploration and Production*, Elsevier, Amstrdam.

Jassim, S. Z. and Buday, T. (2006) "Chapter 6: Units of the Unstable Shelf and the Zagros Suture", in *Geology of Iraq* (first edition) edited by Jassim, S.Z. and Goff, J. C., pp. 71-83. Brno, Czech Republic; Dolin, Prague and Moravian Museum.

Jassim, S. Z. and Buday, T. (2006) "Chapter 14: Latest Eocene-Recent Megasequence AP11", in *Geology of Iraq* (first edition) edited by Jassim, S. Z., and Goff, J. C., pp. 169-184 Brno, Czech Republic; Dolin, Prague and Moravian Museum.

Karim, S. A. (1978) "The genus Borelis de Montfort from Oligocene-Miocene of Iraq", *Journal Geological Society of Iraq*, XI: 106-118.

Khan, M. N. (1989) *Introduction to Wire line Log Interpretation*, Oil and Gas Development Cooperation.

Kharajiany, S. O. A. (2014) "Occurrence of Early and Middle Miocene Rocks (Euphrates, Dhiban, and Jeribe Formation) in Ashdagh Mountain, Sangaw area, Sulaimanyah City, NE Iraq", *Iraqi Bulletin of Geology and Mining*, 10(1): 21-39.

Kharajiany, S. O. A., Qadir, F. M., Hakary, S. H., and Sharbazheri, H. G. (2014) "Oligocene and Miocene Rock Beds in Mamlaha Anticline, Chamchamal Town, Sulaimani City-Kurdistan Region/Iraq", *Journal of Zankoy Sulaimani*, part A (jzs), 16(1): 71-93.

Krygowsky, D. A. (2003) *Guide to Petrophysical Interpretation*, Texas, USA.

Kulyk, V. V. and Bondarenko, M. S. (2016), "Identification of gas reservoirs and determination of their parameters by combination of radioactive logging methods", *Геофизический журнал*, (2) T38:106-119.

Larionov, W. W. (1969) *Radiometrija Skwaschin*, NedraVerlag, Moscow.

Law, A., Megson, J. and Pye, M. (2001) "Low permeability reservoirs: introduction", *Petroleum Geoscience*, 7(1): 2-2.

Lawa, F. A. (1989) "Biostratigraphy and Depositional Environments of the Oligocene–Miocene Sediments in the Mosul –Qaiyarah Area, North Iraq", (Unpublished Report, DGS. Lib., No.180), Baghdad/Iraq.

Lucia, F. J. (1999) "Characterization of Petrophysical Flow Units in Carbonate Reservoirs" *Discussion AAPG Bulletin*, 83(7): 1161-1163.

Lucia, F. J. (2007) *Carbonate Reservoir Characterization*, second Edition, Springer- Verlag Berlin Heidelberg New York.

Mahdi, A. Q. (2015) "Source rock evaluation of the Najmah, Chia Gara, and Balambo formations and related crude oils, Northwestern Zagros Basin, Northern Iraq", *MSc thesis (unpublished)*, Mansura University, Egypt.

Markaryan, Z. M. (2005) "Hydrocarbon generation, migration pathways and their accumulation of the Jeribe Formation in NE Iraq" *M.Sc.thesis*, (unpublished), University of Baghdad, Baghdad, Iraq.

- Miller, M. S. (1970) "Mechanical Well-Logging Methods, Virginia Minerals", 16(4): 29-40.
- Mohagheh, S., Balan, B. and Ameri, S. (1997) "Permeability determination from well log data", *SPE Formation Evaluation*, 12(3): 170-174.
- NOC, (1992) *Internal report*, 29.
- NOC, (1994), *The Annual Report of the reservoirs for the year 1993*.
- North, F. K. (1985) *Petroleum Geology*, Allen and Unwin Inc.
- Numan, N. M. S. (1997) "A Plate Tectonic Scenario for the Phanerozoic Succession in Iraq" *Iraqi Geological Journal*, 30(2): 85-119.
- Parnell, J., Taylor, C. W., Thackrey, S., Osinski, G. R. and Lee, P. (2010) "Permeability data for impact breccias imply focussed hydrothermal fluid flow" *Journal of Geochemical Exploration*, 106(1–3): 171-175.
- Peters, E. J. (2001) *Advanced Petrophysics*, University of Texas, USA.
- Prazak, J. (1974) "Stratigraphy and Paleontology of the Miocene of the Western Desert, W. Iraq" Manuscript report, GUESURV, Baghdad.
- Rider, M. (2002) *The Geological Interpretation of Well Logs*, Second Edition, Rider, Texas, French Consulting Ltd., Aberdeen and Sutherland.
- Rider, M. and Kennedy, M. (2011) *The Geological Interpretation of Well Logs*.
- Rivas, J. J., Busnego, H., Bejarano, C. and Meza, R. (2014) "Modeling of Pore Throat Radio using Pittman Modified Equation for Carabobo Area in the Faja Petrolífera del Orinoco", Heavy Oil (Latin America Conference and Exhibition), Venezuela.
- Sadeq, Q. M., Bhattacharya, S. K. and Wan Yusoff, W. I. B. (2015) "Permeability Estimation of Fractured and Vuggy Carbonate Reservoir by Permeability Multiplier Method in Bai Hassan Oil Field Northern Iraq" *Journal of Petroleum and Environmental Biotechnology*, 6(4): doi:10.4172/2157-7463.1000231

Schlumberger (1972) *Log Interpretation / Charts*: Huston, Schlumberger Well Services, Inc, Vol.1.

Shlumberger (1988) *Log interpretation chart*, Schlumberger Educational Services, U.S.A.

Schlumberger (1989) *Log Interpretation Principles/Applications*, Sguard Land, Texas.

Schon, J. (2015) *Basic Well Logging and Formation Evaluation* (1st Edition), Bookboon.com.

Sharland, P. R., Arche, R., Casey, D. M., Davies, R. B., Hall, S. H., Heward, A. P., Horbury, A. D. and Simmons, M. D. (2001) "Arabian Plate Sequence Stratigraphy" *GeoArabia Special Publication 2*, Manama, Bahrain, Gulf Petrolink.

Sissakian, V. K., Karim, S. A., Al-Kubaisyi, K. N., Al-Ansari, N. and Knutsson, S. (2016) "The Miocene Sequence in Iraq, a Review and Discussion, with emphasize on the Stratigraphy, Paleogeography and Economic Potential" *Journal of Earth Sciences and Geotechnical Engineering*, 6(3): 271-317.

Taghavi, A. A. (2005) "Improved Permeability Estimation through Use of Fuzzy Logic in a Carbonate Reservoir from Southern Iran", Society of Petroleum Engineers (SPE) Inc. In SPE Middle East Oil and Gas Show and Conference.

Teh, W. J. and Willhite, G. P. (2011) "Improved Predictions of Porosity from Microresistivity Logs in a Mature Field through Incorporation of Pore Typing", *SPE-149506-PP*: 1-13.

Thomas, B. H. (2002) Flow unit prediction with limited permeability data using artificial neural network analysis", *PhD Dissertation (unpublished)*, West Virginia University, United States.

Tiab, D. and Donaldson, E.C. (2004) *Petrophysics – Theory and Practice of Measuring Reservoir Rock and Fluid Transport Properties*, 2nd Ed., Boston: Gulf Publishing Co.

Tucker, M. E. (1999) "Sabkha cycles, stacking patterns and controls: Gachsaran (Lower Fars/Fatha) Formation, Miocene, Mesopotamian Basin,

Iraq" *N. Jb. Geol. Palaont. Abh.*, 214, 45-69.

Ulasi, A. I., Onyekuru, S. O. and Iwuagwu, C. J. (2012) "Petrophysical evaluation of uzek well using well log and core data, Offshore Depobelt, Niger Delta, Nigeri" 3(5): 2966-2991.

Van Golf-Racht, T.D. (1982) *Fundamental of fractured reservoir engineering, Development in Petroleum Science*, 12, Elsevier, Amsterdam.

Western Atlas (1995) *Introduction to Wireline Log Analysis*, Houston, Texas.

Appendix A

Well Log Data-Well, Hr-49.

Depth (m)	GR (API)	Δt ($\mu\text{s}/\text{ft}$)	ρ_b (g/cc)	MSFL ($\Omega\cdot\text{m}$)	LLS ($\Omega\cdot\text{m}$)	LLD ($\Omega\cdot\text{m}$)	M	N	(ρ_{ma})a	(Δt_{ma})a
419.50	50.00	61.45	2.43	88.97	102.78	96.49	0.89	0.65	2.62	49.62
420.00	58.63	55.12	2.35	51.31	48.17	46.89	0.99	0.64	2.63	41.55
421.00	18.24	84.05	2.48	754.44	53.67	67.86	0.71	0.63	2.65	63.51
422.00	31.57	79.83	2.31	25.15	21.38	38.43	0.83	0.58	2.71	46.94
423.00	25.29	112.87	2.22	26.07	29.58	43.60	0.62	0.68	2.58	78.24
424.00	19.41	126.18	2.26	36.73	24.92	39.47	0.50	0.71	2.55	94.78
425.00	32.35	118.23	2.23	45.19	113.40	156.91	0.57	0.74	2.51	88.99
426.00	34.71	104.24	2.25	134.58	237.57	356.52	0.68	0.76	2.49	79.78
427.00	32.94	85.94	2.42	22.15	29.03	35.09	0.73	0.62	2.66	60.72
428.00	59.02	75.98	2.42	29.82	33.54	36.04	0.80	0.62	2.67	53.78
429.00	59.41	82.20	2.34	28.25	32.93	41.63	0.79	0.66	2.60	59.32
430.00	29.61	79.23	2.33	24.67	35.71	60.80	0.82	0.67	2.60	57.30
431.00	43.33	83.63	2.31	14.23	15.15	25.11	0.80	0.62	2.67	53.38
432.00	55.10	82.00	2.36	24.22	13.72	25.11	0.79	0.64	2.64	56.86
433.00	59.80	95.02	2.31	22.53	14.22	29.27	0.72	0.67	2.60	66.66
434.00	76.67	103.54	2.31	26.98	10.00	20.58	0.65	0.63	2.64	69.88
435.00	53.14	90.51	2.26	13.35	3.67	6.03	0.78	0.65	2.62	59.05
436.00	54.71	88.97	2.14	28.73	11.34	20.21	0.87	0.72	2.53	58.48
437.00	64.31	114.83	2.24	13.10	9.13	14.73	0.60	0.61	2.68	72.53
438.00	32.94	109.85	2.39	261.83	31.15	45.50	0.57	0.66	2.60	82.47
439.00	54.71	75.65	2.35	179.23	46.32	53.03	0.84	0.69	2.57	58.04
440.00	47.06	83.02	2.33	52.54	43.87	54.47	0.80	0.68	2.58	61.23
441.00	39.02	78.61	2.36	82.48	25.30	24.40	0.81	0.62	2.66	53.27
442.00	36.86	76.02	2.33	382.19	36.95	35.96	0.85	0.69	2.57	57.59
443.00	43.73	76.31	2.32	65.21	30.57	37.28	0.85	0.67	2.60	54.90
444.00	43.73	84.54	2.34	136.62	27.92	32.26	0.78	0.67	2.60	61.24
445.00	59.22	79.56	2.50	118.24	21.30	24.39	0.73	0.58	2.72	55.88
446.00	27.06	68.25	2.59	100.50	19.11	25.28	0.76	0.55	2.77	48.62
447.00	22.55	63.65	2.52	19.11	9.98	12.17	0.83	0.56	2.75	44.78
448.00	27.06	80.12	2.43	27.41	17.77	23.51	0.76	0.60	2.68	55.65
449.00	23.73	84.81	2.45	31.37	14.71	17.93	0.72	0.57	2.74	55.49
450.00	14.71	66.42	2.62	730.75	23.72	29.45	0.76	0.56	2.74	51.31
451.00	29.61	56.74	2.55	704.74	13.55	17.29	0.85	0.57	2.73	43.97
452.00	26.27	73.59	2.45	261.22	8.48	11.11	0.80	0.59	2.71	50.43
453.00	26.47	72.15	2.48	29.17	10.15	12.84	0.79	0.56	2.74	47.91
454.00	35.49	75.88	2.47	39.99	6.76	8.03	0.77	0.56	2.75	49.68
455.00	24.71	71.47	2.47	28.90	13.06	16.67	0.80	0.58	2.71	49.97
456.00	19.41	76.26	2.47	234.26	12.37	16.52	0.77	0.57	2.73	50.96
457.00	27.65	74.53	2.54	39.97	11.41	15.64	0.74	0.54	2.77	49.93
458.00	21.76	63.42	2.68	35.22	12.37	16.81	0.75	0.53	2.80	47.49
459.00	22.16	60.92	2.65	27.36	4.00	6.12	0.78	0.51	2.82	42.73
460.00	27.45	65.61	2.57	24.55	5.44	8.17	0.78	0.52	2.81	43.10
461.00	52.35	70.11	2.53	23.89	6.94	10.14	0.78	0.53	2.79	45.77
462.00	29.22	73.46	2.44	295.89	7.33	10.51	0.80	0.58	2.72	49.17
463.00	30.20	78.92	2.30	29.92	9.43	12.81	0.85	0.64	2.64	51.92

464.00	30.00	86.67	2.23	19.75	7.32	11.29	0.83	0.64	2.63	53.22
465.00	36.86	85.33	2.26	16.49	5.59	7.73	0.82	0.58	2.72	47.35
466.00	42.35	87.24	2.45	14.80	4.88	5.49	0.70	0.52	2.82	50.48
466.50	29.61	73.92	2.62	295.66	4.42	5.29	0.71	0.54	2.78	52.08

Well Log Data-Well, Hr-50.

Depth (m)	GR (API)	Δt ($\mu\text{s}/\text{ft}$)	ρ_b (g/cc)	MSFL ($\Omega.\text{m}$)	LLS ($\Omega.\text{m}$)	LLD ($\Omega.\text{m}$)	M	N	(ρ_{ma}) _a	(Δt_{ma}) _a
525.00	30.46	57.11	2.70	356.87	268.99	215.11	0.78	0.55	2.85	45.40
526.00	52.23	74.21	2.51	208.38	86.04	65.89	0.76	0.50	2.94	39.84
527.00	20.58	63.67	2.65	238.92	126.19	122.35	0.76	0.52	2.89	43.62
528.00	23.61	69.05	2.47	261.73	91.71	93.97	0.81	0.52	2.90	37.64
529.00	66.76	77.60	2.32	176.83	99.55	104.81	0.85	0.53	2.88	36.17
530.00	50.83	78.99	2.32	133.29	53.06	47.92	0.84	0.53	2.88	37.53
531.00	50.03	61.70	2.52	302.85	117.31	92.27	0.84	0.52	2.89	36.60
532.00	44.39	73.43	2.36	75.73	46.28	45.37	0.85	0.53	2.88	36.00
533.00	27.66	75.03	2.49	62.53	27.52	28.26	0.77	0.50	2.93	40.19
534.00	29.48	75.33	2.42	26.29	15.78	17.77	0.80	0.51	2.92	38.00
535.00	53.67	73.84	2.49	58.66	16.36	18.43	0.77	0.49	2.95	38.26
536.00	58.51	73.64	2.43	39.27	13.76	16.08	0.80	0.48	2.96	33.78
537.00	66.58	73.85	2.46	27.27	10.86	14.02	0.79	0.51	2.91	39.03
538.00	84.53	75.04	2.43	7.47	7.20	9.83	0.80	0.51	2.92	37.70
539.00	49.05	72.26	2.49	20.18	7.07	8.98	0.79	0.50	2.93	37.93
540.00	58.93	76.24	2.41	18.76	10.56	14.81	0.80	0.51	2.92	37.80
541.00	59.34	73.46	2.45	45.86	13.89	19.29	0.80	0.52	2.90	39.09
542.00	48.65	80.62	2.39	121.67	8.33	12.23	0.78	0.50	2.93	39.19
543.00	63.17	79.93	2.30	17.28	12.00	14.41	0.84	0.53	2.88	37.27
544.00	70.23	78.84	2.29	20.37	10.00	10.87	0.85	0.50	2.93	32.36
545.00	40.60	78.05	2.39	126.19	19.82	20.55	0.80	0.52	2.89	40.19
546.00	45.04	67.11	2.52	185.08	30.42	32.10	0.80	0.55	2.85	42.64
547.00	49.68	77.06	2.39	26.53	16.07	15.79	0.81	0.49	2.94	35.14
548.00	33.75	71.79	2.50	314.10	24.22	23.78	0.78	0.53	2.87	43.17
549.00	45.45	72.29	2.47	41.48	17.93	16.22	0.79	0.50	2.94	36.70
550.00	35.98	76.37	2.41	95.99	17.60	15.22	0.80	0.52	2.90	38.87
551.00	19.25	58.38	2.67	460.69	66.05	69.59	0.78	0.53	2.88	42.24
552.00	51.91	66.44	2.58	142.07	21.71	21.51	0.78	0.50	2.93	38.54
553.00	26.71	62.37	2.54	106.12	24.44	25.11	0.82	0.51	2.91	36.67
554.00	34.18	76.09	2.38	38.56	18.59	17.61	0.82	0.50	2.94	34.71
555.00	41.64	63.66	2.56	88.42	34.57	34.22	0.80	0.51	2.91	37.91
556.00	46.48	67.05	2.50	101.39	16.36	14.95	0.81	0.53	2.88	39.29
557.00	49.31	78.48	2.37	6.88	7.75	7.15	0.80	0.51	2.92	37.47
558.00	28.75	70.14	2.50	420.54	11.16	10.97	0.79	0.52	2.89	40.66
559.00	44.48	74.51	2.44	12.91	7.75	7.98	0.80	0.54	2.87	42.09
560.00	29.36	66.76	2.45	59.74	13.89	13.65	0.84	0.49	2.95	31.66
561.00	13.84	71.14	2.50	195.49	9.64	9.92	0.78	0.52	2.90	40.77
562.00	17.27	65.38	2.52	95.99	12.00	12.01	0.81	0.50	2.93	35.83
563.00	14.25	61.80	2.59	257.00	15.92	15.79	0.80	0.52	2.89	39.50
564.00	25.14	70.45	2.51	10.37	9.38	8.90	0.78	0.49	2.95	37.01
565.00	24.54	66.98	2.66	373.52	6.76	6.59	0.73	0.51	2.92	43.73
566.00	19.70	59.13	2.69	234.60	9.30	9.40	0.77	0.54	2.87	44.64

567.00	19.50	65.00	2.66	688.12	11.16	10.39	0.75	0.51	2.92	42.62
568.00	25.96	62.41	2.68	20.00	5.89	7.28	0.75	0.51	2.92	41.79
569.00	43.50	67.29	2.60	9.73	5.00	6.41	0.76	0.48	2.98	36.73
570.00	48.34	77.63	2.51	13.76	5.23	6.77	0.74	0.49	2.95	41.32
571.00	30.80	92.44	2.35	16.82	3.70	4.62	0.71	0.49	2.95	43.83
572.00	31.61	77.34	2.33	17.28	3.67	4.46	0.84	0.53	2.88	36.93
573.00	31.21	79.73	2.28	8.18	4.24	4.92	0.85	0.52	2.90	34.31
574.00	34.04	74.16	2.37	20.18	5.48	5.70	0.84	0.51	2.91	35.39
575.00	24.97	75.66	2.41	38.21	10.00	10.11	0.80	0.50	2.94	35.72
576.00	10.26	58.26	2.82	1115.74	26.78	22.31	0.72	0.52	2.90	46.93

Well Log Data-Well, Hr-51.

Depth (m)	GR (API)	Δt ($\mu\text{s}/\text{ft}$)	ρ_b (g/cc)	MSFL ($\Omega.\text{m}$)	LLS ($\Omega.\text{m}$)	LLD ($\Omega.\text{m}$)	M	N	(ρ_{ma})a	(Δt_{ma})a
476.50	11.95	63.08	2.76	190.18	391.99	292.44	0.71	0.55	2.76	53.61
477.00	52.25	74.18	2.51	21.52	60.00	77.54	0.76	0.60	2.69	54.93
478.00	47.32	77.23	2.56	14.38	33.40	40.11	0.72	0.57	2.73	56.00
479.00	36.40	115.05	2.34	8.15	12.89	20.37	0.55	0.63	2.64	81.14
480.00	24.65	116.62	2.24	27.55	17.92	29.65	0.58	0.68	2.58	82.72
481.00	21.99	111.12	2.25	13.62	22.53	47.29	0.62	0.69	2.56	79.04
482.00	34.83	103.46	2.37	16.96	17.27	32.20	0.63	0.60	2.68	69.14
483.00	33.82	95.21	2.35	17.27	15.48	26.56	0.70	0.61	2.68	62.33
484.00	29.51	93.83	2.43	8.54	9.97	14.38	0.67	0.57	2.73	61.10
485.00	39.24	88.92	2.38	14.65	12.09	20.00	0.73	0.61	2.68	59.16
486.00	56.83	81.94	2.40	11.13	15.48	23.37	0.76	0.59	2.70	54.43
487.00	43.43	89.71	2.40	10.25	12.89	21.13	0.71	0.59	2.70	59.00
488.00	38.70	75.95	2.52	13.37	11.44	21.52	0.74	0.56	2.75	52.00
489.00	79.23	79.29	2.46	8.94	6.14	11.23	0.75	0.55	2.76	49.83
490.00	54.87	81.26	2.44	9.18	5.50	10.93	0.75	0.56	2.75	51.17
491.00	73.49	83.61	2.42	8.77	6.55	12.77	0.74	0.54	2.77	50.35
492.00	52.86	87.64	2.47	5.65	3.58	5.55	0.69	0.56	2.75	57.11
493.00	41.94	102.87	2.24	14.12	17.92	29.92	0.70	0.71	2.54	73.59
494.00	43.62	90.39	2.38	13.62	16.96	22.74	0.72	0.61	2.67	61.20
495.00	57.49	87.15	2.37	10.73	17.12	20.00	0.75	0.60	2.68	57.05
496.00	45.32	80.18	2.37	14.25	57.84	49.06	0.80	0.66	2.61	58.48
497.00	39.36	73.79	2.53	35.28	45.59	45.18	0.75	0.60	2.68	56.30
498.00	57.98	81.06	2.36	13.13	19.28	27.81	0.80	0.66	2.61	58.63
499.00	27.84	75.36	2.53	16.05	14.65	15.62	0.74	0.55	2.76	51.29
500.00	28.28	75.56	2.56	45.18	19.82	21.52	0.73	0.54	2.77	51.42
501.00	30.37	72.61	2.62	147.17	20.94	25.84	0.72	0.54	2.78	51.90
502.00	35.36	79.10	2.40	13.13	16.35	16.35	0.79	0.59	2.71	51.15
503.00	40.14	74.77	2.44	12.20	9.10	9.88	0.79	0.59	2.71	50.69
504.00	26.94	65.64	2.65	31.04	20.00	24.02	0.75	0.54	2.78	49.00
505.00	38.33	75.17	2.52	16.65	10.54	13.49	0.75	0.56	2.75	51.67
506.00	18.94	72.42	2.54	12.65	10.73	13.13	0.76	0.54	2.78	48.38
507.00	24.13	73.89	2.49	13.99	14.12	15.91	0.77	0.55	2.77	47.53
508.00	16.92	68.59	2.61	22.32	14.65	17.92	0.75	0.53	2.79	47.87
509.00	14.47	63.48	2.75	138.04	15.76	19.11	0.72	0.52	2.81	49.03
510.00	23.38	71.43	2.65	74.07	7.72	10.35	0.71	0.52	2.81	50.19

511.00	30.02	83.03	2.37	7.86	4.84	6.73	0.77	0.58	2.71	52.37
512.00	28.19	77.92	2.42	9.02	3.68	5.35	0.78	0.56	2.75	48.56
513.00	36.48	76.54	2.50	14.65	4.88	7.58	0.75	0.53	2.79	48.14
514.00	39.60	76.35	2.50	8.85	4.30	5.97	0.75	0.55	2.76	50.28
515.00	25.58	72.22	2.47	14.92	8.77	12.20	0.80	0.56	2.74	47.32
516.00	39.86	71.83	2.50	15.76	8.94	11.76	0.78	0.56	2.75	48.04
517.00	37.00	66.72	2.64	14.52	5.11	7.24	0.75	0.53	2.80	47.81
518.00	26.07	73.99	2.52	9.44	4.58	5.35	0.76	0.55	2.76	49.58
519.00	29.20	72.42	2.66	9.35	4.38	5.81	0.70	0.52	2.80	51.35
520.00	29.85	72.81	2.56	10.35	6.43	8.94	0.75	0.54	2.78	48.82
521.00	36.69	80.18	2.42	11.76	4.88	6.79	0.77	0.58	2.71	52.82
522.00	21.43	82.83	2.33	11.34	5.97	8.30	0.80	0.61	2.68	52.48
523.00	35.92	82.53	2.37	7.44	5.07	6.43	0.78	0.56	2.74	49.29
524.00	36.15	76.54	2.45	9.97	6.67	7.72	0.78	0.56	2.75	48.70
525.00	22.33	75.17	2.51	12.77	6.67	6.67	0.75	0.53	2.80	47.20
525.50	19.25	64.36	2.71	108.80	7.58	6.08	0.73	0.52	2.81	47.67

Appendix B

Well log derived Porosity, Permeability, and Shale volume-well Hr-49.

Depth (m)	Vsh (%)	Øs (%)	Øs co (%)	ØN (%)	ØN co (%)	ØD (%)	ØD co (%)	N-D co (%)	ØF (%)	K-log (md)
419.50	27	9.79	-1.07	7.18	2.52	16.16	9.74	6.13	6.88	9.76
420.00	43	5.32	-11.62	13.08	5.82	20.99	10.98	8.40	16.53	14.23
421.00	1	25.78	25.26	6.96	6.74	13.23	12.93	9.83	0.00	19.28
422.00	8	22.79	19.48	23.51	22.09	23.33	21.37	21.73	8.09	34.88
423.00	5	46.16	44.36	16.38	15.60	28.38	27.32	21.46	0.00	62.48
424.00	2	55.57	54.87	11.09	10.78	26.38	25.96	18.37	0.00	66.70
425.00	9	49.95	46.42	8.53	7.01	27.85	25.76	16.38	0.00	63.82
426.00	11	40.06	35.83	4.74	2.93	26.82	24.31	13.62	0.00	53.33
427.00	9	27.12	23.42	12.21	10.62	17.10	14.91	12.77	0.00	26.99
428.00	44	20.07	2.80	12.77	5.36	17.10	6.89	6.13	4.17	20.11
429.00	45	24.47	6.86	10.82	3.27	21.39	10.98	7.13	2.32	30.77
430.00	7	22.37	19.57	10.93	9.73	21.94	20.28	15.01	1.31	31.03
431.00	19	25.48	18.03	19.12	15.93	23.13	18.73	17.33	4.71	36.02
432.00	36	24.33	10.14	13.72	7.64	20.58	12.19	9.92	2.82	29.80
433.00	45	33.54	15.59	12.83	5.14	23.41	12.80	8.97	0.00	41.95
434.00	100	39.56	0.18	16.96	0.07	23.19	0.00	0.00	0.00	45.90
435.00	32	30.35	17.52	18.07	12.57	26.07	18.49	15.53	3.27	44.54
436.00	35	29.26	15.35	17.46	11.50	33.08	24.86	18.18	7.43	55.18
437.00	56	47.55	25.24	25.10	15.53	27.65	14.46	15.00	0.00	61.77
438.00	9	44.02	40.32	7.38	5.80	18.53	16.34	11.07	0.00	43.17
439.00	35	19.84	5.93	7.05	1.09	21.14	12.92	7.00	2.85	26.31
440.00	23	25.05	15.81	9.06	5.10	22.12	16.65	10.87	0.00	32.86

441.00	14	21.93	16.23	15.41	12.97	20.55	17.18	15.07	3.71	28.50
442.00	12	20.10	15.17	7.95	5.83	22.29	19.37	12.60	1.98	29.20
443.00	19	20.30	12.67	11.63	8.36	22.56	18.05	13.20	4.33	29.96
444.00	19	26.12	18.50	10.35	7.08	21.37	16.86	11.97	0.00	32.76
445.00	44	22.60	5.16	12.97	5.49	12.41	2.10	3.80	0.18	14.44
446.00	6	14.60	12.41	13.36	12.42	7.25	5.96	9.19	0.50	0.30
447.00	3	11.35	10.09	14.81	14.27	11.17	10.42	12.35	5.28	4.34
448.00	6	23.00	20.81	13.70	12.76	16.38	15.08	13.92	0.00	22.63
449.00	4	26.32	24.83	17.60	16.96	14.97	14.09	15.53	0.00	23.54
450.00	0	13.31	13.31	8.63	8.63	5.14	5.14	6.89	0.00	0.00
451.00	7	6.46	3.66	11.14	9.94	9.11	7.45	8.70	6.13	0.00
452.00	5	18.38	16.37	15.04	14.18	15.30	14.11	14.15	2.69	17.09
453.00	5	17.36	15.30	17.00	16.11	13.73	12.51	14.31	3.60	13.80
454.00	11	20.00	15.53	17.61	15.69	14.17	11.52	13.61	2.74	16.56
455.00	4	16.88	15.20	14.05	13.33	13.90	12.90	13.11	2.47	13.43
456.00	2	20.27	19.56	16.39	16.09	14.06	13.64	14.87	1.17	16.91
457.00	6	19.05	16.72	16.34	15.34	10.10	8.72	12.03	0.33	9.07
458.00	3	11.19	10.07	11.32	10.85	1.90	1.24	6.05	0.00	0.00
459.00	3	9.42	8.24	15.45	14.94	3.75	3.05	9.00	3.23	0.00
460.00	6	12.74	10.46	18.13	17.15	7.93	6.59	11.87	4.55	0.32
461.00	31	15.92	3.61	18.07	12.79	10.43	3.15	7.97	5.45	6.33
463.00	7	22.15	19.20	17.24	15.98	23.85	22.11	19.04	5.60	34.63
464.00	7	27.63	24.73	21.64	20.40	28.30	26.59	23.49	6.18	47.12
465.00	12	26.68	21.75	26.94	24.82	26.13	23.22	24.02	8.80	43.01
466.00	18	28.03	21.01	25.05	22.03	15.06	10.90	16.47	1.76	25.32
466.50	7	18.62	15.82	13.29	12.09	5.45	3.79	7.94	0.00	0.60

Well log derived Porosity, Permeability, and Shale volume -well Hr-50.

Depth (m)	Vsh (%)	Øs (%)	Øs co (%)	ØN (%)	ØN co (%)	ØD (%)	ØD co (%)	N-D co (%)	ØF (%)	K-log (md)
525.00	8	57.11	7.59	6.95	4.82	9.20	7.34	6.08	0.00	0.00
526.00	25	74.21	15.66	24.98	18.38	19.22	13.48	15.93	0.27	11.37
527.00	4	63.67	13.09	13.72	12.78	11.78	10.96	11.87	0.00	0.00
528.00	5	69.05	16.51	23.95	22.68	21.16	20.06	21.37	4.86	12.72
529.00	45	77.60	13.60	30.78	18.87	29.68	19.31	19.09	5.49	32.27
530.00	23	78.99	19.27	30.35	24.15	29.68	24.28	24.22	4.94	33.87
531.00	23	61.70	7.57	20.43	14.45	18.73	13.52	13.99	6.42	2.68
532.00	17	73.43	16.76	28.36	23.74	27.41	23.40	23.57	6.81	26.49
533.00	7	75.03	20.22	25.15	23.40	20.51	18.98	21.19	0.97	15.10
534.00	8	75.33	20.23	27.57	25.57	23.85	22.12	23.84	3.62	21.56
535.00	27	73.84	15.06	26.36	19.34	20.13	14.02	16.68	1.62	12.88
536.00	33	73.64	13.63	30.65	22.06	23.31	15.84	18.95	5.32	18.74
537.00	45	73.85	11.09	25.57	13.74	22.02	11.72	12.73	1.64	15.56
538.00	87	75.04	2.72	27.69	4.72	23.63	3.65	4.18	1.47	18.05
539.00	22	72.26	15.04	25.69	19.96	20.56	15.57	17.77	2.73	12.85
540.00	33	76.24	15.29	28.35	19.61	24.38	16.78	18.20	2.91	22.01

541.00	34	73.46	13.26	25.26	16.38	22.44	14.71	15.55	2.29	16.49
542.00	21	80.62	20.87	29.80	24.17	25.51	20.62	22.39	1.53	27.29
543.00	39	79.93	16.49	31.19	20.83	30.42	21.41	21.12	4.63	35.26
544.00	51	78.84	13.06	35.06	21.46	31.07	19.23	20.35	7.29	35.73
545.00	14	78.05	20.59	27.13	23.31	25.40	22.08	22.70	2.11	25.61
546.00	18	67.11	12.30	17.21	12.46	18.77	14.63	13.54	1.24	5.87
547.00	22	77.06	18.20	31.43	25.53	25.78	20.65	23.09	4.89	25.77
548.00	10	71.79	17.28	19.81	17.19	19.80	17.52	17.35	0.07	11.17
549.00	18	72.29	15.78	26.95	22.10	21.20	16.97	19.54	3.75	14.31
550.00	11	76.37	20.13	27.37	24.39	24.81	22.21	23.30	3.17	23.70
551.00	3	58.38	9.56	11.77	10.96	10.68	9.98	10.47	0.91	0.00
552.00	25	66.44	10.40	21.32	14.82	15.75	10.09	12.45	2.06	0.07
553.00	6	62.37	11.62	20.78	19.14	17.53	16.11	17.62	6.01	1.72
554.00	10	76.09	20.18	31.24	28.55	26.10	23.76	26.16	5.98	26.32
555.00	15	63.66	10.53	20.23	16.20	16.34	12.83	14.52	3.98	0.00
556.00	19	67.05	11.98	20.89	15.80	19.84	15.41	15.61	3.63	8.08
557.00	22	78.48	19.26	30.09	24.29	26.47	21.43	22.86	3.60	27.77
558.00	7	70.14	16.74	21.44	19.54	19.73	18.08	18.81	2.07	10.38
559.00	18	74.51	17.49	22.83	18.20	23.24	19.21	18.70	1.21	18.98
560.00	7	66.76	14.35	28.63	26.65	22.37	20.65	23.65	9.30	13.86
561.00	1	71.14	18.73	21.98	21.66	19.68	19.40	20.53	1.80	11.33
562.00	2	65.38	14.52	23.55	22.93	18.49	17.95	20.44	5.92	5.79
563.00	1	61.80	12.28	17.26	16.90	15.09	14.78	15.84	3.56	0.00
564.00	5	70.45	17.33	25.48	24.04	19.08	17.83	20.93	3.60	9.88
565.00	5	66.98	15.00	15.87	14.49	10.99	9.80	12.15	0.00	0.00
566.00	3	59.13	10.04	9.33	8.48	9.75	9.01	8.75	0.00	0.00
567.00	3	65.00	14.09	15.80	14.97	11.21	10.48	12.73	0.00	0.00
568.00	6	62.41	11.73	15.02	13.47	10.13	8.79	11.13	0.00	0.00
569.00	17	67.29	12.70	23.78	19.37	14.33	10.49	14.93	2.23	0.00
570.00	21	77.63	18.88	25.72	20.17	19.08	14.25	17.21	0.00	13.38
571.00	8	92.44	31.84	33.34	31.16	27.65	25.75	28.45	0.00	39.20
572.00	9	77.34	21.36	29.89	27.59	28.99	26.99	27.29	5.93	32.29
573.00	8	79.73	23.05	33.82	31.58	31.53	29.58	30.58	7.53	38.73
574.00	10	74.16	18.87	29.40	26.74	26.67	24.35	25.55	6.67	26.05
575.00	5	75.66	20.93	30.01	28.59	24.52	23.28	25.93	5.01	23.34
576.00	0	58.26	10.11	5.81	5.77	2.79	2.75	4.26	0.00	0.00

Well log derived Porosity, Permeability, and Shale volume -well Hr-51.

Depth (m)	Vsh (%)	Øs (%)	Øs co (%)	ØN (%)	ØN co (%)	ØD (%)	ØD co (%)	N-D co (%)	ØF (%)	K-log (md)
476.50	0	10.95	10.85	3.05	2.96	0.00	0.00	0.00	0.00	0.00
477.00	31	18.80	11.84	9.92	3.73	11.53	6.98	5.36	0.00	9.70
478.00	24	20.95	15.48	10.97	6.10	8.92	5.35	5.72	0.00	7.48
479.00	13	47.70	44.68	15.18	12.49	21.42	19.45	15.97	0.00	51.67
480.00	6	48.81	47.53	14.98	13.84	27.39	26.55	20.20	0.00	62.90
481.00	4	44.92	43.93	13.42	12.55	27.02	26.38	19.46	0.00	58.92

482.00	12	39.50	36.76	17.75	15.32	20.13	18.34	16.83	0.00	42.91
483.00	11	33.67	31.10	18.24	15.96	21.33	19.65	17.80	0.00	40.07
484.00	9	32.70	30.78	18.48	16.78	16.61	15.36	16.07	0.00	31.53
485.00	16	29.22	25.66	16.62	13.44	19.44	17.11	15.28	0.00	32.84
486.00	38	24.29	15.68	16.61	8.95	17.86	12.24	10.60	0.00	25.32
487.00	20	29.78	25.29	17.47	13.48	18.27	15.35	14.41	0.00	31.30
488.00	15	20.05	16.59	14.92	11.84	11.20	8.94	10.39	0.00	11.22
489.00	100	22.41	0.10	19.93	0.09	14.63	0.08	0.08	0.01	17.13
490.00	35	23.80	15.93	19.86	12.86	15.59	10.46	11.66	0.51	21.55
491.00	79	25.47	7.82	22.52	6.82	16.85	5.34	6.08	0.61	24.16
492.00	32	28.32	21.15	17.98	11.61	14.07	9.39	10.50	0.00	22.72
493.00	18	39.09	34.95	11.65	7.97	27.71	25.01	16.49	0.00	54.38
494.00	20	30.26	25.73	15.43	11.40	19.37	16.41	13.91	0.00	33.33
495.00	40	27.97	19.10	17.65	9.77	20.14	14.36	12.06	0.00	32.31
496.00	22	23.04	18.09	10.20	5.80	19.96	16.73	11.26	0.00	27.65
497.00	16	18.52	14.93	7.84	4.65	10.52	8.18	6.42	0.00	8.10
498.00	40	23.66	14.60	10.75	2.68	20.66	14.75	8.72	0.00	28.85
499.00	8	19.63	17.95	15.33	13.83	10.45	9.35	11.59	0.00	9.99
500.00	8	19.77	18.03	15.32	13.77	8.93	7.79	10.78	0.00	7.57
501.00	9	17.69	15.65	12.52	10.71	5.12	3.79	7.25	0.00	0.00
502.00	13	22.27	19.44	18.28	15.76	18.40	16.55	16.15	2.54	25.54
503.00	17	19.22	15.47	15.60	12.27	15.67	13.23	12.75	1.92	18.00
504.00	7	12.76	11.19	11.01	9.62	3.22	2.20	5.91	0.00	0.00
505.00	15	19.50	16.11	14.72	11.71	10.88	8.68	10.19	0.00	10.23
506.00	3	17.55	16.87	16.63	16.03	9.97	9.53	12.78	0.97	7.80
507.00	5	18.59	17.37	18.67	17.58	12.86	12.06	14.82	2.66	13.57
508.00	2	14.84	14.34	14.51	14.07	5.85	5.52	9.80	0.00	0.00
509.00	1	11.23	10.94	9.42	9.16	-2.38	-2.57	3.30	0.00	0.00
510.00	5	16.86	15.72	13.75	12.74	3.54	2.79	7.76	0.00	0.00
511.00	9	25.05	23.07	19.82	18.05	19.72	18.42	18.24	2.09	30.40
512.00	8	21.44	19.71	20.37	18.83	16.81	15.68	17.26	3.46	22.61
513.00	14	20.47	17.44	19.86	17.17	12.21	10.23	13.70	1.49	13.82
514.00	16	20.33	16.69	17.25	14.01	12.44	10.07	12.04	0.36	13.73
515.00	6	17.41	16.01	17.74	16.50	14.31	13.40	14.95	3.74	14.86
516.00	16	17.13	13.44	16.62	13.33	12.19	9.78	11.55	2.15	10.54
517.00	14	13.52	10.39	13.26	10.48	4.08	2.04	6.26	0.00	0.00
518.00	7	18.66	17.20	16.35	15.05	11.08	10.13	12.59	0.55	10.38
519.00	8	17.55	15.68	13.06	11.40	2.98	1.76	6.58	0.00	0.00
520.00	9	17.83	15.87	16.40	14.65	8.89	7.62	11.14	0.00	5.93
521.00	14	23.04	19.97	17.13	14.40	16.92	14.92	14.66	0.68	23.57
522.00	4	24.91	23.99	19.54	18.72	22.41	21.81	20.26	3.47	34.98
523.00	13	24.71	21.77	22.88	20.27	19.87	17.95	19.11	3.87	30.47
524.00	13	20.47	17.49	19.22	16.57	15.15	13.21	14.89	2.64	18.66
525.00	5	19.50	18.47	19.95	19.04	11.45	10.78	14.91	1.98	12.15
525.50	3	11.85	11.14	11.77	11.14	0.27	0.00	5.47	0.00	0.00

Appendix C

Well log derived saturation, well Hr-49.

Depth (m)	Sw (%)	Sxo (%)	ROS (%)	MOS (%)	BVW	BVH	MHI	FZI	Ro	Rxoo
419.50	28.10	74.61	25.39	46.51	0.02	0.04	0.38	0.61	7.62	49.52
420.00	30.35	73.95	26.05	43.61	0.03	0.06	0.41	0.45	4.32	28.06
421.00	21.89	16.74	83.26	0.00	0.02	0.08	1.00	0.40	3.25	21.14
422.00	14.25	44.91	55.09	30.66	0.03	0.19	0.32	0.14	0.78	5.07
423.00	13.53	44.61	55.39	31.08	0.03	0.19	0.30	0.20	0.80	5.19
424.00	16.35	43.22	56.78	26.87	0.03	0.15	0.38	0.27	1.06	6.86
425.00	9.09	43.20	56.80	34.10	0.01	0.15	0.21	0.32	1.30	8.43
426.00	7.12	29.56	70.44	22.43	0.01	0.13	0.24	0.39	1.81	11.76
427.00	24.07	77.24	22.76	53.17	0.03	0.10	0.31	0.31	2.03	13.21
428.00	45.98	100.00	0.00	54.02	0.03	0.03	0.36	0.87	7.62	49.54
429.00	37.34	100.00	0.00	62.66	0.03	0.04	0.32	0.85	5.80	37.73
430.00	15.81	63.27	36.73	47.46	0.02	0.13	0.25	0.26	1.52	9.88
431.00	21.61	73.20	26.80	51.59	0.04	0.14	0.30	0.22	1.17	7.62
432.00	35.72	92.72	7.28	57.00	0.04	0.06	0.39	0.49	3.20	20.82
433.00	36.22	100.00	0.00	63.78	0.03	0.06	0.34	0.69	3.84	24.95
434.00	100.00	100.00	0.00	100.00	0.03	0.00	0.45	0.00	20.00	200.00
435.00	48.65	83.40	16.60	34.75	0.08	0.08	0.58	0.29	1.43	9.28
436.00	23.07	49.34	50.66	26.26	0.04	0.14	0.47	0.25	1.08	6.99
437.00	32.13	86.85	13.15	54.73	0.05	0.10	0.37	0.36	1.52	9.88
438.00	24.03	25.54	74.46	1.51	0.03	0.08	0.94	0.50	2.63	17.08
439.00	33.61	46.61	53.39	13.00	0.02	0.05	0.72	0.81	5.99	38.94
440.00	22.32	57.93	42.07	35.61	0.02	0.08	0.39	0.45	2.71	17.63
441.00	24.85	34.47	65.53	9.61	0.04	0.11	0.72	0.24	1.51	9.80
442.00	24.05	18.81	81.19	0.00	0.03	0.10	1.00	0.33	2.08	13.52
443.00	22.66	43.67	56.33	21.01	0.03	0.10	0.52	0.31	1.91	12.44
444.00	26.61	32.96	67.04	6.36	0.03	0.09	0.81	0.38	2.28	14.84
445.00	85.99	100.00	0.00	14.01	0.03	0.01	0.86	1.55	18.03	117.19
446.00	38.12	48.74	51.26	10.62	0.04	0.06	0.78	0.06	3.67	23.87
447.00	42.11	85.69	14.31	43.58	0.05	0.07	0.49	0.13	2.16	14.03
448.00	27.20	64.22	35.78	37.02	0.04	0.10	0.42	0.25	1.74	11.30
449.00	28.23	54.41	45.59	26.18	0.04	0.11	0.52	0.21	1.43	9.29
450.00	45.77	23.43	76.57	0.00	0.03	0.04	1.00	0.00	6.17	40.10
451.00	48.42	19.34	80.66	0.00	0.04	0.04	1.00	0.00	4.05	26.36
452.00	39.00	20.51	79.49	0.00	0.06	0.09	1.00	0.21	1.69	10.98
453.00	35.90	60.72	39.28	24.82	0.05	0.09	0.59	0.18	1.65	10.75
454.00	47.52	54.28	45.72	6.76	0.06	0.07	0.88	0.22	1.81	11.78
455.00	34.09	66.00	34.00	31.91	0.04	0.09	0.52	0.21	1.94	12.59
456.00	30.59	20.71	79.29	0.00	0.05	0.10	1.00	0.19	1.55	10.04
457.00	38.02	60.64	39.36	22.62	0.05	0.07	0.63	0.20	2.26	14.70
458.00	68.14	100.00	0.00	31.86	0.04	0.02	0.57	0.00	7.81	50.73

459.00	78.98	95.24	4.76	16.26	0.07	0.02	0.83	0.00	3.82	24.81
460.00	53.28	78.35	21.65	25.07	0.06	0.06	0.68	0.04	2.32	15.07
461.00	68.40	100.00	0.00	31.60	0.05	0.03	0.60	0.32	4.74	30.83
462.00	38.54	18.52	81.48	0.00	0.06	0.09	1.00	0.20	1.56	10.15
463.00	27.79	46.37	53.63	18.58	0.05	0.14	0.60	0.18	0.99	6.43
464.00	24.50	47.23	52.77	22.73	0.06	0.18	0.52	0.14	0.68	4.41
465.00	29.03	50.67	49.33	21.64	0.07	0.17	0.57	0.13	0.65	4.23
466.00	48.41	75.14	24.86	26.74	0.08	0.08	0.64	0.20	1.29	8.35
466.50	95.01	32.40	67.60	0.00	0.08	0.00	1.00	0.10	4.78	31.04

Well log derived saturation -well Hr-50.

Depth (m)	Sw (%)	Sxo (%)	ROS (%)	MOS (%)	BVW	BVH	MHI	FZI	Ro	Rxoo
525.00	18.95	38.35	61.65	19.41	0.01	0.05	0.49	0.00	7.72	52.50
526.00	14.39	21.10	78.90	6.71	0.02	0.14	0.68	0.14	1.36	9.28
527.00	13.76	25.67	74.33	11.92	0.02	0.10	0.54	0.00	2.32	15.75
528.00	9.25	14.45	85.55	5.20	0.02	0.19	0.64	0.09	0.80	5.47
529.00	9.69	19.46	80.54	9.77	0.02	0.17	0.50	0.17	0.99	6.70
530.00	11.58	18.10	81.90	6.52	0.03	0.21	0.64	0.12	0.64	4.37
531.00	13.67	19.68	80.32	6.01	0.02	0.12	0.69	0.08	1.72	11.73
532.00	12.19	24.60	75.40	12.41	0.03	0.21	0.50	0.11	0.67	4.58
533.00	17.00	29.80	70.20	12.80	0.04	0.18	0.57	0.10	0.82	5.55
534.00	19.28	41.32	58.68	22.04	0.05	0.19	0.47	0.10	0.66	4.49
535.00	26.10	38.15	61.85	12.05	0.04	0.12	0.68	0.14	1.26	8.54
536.00	24.92	41.58	58.42	16.66	0.05	0.14	0.60	0.13	1.00	6.79
537.00	38.16	71.37	28.63	33.20	0.05	0.08	0.53	0.24	2.04	13.89
538.00	100.00	100.00	0.00	0.00	0.04	0.00	0.33	10.00	15.14	102.92
539.00	35.34	61.46	38.54	26.12	0.06	0.11	0.57	0.12	1.12	7.62
540.00	26.93	62.38	37.62	35.46	0.05	0.13	0.43	0.16	1.07	7.30
541.00	27.19	45.97	54.03	18.79	0.04	0.11	0.59	0.18	1.43	9.69
542.00	24.58	20.32	79.68	0.00	0.06	0.17	1.00	0.12	0.74	5.03
543.00	23.87	56.84	43.16	32.97	0.05	0.16	0.42	0.15	0.82	5.58
544.00	28.43	54.16	45.84	25.73	0.06	0.15	0.52	0.16	0.88	5.97
545.00	18.74	19.72	80.28	0.98	0.04	0.18	0.95	0.11	0.72	4.91
546.00	23.86	25.91	74.09	2.05	0.03	0.10	0.92	0.13	1.83	12.43
547.00	21.05	42.33	57.67	21.29	0.05	0.18	0.50	0.11	0.70	4.76
548.00	22.18	15.91	84.09	0.00	0.04	0.14	1.00	0.12	1.17	7.95
549.00	24.14	39.36	60.64	15.22	0.05	0.15	0.61	0.11	0.95	6.43
550.00	21.26	22.08	77.92	0.82	0.05	0.18	0.96	0.10	0.69	4.68
551.00	20.43	20.71	79.29	0.28	0.02	0.08	0.99	0.00	2.91	19.75
552.00	31.43	31.89	68.11	0.46	0.04	0.09	0.99	0.02	2.13	14.45
553.00	21.29	27.00	73.00	5.71	0.04	0.14	0.79	0.05	1.14	7.74
554.00	17.82	31.39	68.61	13.58	0.05	0.21	0.57	0.09	0.56	3.80
555.00	21.71	35.22	64.78	13.51	0.03	0.11	0.62	0.00	1.61	10.97

556.00	30.78	30.82	69.18	0.04	0.05	0.11	1.00	0.12	1.42	9.63
557.00	31.56	83.89	16.11	52.34	0.07	0.16	0.38	0.12	0.71	4.84
558.00	30.37	12.79	87.21	0.00	0.06	0.13	1.00	0.10	1.01	6.88
559.00	35.80	73.39	26.61	37.58	0.07	0.12	0.49	0.14	1.02	6.95
560.00	22.16	27.61	72.39	5.46	0.05	0.18	0.80	0.08	0.67	4.56
561.00	29.52	17.34	82.66	0.00	0.06	0.14	1.00	0.09	0.86	5.88
562.00	26.93	24.84	75.16	0.00	0.06	0.15	1.00	0.07	0.87	5.92
563.00	29.55	19.10	80.90	0.00	0.05	0.11	1.00	0.00	1.38	9.37
564.00	30.63	73.97	26.03	43.34	0.06	0.15	0.41	0.08	0.83	5.68
565.00	58.08	20.12	79.88	0.00	0.07	0.05	1.00	0.00	2.22	15.12
566.00	65.37	34.12	65.88	0.00	0.06	0.03	1.00	0.00	4.02	27.31
567.00	44.36	14.21	85.79	0.00	0.06	0.07	1.00	0.00	2.04	13.90
568.00	59.76	94.04	5.96	34.28	0.07	0.04	0.64	0.00	2.60	17.69
569.00	48.91	100.00	0.00	51.09	0.07	0.08	0.47	0.00	1.53	10.43
570.00	41.87	76.60	23.40	34.72	0.07	0.10	0.55	0.13	1.19	8.07
571.00	32.24	44.07	55.93	11.83	0.09	0.19	0.73	0.09	0.48	3.27
572.00	34.09	45.13	54.87	11.04	0.09	0.18	0.76	0.09	0.52	3.52
573.00	29.27	59.21	40.79	29.94	0.09	0.22	0.49	0.08	0.42	2.87
574.00	32.00	44.32	55.68	12.33	0.08	0.17	0.72	0.09	0.58	3.97
575.00	23.70	31.78	68.22	8.08	0.06	0.20	0.75	0.09	0.57	3.86
576.00	81.07	29.89	70.11	0.00	0.03	0.01	1.00	0.00	14.66	99.69

Well log derived saturation, well Hr-51.

Depth (m)	Sw (%)	Sxo (%)	ROS (%)	MOS (%)	BVW	BVH	MHI	FZI	Ro	Rxoo
476.50	100.00	100.00	0.00	0.00	0.00	0.00	0.27	0.00	12.00	150.00
477.00	35.38	100.00	0.00	0.65	0.02	0.03	0.18	0.75	9.70	87.33
478.00	46.36	100.00	0.00	0.54	0.03	0.03	0.20	0.59	8.62	77.57
479.00	25.82	100.00	0.00	0.74	0.04	0.12	0.21	0.30	1.36	12.23
480.00	17.33	53.92	46.08	0.37	0.03	0.17	0.32	0.22	0.89	8.01
481.00	14.19	80.19	19.81	0.66	0.03	0.17	0.18	0.23	0.95	8.56
482.00	19.60	81.89	18.11	0.62	0.03	0.14	0.24	0.25	1.24	11.13
483.00	20.51	77.13	22.87	0.57	0.04	0.14	0.27	0.22	1.12	10.05
484.00	30.56	100.00	0.00	0.69	0.05	0.11	0.26	0.23	1.34	12.09
485.00	27.12	96.12	3.88	0.69	0.04	0.11	0.29	0.26	1.47	13.24
486.00	34.87	100.00	0.00	0.65	0.04	0.07	0.23	0.41	2.84	25.58
487.00	27.81	100.00	0.00	0.72	0.04	0.10	0.23	0.27	1.63	14.70
488.00	36.98	100.00	0.00	0.63	0.04	0.07	0.26	0.28	2.94	26.49
489.00	100.00	100.00	0.00	0.00	0.03	0.00	0.30	0.00	2000	1960
490.00	46.79	100.00	0.00	0.53	0.05	0.06	0.31	0.32	2.39	21.53
491.00	77.78	100.00	0.00	0.22	0.05	0.01	0.28	0.97	7.73	69.54
492.00	72.13	100.00	0.00	0.28	0.08	0.03	0.34	0.39	2.89	25.99
493.00	20.70	91.39	8.61	0.71	0.03	0.13	0.23	0.29	1.28	11.54
494.00	27.69	100.00	0.00	0.72	0.04	0.10	0.26	0.30	1.74	15.68

495.00	33.55	100.00	0.00	0.66	0.04	0.08	0.24	0.37	2.25	20.26
496.00	22.78	100.00	0.00	0.77	0.03	0.09	0.18	0.39	2.55	22.92
497.00	39.40	100.00	0.00	0.61	0.03	0.04	0.29	0.51	7.01	63.12
498.00	38.11	100.00	0.00	0.62	0.03	0.05	0.23	0.60	4.04	36.36
499.00	39.36	100.00	0.00	0.61	0.05	0.07	0.34	0.22	2.42	21.77
500.00	35.78	74.91	25.09	0.39	0.04	0.07	0.48	0.22	2.76	24.80
501.00	46.67	59.32	40.68	0.13	0.03	0.04	0.80	0.00	5.63	50.66
502.00	28.53	96.58	3.42	0.68	0.05	0.12	0.30	0.20	1.33	11.98
503.00	45.41	100.00	0.00	0.55	0.06	0.07	0.37	0.26	2.04	18.34
504.00	58.21	100.00	0.00	0.42	0.03	0.02	0.38	0.00	8.14	73.25
505.00	47.53	100.00	0.00	0.52	0.05	0.05	0.37	0.28	3.05	27.43
506.00	39.32	100.00	0.00	0.61	0.05	0.08	0.33	0.17	2.03	18.27
507.00	31.25	100.00	0.00	0.69	0.05	0.10	0.31	0.17	1.55	13.98
508.00	42.75	100.00	0.00	0.57	0.04	0.06	0.37	0.00	3.27	29.47
509.00	100.00	100.00	0.00	0.00	0.04	0.00	0.90	0.00	23.25	209.23
510.00	69.35	78.61	21.39	0.09	0.05	0.02	0.89	0.00	4.98	44.78
511.00	39.87	100.00	0.00	0.60	0.07	0.11	0.36	0.18	1.07	9.63
512.00	46.99	100.00	0.00	0.53	0.08	0.09	0.43	0.17	1.18	10.64
513.00	48.61	100.00	0.00	0.51	0.07	0.07	0.46	0.20	1.79	16.11
514.00	61.48	100.00	0.00	0.39	0.07	0.05	0.41	0.24	2.26	20.32
515.00	35.42	97.13	2.87	0.62	0.05	0.10	0.37	0.18	1.53	13.77
516.00	45.48	100.00	0.00	0.55	0.05	0.06	0.39	0.23	2.43	21.89
517.00	100.00	100.00	0.00	0.00	0.06	0.00	0.47	0.00	7.33	65.98
518.00	62.39	100.00	0.00	0.38	0.08	0.05	0.44	0.20	2.08	18.75
519.00	100.00	100.00	0.00	0.00	0.07	0.00	0.42	0.00	6.70	60.31
520.00	53.94	100.00	0.00	0.46	0.06	0.05	0.36	0.18	2.60	23.40
521.00	48.31	100.00	0.00	0.52	0.07	0.08	0.44	0.23	1.58	14.26
522.00	32.65	84.75	15.25	0.52	0.07	0.14	0.39	0.16	0.89	7.97
523.00	39.11	100.00	0.00	0.61	0.07	0.12	0.36	0.17	0.98	8.85
524.00	44.68	100.00	0.00	0.55	0.07	0.08	0.38	0.20	1.54	13.87
525.00	48.01	100.00	0.00	0.52	0.07	0.08	0.46	0.16	1.54	13.83
525.50	100.00	88.87	11.13	0.00	0.07	0.00	1.00	0.00	9.34	84.05

الخلاصة

تم دراسة و تقييم تكوين الجريبي (المايوسيني الاوسط) من حيث كفاءته المكنية في ثلاث آبار مختارة في حقل حميرين النفطى ، شمال العراق. تعتبر الشرائح الرقيقة المستحضرة من النماذج الصخرية الفتاتية مع المجسات البئرية المختلفة للآبار Hr-51 و Hr-50 و Hr-49 المصادر الرئيسية لأستقاء للمعلومات في هذه الدراسة.

ظهرتكوين الجريبي فى آبار الدراسة بسمك حوالي 50 مترا متكونا من الحجر الجيري، الحجر الجيري الدولوميتى، والدولومايت مع احتوائه على نسب مختلفة من السجيل المتناثر علما ان أعلى نسبة سجيل تم ملاحظتها كانت في الجزء الاوسط من التكوين. لقد تم تحديد الأنواع المختلفة من السحنات المجهرية الدقيقة مع ما تحتويها من أنواع المسامات و ما رافقتها من عمليات تحويرية و ذلك من خلال الدراسة المجهرية للشرائح الرقيقة المحضرة من النماذج الصخرية المختارة.

المسامية المحتسبة من خلال معطيات مجسات المسامية المتكونة من المجس الصوتي ومجس الكثافة مع مجس النيوترون قد تم تصحيحها جميعا من تأثير السجيل. لقد ظهر بأن للتكوين مسامية تتراوح بين اقل من 5% في الانطقة الغنية بالسجيل إلى أكثر من 20% في الجزء الأسفل والأعلى من التكوين ذات الأقل احتواء للسجيل.

تم الاستدلال على وجود الغاز في تكوين الجريبي في البئرين Hr-51 و Hr-49 من خلال ملاحظة العلاقة بين معطيات مجسي الكثافة و النيوترون كما تم الاستدلال على وجود المسامية الثانوية بنسب مختلفة بلغت اقصاها حوالي 7% في بعض الانطقة من التكوين .

تم احتساب النفاذية للتكوين بطريقة الانحدار الخطي المتعدد معتمدين على معطيات اختبار اللباب (المسامية و النفاذية) لنماذج مختارة من تكوين الجريبي في البئر Hr-2 وقد تم تطبيق هذه المعادلة المستخلصة بالطريقة الرياضية والتي مثلت العلاقة بين القراءات للمجسات المختلفة والنفاذية المحتسبة من اختبار اللباب للبئر Hr-2 على بقية ابار الدراسة.

ان النفاذية المحتسبة للجزء الأعلى من التكوين قد تجاوزت 30مللي دارسي وخصوصا في البئر Hr-49 بينما ابدى التكوين تذبذبا في قيمة النفاذية في جزئيه الأوسط و الأسفل في البئرين الأخرين نتيجة لطبيعة التكوين غير المتجانسة فيهما.

أربع وحدات مكنية تم تمييزها في التكوين على اساس التباين في قيم المحتوى

السجيلي و المسامية، والنفاذية وقد تم تقسيم الوحدات من الأسفل نحو أعلى التكوين RU-1، RU-2، RU-3 و RU-4 علماً بان الودحتين المكنيتين RU-3 و RU-4 كلّ قد تم تقسيمها الى وحتين ثانويتين.

ان قيم التشبع المائي التي تم احتسابها للتكوين من خلال معطيات مجسات المقاومة قد اظهرت نسبا اعلى في البئر Hr-51 مقارنة بالبئرين الاخرين. من ناحية اخرى تم الاستدلال على ان معظم الهيدروكربونات الموجودة في التكوين في البئر Hr-51 لها قابلية الحركة وذلك بعكس الهيدروكربونات الموجودة في التكوين في البئر Hr-50 التي ظهر بان معظمها هيدروكربونات متبقية غير قادرة على الحركة.

من المتوقع ان تصاحب الهيدروكربونات التي يتم انتاجها من التكوين كميات مختلفة من المياه المصاحبة. كما يتوقع ان تكون اقل كمية من المياه المصاحبة للهيدروكربونات المنتجة هي امل من الوحدة المكنية RU-1 والوحدة المكنية الثانوية RU-4B واكثر كمية من المياه المصاحبة تكون من الوحدة المكنية الثانوية RU-3A.

بيّنت الدراسة بان الحجر الحبيبي / المرصوص و الحجر الدولومايتي المرصوص هما الغالبان كنسيج صخري مكوّن لتكوين الجريبي في ابار الدارسة عدا في الودحتين المكنيتين RU-1 و RU-2 من البئر Hr-50 اللتين اظهرتا نسيجا صخريا معظمه حجر مرصوص وحجرواكي.

فيما يخص المسافات البينية و الرابطة بين المسامات فقد ظهر بأنها غالبا ما تبلغ 1.0 و 2.0 ميكرونا مع كون 2.0 ميكرون هو الاغلب. كما ان مسافات بينية بمقدار 0.5 ميكرون قد تم ملاحظتها بالرغم من ندرتها و خصوصا في الوحدة المكنية RU-2 في البئر Hr-49. فيما يخص تحديد نوعية أنسيابية الجريان للتكوين فمن خلال العلاقة بين المسامية و النفاذية تبين بأن كل من المسامات الموجودة في الملاط الصخري للتكوين مع الكسور الدقيقة قد وفرتا النفاذية المطلوبة للجريان.

أربعة انطقة جريان دالة (FZI) هي كل ما تم تمييزها في تكوين الجريبي ممثلة لأربعة أنطقة جريان هيدروليكية (HFU) في هذه الدراسة و ذلك اعتماداً على العلاقة بين الدالة المكنية النوعية (RQI) و الدالة المسامية المتطبعة (ϕz).

ان النسب المكنية و العطائية والمنتجة الصافية من تكوين الجريبي في ابار الدراسة قد تم احتسابها معتمدين قيم حديّة للمحتوى السجيلي والمسامية والنفاذية و التشبع المائي مع الاخذ بعين الاعتبار قابلية الهيدروكربونات للحركة. ان اعلى القيم للنسب المذكورة انفاً قد تم

احتسابها في البئر Hr-51 وكانت 79.83% للنسبة المكمية الصافية و 79.33% للنسبة العطائية الصافية و 78.68% للنسبة المنتجة الصافية. بينما اقل القيم الامل قد تم احتسابها في البئر Hr-50 وكانت 58.93% و 54.31% و 25.98% للنسب المذكورة تباعاً. ان تكوين الجريبي في البئر Hr-51 يملك الأعلى سمكاً من الانطقة المنتجة و البالغة جمعاً 37متراً بينما يملك التكوين في البئر Hr-50 الأقل سمكاً من الانطقة المنتجة و البالغة جمعاً 13.25 متراً.

التقييم المكمني لتكوين الجريبي (المايوسين الاوسط) من أبار مختارة في حقل حميرن النفطي, شمال العراق

رسالة

مقدمة الى مجلس كلية العلوم
في جامعة السليمانية كجزء من متطلبات
نيل شهادة ماجستير في علوم
الجيولوجيا
(جيولوجيا النفط)

من قبل

محمد برهان محمد سعيد

بكالوريوس جيولوجي، (٢٠٠٩) جامعة السليمانية

باشراف

د. دلير حسين بابان

استاذ مساعد

پوختە

لەم توپزىنەوويەدا ھەئسەنگاندىن بۇ پېكھاتووى جىرەبى، تەمەنى مايۆسىنى ناوەرەست، لەرووى تايبەتمەندىيى و تواناى وەك كۆگەى نەوتى لە سى بىرى ھەئبژىردراوى كىلگەى ھەمىرىن لە باكورى عىراق ئەنجامدراوہ.

تېروانىن بۇ بىرگەى تەنك ئەنجام دراوہ، كە لە نموونەى بەردى ووردبووہوہ دروستكراوہ، لەگەئ لىكدانەوہى ئەو لۇگ(تۆمار) و داتايانەى كە بەرچەستەن لە ھەر يەكە لە بىرى ھەمىرىن 49 و ھەمىرىن 50 و ھەمىرىن 51 بەكارھاتوون بۇ خستەن رووى سيفتە و تايبەتمەندىيەكانى كۆگەكە. پېكھاتووى جىرەبى لەو بىرانەى لىكۆلنەوہىيان لەسەر كراوہ، ئەستورىيەكەى نىكەى 50 مەترە و پېكھاتووہ لەبەردى كلسى و بەردى كلسىي دۆلۆمىتى و دۆلۆستون. جۆرەھا شىوازى وورد (مايكروفەش) و جۆرى كونىلە و جۆرەھا گۆرانەكردارەكان دەردەكەوئت لە ژىر مايكروۆسكۆب لە نىو بەردى نمونەى ھەئبژىردراو، پېكھاتەكە بىرى رېژەى جىاواز لە قورە كەفرى پەرەبى (Shale) نىشان دەدات كە زۆربەى زۆرى لە جۆرى قورى پەرەبى پەرش و بلاو، وە سەرنجمانداوہ زۆربەى زۆرى رېژەى قورە كەفرى پەرەبى لە بەشى ناوەرەستى پېكھاتەكەدايە.

ئەژماركردنى كونۆچكەدارى يان كونىلەدارى راستكراوہتەوہ بۇ كارىگەرى قورە كەفرى پەرەبى بۇ تەواوى داتا پىوانەكراوى لۇگى سۆنىك و دىنستى و نىوترۆن، كونۆچكەدارى لە و بەشەى كەفەرە قورى كەفرى پەرەبىيە لە 5% كەمترە و لە بەشى سەرەوہ و خوارەوہى پېكھاتووہكەدا زىاتر 20% دەبىت. بوونى گاز لە پېكھاتووى جىرەبى لە بىرى ھەمىرىن 49 و ھەمىرىن 51 ديارى كراوہ لە پەيوەندى نىوان ھەردوو لۇگى دىنستى و نىوترۆن وە بوونى كونىلەى دووہمى بە رېژەى جىاواز لە ھەندى شوئن دەگاتە لە 7% . ئەژماركردنى دەلاندن لە پېكھاتووى جىرەبى بە پشت بەستەن بە ھاوكىشەى مەئتى لىنەر رېگريشن و بە بوونى بەھاي كونۆچكەدارى و دەلاندن كە لە لىكدانەوہى داتاي كۆرەوہ (Core data analysis) و ئەژماركردنى لۇگ لە بىرى ھەمىرىن 2 وەرگىراوہ. ئەم

ھاۋا كېشەيە گونجاوترىن پەيوەندى نىۋان لۆگ و داتا ۋە بەھاي دەلاندن لە داتاى كۆرەۋە لە بىرى
ھەمىرىن 2 پىشان دەدات و لە سەر داتاى لۆگى سى بىرى باسكراۋ جىبەجىكراۋە. دەلاندن لەبەشى
سەرۋەى پىكھاتوۋەكە لە 30% ملیدارسى زياتر پىشان دەدات، بە تايبەتى لە بىرى ھەمىرىن 49 دا.
بە روۋنى بەرزى و نزمى لە بەھاي دەلاندن لە بەشى سەرۋە و خوارۋەى ئەم پىكھاتوۋەدا لە ناو
ھەردوۋ بىرى ھەمىرىن 50 و 51 دەبىنرېت، كە نىشانەى نا چوۋنىيەكى سىروشتى پىكھاتوۋەكەيە.

پىكھاتوۋى جىرەبى بۇ چوار يەكەى كۆگەيى دابەش كراۋە بە پىشتەستىن بە جۆرى بىرى قورە كەقرى
پەرەيى و كۈنيلەدارى و دەلاندن. يەكە كۆگەيىيەكان لە خوارۋە بۇ سەرۋە ناۋنراۋە ، ۋەكو كۆگەى
يەكەى يەك و كۆگەى يەكەى دوو و كۆگەى يەكەى سى، كە بەوردى دابەش كراۋە بۇ دوو كۆگەى
لاۋەكى (ا،ب) و كۆگەى يەكەى چوار، كە دابەش كراۋە بۇ دوو كۆگەى لاۋەكى (ا،ب).

تېرىبونى ئاۋى لە پىكھاتوۋى جىرەبى بەھاي بەرزى لە بىرى ھەمىرىن 51 دا تۆماركردوۋە
بەبەرۋارد لەگەل دوو بىرەكەى تردا و بە تايبەتى لە بەشى خوارۋەى بىرەكەدا و زياتر كۆگەى
ھايدىرۆكاربۇنى جوۋلاۋە لە بىرى ھەمىرىن 51 ، بە پىچەۋانەى بىرى ھەمىرىن 50 كە بەرزترىن
ھايدىرۆكاربۇن قەتسىبوۋ دەردەكەۋىت.

پىكھاتوۋى جىرەبى لە بىرەكاندا بەرھەمى ھايدىرۆكاربۇنى لەگەل ئاۋدا ھەيە بەرپىژەى جىاۋاز
كە پەيوەستە بە قەبارەى جىاۋازى ئاۋ. كەمترىن بەرھەمى ئاۋ لەناو كۆگەى يەكەى يەك و كۆگەى
لاۋەكى يەكەى چوار (ب) دا يە ۋە بەرزترىن بەرھەمى ئاۋ لەناو كۆگەى لاۋەكى يەكەى چوار (ا) دا يە.
پاكستۇنى دەنكۆلەيى و پاكستۇنى دۆلۆمايتى بلاۋە لە بەردى پىكھاتوۋى جىرەبىيى بىچگە لە كۆگەى
يەكەى يەك و دوو لە ناو بىرى ھەمىرىن 50 كە پاكستۇن و ۋاك ستۇنى فرە قور بلاۋە. قەبارەى
كەنالى نىۋان كۈنيلەكان زياتر لە مەۋداى 1-2 مايكرون دا يە كە بوۋنى 2 مايكرون زياتر بلاۋە،
قەبارەى كەنالى نىۋان كۈنيلەكان لە جۆرى 0.5 مايكرون بوۋنى كەمە لە كۆگەى يەكەى دوو لە بىرى
ھەمىرىن 49 دا. شلە رۇين دەلاندن سەرەكى لە پىكھاتوۋى جىرەبى دەردەكەۋىت لە نىۋان كۈنيلەى
ماترىكس و وورديفراگجەر.

چوار پشتينەى رېبەرىي شلە رۆين ديارىكراوه و نيشانەى چوار يەكەى هايدروئىكى ناسراوى
پىكھاتووى جىرەبى يە كە پەيوەندى نىوان ئەژماركردنى هاوكۆلكەى جۆرىي كۆگە و هاوكۆلكەى
كونىلەدارى پىوانەىي پيشان دەدات.

رېژەگانى نىوان پوختەى كۆگە و پىدان و بەرھەم (Net to Gross ratios) له
پىكھاتووى جىرەبىدا ئەژماركراوه بە بە بەكارھىننى كەمترىن مەوداگانى (Cutoffs) بىرى قورە
كەفرى پەرەبى و كونىلەدارى و دەلاندن و تىربون بەئاو لەگەل رەچاوكردنى بەھى پشتينەى
هايدروكاربونى جوولاًو . بەرزترىن رېژە پوختەى كۆگە و پىدان و بەرھەم له پىكھاتووى جىرەبى له
ناو بىرى حەمرىن 51 دايە (79.83% و 79.33% و 78.68% يەك لەداوى يەك) وە كەمترىن له ناو
بىرى حەمرىن 50 دايە (62.25% و 57.35% و 25.98% يەك لەداوى يەك) . بىرى حەمرىن 51
بەرزترىن ئەستوورىي بەرھەمەينى پىكھاتووى جىرەبى له خۇدەگرىت لەنىوان ھەرسى بىرى باسكراو،
كە كۆى دەگاتە 37 مەتر، لەكاتىكدا بىرى حەمرىن 50 كەمترىن ئەستوورىي له خۇدەگرىت كە كۆى
دەگاتە 13.25 مەتر.

تایبەتمەندییەکانی کۆگەى نەوتى پیکهاتووی جیڤهیبی
(مایۆسىنى ناوهراست) له چەند بیرىكى هەلبژیراوی کىلگەى
نەوتى حەمرین له باکوورى عىراق

نامەیهکە

پیشکەشکراوه به ئەنجومەنى کۆلیجى
زانست له زانکۆى سلیمانى وهك بهشیک له پیداوایستیهکانى
بهدهستهینانى پروانامەى ماستەر
له زانستى جیۆلۆجى
(جیۆلۆجیای نەوت)

له لایەن

محمد برهان محمد سعید
بهکالوریۆس له جیۆلۆجى، (2009) زانکۆى سلیمانى

بهسەرپهەرشتى

د. دلیر حسین بابان
پروفیسۆرى یاریدهدر